

University of Alberta

Winter Ice Regime of the Lower Athabasca River

by

Juan Nicolas Abarca



A thesis submitted to the faculty of Graduate Studies and Research in partial fulfillment
of the requirements for the degree of Master of Science

in

Water Resources Engineering

Department of Civil and Environmental Engineering

Edmonton, Alberta

Fall 2007



Library and
Archives Canada

Bibliothèque et
Archives Canada

Published Heritage
Branch

Direction du
Patrimoine de l'édition

395 Wellington Street
Ottawa ON K1A 0N4
Canada

395, rue Wellington
Ottawa ON K1A 0N4
Canada

Your file *Votre référence*
ISBN: 978-0-494-33185-9
Our file *Notre référence*
ISBN: 978-0-494-33185-9

NOTICE:

The author has granted a non-exclusive license allowing Library and Archives Canada to reproduce, publish, archive, preserve, conserve, communicate to the public by telecommunication or on the Internet, loan, distribute and sell theses worldwide, for commercial or non-commercial purposes, in microform, paper, electronic and/or any other formats.

The author retains copyright ownership and moral rights in this thesis. Neither the thesis nor substantial extracts from it may be printed or otherwise reproduced without the author's permission.

AVIS:

L'auteur a accordé une licence non exclusive permettant à la Bibliothèque et Archives Canada de reproduire, publier, archiver, sauvegarder, conserver, transmettre au public par télécommunication ou par l'Internet, prêter, distribuer et vendre des thèses partout dans le monde, à des fins commerciales ou autres, sur support microforme, papier, électronique et/ou autres formats.

L'auteur conserve la propriété du droit d'auteur et des droits moraux qui protègent cette thèse. Ni la thèse ni des extraits substantiels de celle-ci ne doivent être imprimés ou autrement reproduits sans son autorisation.

In compliance with the Canadian Privacy Act some supporting forms may have been removed from this thesis.

Conformément à la loi canadienne sur la protection de la vie privée, quelques formulaires secondaires ont été enlevés de cette thèse.

While these forms may be included in the document page count, their removal does not represent any loss of content from the thesis.

Bien que ces formulaires aient inclus dans la pagination, il n'y aura aucun contenu manquant.


Canada

ABSTRACT

Water withdrawals from the Lower Athabasca River will increase with the expansion of the oil sands mining operations, and may affect the ice regime of this reach. A three-year program was established to develop an appropriate modeling tool to address this issue. The main purpose of this first year of study was to establish the main conditions describing the winter ice regime of an 80 km reach of the Athabasca River, spanning from Fort McMurray to Bitumont. Hydrometeorological and ice cover characterization data was collected for the 2006/07-winter season through the implementation of an extensive field monitoring program. Preliminary numerical modeling of thermal and hydraulic processes was conducted in River1D and River2D. The ice regime of the reach was observed to be highly two-dimensional, due to the presence of numerous islands, sand bars and industrial warm water outfalls. To account for these factors, several limitations of the models must be addressed.

ACKNOWLEDGEMENTS

The author greatly acknowledges Dr. Faye Hicks, for being a true mentor and a wonderful friend. Her support and advice were invaluable throughout the development of this project, and her passion for river ice was both awe inspiring and stimulating. Thanks are also extended to her brilliant river ice group: Robyn Andrishak for his acumen and good judgment during the ice slicing and modeling stages of the project; Chris Krath who made of fieldwork a safe and enjoyable experience; Amy She and Karen Dow who made of our discussion groups something to look forward to; Brett Howard for always being willing to undertake tedious tasks; Perry Fedun, whose technical expertise made everything work seamlessly; and especially David Keller, who not only makes beautiful maps, but whose friendship and honesty are priceless.

For agreeing to be on the examining committee for the defence of this project, the author acknowledges Dr. Mark Loewen from the Water Resources group and Dr. Gerhard Reuter from the Earth and Atmospheric Sciences group. Their participation in such short notice is greatly appreciated.

High amounts of data were provided by Chandra Mahabir from Alberta Environment; Chris Katopodis and Haitham Ghamry from the Department of Fisheries and Oceans; Yves Gauthier and Monique Bernier from INRS-ETE; C-CORE; Water Survey of Canada; Golder Associates; and the Cumulative Environmental Management Association. These records are greatly acknowledged. Funding for this project was

provided by Alberta Ingenuity; their support is truly appreciated. Funding for the equipment used in this study was provided by the Natural Sciences and Engineering Research Council of Canada, and this support is also gratefully acknowledged.

None of this would have been possible without the support and love of my parents, Juan Agustin and Laura Beatriz, my beautiful wife Jenny, who was there with me every step of the way, and my grandmother Soledad, who passed away as this project was taking shape, but who would have surely been happy and proud of the outcome.

TABLE OF CONTENTS

CHAPTER 1 INTRODUCTION.....	1
1.1. AN INTRODUCTION TO RIVER ICE PROCESSES	2
1.2. RESEARCH OBJECTIVES.....	4
1.3. PREVIOUS STUDIES	5
1.4. EXISTING DATA.....	8
CHAPTER 2 FIELD PROGRAM AND DATA ANALYSIS	15
2.1. INTRODUCTION.....	15
2.2. DESCRIPTION OF THE STUDY REACH.....	16
2.3. METEOROLOGICAL DATA	18
2.3.1. Existing Meteorological Records.....	18
2.3.2. Instrumentation and Methodology.....	20
2.3.3. Data Analysis.....	20
2.4. HYDROMETRIC DATA.....	22
2.4.1. Existing Hydrometric Stations.....	23
2.4.2. Instrumentation and Methodology – Water Level.....	25
2.4.3. Instrumentation and Methodology – Discharge.....	27
2.4.4. Water Level Data Analysis.....	29
2.4.4.1. Freeze-up.....	30
2.4.4.2. Breakup	31
2.4.5. Discharge Data Analysis.....	32
2.5. WATER TEMPERATURE DATA.....	33
2.5.1. Existing Data.....	34
2.5.2. Instrumentation and Methodology.....	35

2.5.3. Data Analysis.....	37
2.5.3.1. Freeze-up.....	37
2.5.3.2. Breakup.....	40
2.6. ICE COVER CHARACTERIZATION.....	41
2.6.1. Surface Ice concentration.....	42
2.6.2. Aerial Surveillance of Ice Cover Formation and Deterioration.....	44
2.6.2.1. Freeze-up.....	44
2.6.2.2. Breakup.....	46
2.6.3. Satellite Imagery.....	48
2.6.3.1. Freeze-up.....	48
2.6.3.2. Breakup.....	51
2.6.3.3. Discussion.....	52
2.6.4. Ice Cover Thickness Measurements.....	52
2.6.4.1. Operating Principles of Ground Penetrating Radar.....	53
2.6.4.2. GPR for Ice Cover Characterization – Previous Studies.....	55
2.6.4.3. Fieldwork Procedures and Data Analysis.....	57
2.6.5. Ice Core Sampling.....	60
2.7. SUMMARY.....	63
CHAPTER 3 THERMAL AND HYDRAULIC MODELING.....	122
3.1. ONE-DIMENSIONAL MODELING.....	122
3.1.1. Model Description.....	123
3.1.2. Model Implementation.....	125
3.1.3. Discussion of Results.....	128
3.2. TWO-DIMENSIONAL MODELING.....	135
3.2.1. Model Description.....	137
3.2.2. Evaluation of the CEMA Reach 1 <i>River2D</i> Model.....	139

3.3. SUMMARY	142
CHAPTER 4 SUMMARY AND RECOMMENDATIONS.....	153
CHAPTER 5 REFERENCES.....	160
- APPENDIX A -	165
Appendix A1 Campbell Scientific air temperature sensor (model 44212) - Specification sheet.....	166
Appendix A2 Van Essen Instruments Divers – Specification sheet	168
Appendix A3 Sontek Acoustic Doppler Current Profiler – Specification sheet	170
Appendix A4 Campbell Scientific soil/water temperature probe (model 107B) – Specification sheet	172
Appendix A5 RTD Platinum Thermometer – Specification sheet	175
- APPENDIX B -.....	177
Appendix B1 Ice cover mapping – November 5, 2006	178
Appendix B2 Ice cover mapping – November 10, 2006	187
Appendix B3 Ice cover mapping – November 17, 2006	196
Appendix B4 Ice cover mapping – March 30, 2007.....	205
Appendix B5 Ice cover mapping – April 12, 2007.....	214
Appendix B6 Ice cover mapping – April 16, 2007.....	223
Appendix B5 Ice cover mapping – April 17, 2007.....	232

LIST OF TABLES

Table 2.1	Automated monitoring stations installed along the study reach on September 2006.	66
Table 2.2	Location of major islands and landmarks along the study reach.....	67
Table 2.3	Existing meteorological stations on the study area.....	68
Table 2.4	Existing hydrometric stations operated by WSC on the study area.....	69
Table 2.5	Areas of open water, border ice, juxtaposed ice and hummocky ice (km ²) along the reach during the freeze-up and breakup periods, obtained from aerial surveillance.	69
Table 2.6	Location of warm water outfalls and extent of the resulting open leads as observed during the freeze-up 2006 surveillance flights.	70
Table 2.7	RADARSAT-1 SAR images of the study reach obtained, with included ice cover classification.	70
Table 2.8	Summary of GPR transects and mean ice thicknesses obtained from.....	71
Table 2.9	Summary of ice core samples obtained from CEMA Reach 1.	71
Table 2.10	Average crystal sizes of ice core samples obtained from cold room laboratory analysis.....	72
Table 2.11	Air content of ice core samples obtained from cold room laboratory analysis.	73

Table 3.1	Summary of available records for <i>River1D</i> model implementation and calibration, obtained for the 2006/07-winter season.....	145
Table 3.2	Summary of ice modeling parameters adopted from Andrishak, 2006 for <i>River1D</i> model implementation.....	146

LIST OF FIGURES

Figure 1.1	Overview of the Athabasca River spanning from the Town of Athabasca to Bitumont.....	11
Figure 1.2	Mean monthly flows on the Athabasca River at Fort McMurray, Alberta (Data Source: Water Survey of Canada, available record from 1957 to 2004).....	12
Figure 1.3	Conceptual diagram of river ice formation processes (adapted from Michel, 1971).	12
Figure 1.4	Border ice, pans and rafts seen in the Lower Athabasca River on November 4 th , 2006.....	13
Figure 1.5	Juxtaposed Ice cover seen on the Lower Athabasca River near Fort MacKay on November 3 rd , 2006.	13
Figure 1.6	Hummocky ice cover seen on the Lower Athabasca River near Fort McMurray on November 10 th , 2006.....	14
Figure 1.7	Thermally deteriorated Ice Cover seen on the Lower Athabasca River on April 16, 2007.....	14
Figure 2.1	Overview of the study area.	74
Figure 2.2	Athabasca river longitudinal profile from the Town of Athabasca to Lake Athabasca (after Kellerhalls et al., 1972, adapted from Robichaud, 2003). Note: vertical scale exaggerated.	75
Figure 2.3	Islands and sand bars on the Lower Athabasca River at Morton Island – September 2006.....	76

Figure 2.4	Historical records of air temperature at Fort McMurray from 1944 to 2005 obtained from the meteorological station at Fort McMurray airport.....	76
Figure 2.5	Air Temperature sensor above the data-logger shelter installed at river station M216.7.....	77
Figure 2.6	Air temperature records obtained from Station M216.7, UA Met station and AE Met Station– Sept. 2006 to April 2007.....	77
Figure 2.7	Mean daily air temperature (°C) at UA meteorological station versus river station M216.7 from October 2006 to April 2007.	78
Figure 2.8	Historical record of Mean monthly air temperature at Fort McMurray airport between October and April.	78
Figure 2.9	Historical versus 2006/07 mean monthly discharges obtained from the WSC gauge below Fort McMurray.	79
Figure 2.10	Mean daily discharges obtained from the WSC gauge below Fort McMurray for the 2006 pre-freeze-up period.	79
Figure 2.11	Recorded water levels at the WSC Gauge below Fort McMurray during the 2006 freeze-up period.....	80
Figure 2.12	2006 Freeze-up water levels recorded at a) Beaver River above Syncrude, b) Steepbank River near Fort McMurray, c) Muskeg River near Fort MacKay and d) MacKay River near Fort MacKay.	81
Figure 2.13	Recorded water levels at the WSC gauge below Fort McMurray, during the 2007 breakup period.....	82
Figure 2.14	2007 breakup water levels recorded at a) Beaver River above Syncrude, b) Steepbank River near Fort McMurray, c)	

	Muskeg River near Fort MacKay and d) MacKay River near Fort MacKay.	83
Figure 2.15	Setup used for Diver [®] installation in the field - September 2006.....	84
Figure 2.16	Remaining cable-clamps as they were detached from the concrete pad – May 2007.....	84
Figure 2.17	Location of ADCP, GPR, ice core samples and ice cover thickness measurements at CEMA Reach 1 – March 2007.....	85
Figure 2.18	Measured Water Levels at Stations M288.1 and M268.1 – October 2006 to April 2007.....	86
Figure 2.19	Measured water level fluctuation during ice cover formation at stations M288.1 and M268.1.	86
Figure 2.20	Measured ice jam release waves at stations M288.1 and M268.1 - April 2007.....	87
Figure 2.21	Discharge and velocities recorded with the ADCP at the upstream boundary of CEMA Reach 1 on March 6, 2007.	88
Figure 2.22	Discharge and velocities recorded with the ADCP at the downstream boundary of CEMA Reach 1 on March 6, 2007.....	89
Figure 2.23	Discharge and velocities recorded with the ADCP at the island split section of CEMA Reach 1 on March 6, 2007.....	90
Figure 2.24	Water temperature variation during the 2006 freeze-up period recorded at the Town of Athabasca.	91
Figure 2.25	Concrete pad holding the air temperature sensor and the Diver prior to station installation.	91

Figure 2.26	Conceptual diagram of the typical monitoring station installation (separate concrete pads).....	92
Figure 2.27	Manual water temperature measurements at stations a) M288.1, b) M268.1, c) M245.6 and d) 216.7 obtained in September 2006, prior to station installation.....	93
Figure 2.28	Water temperature variation data collected by the automated stations during the 2006 freeze-up period.....	94
Figure 2.29	Mean daily water temperature recorded at a) station M288.1 and b) station M268.1 using Campbell Scientific 107B soil/water temperature probes and Van Essen Instruments Divers	95
Figure 2.30	Arrival of the zero degree isotherm measured at all four monitoring stations.....	96
Figure 2.31	Water temperature variation data collected before, during and after breakup 2007 by station M288.1 and M268.1.....	96
Figure 2.32	Water temperature and water level variation before, during and after breakup at river station M288.1.....	97
Figure 2.33	Water temperature and water level variation before, during and after breakup at river station M268.1.....	97
Figure 2.34	Overnight appearance of border ice and frazil floes as captured by the surveillance cameras at Stations M288.1 (a,c) and M216.7 (b,d).....	98
Figure 2.35	Superimposed grid created in CAD software to determine surface ice concentrations at station M288.1.....	99

Figure 2.36	Surface ice concentration data at Station M288.1, as obtained from images captured by the surveillance camera.	99
Figure 2.37	Relationship of cumulative degree-days of freezing and thaw, with percentage of surface ice concentration and open water, respectively.	100
Figure 2.38	Open leads in the vicinity of Willow Island as seen on November 5, 2006.	101
Figure 2.39	Open lead resulting from a warm water outfall near the Suncor Bridge, as seen on November 5, 2006.	101
Figure 2.40	Appearance of frazil ice pans in an open lead. Thermal growth formations around islands and sand bars. November 5, 2006.	102
Figure 2.41	Open lead generated downstream of Suncor Bridge. Thermal deterioration of the ice cover during breakup. April 12, 2006.	102
Figure 2.42	Ice cover classification of the RADARSAT SAR image taken on 1-Nov-06 (km 290 to 285) compared to the image recorded by the digital camera at station M288.1.	103
Figure 2.43	Ice cover classification of the RADARSAT SAR image taken on 01-Nov-06 (upstream of the Suncor Bridge), compared to observations during the surveillance flight undertaken on 05-Nov-07.	104
Figure 2.44	Suspected outfall locations near the Suncor Bridge seen during aerial surveillance and identified in ice cover classification of the RADARSAT SAR image taken on 05-Nov-06.	105
Figure 2.45	Suspected outfall locations downstream of Peter Lougheed Bridge seen during aerial surveillance and identified in ice	

	cover classification of the RADARSAT SAR image taken on 05-Nov-06.....	106
Figure 2.46	Discrepancies in ice cover classification near station M288.1, between satellite imagery (left) and aerial surveillance (right) – 05-Nov-06.....	107
Figure 2.47	Presence of floating ice pans identified during aerial surveillance, compared to the RADARSAT SAR image taken on 05-Nov-06 (km 261 to 253).....	108
Figure 2.48	Ice cover classification of the RADARSAT SAR image taken on 15-Apr-07 (km 293 to 276), compared to observations during the surveillance flight undertaken on 16-Apr-07.....	109
Figure 2.49	Ice cover classification of the RADARSAT SAR image taken on 18-Apr-07 (km 265 to 250), compared to observations during the surveillance flight undertaken on 17-Apr-07.....	110
Figure 2.50	Use of a snowmobile to tow the GPR antenna along the ice cover.....	111
Figure 2.51	2-D scan display line acquired at the downstream boundary of CEMA Reach 4 - 900 MHz antenna.....	111
Figure 2.52	Thickness of the ice cover as obtained from GPR scans compared to measured values at the upstream boundary of CEMA Reach 1 (Transect 1).....	112
Figure 2.53	Thickness of the ice cover as obtained from GPR scans compared to measured values at the downstream boundary of CEMA Reach 1 (Transect 2).....	112

Figure 2.54	Thickness of the ice cover as obtained from GPR scans compared to measured values at the split section of CEMA Reach 1 (Transect 3).	113
Figure 2.55	Air inclusions and crystal structure analysis of core sample obtained at the upstream boundary of CEMA Reach 1 – 130 m from the west bank.	114
Figure 2.56	Air inclusions and crystal structure analysis of core sample obtained at the split section of CEMA Reach 1 – 30 m from the west bank.	115
Figure 2.57	Air inclusions and crystal structure analysis of core sample obtained at the split section of CEMA Reach 1 – 100 m from the west bank.	116
Figure 2.58	Air inclusions and crystal structure analysis of core sample obtained at the split section of CEMA Reach 1 – 200 m from the west bank.	117
Figure 2.59	Air inclusions and crystal structure analysis of core sample obtained at the downstream boundary of CEMA Reach 1 – 60 m from the west bank.	118
Figure 2.60	Air inclusions and crystal structure analysis of core sample obtained at the downstream boundary of CEMA Reach 1 – 180 m from the west bank.	119
Figure 2.61	Air inclusions and crystal structure analysis of core sample obtained at the downstream boundary of CEMA Reach 1 – 240 m from the west bank.	120
Figure 2.63	Cumulative freezing degree-day records for the 2006/07-winter season, obtained from Ta records at Fort McMurray.	121

Figure 3.1	River1D water temperature calibration to measured values at Station M268.1.....	147
Figure 3.2	River1D water temperature calibration to measured values at Station M245.6.....	147
Figure 3.3	River1D water temperature calibration to measured values at Station M216.7.....	148
Figure 3.4	River1D water temperature simulation using hourly input data at Station M268.1 – $H_{wa} = 10 \text{ W/m}^2/\text{°C}$	148
Figure 3.5	River1D water temperature simulation using hourly input data at Station M245.6 - $H_{wa} = 10 \text{ W/m}^2/\text{°C}$	149
Figure 3.6	River1D water temperature simulation using hourly input data at Station M216.7 - $H_{wa} = 10 \text{ W/m}^2/\text{°C}$	149
Figure 3.7	Suspended frazil ice concentrations at station M288.1 as obtained from simulations run from the Town of Athabasca.	150
Figure 3.8	Observed vs. River1D simulated surface ice concentration at stations M268.1, M245.6 and M216.7.....	150
Figure 3.9	Aerial Photograph of CEMA Reach 1 – November 10 th , 2006.	151
Figure 3.10	Cumulative Discharge at CEMA Reach 1 obtained from <i>River2D</i> simulations.....	152

LIST OF SYMBOLS

- A = cross sectional flow area (m^2)
- B = width of the rectangular cross section (m)
- F = mass or energy flux (*units vary*)
- g = acceleration due to gravity (m/s^2)
- H = depth of flow (m)
- h_{wa} = linear heat transfer coefficient ($W/m^2/^\circ C$)
- K_{wa} = linear heat transfer constant (W/m^2)
- Q = discharge (m^3/s)
- q_x, q_y = discharge intensity in the x- and y-directions (m^3/s)
- S_0 = longitudinal channel bed slope (*dimensionless*)
- S_{0x}, S_{0y} = bed slope in the x- and y-directions (*dimensionless*)
- S_f = Longitudinal boundary friction slope (*dimensionless*)
- S_{fx}, S_{fy} = friction slope in the x- and y-directions (*dimensionless*)
- T_a = air temperature ($^\circ C$)
- T_w = water temperature ($^\circ C$)
- U_l = cross sectional average longitudinal velocity (m/s)
- U_i = the applicable mean or surface ice velocity (m/s)
- U = depth averaged velocity in the x-direction (m/s)
- V = depth averaged velocity in the y-direction (m/s)
- x, t = longitudinal and temporal coordinates (s, m)
- ρ = density of water (kg/m^3)

ϕ_{wa} = net rate of heat exchange per unit area between water and air (W/m^2)

ϕ_R = net rate shortwave solar radiation reaching the water surface (W/m^2)

Φ = the solution variable of interest

τ_{xx} , τ_{xy} , τ_{yx} , τ_{yy} = components of the horizontal turbulent stress tensor (N/m^2)

CHAPTER 1 INTRODUCTION

The oil sands mining projects in the vicinity of the Athabasca River below Fort McMurray (Figure 1.1) have raised the demand for water in the area. As a consequence, the rate of water withdrawals from the river has increased significantly and will continue to do so in years to come. Woynillowicz (2006) reports that nearly 65% of the total water withdrawn from the Athabasca River is destined for oil sands mining operations, representing approximately 350 million cubic meters (m^3) of water per year; planned projects will push this number to 549 million m^3 .

Figure 1.2 shows the historical record of mean monthly flows in the Athabasca River at Fort McMurray. During the winter period, water levels reach their lowest point throughout the year. Ice cover development is highly dependent upon flow rates and streamflow hydraulics, both of which can be affected by additional water withdrawals. Given the unregulated nature of the Athabasca River, this may result in even less availability of liquid water during the winter months, if these changes in channel hydraulics result in thicker ice covers.

In order to ensure the sustainability of the mining projects and the ecological integrity of the river, it is necessary to quantify winter ice processes along this reach. By understanding the nature of ice cover formation and deterioration in the area, a predictive numerical model can be constructed in the long term, in order to assess the impacts of additional water withdrawals and potential climate change scenarios.

1.1. AN INTRODUCTION TO RIVER ICE PROCESSES

The development of an ice cover in northern rivers is the result of a wide variety of dynamic and thermal processes. The nature of ice cover formation and deterioration depends on specific atmospheric conditions and streamflow hydraulics, which vary greatly with time and location. As a result, the physical characteristics of the fully formed ice cover, such as thickness and strength, are unique for each river.

The formation phase of an ice cover, also known as freeze-up (shown conceptually in Figure 1.2), begins with the decrease in air temperature as the winter season approaches, and is most often the result of convective heat loss from the water surface to the colder atmosphere on top. As water temperatures drop a few hundreds of a degree below zero degrees Celsius (known as supercooling), ice formation will begin.

In lakes and other calm water bodies, ice formation is the result of thermal growth of a thin layer of skim ice, which forms on the surface under supercooled conditions. Along the banks of the river, where velocities are negligible, ice will grow thermally as on a lake; this is known as “border ice” and is illustrated in Figure 1.4. However, away from the river banks where water is fast flowing and turbulent, vertical mixing leads to the entire water body to cool down at the same rate as the water surface (Michel, 1971). Small particles known as “frazil” will begin to appear and agglomerate to form slush, often termed “frazil flocs”. As the size of frazil flocs increases, so do the buoyant forces acting upon them until they eventually float to the

surface. These are frequently seen in the form of large sized discs with rough upturned edges, known as “frazil pans”, which float downstream on the water surface, either individually or together in large groups or “rafts”; this is also illustrated in Figure 1.4.

As surface ice concentration reaches 80 to 90%, pans and rafts will eventually congest. The location at which this arrest occurs, or “bridging point” is a characteristic of the river itself, and is often the same every winter. Typical bridging sites include islands, tight bends, bridge crossings and natural or artificial constrictions, which can even be caused by large extents of border ice.

Once “bridging” occurs, the incoming pans and rafts from upstream can accumulate edge-to-edge, covering the entire water surface. The resulting “juxtaposed” ice cover is illustrated in Figure 1.5. Further heat loss causes freezing between the pans and of the pore water within the frazil slush located on the underside of the pans, strengthening the accumulation. Additional thermal thickening of the ice cover typically occurs over the course of the winter. However, the insulating effects of snow can mitigate this process.

Often times drag forces beneath the ice cover are high enough to collapse it. This causes the ice floes in the accumulation to tip and rotate, creating a much thicker and stronger ice cover, known as a “freeze-up ice jam” or “hummocky” ice cover. This is illustrated in Figure 1.6.

Air temperature and solar radiation increase with the coming of spring, and snow on top of the ice cover, as well as the ice cover itself will begin to melt (Figure 1.7). As open water areas become more prominent, both the warm overlying air and solar radiation will cause further heating of the water, and consequently, additional melt of the ice cover from underneath. However, meteorological processes do not always dominate breakup, and often times large waves associated with spring runoff can cause the intact ice cover to break into discrete pieces. In such cases ice sheets and floes are carried downstream by the flood flow and ice jams can eventually form if this ice run is arrested. This is a common phenomenon in north flowing rivers, where ice cover deterioration occurs much later in the downstream reaches. Ice runs from upstream will eventually arrest as they encounter the still intact ice cover further downstream.

1.2. RESEARCH OBJECTIVES

The primary objective of this study was to establish the main conditions describing the winter regime of the Lower Athabasca River along an 80 km reach spanning from Fort McMurray to Bitumont (Figure 1.1). By developing a monitoring program, qualitative and quantitative data concerning ice cover formation and deterioration in the reach, were obtained for the 2006/07-winter season. This data constitutes the first out of a three-year record that will be used for numerical ice process model calibration and validation purposes. Additionally, given the extensive fieldwork required for data collection, an evaluation of the different techniques,

equipment and the quality of the obtained data was also accomplished as part of this study.

The thermal river ice process model *River1D* was used as an analytical tool to evaluate ice cover formation processes along the reach. Initial calibration of modeling parameters based on the 2006/07 collected data was completed; however, exhaustive calibration and validation of the model are beyond the scope of this work, due to the lack of available historical records. These calibrated *River1D* modeling components will constitute the basis for further enhancements to the two-dimensional depth-averaged model *River2D* simulation capabilities. By incorporating thermal and dynamic ice formation processes into this two-dimensional model, key sites such as water intakes and warm water outfalls can be evaluated in detail in further studies. Preliminary *River1D* and *River2D* model simulations were conducted in order to evaluate and direct the future field monitoring program and model development plans.

1.3. PREVIOUS STUDIES

Hydrologic and hydraulic studies of the Lower Athabasca River date back to the late 1970's, most of which focus on the environmental impact the oil sands mining efforts has had over river ecology. However, no studies dedicated to river ice processes in the reach were found as a result of this investigation. That being said, a number of these studies do contain information regarding winter river hydraulics and ice cover characteristics.

Doyle (1977) characterized hydrology and hydraulics of the Lower Athabasca River spanning approximately 180 km from Fort McMurray to Embarras. Dissemination of data collected by Alberta Research Council and other agencies, provide an insight into the behavior of the river in this reach. Ice cover formation processes are not discussed in this study; however, it does contain information regarding historical accounts of ice jam related flooding events at some locations downstream of Fort McMurray. These include Inglis Island (23 km downstream), Ells River (73 km downstream), Morrison Island (91 km downstream) and Embarras (187 km downstream).

Beltaos (1979) studied mixing characteristics of the Athabasca River under ice-covered conditions, spanning approximately 300 km from Fort McMurray to Lake Athabasca. As part of a research program to investigate mixing characteristics of rivers in Alberta, this study contained hydrometric information and geomorphic characteristics of the reach, as well as information regarding the thickness of the fully formed ice cover. However, no data pertaining to ice cover formation or deterioration processes was provided.

Van Der Vinne (1993) also conducted winter low flow tracer dye studies in the reach of the Athabasca River spanning 80 km from Fort McMurray to Bitumont. As part of the Northern River Basins Study, this investigation focused on characterizing the cumulative effects of development on the water and aquatic environment of the study area. Field investigation was conducted under relatively low discharges, ranging from 81 to 188 m³/s, and travel times for the reach were

defined relative to its hydraulic characteristics. Even though winter ice processes were not characterized, the information regarding the hydraulics of the reach, such as times-of-travel and the variation of Manning's roughness was found useful to this study, for modeling purposes.

Since 1998, the University of Alberta in cooperation with Alberta Environment has undertaken an extensive monitoring program of breakup processes in the reach upstream of Fort McMurray, spanning approximately 40 km to Crooked Rapids. Even though their focus has primarily been dynamic ice jam formation and release events along this area, occasional monitoring of the reach downstream of Fort McMurray during the breakup period has also taken place. This was found in Kowalczyk (2003), who reported on the behavior of ice runs as they went passed Fort McMurray, briefly stalling and rebuilding due to the numerous islands and sand bars characteristic of this lower reach.

Most recently, the Regional Aquatics Monitoring Program (RAMP) and the Cumulative Environmental Management Association (CEMA) have worked together to assess the ecological health of the Athabasca River in the vicinity of the oil sands mining operations. As a result, private consultants were hired to conduct field measurements regarding winter bathymetry and ice cover characteristics at several sites along the reach. Additionally, CEMA also funded the efforts to improve the *River2D* modeling capabilities, by enabling it to consider the effects of an ice cover on streamflow hydraulics. Their data has been made available to this project, as part of an informal collaboration.

Katopodis and Ghamry (2005) of the Department of Fisheries and Oceans (DFO) used the data collected by CEMA to develop two-dimensional models of the sites and evaluate the ability of *River2D* to simulate ice-covered channel hydraulics. Even though most of these latest efforts focus on evaluating the river from an ecological perspective, collected data and simulation results were considered important for validating future ice process components, as they are incorporated to the *River2D* model.

1.4. EXISTING DATA

Basic data requirements for simulating thermal river ice processes consist of geometric characteristics and air temperature records along the reach of interest, inflow water temperature and inflow discharge (Andrishak, 2007). However, data requirements for model calibration and validation demand additional historical records of ice cover formation related data. This includes water temperature, solar radiation, surface ice concentrations and even rate of progression of the ice front. Even though most of these records are unavailable for the Lower Athabasca River, comprehensive hydrometeorological data sets are accessible for the present study.

Hydrometeorological data was mostly available online. The primary record of air temperature was obtained from the database of historical climate data of the Environment Canada (EC) website (<http://www.climate.weatheroffice.ec.gc.ca>). Comprehensive hourly and mean daily air temperature records were found. However, some gaps did exist in the database.

Hydrometric records were obtained from the Water Survey of Canada (WSC) website (<http://www.wsc.ec.gc.ca>). Water levels are recorded in half hour intervals and published discharges are obtained from these levels by the use of rating curves. However, rating curves are not applicable under ice affected (backwater) conditions. Therefore, winter discharge is typically estimated based on interpolation between direct measurements. Published discharges at freeze-up and breakup are crude estimates only, and during these periods, only the water level was considered.

Limited geometric data was available for modeling. However, these constraints are minimal given that a rectangular channel approximation was used for one-dimensional simulations. Spaced at 1 km intervals, rectangular cross-sections were derived in previous studies from National Topographic Series (NTS) maps, to create a flood routing model of the Athabasca River using *River1D*, spanning from Whitecourt to Lake Athabasca. The gradient of the river bed was obtained from longitudinal water surface profiles given in Kellerhalls et al. (1972).

Winter bathymetric data collected by CEMA for research on fish habitat in the winter period of low flow was available for this study. The data consists of two-dimensional detailed bathymetry in three sites along the Lower Athabasca River. The location of these sites is shown in Figure 1.1. Corresponding data describing snow depth on the ice cover, ice cover thickness, water depth and bed elevation, as well as water velocity, were collected over a period of four years.

In order to complete the data record required for model calibration and validation, an extensive field program was undertaken during a period of eight months, starting in September 2006. Chapter 2 presents the details of this program, along with a discussion on instrumentation and data collection techniques, and an analysis of the obtained data. Included in this chapter is a description of the various observations made during this period, on the different stages of formation and deterioration of the ice cover in the study reach.

Calibration of the *River1D* model using this data and available historical records is discussed in Chapter 3. A preliminary evaluation of the *River2D* model of two of the CEMA reaches is also included within this chapter. Given that this project is the first phase of a three-year study, some recommendations for future modeling work and data collection are discussed in Chapter 4.

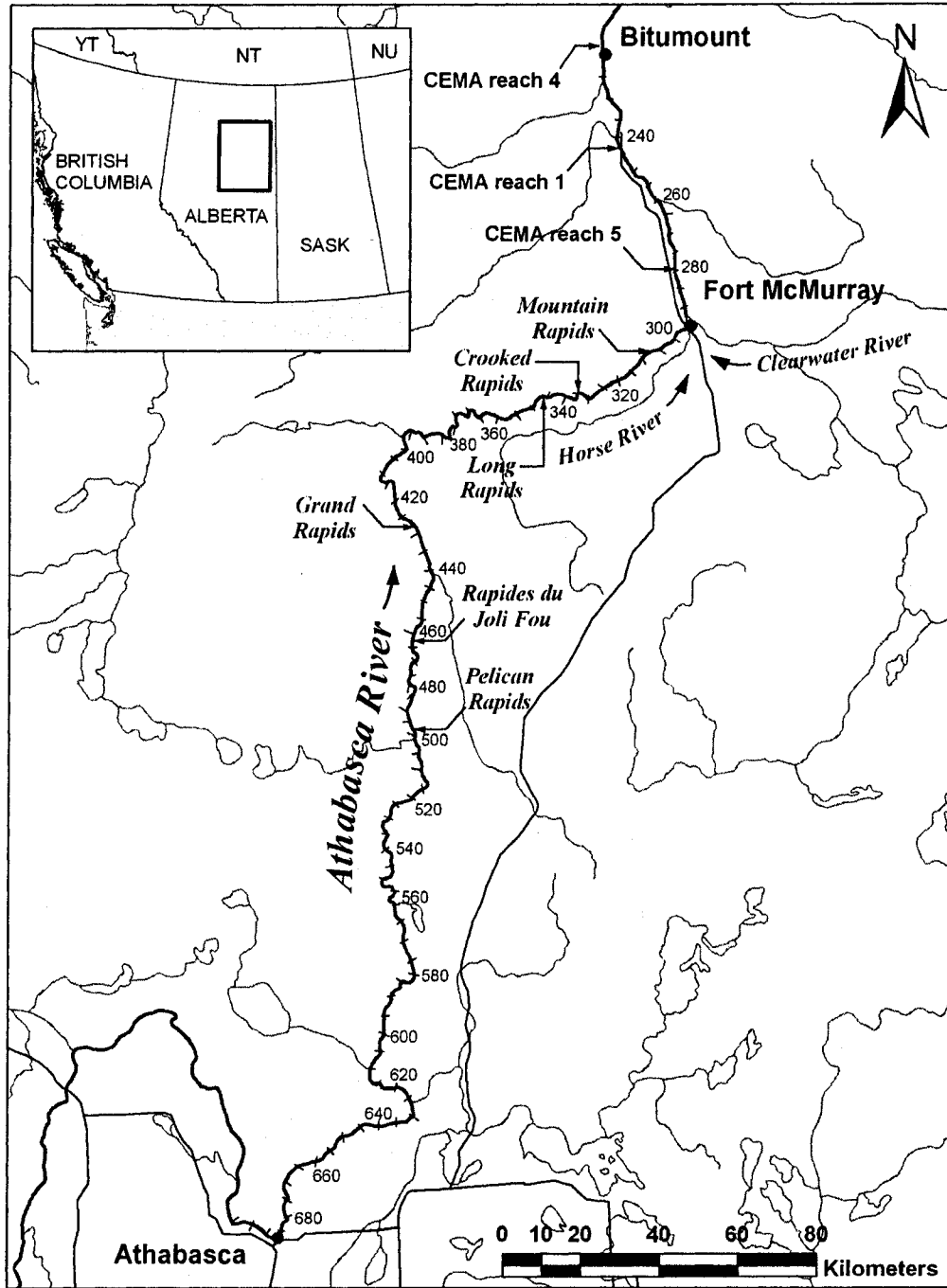


Figure 1.1 Overview of the Athabasca River spanning from the Town of Athabasca to Bitumont.

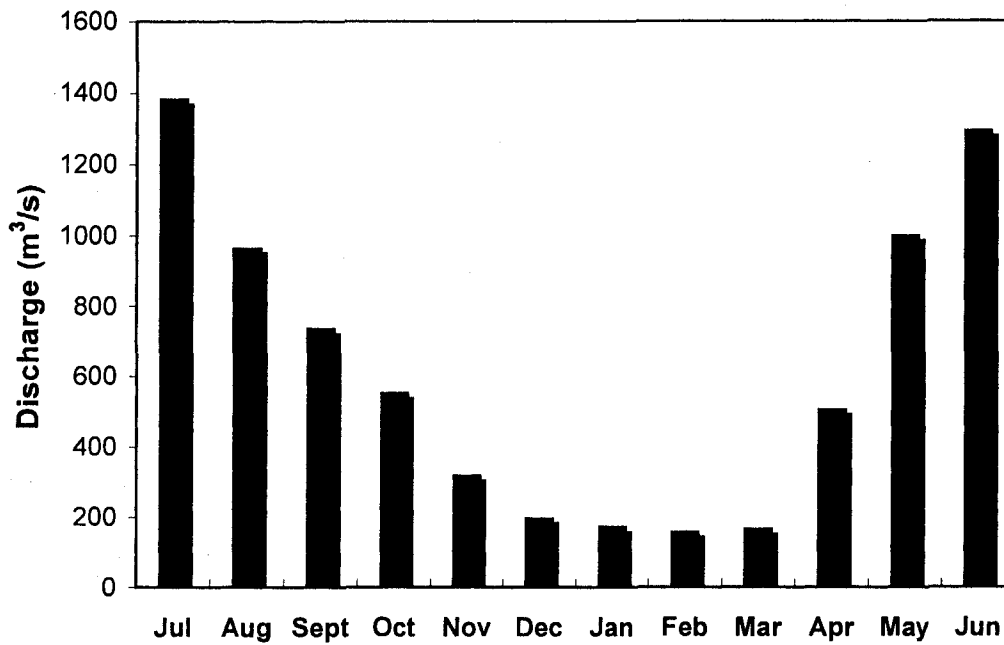


Figure 1.2 Mean monthly flows on the Athabasca River at Fort McMurray, Alberta (Data Source: Water Survey of Canada, available record from 1957 to 2004).

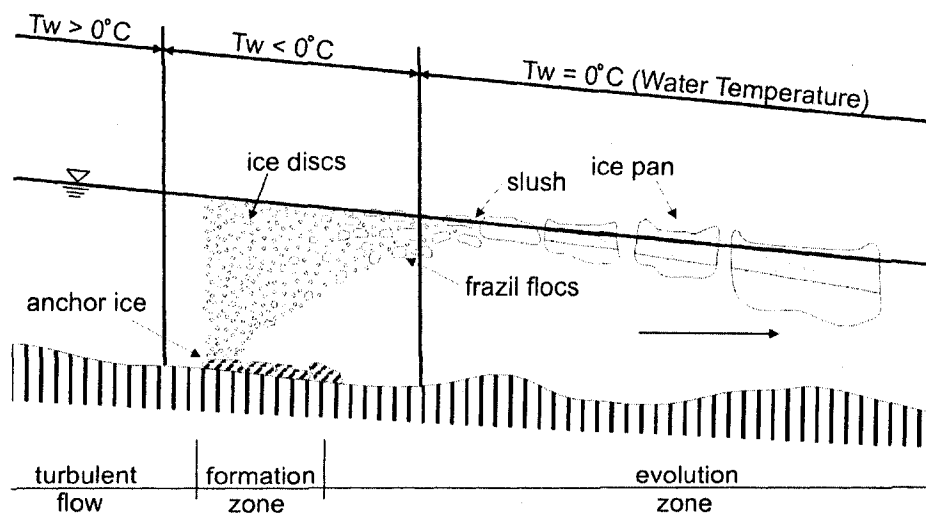


Figure 1.3 Conceptual diagram of river ice formation processes (adapted from Michel, 1971).

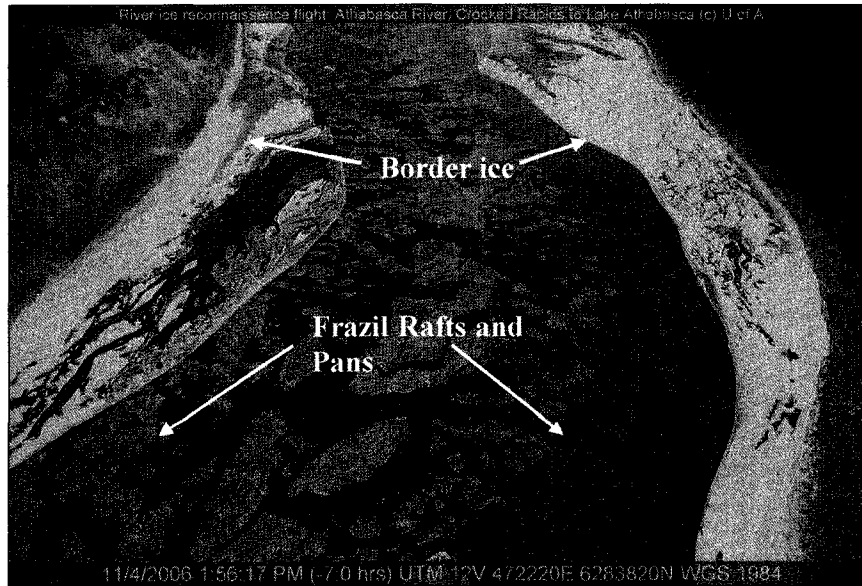


Figure 1.4 Border ice, pans and rafts seen in the Lower Athabasca River on November 4th, 2006.



Figure 1.5 Juxtaposed Ice cover seen on the Lower Athabasca River near Fort MacKay on November 3rd, 2006.



Figure 1.6 Hummocky ice cover seen on the Lower Athabasca River near Fort McMurray on November 10th, 2006.



Figure 1.7 Thermally deteriorated Ice Cover seen on the Lower Athabasca River on April 16, 2007.

CHAPTER 2 FIELD PROGRAM AND DATA ANALYSIS

2.1. INTRODUCTION

A field program was established in 2006/07 to study the winter ice regime of the Athabasca River below Fort McMurray; Figure 2.1 presents an overview of the study reach. For a period of 8 months, starting in September 2006, river ice processes were monitored through periodic aerial surveillance and the collection of hydrometeorological data. Ice cover characterization also took place during the months of February and March of 2007.

Hydrometric and meteorological records, established through existing monitoring stations, were complemented with the installation of four additional stations along the reach, which took place in September 2006. Information regarding the location and data collected at each of these stations is contained in Table 2.1 and their locations are illustrated in Figure 2.1. Station locations were selected based on hydraulic conditions at each site. Accessibility to the sites was also an issue; however, these four stations were spaced as equally as possible along the reach, with approximately 25 km between adjacent stations.

This chapter will provide a description of the study reach, and details of existing monitoring stations and available hydrometeorological data. It will also provide an analysis of our efforts in complementing this existing data to obtain an appropriate record for the purposes of hydraulic and thermal numerical modeling.

Each data record is analyzed by type, along with a description of the instrumentation used and the methodology applied in each case. A discussion of the different problems and setbacks encountered during data collection and equipment installation is also included.

2.2. DESCRIPTION OF THE STUDY REACH

The reach of the Lower Athabasca River chosen for this research extends approximately 80 km, spanning from Fort McMurray to the town of Bitumont (illustrated in Figure 2.1). This lower portion of the Athabasca River drains a total of 58,000 km², which includes the Clearwater River Basin (Conly, *et al.*, 2002). Major tributaries along the reach include the Steepbank, Beaver, Muskeg and MacKay Rivers, which together drain approximately 8220 km². Their contribution to the total flow of the river at this reach is close to four percent (Doyle, 1977). A summary of key sites along the reach is contained in Table 2.2. A profile of the Athabasca River spanning from the Town of Athabasca to the Peace Athabasca Delta is illustrated in Figure 2.2.

Downstream of Fort McMurray, the Athabasca River flows north through lowlands and the Athabasca tar sands deposits, with an average slope of 0.13 m/km (Kellerhalls, *et al.*, 1972). According to Conly *et al.* (1972) the river is laterally stable and deeply entrenched in its valley, flowing straight with occasional islands and sand bars of considerable size (illustrated in Figure 2.3). Doyle (1977) states that the thalweg shifts within a year in much of the reach downstream of Fort McMurray

and dredging in many places is often required to maintain an adequate navigation channel. Bed material is predominantly sand, with local gravel over limestone, and Manning's roughness values range between 0.018 and 0.030 for the entire reach at different flood frequencies. (Kellerhalls, *et al.*, 1972). Van der Vinne *et al.* (1993) reports a roughness coefficient of 0.017 for the entire reach under ice-covered conditions; however, they estimated this value to be low due to the inaccuracy in determining the under ice top width.

Doyle (1977) describes the climate of the study area as a "typical continental climate with warm summers and cold winters". Very few studies regarding the winter regime of this reach were found as a result of this investigation, and no historical accounts on freeze-up processes were available. However, as mentioned in Chapter 1, breakup has been extensively studied in the reach upstream of Fort McMurray. The river in the upstream reach has an average bed slope of 0.0010 and is characterized by a series of rapids, which span for approximately 140 km (Figure 2.2). Kowalczyk and Hicks (2007) describe breakup in this upstream reach as being highly dynamic, progressing as a cascade of ice jam formation and release events, along the entire reach up to Fort McMurray, where the bed flattens noticeably (see Figure 2.2). Breakup in the reach downstream of Fort McMurray is dominated by thermal deterioration. However, it was observed that ice runs from upstream often arrest in the channel due to the presence of islands and sand bars (Kowalczyk and Hicks, 2007). As mentioned earlier, Doyle (1977) reports without much detail, the occurrence of a series of ice jam events taking place in the study reach in 1974 and 1977. No additional historical accounts of ice jam events were found.

2.3. METEOROLOGICAL DATA

The nature of ice cover formation and deterioration in a river depends largely on atmospheric conditions, as solar radiation and air temperature are dominating variables within the overall energy budget of the system. In addition, ice process modeling requires meteorological data as input, particularly air temperature, as it is a key variable influencing many temperature dependant heat transfer processes. The quantification of meteorological data also plays a major roll in the evaluation of potential climate change scenarios, which will inevitably affect ice cover development. The following sections discuss the availability and quality of existing meteorological records in the study area, as well as the methodology and instrumentation employed to complement these records during the 2006/07 field program.

2.3.1. Existing Meteorological Records

Existing meteorological records for the study area were found from three distinct sources. (1) Environment Canada (EC) controls a meteorological station located at the Fort McMurray airport. (2) The University of Alberta (UA) operates a meteorological station in Fort McMurray, which is located in the city services compound at the northwest corner of McKenzie Boulevard and MacAlpine Crescent. (3) Golder Associates operates the Aurora Climate station, which was established in May, 1995 to monitor climate conditions in the Muskeg River Basin. The station is located in proximity to the study area, 800 m east of Jackpine Creek, near an abandoned airstrip just south of a two wheel drive road. Table 2.3 contains

information regarding Universal Transverse Mercator (UTM) coordinates, sensors and data availability at each of these stations.

Excellent correlations exist for the records between the UA station, the Fort McMurray airport station and the Aurora Station for mean daily temperature and solar radiation. Robichaud (2003) conducted an extensive analysis of this data, filling in missing values using standard analysis techniques. She found that air temperature records from the Fort McMurray airport station could be transposed to the UA meteorological station through linear regression. A coefficient of determination (R^2) value equal to 0.991 was found, showing an excellent correlation between air temperatures measured at each station. In a similar manner, solar radiation data records obtained from the UA meteorological station showed good correlations with the records obtained from the Aurora climate station. Linear regression for the relationship between these data sets resulted in a value of R^2 equal to 0.950.

Historical records of air temperature obtained from the Fort McMurray airport meteorological station (illustrated in Figure 2.4) show mean monthly temperatures reaching their lowest in the month of January, with a record minimum of -39.4°C in 1950. An overall tendency of air temperatures to remain constant at an average of -8°C during February and March is noticeable, as well as a significant increase in temperature as spring approaches during the month of April. An average air temperature of -9.7°C was calculated between the months of October and April.

2.3.2. Instrumentation and Methodology.

Given that the three existing meteorological stations are not actually at river level, there were some doubts as to whether data records would be truly representative for modeling thermal ice processes. To investigate this question, an additional air temperature sensor was installed at the most downstream of the monitoring stations, setup during September, 2006.

This additional air temperature gauge installed at river station M216.7 (see Table 2.1), consisted of a Campbell Scientific air temperature sensor (model 44212) mounted inside a Young radiation shield (model 41303-5A). The sensor was connected to a Campbell Scientific data-logger (Model CR510) by a lead cable protected with electrical conduit. The radiation shield containing the sensor was bolted to a tree above the data-logger enclosure as shown in Figure 2.5. The data-logger was used to collect all measured data at an hourly rate. Appendix A provides the specification sheet for the temperature sensor, which has an operating linear range of -50°C to $+50^{\circ}\text{C}$ and an accuracy of $\pm 0.1^{\circ}\text{C}$.

2.3.3. Data Analysis

Figure 2.6 shows the records of air temperature data obtained from the UA meteorological station, the Fort McMurray airport station and the sensor at river station M216.7, for the 2006/07 ice season. As seen in the figure, air temperature data between stations are comparable. Further analysis was done to determine the spatial correlation between the air temperature data obtained at station M216.7 and

the UA meteorological station. Figure 2.7 presents the result of the linear regression. Most of the readings are very close to the trendline, resulting in an R^2 of 0.957. There appears to be some seasonal variation in correlation during the months of December and January, for which data points seem to deviate significantly from the trendline. Overall correlation between the stations is very good, particularly for temperatures above 0°C ; however, as air temperature decreases, readings from both stations tend to disagree, as illustrated in Figure 2.7, where data points deviate from the 45° line for temperatures below freezing. This tends to suggest that the UA meteorological station does not accurately depict the air temperature as it occurs at river level, especially during the colder periods.

Historical trends of air temperature during the winter season alone are shown in Figure 2.8. Mean monthly air temperature records during the past decade show an overall average increase of 2°C with respect to the records from 1944 to 1997. It is also seen that the 2006/07-winter season was warmer than average (during the months of December and January); mean monthly temperatures were nearly 6°C higher than average compared to the last decade. However, it is important to note that during the freeze-up period, air temperatures were significantly lower than average for the 2006/07 winter season, by approximately 7°C , compared to the previous decade. Temperatures during the breakup season were relatively consistent with historical trends, showing an average variation of only $\pm 1^{\circ}\text{C}$.

2.4. HYDROMETRIC DATA

River hydraulics modeling requires inflow discharge data at the upstream boundary. WSC has a comprehensive database of flow records, which dates back to the early 1900's. This discharge data is derived from water level measurements using calibrated rating curves. However, as mentioned earlier, the use of rating curves during the winter season is not considered to be adequate, given that under ice-covered conditions, discharges are not a function solely of point water levels. It is worth mentioning that WSC performs direct measurements under ice-covered conditions at least 2 to 3 times during the winter season. This has allowed them to obtain reasonable winter discharges by simple interpolation. For the 2006/07 winter period, three discharges were measured on 20-Dec-06, 17-Jan-07 and 15-Mar-07. From these measurements, mean daily discharge data between November and April was obtained by linear interpolation, for one-dimensional modeling of freeze-up processes. In the case of two-dimensional modeling, evaluating the results of simulated flow splits around an island requires knowledge of the total inflow discharge and the discharge at the split. Discharge under ice-covered conditions was measured on March 2007 for this purpose, using an Acoustic Doppler Current Profiler (ADCP).

Monitoring water level fluctuations provides an insight into the dynamics of ice cover formation and deterioration, as ice front progression, bridging front development, the retreat of an ice cover and waves related with breakup ice runs, are all associated with changes in river stage. An ice cover increases the wetted

perimeter in a river (by a factor of ~2), especially when the width to depth ratio is large, as is the case of the Lower Athabasca River. In addition, the submerged portion of the ice cover also obstructs the flow. The net result is a reduction in flow velocity, which for the same discharge conditions, translates into an increase in river stage. Backwater effects, due to ice cover development downstream, also results in an increase in water levels. When bridging fronts occur upstream of a monitoring gauge, a decrease in water level can also be observed, as water goes into storage upstream.

The following sections provide information regarding existing hydrometric records in the study area, as well as the methodology, instrumentation and setbacks encountered during the 2006/07 data collection program, which includes water level monitoring at each of the automated monitoring stations installed, and the use of the ADCP at CEMA Reach 1 to obtain flow data for two dimensional modeling.

2.4.1. Existing Hydrometric Stations

WSC reports continuous discharge data at station 07DA001, which is located on the east bank of the Athabasca River, 0.9 km upstream of the study reach inflow section at M288.1. Several other hydrometric stations operated by the WSC are located within the study area, at a number of the tributaries, before they enter the main channel. Table 2.4 presents a summary of the existing hydrometric stations with available records, located within the study area.

As mentioned in Chapter 1, historical records of mean monthly flows obtained from station 07DA001 (Figure 1.2) show a general trend of discharge decrease during the winter period in the Lower Athabasca River, reaching as low as only 20% of the average flow for the entire year. Available mean monthly flow records for the 2006/07-winter season compared to historical trends are shown in Figure 2.9. Discharge records for the months of September and October show that 2006 flows were relatively lower than the historical average, being 42% and 15% lower, respectively. Additionally, records for the post breakup period show that 2006 discharges were 66% higher than the historical average. Flows during the 2006/07 ice covered period (November through March) appeared to be comparable to historical trends. Figure 2.10 shows the mean daily flow records for the pre-freeze-up period, obtained from the WSC gauge below Fort McMurray. These records were used as input data for one-dimensional hydraulic modeling.

Figures 2.11 and 2.12 show recorded water levels obtained from the five existing hydrometric stations (summarized in Table 2.4) during the 2006 freeze-up period. The WSC gauge below Fort McMurray captured the arrival of the ice front on the Athabasca River at this location, taking place on 3-Nov-06. In a similar manner, the gauges located on the Muskeg and MacKay Rivers also captured this event at these tributaries, taking place on 29-Oct-6 and 1-Nov-06 respectively. However, it is possible that these water level rises at the tributaries were a result of backwater from the main channel. These effects are less obvious in the records obtained from the gauge located at the Beaver River above Syncrude, where no peak associated with ice front progression is noted. However, a bridging front might have

taken place at a location upstream of the gauge on 29-Oct-06, as water going into storage results in a decrease in water levels further downstream. No records for the 2006 freeze-up period were found at the Steepbank River gauge. It is important to note however, that most of these tributaries could be intermittent.

Figures 2.13 and 2.14 show water level records obtained from these five gauges during the 2007 breakup period. The record from the gauge located on the Athabasca River below Fort McMurray shows three major peaks, associated with the formation and release of an ice jam from the upstream reach. The release wave resulted in a water level rise of 0.96 m peaking at 21:00 on 19-Apr-07. Water levels recorded at the four tributaries show the backwater effects resulting from the release of this ice jam. This is particularly noticeable on the Steepbank and MacKay Rivers, where water levels rose approximately 1 m due to backwater. These effects were much less pronounced on the Beaver and Muskeg Rivers.

2.4.2. Instrumentation and Methodology – Water Level

As mentioned in the previous section, aside from water level records at various tributaries, existing records for the Lower Athabasca River could only be obtained from the WSC gauge below Fort McMurray. In order to monitor water level fluctuations along the entire channel, it was decided during initial planning to install pressure transducers at all four monitoring stations. The transducers would be connected to the data-loggers, which would record data at an hourly interval. Additional self-contained units, known as Diversers[®] would be placed in concrete pads

at the bottom of the channel to provide backup water level and water temperature data. Unfortunately, the vendor was unable to supply the pressure transducers on time for station installation. Consequently, the Divers® were the only water level measurement device used during the 2006/07 monitoring program.

Van Essen Instruments' Divers® are autonomous instruments that contain temperature sensors, pressure transducers and an internal memory of 24,000 measurements per parameter. Water temperature is measured at a range of -20°C to +80°C with an accuracy of $\pm 0.1^\circ\text{C}$ and a resolution of 0.01°C . Pressure is measured with an accuracy of 0.5 cm H₂O and a resolution of 0.2 cm H₂O. Appendix A provides the specification sheet for these units. It is important to note that these are self-contained units that store data internally. Therefore, data can only be retrieved by removing the unit from the water and downloading it to a computer.

It is worth mentioning, that in order to ensure an adequate installation depth for the sensors, the outsides of bends were chosen as ideal station locations, to take advantage of the deep, naturally maintained thalwegs that tend to develop near the outer banks in such cases. Figure 2.15 shows the methodology used for field installation of the Divers®. As seen in the figure, the units were placed inside 15 cm long sections of ¾" diameter PVC pipe and attached to 16" x 16" x 2" concrete pads for weighting. The concrete pads were then set at the bottom of the river channel and moored to a tree on the river bank using a ½" diameter steel cable. PVC was chosen as the material for the sensor enclosures to minimize the risk of frazil ice adhering to the units. Manual water level measurements using a rod and precision

level, took place during station installation and unit retrieval to determine if any sensor movement occurred.

Several problems were encountered during unit retrieval, which took place in May 2007. The Divers[®] at river stations M288.1 and M268.1 were recovered along with all collected data. The concrete pad at Station M245.6 remained in the bottom of the channel, buried beneath the bed material and retrieval of the unit was not possible (this may be a good indication of high amounts of sediment transport occurring during the passage of the ice jam release wave in April 2007). Additionally, it is important to remember that sensors were installed along the naturally maintained thalwegs, and consequently, were exposed to higher stream velocities. At Station M216.7, the concrete pad was detached from the steel cable that secured it to the bank; this is illustrated in Figure 2.16. The reason for this occurrence is uncertain; however, it is suspected this was due to severe breakup ice runs as they passed through this station location. Unfortunately, since these units store data internally, no water level records were obtained from river stations M245.6 and M216.7 for the 2006/07 winter season.

2.4.3. Instrumentation and Methodology – Discharge

The *River2D* model requires discharge data as input for the inflow boundary. As discussed in Chapter 1, detailed bathymetric data was obtained for this study from surveys conducted by CEMA at three reaches located within the study area. In order to evaluate the calibrated two-dimensional models developed for these reaches

by Katopodis and Ghamry (2005), discharge data would be needed at the inflow and outflow (for calibration) boundaries of each of these reaches. Additional flow data is required at areas where islands split the flow to evaluate the performance of the model in simulating this occurrence. However, due to time and money constraints, discharge data under ice-covered conditions was only collected for CEMA Reach 1, which spans 3.2 km and is located downstream of Peter Lougheed Bridge. Measurements with the ADCP took place on 6-, 7-, 8-Mar-2007 at the upstream boundary, downstream boundary and the split section of the reach, respectively. The location where ADCP measurements took place within CEMA Reach 1 is illustrated in Figure 2.17

Appendix A contains information regarding the technical specifications of the ADCP. The unit measures velocities in a range of ± 10 m/s, with a resolution of 0.1 cm/s and an accuracy of ± 10.5 cm/s. It also contains several other sensors, which include a pressure sensor with an accuracy of 0.1% and a temperature sensor with an accuracy of $\pm 0.1^\circ\text{C}$. The ADCP unit consists of three acoustic transducers used for 3D profiling based on the physical principle of Doppler Shift. Each transducer generates a pulse of sound at a user-known frequency, which is reflected in all directions by foreign particles traveling within the water, such as sediment or biological matter. Some of the reflected energy travels along the transducer axis back to the transducer, where the Doppler shift is measured. Each transducer measures the frequency change along the axis of the beam; three transducers translate into three-dimensional velocity measurements. Spatial resolution can vary from 0.15 m to 10 m depending on the frequency of operation, which varies from 3000 KHz to 250 KHz.

For under-ice usage, stationary measurements were required. The procedure involved making depth and mean velocity profile measurements at a certain number of locations across each transect spaced approximately 20 m apart. It was assumed that the velocity profile at each station represents the mean velocity for the entire rectangular station area. The ADCP was held stationary at each location for approximately 1 minute; 2 to 3 minutes were required for areas of turbulent flows or rapid changes in stage. It is worth mentioning, that the quality of the obtained data depended largely on the quantity of locations along each transect in which the ADCP was submerged. In areas where the flow is the fastest (i.e. along the thalweg), shortening of the spacing between stations (to less than 10 m) is highly recommended for future usage of the unit.

2.4.4. Water Level Data Analysis

Figure 2.18 illustrates the variations in water level during the 2006/07 winter season, as obtained from the recovered Divers[®] at stations M288.1 and M268.1. It is important to note that these submersible water level loggers contain unvented pressure transducers, and their precision is limited to about 8 cm of head (Robichaud, 2001). However, this was corrected with barometric pressure data collected at the UA meteorological station. It is worth mentioning that the reported values of water level correspond to the depth at which the sensor is installed, relative to the bed. Even though water levels were referenced during station installation, to an arbitrary datum located in the river banks, using manual rod and level measurements, these benchmarks are not tied to any known elevation point. As a consequence, only

relative variations in water level were considered in this analysis. Future referencing of these temporary benchmarks to a known elevation is needed to obtain absolute water level values. Rod and level measurements also took place on May 2007, to verify the location of the sensor with respect to its original position. It was found that the sensor at station M288.1 was located 70 cm below its installation depth, and the sensor at station M268.1 was 14 cm below. This translates into either local bed scour occurring at the sensor locations, or rather the sensors being relocated to deeper locations within the reach (likely during passage of the ice jam release wave in April 2007).

2.4.4.1. Freeze-up

Figure 2.19 shows recorded water level variations during the freeze-up period in 2006. Sudden peaks in the water levels at both stations occurring during the night of 2-Nov-06 and early morning of 3-Nov-06 respectively, show the arrival of the ice front at these locations, with approximately 5 hours difference between them as it progressed upstream. However, a decrease in water level at river station M268.1 on the morning of 31-Oct-06 indicates bridging might have occurred between this location and station M288.1, and the ice cover could have progressed from multiple fronts through the upstream half of the study reach. Changes in water level at station M288.1 were 70 cm higher in average than those at M268.1 and it is observed in the figure that water levels at station M288.1 rose at a much faster rate. This may be indicative of the overall thickness of the ice cover at this location being larger, which is also corroborated by further characterization of the ice cover at these stations. It is

worth noting that once the ice cover was completely formed, water levels remained relatively constant throughout the entire winter season, indicating that discharge fluctuations during this period were minimal.

2.4.4.2. Breakup

As reported by Kowalczyk (2003), even though breakup in the study reach is typically dominated by thermal deterioration processes, it does undergo a series of ice runs resulting from the release of ice jams formed upstream of Fort McMurray. As this study reach contains numerous islands and sand bars, such ice runs are prone to stall briefly at several locations along the reach. If significant thermal deterioration of the ice cover occurs before these ice jams are released, subsequent ice runs will remove most of the remaining ice cover in the reach. However, if the ice runs encounter a relatively undeteriorated ice cover in the vicinity of Fort McMurray and stop, significant flooding can occur in the city's downtown area.

Recorded water levels between 18- and 24-Apr-07 show the ice jam release wave as it passed stations M288.1 and M268.1 (Figure 2.20). As mentioned earlier, water levels recorded at the WSC gauge below Fort McMurray also show the release wave, with a rise of 0.96 m peaking at 21:00 on 19-Apr-07. Further downstream, at station M288.1, the water level rose 2.19 m, peaking at 02:00 on 20-Apr-07. This significant increase in wave height tends to suggest that the ice run stalled briefly before reaching Station M288.1 (She, *et al.* 2007), corroborating the observations made by Kowalczyk and Hicks (2007), which were noted earlier. It is worth noting

that two peaks are seen in both stations during the main release event. According to She, *et al.* (2003), the first smaller peak (illustrated in Figure 2.20) is associated with the dynamic forerunner while the second peak corresponds to the ice run itself. At Station M268.1, water levels rose 1.56 m with the peak reached at 09:30 on 20-Apr-07. The velocity of the release wave peak was calculated as 0.75 m/s.

Two additional peaks were captured by both monitoring stations, one prior, and the other after the main ice jam release event. It is possible that the first disturbance, occurring 24 hours in advance of the release event, corresponds to the wave associated with the formation of the ice jam upstream of Fort McMurray (She *et al.*, 2007). The second peak, occurring during the night of 22-Apr-07, might be associated with the ice run stalling briefly on the downstream half of the study reach (the precise location of this occurrence is unknown).

2.4.5. Discharge Data Analysis

Figures 2.21 to 2.23 show the results of the ADCP measurements undertaken on March 2007 at CEMA Reach 1. Measured discharges at both the upstream and downstream boundaries are comparable, at an average of 128 m³/s, thus, corroborating the validity of the measurements. This was also supported by measured discharges obtained from WSC, who reported 130 m³/s on March 15 2007. These measured discharges show that 2007 was a period of particularly low flow, as historical mean monthly discharge records obtained from the WSC gauge below Fort McMurray (Figure 1.2) report average lows of approximately 165 m³/s during the

months of February and March. Discharge in the island split section was measured to be $109 \text{ m}^3/\text{s}$, which translates into approximately 85% of the total flow at this reach deviating to the west side of the island (Figure 2.17). Normalized velocities are reported to range between 0.2 and 0.5 m/s.

Fast flowing areas, where more than 10% of the total discharge is contained for a particular transect, are represented as red bars in the aforementioned figures. These are areas where spacing between measurements was reduced to at least 10 m or less, in order to minimize error in the estimation of the total flow. It is worth noting that the horizontal velocity distribution and the variation in depth at each transect provides an estimation of the location of the thalweg in the reach, which shifts considerably to the east as flow progresses downstream.

2.5. WATER TEMPERATURE DATA

Water temperature data is essential for the modeling of thermal processes in rivers, as water cooling is the primary mechanism leading to river ice formation. As a consequence, an adequate simulation of water temperature variation, which is largely based on reliable input water temperature data at the upstream boundary, is a highly influencing factor affecting the simulation results of all other ice related conditions (Andrishak, 2006).

The formation of suspended frazil ice in a river is governed by the supercooling of its waters. In the thermal component of the *River1D* model, the

simulation of any ice related conditions begins with the arrival of the zero degree isotherm. The quality of the results depends largely on the capability of the model to accurately portray water temperature cooling to the point at which a condition of zero degrees Celsius is achieved. For this reason, simulation results for water temperature along the entire reach should be calibrated prior to and independent of any ice related parameters (Andrishak, 2006). This requires a comprehensive record of water temperature variation along the entire modeled reach. The following sections contain information regarding the availability of water temperature records in the study area and the results of water temperature monitoring during the 2006/07-data collection program. This includes a discussion regarding the instrumentation used and the quality of the obtained records.

2.5.1. Existing Data

No records of water temperature variations along the study reach prior to 2006 were found as a result of this investigation. However, water temperature was monitored throughout the 2006 cooling period at the wastewater treatment plant in the Town of Athabasca, located approximately 400 km upstream of the study area; these records were provided for this study. Water temperature at this facility was measured using a Barbstead glass thermometer at a resolution of 0.1°C, from a raw water tap, where the water flows from the river by gravity and is later pumped into the piping system; data was measured at a daily rate. Figure 2.24 shows the data obtained for the 2006 pre-freeze-up period, as measured at this facility.

2.5.2. Instrumentation and Methodology

Ample water temperature records are needed for modeling purposes, as an inflow time series is required at the upstream boundary, and additional records along the reach are necessary for calibration of the simulated results. Given its importance and the insufficiency of the existing records, water temperature was monitored at each of the locations at which automated stations were setup in September 2006. Each station was comprised of two distinct sensors for this purpose. The main sources of data collection consisted of Campbell Scientific soil/water temperature probes (model 107B) connected to a data-logger of the same brand (Model CR510), which recorded data at an hourly rate. The second source was designed to provide backup data, and consisted of the aforementioned Diversers[®]. As mentioned earlier, these self contained units measure water temperature at a range of -20°C to +80°C with an accuracy of $\pm 0.1^\circ\text{C}$ and a resolution of 0.01°C (Appendix A)

Campbell Scientific soil/water temperature probes operate at a range of -35°C to +50°C, with a resolution of 0.01°C and an accuracy of $\pm 0.2^\circ\text{C}$. The specification sheet for these sensors can be found in Appendix A. The entire 100 ft lead length of the sensors was protected with a seal-tight flex armored cable with a PVC jacket. The sensor tip was encased in a 14" long, $\frac{3}{4}$ " diameter Iplex shed 80 PVC pipe and placed on a 16" x 16" x 2" concrete pad, similarly to the Diversers[®]. Preliminary measurements of water depth versus distance from the banks was conducted prior to station installation, to determine whether an appropriate installation depth for the sensors could be achieved at the governing length of 100 ft. If this depth was not

adequate, it was decided the Divers[®] should be installed at a greater distance from the banks. As a result, for river stations M288.1 and M245.6, separate concrete pads were used for each sensor, while on the remaining two stations, the same pad was used to hold both sensors (illustrated in Figure 2.25). As mentioned in section 2.4.2, the concrete pads were set at the bottom of the river channel and moored to a tree on the river bank using a steel cable. A conceptual diagram of the station setup (using separate concrete pads) is shown in Figure 2.26.

Manual water temperature readings were taken during station installation at each of the locations, to evaluate the temperature gradient with distance from the banks. These measurements were conducted using an RTD platinum thermometer, which can measure temperature at a range of -50°C to 400°C, with an accuracy of $\pm 0.1^\circ\text{C}$; detailed specifications for this unit are provided in Appendix A. The results of these measurements are illustrated in Figure 2.27. As seen in the figure, small variations of water temperature with distance from the bank of $\pm 1^\circ\text{C}$ were observed at stations M288.1 and M268.1. However, water temperature at stations M245.6 and M216.7 remained constant. This supports the validity of the approximation of using a constant water temperature along the entire width of the channel, as assumed in one-dimensional modeling. However, it is important to note that this may not be true at locations where industrial outfalls are present, given that water from these outfalls is generally at a higher temperature than that of the river. With these measurements it was also possible to verify that the readings obtained from the Campbell Scientific probes were within an acceptable range and accuracy.

As discussed in Section 2.4.2, some of the concrete pads were detached from the steel cable, and severe damage to the armored conduit that protected the sensor was observed during station servicing in May 2007. At both river stations M288.1 and M245.6, where two separate pads were used for each sensor, it was observed that the pads containing the Campbell Scientific probes were detached from the steel cable. However, at station M288.2, the sensor was not disconnected from the data-logger and was still functioning by the time of servicing. The sensors at stations M245.6 and M216.7 were disconnected from the data-loggers; however, the use of male-female quick-connect terminals prevented any harm to the logger itself.

In summary, water temperature data was collected continuously at all four stations during the entire season. Once water cooling ended and the ice cover was completely formed, water temperature remained at a value 0°C, until mid April when temperatures began to rise with the coming of spring. It is important to note that during breakup, data was only collected at river stations M288.1 and M268.1. Backup data was recovered only for these two stations as well, given that the Diversers[®] were lost at the remaining two locations.

2.5.3. Data Analysis

2.5.3.1. Freeze-up

Figure 2.28 illustrates the water temperature records obtained from the automated monitoring stations during the cooling period spanning from 1-Oct-06 to 3-Nov-06. The water temperature decreased continuously from approximately 12°C

on 1-Oct-06 to 2°C by 19-Oct-06. This was followed by a slightly warmer period, during which the water temperature increased by about 1.5°C. On 28-Oct-06 the weather turned cold again, and water temperatures reached 0°C within the ensuing four days.

Even though a comparable cooling trend was observed at all four stations, diurnal fluctuations in water temperatures were more noticeable at station M288.1, reaching high temperature peaks during the late afternoons and lows during the early mornings. The remaining stations also show similar diurnal tendencies; however less pronounced. This was corroborated by a standard deviation ' σ ' analysis of diurnal fluctuations of water temperature at all four stations during the cooling period, which resulted in a value of $\sigma = 0.52$ for station M288.1, while at the remaining stations ' σ ' ranged between 0.20 and 0.25. It is suspected that this difference is due to the insulating conditions in which the sensors were installed at these three stations, compared to station M288.1. Bed material at stations M245.6 and M216.7 was comprised mostly of sand, as seen during station installation. Additionally, since the concrete pad at station M245.6 was buried, rendering it impossible to retrieve, high amounts of sediment transport are suspected to have taken place during the winter season. The bed material at station M268.1 was comprised of gravel; however, the sensor was installed at a relatively high depth (above 3 m). Both situations created isolating conditions for the sensors, minimizing their exposure to solar radiation during noon and late afternoons. The sensor at station M288.1 was located on a gravel bed, at a relatively low depth, making it more exposed to the effects of solar radiation.

As mentioned earlier, the Divers[®] were only recovered at stations M288.1 and M268.1. Correlation between the water temperature recorded by these units and the Campbell Scientific 107B sensors, at these stations during the cooling period, is shown in Figure 2.29. As seen in the figure, correlation between the two sensors is excellent. Linear regression resulted in R^2 values of 0.998 and 0.999 at stations M288.1 and M268.1 respectively. It is worth noting that the regression equation for both cases essentially represents the 45° line illustrated in Figure 2.29

The location along the river at which the water temperature drops to the freezing point is referred to as the “zero degree isotherm”. In the fall cooling period, a water parcel travels downstream, continuously losing heat until it reaches a condition of 0°C. It is also governed by the ratio of the surface area of cooling water to the volume of water underneath it. Figure 2.30 shows a detail of the arrival of the zero degree isotherm at each of the monitoring stations. It is seen in the figure that the water temperature cools to 0 °C practically simultaneously at all locations on 29-Oct-06. This is logical, given that the geometry of the river, where the surface area to volume ratio, is similar at all four stations; thus, under equal meteorological conditions, the river cooled at the same rate at all four locations. It is important to note that the influence of industrial warm water outfalls is not noticeable in the recorded data, as the monitoring stations were not located in the vicinity of any of the suspected outfall sites. However, the sensors did capture the supercooling of the water, with the lowest value of recorded water temperature being -0.105°C.

2.5.3.2. Breakup

Figure 2.31 shows the variation in water temperature before, during and after the breakup period at stations M288.1 and M268.1, relative to variations in air temperature. Even though air temperature began rising above 0°C as early as 10-Apr-07, water remained at freezing temperature for an additional 8 days, due to the insulating effect of the ice cover. Figure 2.31 also shows water temperatures at station M288.1 rising briefly above freezing for a period of 5 days, beginning on 14-Apr-07, indicating thermal decay of the ice cover was more pronounced at this location than at station M268.1, where water temperature remained at a constant 0°C. It is worth reiterating that both the Campbell Scientific probes and the Divers were lost at stations M245.6 and M216.7 during the passing of the ice run at these locations on 20-Apr-07, at 06:00 am and 07:00 am respectively. The exact time of the passing of the ice runs at these locations was obtained from the water temperature data collected with the 107B probes, which ended abruptly as the sensors were disconnected from the data-loggers. However, as a result, no water temperature data is available at these locations after breakup.

Figures 2.32 and 2.33 illustrate the variation in water temperature relative to changes in stage at stations M288.1 and M268.1. It is seen in the figure that the aforementioned 5-day rise in water temperature at station M288.1 ended abruptly as the ice run passed through this location. This influence of the ice runs on the temperature of the water is less evident at station M268.1, as it remained constant throughout the entire period before the ice runs passed through. It is worth noting

that water temperature rose at a rate of approximately 1.3°C/day for a period of 6 days after the breakup ended.

2.6. ICE COVER CHARACTERIZATION

Characterization of the ice cover is essential for understanding the nature of its development as it relates to hydrometeorological and geomorphic conditions on the river. From aerial surveillance flights undertaken during the freeze-up and breakup periods, a qualitative evaluation of ice cover formation and deterioration processes was accomplished. Later mapping from air photographs allowed a quantitative estimation of the total area of open water versus ice for the different days in which surveillance took place. The results are summarized in Table 2.5 the resulting maps for each flight are found in Appendix B.

Thermal modeling requires knowledge of surface ice concentration variation during ice cover development. This constitutes one of the four upstream ice boundary conditions in the *River1D* model (the others being suspended frazil ice concentration, and frazil and solid ice thicknesses). If water temperature remains above freezing at the upstream boundary, these four model components can be set equal to zero and the only thermal boundary condition required is the inflowing water temperature time series (Andrishak, 2006). However, this is typically only the case for unregulated rivers. In this particular study area the river is not regulated and the upstream boundary freezes at a similar time as the rest of the simulated reach, as the water temperature data presented above indicated. This section details the various

observations and analysis conducted to characterize ice cover development processes.

2.6.1. Surface Ice concentration

The quantification of surface ice concentration at any given location along the reach has proven to be quite challenging. Satellite imagery has been used extensively to characterize river ice, but the appropriate analysis algorithms for image interpretation are still under development (Gherboudj, 2006). Additionally, remote-sensing tools such as RADARSAT imagery cannot be used in real-time, since the position of the satellite itself is not stationary.

The need for a surface ice concentration time series for modeling purposes, led to the installation of automated digital cameras at both the upstream and downstream boundaries of the study reach. Both cameras were installed at high spots on trees along the banks, in order to obtain the most adequate view of the entire cross sectional area at each location. Unfortunately, the camera at station M216.7 tilted up from its original perspective before ice cover initiation (possibly by wildlife), and as a result, no meaningful surface ice concentration data could be obtained from it.

At the upstream boundary of the study reach, photos were taken at 30-minute intervals during daylight hours only. For this reason, surface ice concentration data obtained from these images contains gaps, as no data was collected during the night. This is unfortunate, as most often the initial appearance of ice in a river occurs

during night time, when air temperatures are lowest (as reflected in the temperature plots presented earlier). Thermal imaging sensors might be effective for 24 hour monitoring. Figure 2.34 shows the overnight appearance of border and frazil ice as captured by these cameras on 29-Oct-2006. Worth noting is the rather pronounced distortion of the images caused by the use of short focal length lenses. This limits computer automated post-processing, as complex algorithms need to be developed to take into account the variability of the number of pixels per unit length across the channel, imposed by the deforming perspective. As a result, it would be advisable in the future not to employ such distortions.

A simple three-dimensional model of the reach at Station M288.1 was developed using CAD software, based on GPS points taken during field installation of the cameras. These points were taken by boat, as the camera recorded images simultaneously. The location of the camera, its angle of vision and focal length were recorded and translated into the CAD software to create a perspective view of the model. As illustrated in Figure 2.35, this model allowed the creation of 50 m x 100 m gridlines, which were used as a reference to account for cross-sectional distance distortion in the images, enabling the determination of percentage values of surface ice concentration on each image. A total of approximately 100 images account for the 5-day period that spans from the first appearance of ice on 29-Oct-06, until the intact ice cover had completely formed at this location on 3-Nov-06. Figure 2.36 illustrates the resulting surface ice concentration data obtained at river station M288.1, compared to the measured water levels. Even though surface ice

concentrations at this location had reached 100% by 07:00 on 3-Nov-06, the increase in river stage does not occur until late afternoon of the same day.

2.6.2. Aerial Surveillance of Ice Cover Formation and Deterioration

2.6.2.1. Freeze-up

Surveillance flights during the freeze-up period were undertaken on 4, 5, 10 and 17-Nov-06. An additional set of observations was scheduled for 1-Nov-06, but had to be abandoned due to aircraft mechanical problems on the commercial flight to Fort McMurray. Both digital photography and video were used to document ice cover development during these flights. As mentioned in Section 2.6.1, at locations such as station M288.1, the conveyance of ice pans had ceased and a fully formed ice cover was already in place by 3-Nov-06. However, large open water leads were still evident in most of the study reach at this time. The square km of open water and surface ice coverage for the entire study area at the time of each flight are summarized in Table 2.5 and illustrated in the resulting maps, contained in Appendix B. A simple linear relationship between the accumulated degree-days of freezing (AFDD) and the percentage of surface ice coverage in the study area was found. The results are shown in Figure 2.37. Only three points (corresponding to each flight) were used and the approximation is considered crude. Nevertheless, it might be used as a guideline for field planning in upcoming years.

The extent and the nature of the open leads varied considerably along the reach. As illustrated in Figure 2.38, natural constrictions created by large extents of

border ice formations along the banks and around islands and sand bars, resulted in isolated areas of open water, where floating ice pans were unable to enter. By 4-Nov-06 surface ice concentrations in the area spanning from station M288.1 to M268.1 had reached close to 100%. However, it was observed during the flight that several small-sized (<200 m long) open leads developed as a result of these multiple bridging points. By 17-Nov-06, thermal growth had taken place in most of these open water areas, reducing their sizes to negligible proportions.

Other, significantly larger, open leads developed along the reach as a result of industrial warm water outfalls, which kept the water temperature above freezing, early in the winter. An example of one of these open leads is shown in Figure 2.39. The location of these outfalls as identified during the flights, and the extent of the resulting open leads is summarized in Table 2.6 and illustrated in the resulting mapping, contained in Appendix B. Frazil ice production within these open leads had sufficient developmental length for ice pans to form (Figure 2.40) and eventually juxtapose further downstream. As the ice fronts progressed in the upstream direction, frazil production was reduced to the point where ice pans were no longer generated. The remainder of the ice cover in these leads developed as a result of thermal growth, which by 17-Nov-06 was essentially complete.

At the time observations began, most of the border ice in the reaches with open leads had already formed. As discussed earlier, thermal growth was noticeable not only along the banks, but also in the vicinity of islands and sand bars (Figure 2.40), where velocities and water depths tend to be quite low. In the same manner,

narrower channels and other isolated open water areas were also subject to thermal growth of the ice cover. The extents of border ice varied noticeably between flights, as “buttering” by frazil ice pans enhanced border ice development.

By 17-Nov-06 surface ice concentrations had reached approximately 97% in the entire reach. The resulting ice cover was, for the most part, the byproduct of juxtaposition, with approximately 61% of the total area corresponding to thermal (border ice) growth formations. The only hummocky area observed, spanned approximately within the first 8.5 km of the study reach, downstream of station M288.1. Hydraulic analyses of this reach should be considered in the future to examine the cause. However, this will require channel surveys.

2.6.2.2. Breakup

Surveillance flights during the breakup period were undertaken on 30-Mar-06 and, 12, 16 and 17-Apr-07. It was observed that breakup in the study reach was largely dominated by thermal deterioration, which was itself greatly influenced by the presence of industrial warm water outfalls. The total area of open water and ice in the study reach, at the time of each flight undertaken during breakup, is summarized in Table 2.5. In a similar manner as with the data collected during freeze-up, a simple relationship was established between degree-days of thaw and percentage of open water during breakup. However, thermal deterioration for the reach is dependant on several other factors, such as solar radiation and warm

underlying water from the outfalls. As a consequence, this relationship might not be entirely meaningful.

As seen on 30-Mar-07, the first significant open lead, spanning 7.3 km, was observed downstream of an outfall located approximately 650 m downstream of the Suncor Bridge (Figure 2.41). By 17-Apr-07, this open lead had extended to 13 km in length, with the occasional presence of arrested pieces of the remaining ice cover melting in place. Most of the deterioration in the study reach was generated at outfall locations and very few dynamic processes took place. However, a few sheet accumulations were observed in the vicinity of Poplar and Morton Islands. By the time the ice runs (resulting from the release of ice jams formed upstream of Fort McMurray) passed through the study reach, the ice cover was significantly deteriorated.

An additional flight took place on 23-Apr-07, during which it was observed that the ice runs had passed completely through the study reach. As a result, the precise location at which the ice run might have stalled was not determined. However, as mentioned in Section 2.4.4, recorded water levels at stations M288.1 and M268.1 show the ice run stalled briefly between the WSC gauge below Fort McMurray and station M288.1. It is worth noting that this ice run, which resulted from an ice jam release from within Fort McMurray at 20:00 on 19-Apr-07, persisted for more than 18 hours. During aerial surveillance on 23-Apr-07, it was observed that shear walls of significant size (~2 to 3 m) were left behind from this ice run.

2.6.3. Satellite Imagery

River ice classification and characterization of Synthetic Aperture Radar (SAR) imagery has been studied extensively in recent years (Weber *et al.*, 2003; Pelletier *et al.*, 2005; Gauthier *et al.*, 2006; Drouin *et al.*, 2007). As a result, researchers from the University of Alberta, INRS-ETE in Québec, and C-CORE in Newfoundland, have been collaborating to investigate its viability for mapping ice cover development and breakup on the Athabasca River. RADARSAT-1 SAR images of the study reach were taken during the 2006/07-winter season; most were made available for comparison with data from this study, post-classification, facilitating an independent evaluation of the current classification schemes being used by the respective organizations. Table 2.7 contains information regarding the source of these images and the dates on which they were taken. A total of two images were obtained for the freeze-up period and five images for breakup. One additional image was taken on 15-Dec-06, after freeze-up was complete.

2.6.3.1. Freeze-up

From the two images obtained for the 2006 freeze-up period, one of them was taken on 5-Nov-06, which also corresponds to a day when ice classification was accomplished through aerial surveillance. The remaining image was taken on 01-Nov-06, which, as discussed earlier, was the date of a scheduled observation flight over the study reach; however, this could not be completed due to the airline's cancellation of the trip to Fort McMurray (due to mechanical difficulties). Therefore, the only ground truthing available for this image was from the cameras at

stations M288.1 and M268.1. Classification of the ice cover in these two satellite images was accomplished as part of the FRAZIL project, which was initiated in 2005 with the purpose of developing a GIS-based system in support of winter river flow modeling and ice-related flood forecasting. At INRS-ETE, these RADARSAT-1 Synthetic Aperture Radar (SAR) images underwent a process of automated ice classification, based on pixel backscattering and texture. As a result, nine different categories along the channel were determined on each of the images, which include open water, the presence of floating ice pans, border ice, thick columnar ice, mixed frazil and columnar ice sheets, juxtaposed ice, and lightly to heavily consolidated ice (hummocky ice).

The RADARSAT-1 SAR image taken on 01-Nov-06 shows most of the ice in the upstream portion of the reach was comprised of juxtaposed ice and sheets dominated by columnar ice, before being moderately consolidated into the hummocky ice cover seen three days later. Figure 2.42 shows the satellite image ice cover classification of this upstream reach, compared to the image obtained with the digital camera at station M288.1. As seen in the figure, border ice was correctly classified in the satellite image, however, the extents of open water areas with presence of floating ice pans appear to be underestimated. Further downstream, where the ice cover is affected by warm water outfalls, the satellite image shows that a predominantly columnar ice sheet was present in what was observed to be open water by 04-Nov-06; this is illustrated in Figure 2.43. The figure also illustrates that areas outlining border ice formations, classified as juxtaposed and slightly

consolidated ice in the satellite images, might actually be areas of “buttering” of the border ice.

Ice cover classifications in the RADARSAT-1 SAR image obtained on 05-Nov-06 were consistent with the observations made during aerial surveillance. The location and extent of open water areas, along with the suspected location of industrial water outfalls were highly comparable. All suspected industrial outfalls were identified in the satellite images. Areas of thermal growth in the small open leads created by constrictions by border ice were also consistent; this is illustrated in Figures 2.44 and 2.45. The figures also show how areas identified during aerial surveillance as simply juxtaposed ice, were identified in the satellite image as being slightly consolidated ice, with small areas of moderate consolidation at the points of ice arrest (where incoming ice pans had slightly disrupted the previously arrested ones). It is interesting to note how this phenomenon is recurring at the suspected outfall locations, which do not constitute actual bridging points, as persistent open leads are more likely to occur downstream, rather than bridging upstream.

Some discrepancies between the images and the observations were also noted; these are illustrated in Figure 2.46. For example, the extent of the hummocky ice cover, which was identified during aerial surveillance as spanning 8.5 km downstream from station M288.1, was classified in the satellite image as extending for approximately 11 km. Along this upstream reach, the extents of border ice were also dissimilar, and most of what was classified from aerial surveillance as border ice, was identified in the satellite image as slightly consolidated ice. It is important to

note that aerial surveillance classification was accomplished visually, and snow on top of the ice cover would often times mask the real nature of the underlying ice, which is not an issue with radar imagery. Therefore, the visual observations are not necessarily more accurate than the satellite SAR images. In a similar manner, a discrepancy was seen in terms of the quantity of floating ice pans identified in the satellite image, compared to what was observed during the flight (Figure 2.47). Classification in the satellite image shows frazil pans along the entire length of the leads, which was not observed during aerial surveillance. However, light conditions during the time of the flight might not have been appropriate to identify developing pans.

2.6.3.2. Breakup

Five RADARSAT-1 SAR images were obtained during the 2007 breakup period. Ice cover classification was performed by C-CORE, in conjunction with the Polar View project, as part of a pilot program with Alberta Environment to identify ice jams for flood forecasting purposes with SAR imagery. The ice classification employed five categories, which include open water, light ice, intact ice, and lightly and heavily consolidated ice. The images taken on 11, 14, 15, 18-Apr-07 show the ice cover was mostly comprised of light ice and open water areas, most of which were consistent with what was observed during aerial surveillance, in terms of location (Figure 2.48). However, the identified extent of these open water areas was greater in the classified images, than what was actually observed in the field, most likely due to the coarse resolution of these satellite images (>20 m, Table 2.7).

Figure 2.49 illustrates the main open lead, suspected to have been generated by warm water outfalls located downstream of the Suncor bridge (Section 2.6.2.2), which was also correctly identified in these RADARSAT-1 SAR images, particularly in the image taken on 18-Apr-07. It is also worth mentioning that sheet accumulations at the downstream end of this open lead were also correctly identified.

2.6.3.3. Discussion

The results of ice cover classification in RADARSAT SAR imagery are promising, as correspondence of the different types of ice with what was observed during aerial surveillance, is relatively high. However, this is true mostly for the higher resolution images obtained during the freeze-up period, where open water, thermal, juxtaposed and hummocky areas were all highly comparable to field observations. Images obtained during breakup were less accurate, as resolution was significantly lower. Additionally, the state of thermal decay of the ice cover can have a significant effect on its scattering coefficient, which is largely controlled by surface wetness (Pelletier *et al.*, 2005) Some of the observed discrepancies might also be attributable to the different image modes and incidence angles between images, which according to Pelletier *et al.* (2005), affect calculated backscatter coefficients.

2.6.4. Ice Cover Thickness Measurements

Ice thickness measurements are usually accomplished with the use of a manual ice thickness gauge, for which holes must be drilled in the ice cover for every individual measurement. However, in order to obtain a detailed depiction of

the variation of the thickness of the entire ice cover, a large number of these measurements must be conducted, which proves to be a challenging task, especially in a hostile winter environment. For this reason, the use of Ground Penetrating Radar (GPR) as a tool for determining ice cover thickness was evaluated at several locations within the study reach. The location at which GPR transects were taken was illustrated earlier in Figure 2.17. The figure also illustrates the locations of manual ice thickness measurements.

2.6.4.1. Operating Principles of Ground Penetrating Radar

GPR uses the principle of scattering of electromagnetic waves as the basis for its functionality. The waves are radiated by the transmitting antenna and travel through the material at a velocity determined primarily by its dielectric permittivity (the velocity is proportional to the inverse square root of the permittivity of the material). The dielectric constant of the material varies as a function of its moisture content. When encountering a material of different electrical properties, the wave is scattered and its reflection detected by the receiving antenna. In other words, the signal passed through two materials with different electrical properties over the same distance will arrive at different times (Daniels, 2000). The greater the change in velocity, the higher the amplitude of the reflected wave will be.

Travel times, which are defined as the time the wave takes to travel from the transmitting antenna to the receiving antenna, are usually expressed in nanoseconds (10^{-9} seconds). If the dielectric constant the material is known, hence the velocity at

which the wave travels through the material is also known, the depth at which a layer boundary is encountered can be accurately identified. The time-history of the travel of a single pulse from the transmitting to the receiving antenna, which includes all of its travel paths, is called a “trace”. As the antenna is towed across the surface (as shown in Figure 2.50) while recording traces at a fixed spacing, a time-distance record section of traces is created. This can be viewed as a two-dimensional image of the subsurface, with the horizontal axis representing the distance along the transect, and the vertical axis being the two-way travel time of the radar wave. The vertical axis can also portray distance if the permittivity of the medium is known.

A scan display is obtained by assigning a color (or a variation of color intensity) to the different amplitude ranges on the trace (Daniels, 2000). Black and white images, as shown in Figure 2.51 are displayed in real time on the console while towing the unit across the surface. Strong reflections, produced by pronounced differences in the permittivity of the distinct boundary layers, generate easily identifiable black bands, while medial reflections generate shades of gray.

The frequency of the antenna determines its penetrating capabilities. Low frequency antennas generate long-wave radar energy, which can penetrate up to 50 *m* under certain conditions, but are capable of resolving only large subsurface features. On the other hand, high frequency antennas can resolve features down to a few centimeters in diameter, but are capable of penetrating only a few meters in depth.

2.6.4.2. GPR for Ice Cover Characterization – Previous Studies

Ground Penetrating Radar (GPR) has proven to be a useful tool for subsurface characterizations over the past few years, and is a fairly common device used in geophysical and archaeological investigations. However, very few studies were found as a result of this investigation on the use of GPR as a tool for actual mapping of ice cover thickness (none of them related to ice covers in rivers).

Moldoveanu-Constantinescu (2004) conducted one such study of relevance on the use of GPR for surveys on a frozen river lagoon in Calgary, Alberta, obtaining reasonable results using a 250 MHz antenna on an ice surface of 25 m by 45 m. The thickness of the ice cover was interpreted in each of the scans and validated with manual ice thickness measurements. Also worth mentioning is the use of actually calculated values of the velocity of propagation of the electromagnetic waves in the ice, to migrate travel times to actual vertical distances. This velocity was determined during data acquisition by fitting a hyperbola to diffracting objects in the ice. A velocity of 0.15 m/ns was established in their study.

Moorman (1998), studying the use of GPR for applications in glacial hydrology, used very low frequency antennas to determine the exact location and interconnections of englacial and subglacial drainage networks, taking advantage of the high contrast between the dielectric constants of ice, air and water. Relevant to the present study was Moorman's (1998) determination of the average propagation velocities for different types of ice, which are essential for evaluating the capability

of GPR for subsurface characterizations of layering within the ice cover itself (i.e. frazil vs. columnar ice). It is important to note however, that detailed stratigraphy of the ice, as encountered in river ice covers, was not correctly identified in Moorman's study, given the coarse resolution provided by the low frequency antennas used.

Snow has a unique dielectric constant, which varies as a function of its air and moisture content. In a sense, the permittivity of snow is highly dependent upon local climate conditions, and a dielectric constant can be obtained as a weighted average of that for air, water and ice (Moorman, 1998). In other words, under conditions of higher humidity, the dielectric constant of snow will be much more dissimilar than that of ice, making the snow/ice cover interface much more evident in GPR scans. Under dryer environments, where the permittivity of both snow and ice are much more similar, this interface would be less obvious as scatter of the electromagnetic waves is reduced. Additionally, the thickness of the snow cover is not being properly portrayed in the scans, as the scale of the vertical axis is determined by defining the dielectric constant of the principal medium, which is in this case solid ice. However, the thickness of the ice cover can be properly obtained as the distance between the two identified boundary layers.

It is important to note that river ice covers are comprised of multiple types of ice, ranging from frozen frazil slush to thermal ice. As a result, determining a single dielectric constant for travel time migration is rather difficult. This may affect the results of thickness estimations from the GPR data when the percentages of different types of ice within the ice cover are unknown. A single weighted averaged dielectric

constant cannot be assigned for an entire transect, given the high variations in the percentages of thermal versus frazil ice as the ice cover reaches and/or is distanced from the banks.

2.6.4.3. Fieldwork Procedures and Data Analysis

For the present study, 400 MHz and 900 MHz antennas were used at each transect, which were towed both on foot and with the use of snowmobiles (as illustrated in Figure 2.50). Maintaining a constant velocity while towing the antennas is critical for a correct normalization of the horizontal distance, which is based on the number of scans per minute and the distance between markers. These markers were also used for validation of the obtained ice cover thickness, as they also correspond to points of known thickness, measured manually in the field. Table 2.8 summarizes mean ice thicknesses for each transect, comparatively between antennas and manual measurements. Figures 2.52 through 2.54, illustrate these results graphically, showing that the correspondence of measured values of ice cover thickness with the interpreted values obtained from the GPR data is reasonably good. The ice cover was identified in the GPR scans as the area between the first two significantly distinguishable black bands, as seen previously in Figure 2.51. These would most likely correspond to the snow/ice and ice/water interfaces, given the accentuated contrast between the dielectric constants of ice and water (3.2 for ice and 80 for water).

Scans from the 400 MHz antenna show very similar results to those from the 900 MHz antenna, and were for the most part highly comparable to actual measured values. However, given that the low frequency antenna is capable of resolving only large subsurface features, proper identification of ice cover thickness within a reasonable accuracy range becomes more difficult and less reliable. The 900 MHz antenna shows a better result in terms of detail and accuracy. This was corroborated by a root mean square deviation (RMSD) analysis, which resulted in average values of 0.058 for the 400 MHz antenna and 0.043 for the 900 MHz antenna. The results of each individual RMSD analysis are shown in Figures 2.52 to 2.54. In a general sense, ice thickness measurements from the 900 MHz antenna always showed a better correspondence to actual measured values.

Most sources of error in the collected data can be attributable to field operation techniques. Since data is being collected in continuous acquisition mode and pulses are being generated at a pre-programmed rate, the operator must not only move at a constant speed, but also be very attentive to following the designated surface markers. Failure to do so may result in large errors in horizontal scale normalization, rendering the data virtually incomparable to actual measured values, as markers may be misplaced. Additionally, augered holes in the ice cover corresponding to surface marker positions were not located directly beneath the GPR path, as manual thickness measurements were being conducted at the same time as the GPR runs. Obviously, this can contribute to inaccuracies in the comparison data, given that significant variations in ice cover thickness can occur over relatively short distances.

As mentioned earlier, both the use of snowmobiles to tow the antenna and doing so by foot have been examined. The former allows for better control over the speed and handling of the instrument making the normalization process much more precise. However, higher speeds translate into a loss of accuracy, as a lesser number of scans can be accomplished per traveled distance. The latter on the other hand, presents itself as a challenge in terms of the uniformity of the towing velocity and the correct positioning of the antenna. During data collection it is important to ascertain that the position and orientation of the antenna above the snow remain constant. Changes in antenna orientation with respect to the underlying structure can cause variations in the recorded reflections, which can be confused with real changes in the subsurface. This phenomenon is also known as “antenna coupling loss” (Daniels, 2000).

Given the above analysis, it is clear that GPR has the potential to be a valuable tool for ice cover thickness mapping in rivers, but the accuracy of the results may be much more dependent on proper field data collection techniques, than the capabilities of the instrument or the post-processing software. The results of this preliminary attempt in the use of radar signals to map river ice covers show promise, but only if the problems encountered during data collection can be surpassed.

Even though mapping of ice cover thickness has shown potential, the identification of multiple layers within the ice cover has not proven itself to be viable. In order to fully appreciate distinct layering within the ice, permittivity of the

different layers should be sufficiently dissimilar, but unfortunately, dielectric constants for different types of ice do not vary greatly.

Moorman (1998) determined the propagation velocities for wet slush to bubbly ice and blue ice as being 0.12 to 0.17 m/ns, which translates into dielectric constants of 6.25 to 3.2 respectively. The 900 MHz antenna provided reasonably detailed ice cover thickness characterizations. However, the contrast in permittivity between the different layers within the ice cover is not sufficient for the GPR to properly identify these interfaces, without them being mistaken for noise resulting from antenna coupling loss.

2.6.5. Ice Core Sampling

Core samples of the ice cover were taken at numerous sites, most of which were located along CEMA Reach 1, as this was the primary subject of 2-dimensional modeling in this phase of the project. Figure 2.17 shows the locations on this reach where ice core samples were obtained. A mapping of the ice cover as shown in the figure, provided a relative location of where samples were to be extracted, in order to obtain a representative depiction of ice cover formation (i.e. border ice versus juxtaposed ice). Table 2.9 contains information regarding these locations, total thickness, and the different sections of the ice core samples transported back to the University of Alberta for further analysis in the laboratory cold room. This analysis included a characterization of crystal structure and sizes, as well as porosity and air inclusions, determined for each distinct layer observed within the samples.

Quantitative results of this analysis are summarized in Tables 2.10 and 2.11 respectively.

In a general sense, the samples extracted show an average ice cover thickness of 55 cm; this is true mostly for areas of juxtaposed ice, where the total thickness of the ice cover was fairly consistent between samples. Samples obtained from border ice were thicker, averaging 70 cm. In most cases, it was observed during sample extraction that the border ice had no flowing water underneath. This accounts for the thickness of the samples extracted from these formations being relatively larger, as thermal growth of the slow flowing underlying water would continue throughout the season until reaching the bed.

Figures 2.55 to 2.61 qualitatively illustrate the results of the laboratory analysis of the samples. Each distinct layer was identified in regards to changes in air content and/or crystal structure. This analysis shows that the ice cover was comprised for the most part of snow ice, frazil ice and columnar ice. It is important to note that distinctions between snow and frazil ice in terms of crystal structure, are relatively difficult, as average crystal sizes for both types of ice tend to be quite similar. For this reason, no definitive stratification could be obtained between these two ice types from this analysis. Snow ice is formed when freezing occurs to the overlying snow, which has been saturated with water from rainfall or seepage through cracks in the ice cover. As a result, there is some logic in assuming that snow ice layers can only be located at the top portion of the samples. However, when these layers are immediately followed by frazil ice, the distinction between the two

becomes less obvious. Under normal lighting conditions, snow ice tends to look milky colored. However, frazil can also have an opaque appearance. Essentially then, it was not possible to distinguish between the two in these samples.

Frazil layers, identified as those containing large amounts of impurities and embedded bed material, tend to suggest an average initial pan thickness of 35 cm. However, determining this thickness purely from core sample analysis is rather subjective and inaccurate, given that subsequent accumulations of additional frazil slush (produced and transported from upstream open areas) is also entirely possible.

Frazil production was estimated to have stopped entirely by the time the core samples were collected. This was based on the fact that the ice cover was completely formed and no significant open leads were present, in addition to the fact that no frazil slush was observed in the flowing water at the time the samples were extracted. This deduction is also supported by the layers of columnar ice observed at the bottom of the majority of the extracted samples.

Samples taken at zones of fast flow under a juxtaposed ice cover (Figures 2.56 and 2.59) show areas of columnar ice growth embedded within the frazil ice layers. This was not evident on other samples taken in the juxtaposed ice, where the underlying flow was significantly slower. This possibly suggests that higher velocities cause a disruption and consequently larger pores within the frazil slush, which saturated with water, would eventually freeze and grow thermally, resulting in large organized crystals, similar to those seen in columnar ice layers.

According to Gherboudj *et al.* (2007), ice rejects all air in the water during solidification and the effects of rapid freezing, along with high turbulent velocities, may contribute to larger and more prevalent air inclusions. In other words, the characteristics of air inclusions present in the ice cover may depend on the rate of freezing and the hydraulics of the channel. Given the mild slope of the study reach and its relatively low velocities, air inclusions seen in the samples may possibly be attributable only to periods of rapid freezing. Figure 2.62 shows these periods of rapid freezing occurring both in November 2006 and January 2007.

Here, the characteristics of air inclusions were found to depend largely upon ice type. Layers of columnar ice in the bottom of the samples were for the most part free of air. Air inclusions appeared to be concentrated in the top 20 cm in most of the samples. The top most layers, which might be considered snow ice, were found to be relatively more porous, showing air porosities ranging from 9 to 11%. Deeper within the samples, air porosities were found to be relatively lower, ranging from 1 to 5%. Bubble sizes also appeared to be larger overall in the top most layers, ranging from 0.8 to 1.5 mm in average.

2.7. SUMMARY

River ice processes in the study reach were documented for the entire 2006/07-winter season. Ice cover formation and deterioration processes were observed to be highly two-dimensional. The ice cover in most of the study area was formed through juxtaposition, with the exception of the first 8.5 km where a

hummocky ice cover developed. An average thickness of 55 cm was seen in most of the juxtaposed locations. Areas of low flow along the banks and around the numerous islands and sand bars resulted in border ice type formations, representing approximately 61% of the total ice cover at this reach. Additionally, natural constrictions created by the extents of these border ice formations resulted in numerous bridging points and small sized open leads that froze thermally over the course of the winter.

Industrial warm water outfalls, which maintained the water temperature above freezing at each site early in the winter, created open leads of significant size that affected the nature of both freeze-up and breakup processes. In areas unaffected by these outfalls (the first 25 km of the reach spanning from Stations M288.1 to M268.1), an intact ice cover was formed within a period of 5 days. However, along these large open leads generated by the outfalls, frazil production continued over the course of the following weeks. If the length of the lead was sufficient, frazil production continued to generate ice pans that eventually formed the juxtaposed ice cover. This occurred until surface ice coverage in the lead reached approximately 90%, after which time, thermal growth of the ice cover took place in the remainder of the lead. Breakup was also initiated at these outfalls, creating large open leads before any significant deterioration of the ice cover due to heat exchanges with the atmosphere took place. Very few dynamic processes took place in the reach during breakup, and ice cover deterioration occurred thermally, until ice runs from the ice jam releases upstream of Fort McMurray passed through.

A comprehensive record of hydrometeorological and ice characterization data was obtained for the 2006/07 winter season. This includes air temperature, water temperature, water level, surface ice concentration and ice cover thickness data along a period of 8 months, starting in September 2006. Several techniques for automated data collection and ice cover characterization were evaluated in terms of the accuracy of the obtained records. These records comprise the first out of a three-year set, which will be used to develop a predictive numerical model for the study reach. Preliminary one- and two-dimensional modeling using the collected data is discussed in the following chapter.

Table 2.1 Automated monitoring stations installed along the study reach on September 2006.

Station Name	UTM Coordinates	Location Description	Installation Date	Data Collected
M288.1	474833 E 6294018 N	West bank, 6 km downstream of MacEwan Bridge at Fort McMurray	26-Sep-06	Water Temperature, Water Level, Surface Ice Concentration
M268.1	472159 E 6312632 N	West Bank across Shipyard Lake, 5 km upstream of Suncor Bridge.	28-Sep-06	Water Temperature, Water level
M245.6	463672 E 6331808 N	East Bank, 1 km upstream of Peter Lougheed Bridge	28-Sep-06	Water Temperature, Water level
M216.7	460475 E 6357980 N	East Bank, 2 km upstream of the town of Bitumont	27-Sep-06	Water Temperature, Water Level, Surface Ice Concentration, Air Temperature

Note: All stations record data at an hourly rate.

Table 2.2 Location of major islands and landmarks along the study reach.

Island/Landmark	Location (km)
Waste Water Treatment Plant	290.5
Poplar Island	284.8 – 285.9
Willow & Stony Islands	276.8 – 279.0
Inglis Island	270.0 – 271.4
Shipyard Lake	267.7
Suncor Bridge	262.8
Steepbank River	260.0
Saline Lake	252.5
Morton Island	249.8 – 252.1
Muskeg River	245.0
Peter Lougheed Bridge	244.6
Alexander Island	242.5 – 243.4
MacKay River	240.8
Haight Island	234.8 – 236.7
Ings Island	228.5 – 233.2
Daphne Island	224.7 – 228.3
Ells River	223.4
Sutherland Island	220.0 – 222.0
McDermont Island	218.0 – 219.3
Lafont Island	211.6 – 214.3

Note: River km referenced to an origin in the Peace – Athabasca Delta

Table 2.3 Existing meteorological stations on the study area.

Station Name	Operator	Location	Data Collected	Record Period
Fort McMurray Meteorological Station	Alberta Environment	513281 E 6278447 N	Air Temperature, Humidity, Wind Speed, Barometric Pressure	January, 1944 - present
Aurora Climate Station	Golder Associates	475800 E 6343750 N	Wind Speed, Solar Radiation, Air Temperature, Humidity, Precipitation, Sunshine	May, 1995 - present
UA Meteorological Station	University of Alberta	479737 E 6279743 N	Wind Speed, Solar Radiation, Air Temperature, Precipitation, Barometric Pressure	October, 2000 - present

Table 2.4 Existing hydrometric stations operated by WSC on the study area.

Station Code	Description	Location	Available Record
07DA001	Athabasca River below McMurray	524441 E 6293024 N	1957 - present
07DA018	Beaver River above Syncrude	537917 E 6255376 N	1975 – present
07DA006	Steepbank River near Fort McMurray	525223 E 6318111 N	1972 – present*
07DA008	Muskeg River near Fort MacKay	534330 E 6338864 N	1974 - present
07DB001	MacKay River near Fort MacKay	541879 E 6341037 N	1972 - present

* No record available for the 2006 freeze-up period

Table 2.5 Areas of open water, border ice, juxtaposed ice and hummocky ice (km²) along the reach during the freeze-up and breakup periods, obtained from aerial surveillance.

Date of Flight	Total Area of ice (km²)	Total area of open water (km²)
November 5, 2006	33.89	9.18
November 10, 2006	39.36	3.66
November 17, 2006	41.98	1.04
March 30, 2007	43.33	0.54
April 12, 2007	41.92	1.95
April 16, 2007	31.17	12.70
April 17, 2007	28.41	15.46

Table 2.6 Location of warm water outfalls and extent of the resulting open leads as observed during the freeze-up 2006 surveillance flights.

Suspected Outfall Location	Length of resulting open lead (km)		
	November 5	November 10	November 17
472238 E, 6312878 N	0.75	0.49	0.47 (half width)
473289 E, 6316531 N	14.0	3.0	0.67
462084 E, 6335730 N	1.53	1.50	1.50
462941 E, 6339575 N	>25	9.7	2.0

Table 2.7 RADARSAT-1 SAR images of the study reach obtained, with included ice cover classification.

Image Date	SAR Mode	Nominal Resolution (m)	Incidence Angle (deg)	Ice Cover Classification
1-Nov-06	Fine 5 –Descending.	8	49	FRAZIL
5-Nov-06	Fine 2 – Ascending	9	35	FRAZIL
15-Dec-06	Wide 2 – Descending	27	45	C-Core / Polar View
11-Apr-07	Standard 6 – Descending	22	20	C-Core / Polar View
14-Apr-07	Wide 2 – Descending	27	20	C-Core / Polar View
15-Apr-07	Wide 3 – Ascending	23	45	C-Core / Polar View
18-Apr-07	Standard 7 – Descending	21	49	C-Core / Polar View
19-Apr-07	Standard 2 – Ascending	22	20	C-Core / Polar View

Table 2.8 Summary of GPR transects and mean ice thicknesses obtained from manual readings, and GPR 400 MHz and 900 MHz antennas.

Transect	UTM Coordinates		Mean Ice Thickness (m)		
	Start Point	End Point	Measured	GPR 400 MHz	GPR 900 MHz
1	462857 E 6332683 N	463172 E 6332718 N	0.58	0.57	0.57
2	461970 E 6335322 N	462221 E 6335391 N	0.56	0.52	0.52
3	462216 E 6333767 N	462509 E 6333778 N	0.52	0.50	0.53
4	463013 E 6332701 N	462268 E 6333767 N	0.52	0.51	-
5	462268 E 6333767 N	462182 E 6334565 N	0.52	0.49	-
6	462182 E 6334565 N	462008 E 6335334 N	0.53	0.46	-

Table 2.9 Summary of ice core samples obtained from CEMA Reach 1.

Sample No.	UTM Location	Ice Type	Thickness (cm)	Section analyzed in cold room (cm)
1	462974 E, 6337698 N	Juxtaposed ice	53	11-53
2	462237 E, 6333765 N	Juxtaposed ice	40	0-40
3	452368 E, 6333769 N	Juxtaposed ice	53	21-53
4	467473 E, 6333775 N	Border ice	65	0-20 and 53-65
5	462027 E, 6335341 N	Juxtaposed ice	45	0-33
6	462142 E, 6335373 N	Juxtaposed ice	60	0-60
7	462200 E, 6335337 N	Border ice	50	0-26

Table 2.10 Average crystal sizes of ice core samples obtained from cold room laboratory analysis.

Sample No.	Location from top (cm)	Average Crystal Size (mm ²)
1	2.0	3.8
	4.0	2.6
	14.0	4.5
	16.5	3.9
	36.0	38.8
2	7.0	2.0
	13.0	4.0
	24.0	3.2
3	6.5	5.1
	19.5	5.5
	22.0	8.4
4	1.0	1.7
	5.0	1.7
	10.0	1.6
	19.0	14.8
	53.5	No crystals visible
5	5.5	2.3
	13.5	3.7
	24.5	2.4
6	11.0	3.1
	39.5	3.1
	52.5	14.7
7	12.0	3.5
	17.0	0.6
	24.0	25.3

Table 2.11 Air content of ice core samples obtained from cold room laboratory analysis.

Sample No.	Ice type*	Location from top (cm)	Porosity (%)	Bubble Size (mm)		
				Average	Maximum	Minimum
1	J	2.0	11.20	0.83	4.27	0.20
		4.0	11.20	0.41	3.11	0.10
		14.0	2.95	0.54	4.15	0.14
		16.5	5.66	1.09	4.72	0.18
		36.0		No air content		
2	J	7.0	9.10	1.47	3.86	0.34
		13.0	11.94	1.48	5.23	0.59
		24.0	1.02	0.54	3.65	0.15
3	J	6.5	3.83	1.34	4.46	0.36
		19.5		No air content		
		22.0		No air content		
4	B	1.0	2.33	0.45	3.54	0.16
		5.0		No air content		
		10.0	7.65	0.83	2.44	0.27
		19.0		No air content		
		53.5		No air content		
5	J	5.5	4.12	1.38	2.92	0.43
		13.5		No air content		
		24.5		No air content		
6	J	11.0	3.47	0.92	2.63	0.20
		39.5	0.64	0.69	3.00	0.26
		52.5		No air content		
7	B	12.0	5.27	0.55	1.43	0.15
		17.0	7.31	0.41	0.88	0.15
		24.0		No air content		

*J = Juxtaposed ice; B = Border Ice

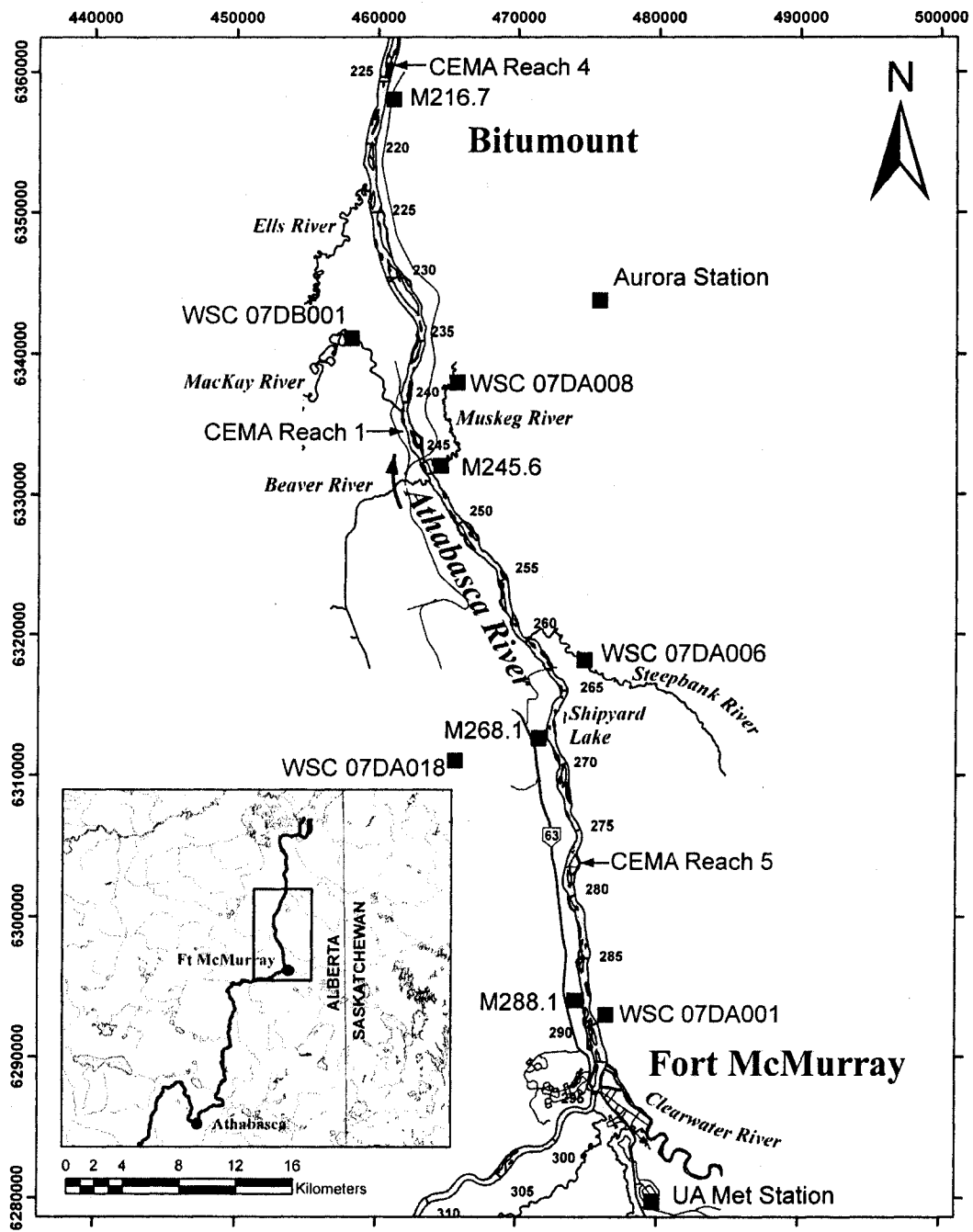


Figure 2.1 Overview of the study area.

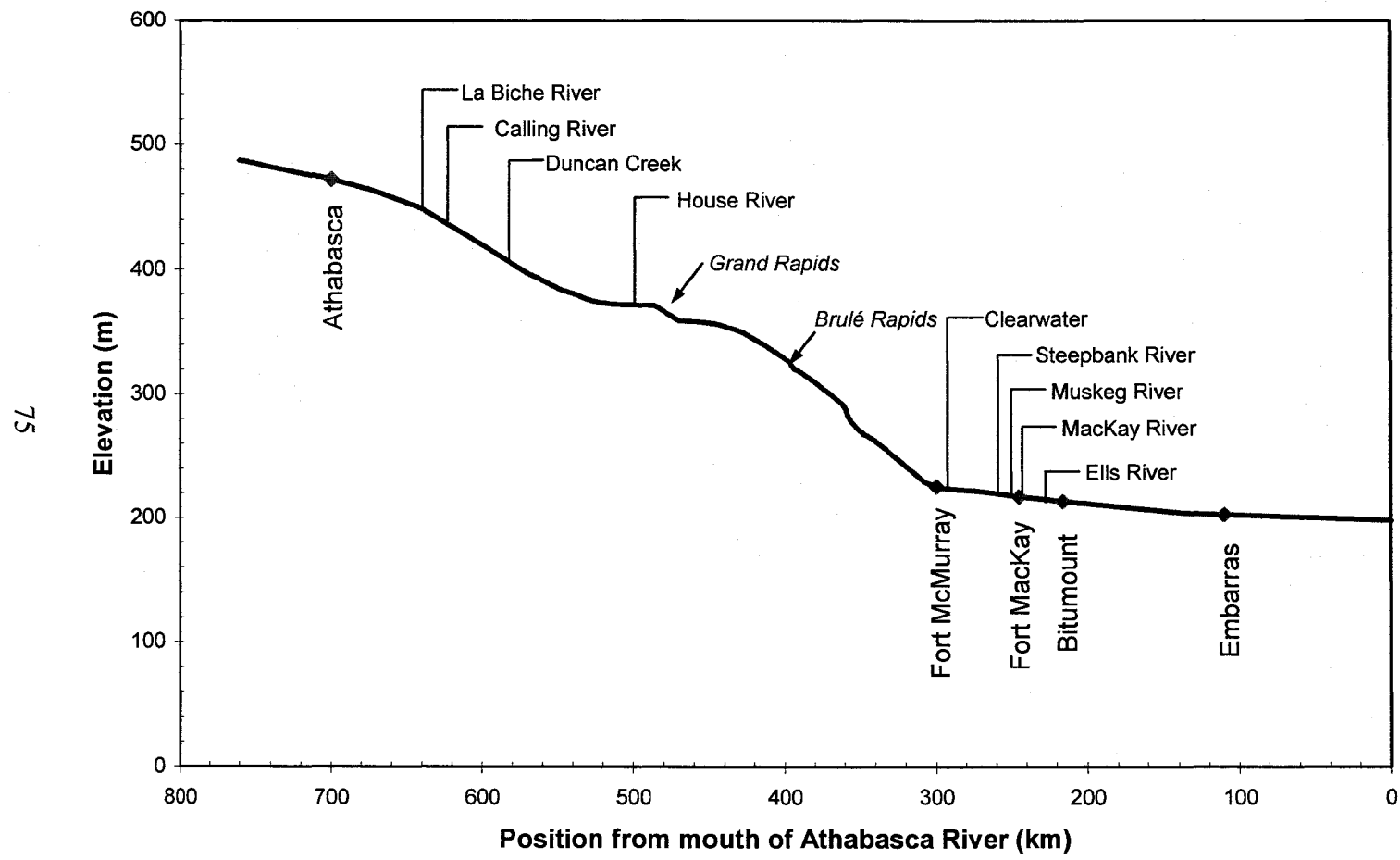


Figure 2.2 Athabasca river longitudinal profile from the Town of Athabasca to Lake Athabasca (after Kellerhalls et al., 1972, adapted from Robichaud, 2003). Note: vertical scale exaggerated.



Figure 2.3 Islands and sand bars on the Lower Athabasca River at Morton Island – September 2006.

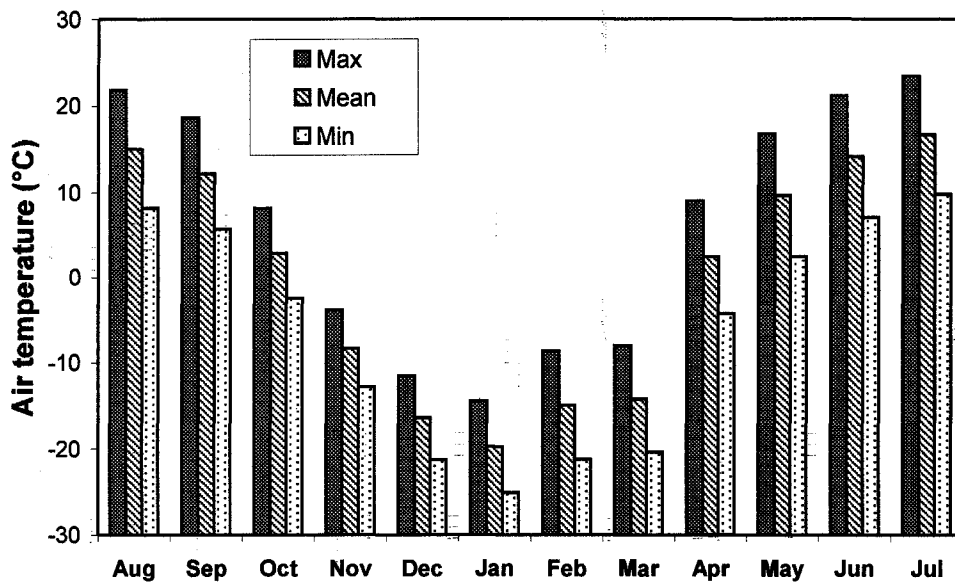


Figure 2.4 Historical records of air temperature at Fort McMurray from 1944 to 2005 obtained from the meteorological station at Fort McMurray airport.

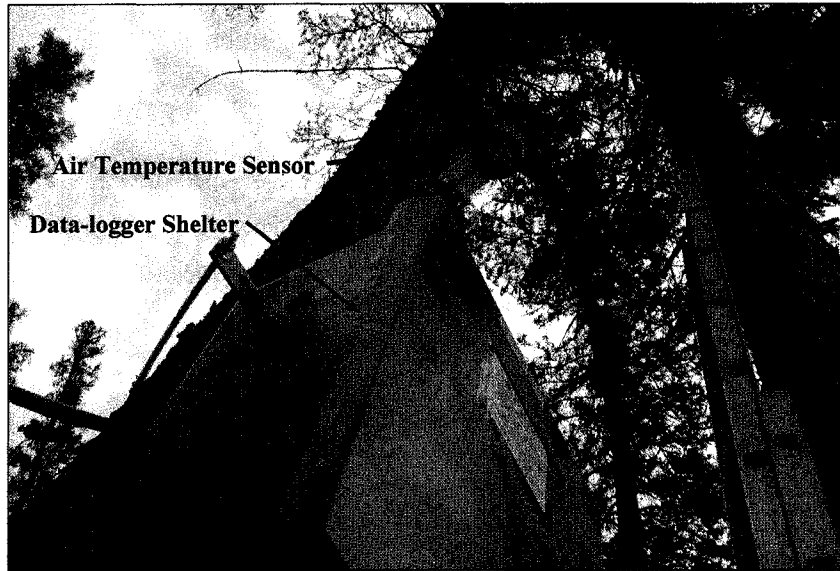


Figure 2.5 Air Temperature sensor above the data-logger shelter installed at river station M216.7.

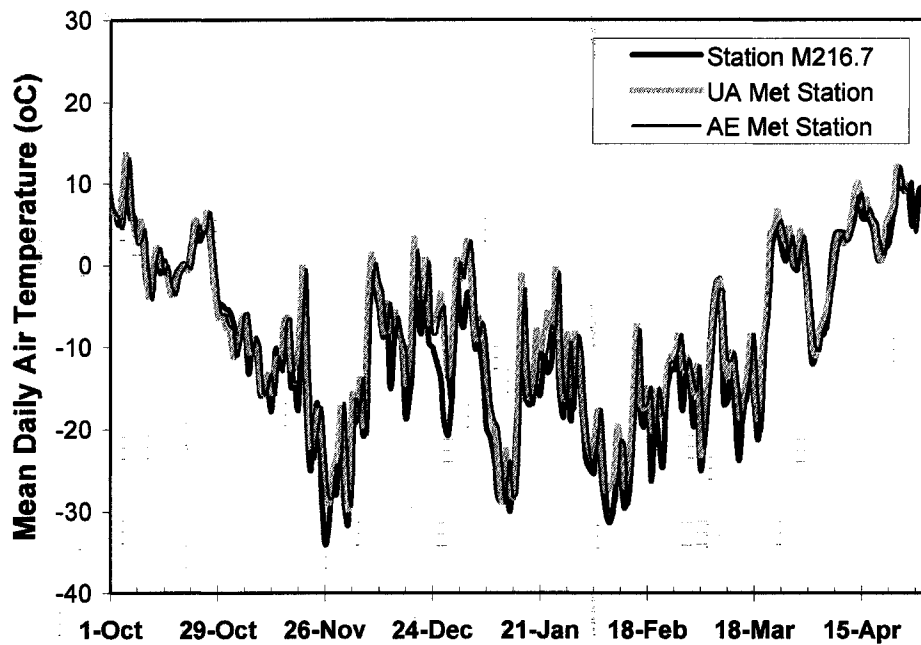


Figure 2.6 Air temperature records obtained from Station M216.7, UA Met station and AE Met Station— Sept. 2006 to April 2007.

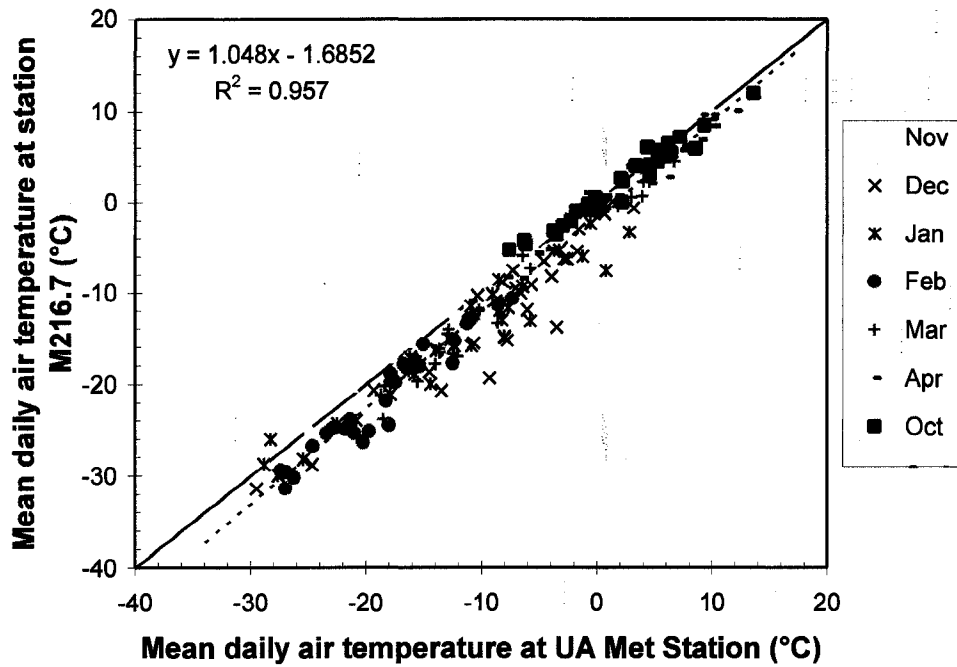


Figure 2.7 Mean daily air temperature (°C) at UA meteorological station versus river station M216.7 from October 2006 to April 2007.

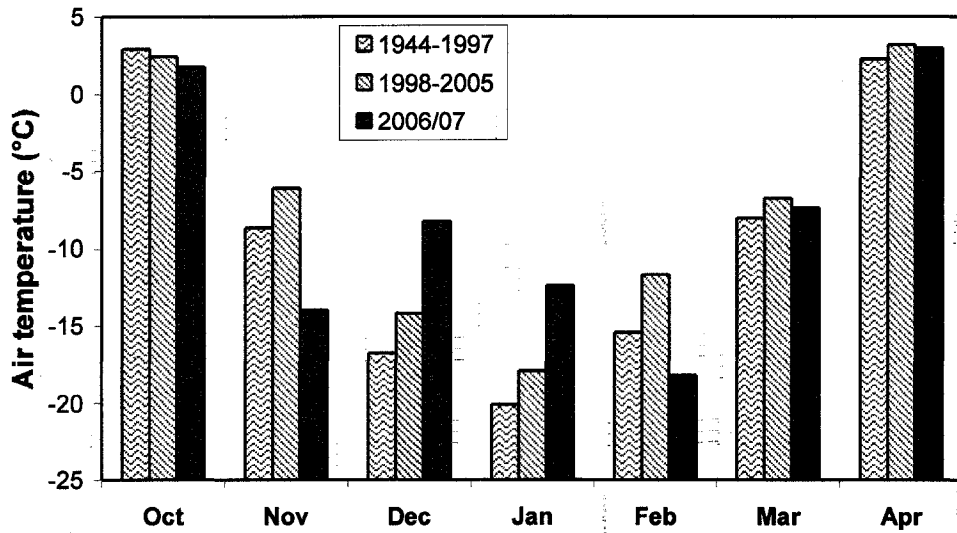


Figure 2.8 Historical record of Mean monthly air temperature at Fort McMurray airport between October and April.

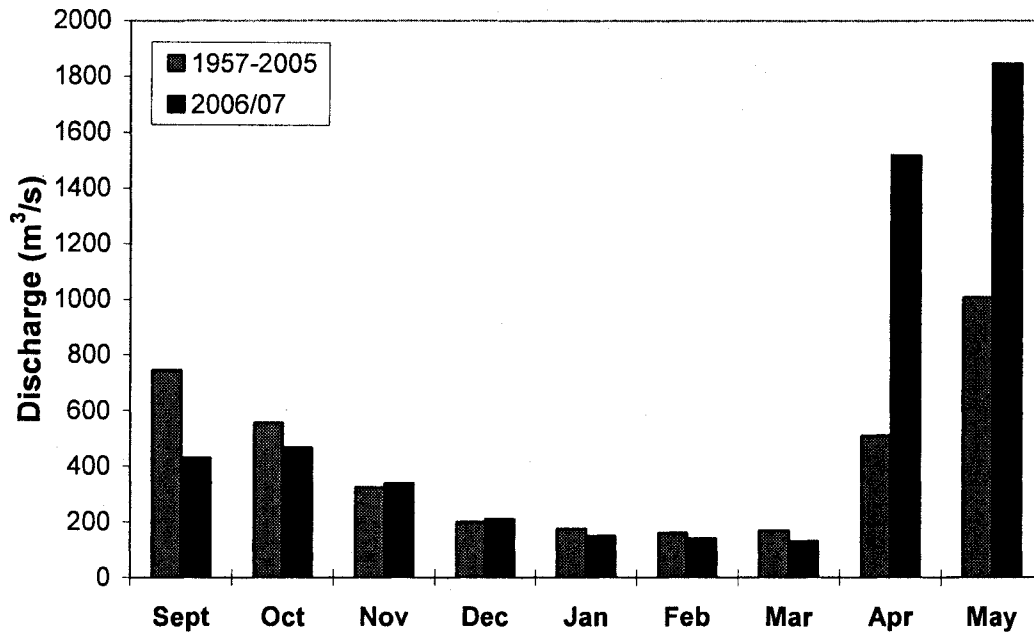


Figure 2.9 Historical versus 2006/07 mean monthly discharges obtained from the WSC gauge below Fort McMurray.

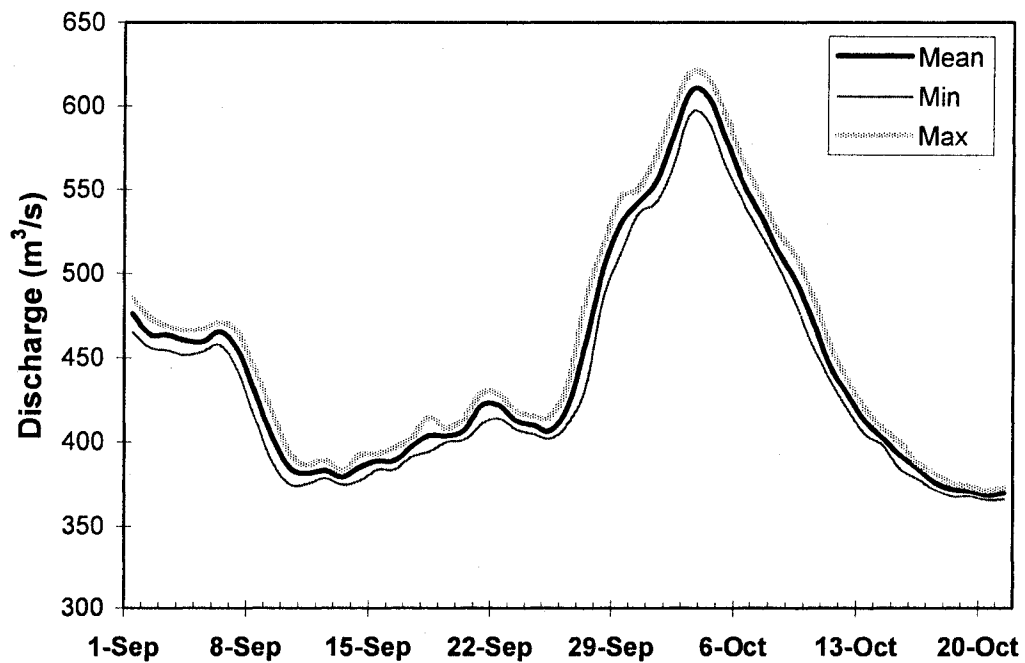


Figure 2.10 Mean daily discharges obtained from the WSC gauge below Fort McMurray for the 2006 pre-freeze-up period.

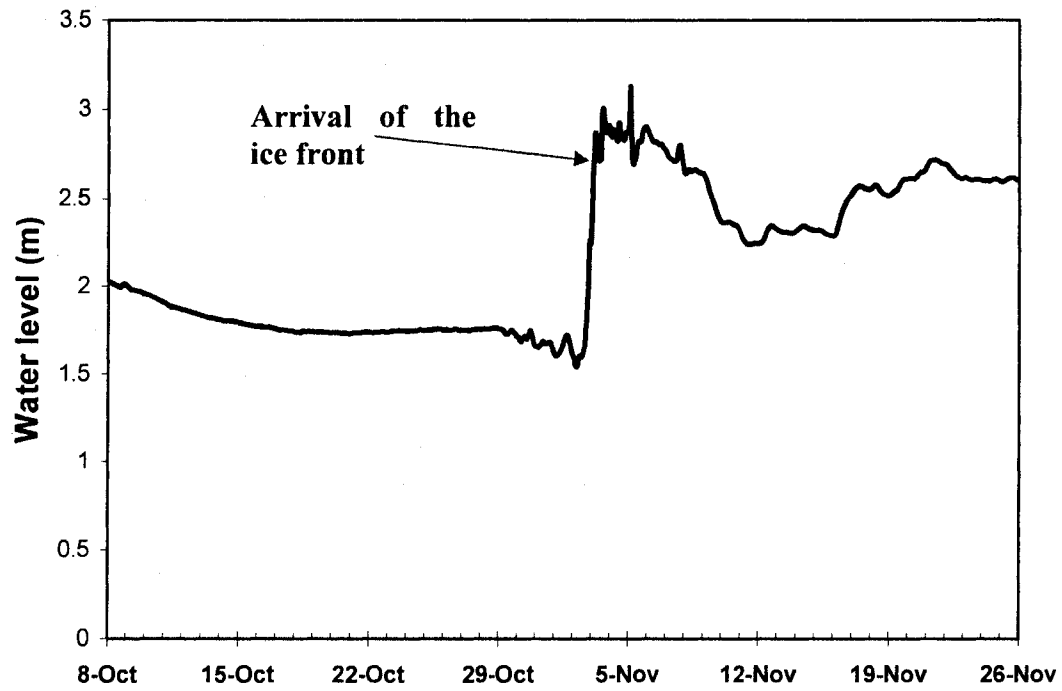


Figure 2.11 Recorded water levels at the WSC Gauge below Fort McMurray during the 2006 freeze-up period.

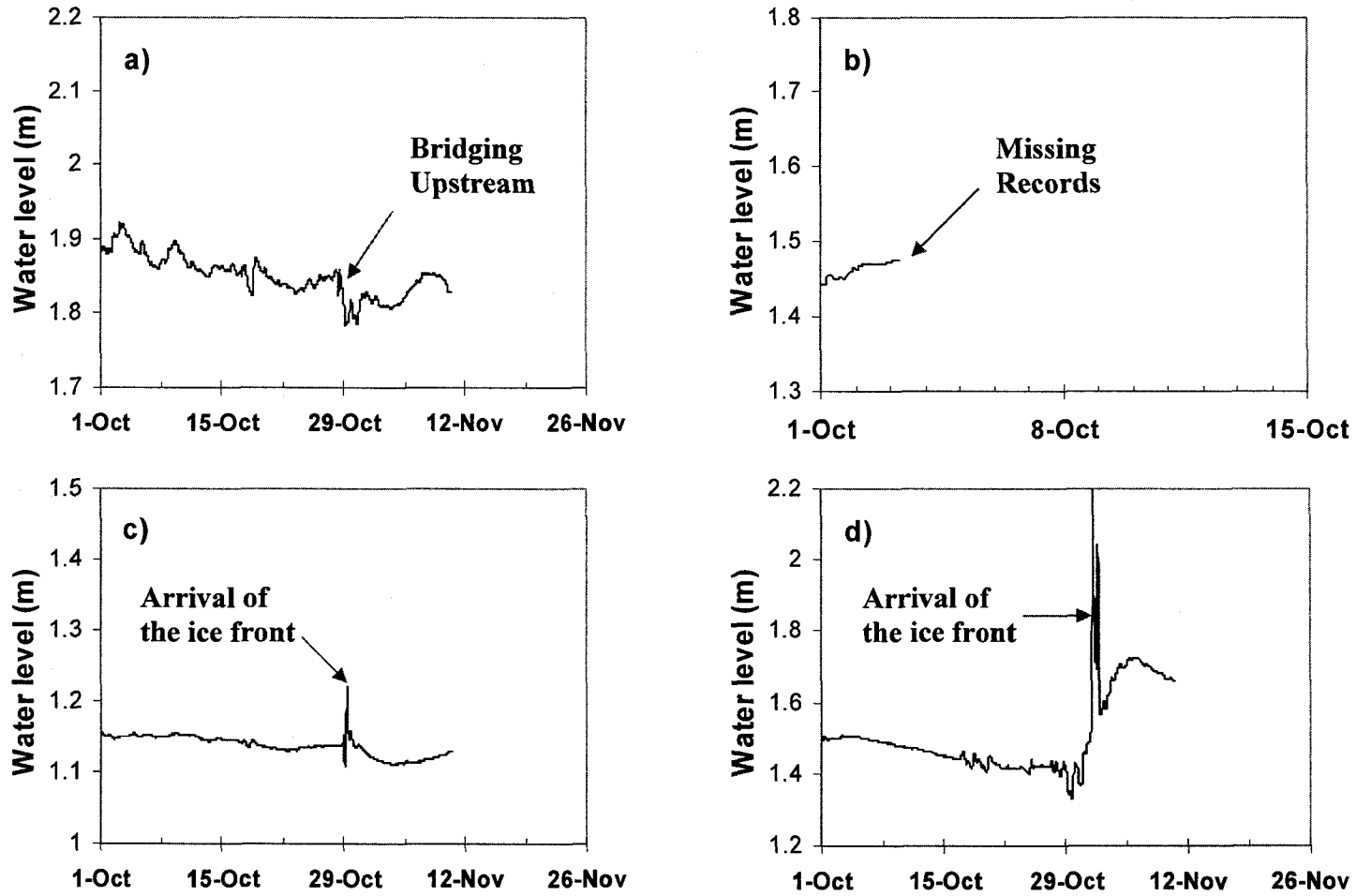


Figure 2.12 2006 Freeze-up water levels recorded at a) Beaver River above Syncrude, b) Steepbank River near Fort McMurray, c) Muskeg River near Fort MacKay and d) MacKay River near Fort MacKay.

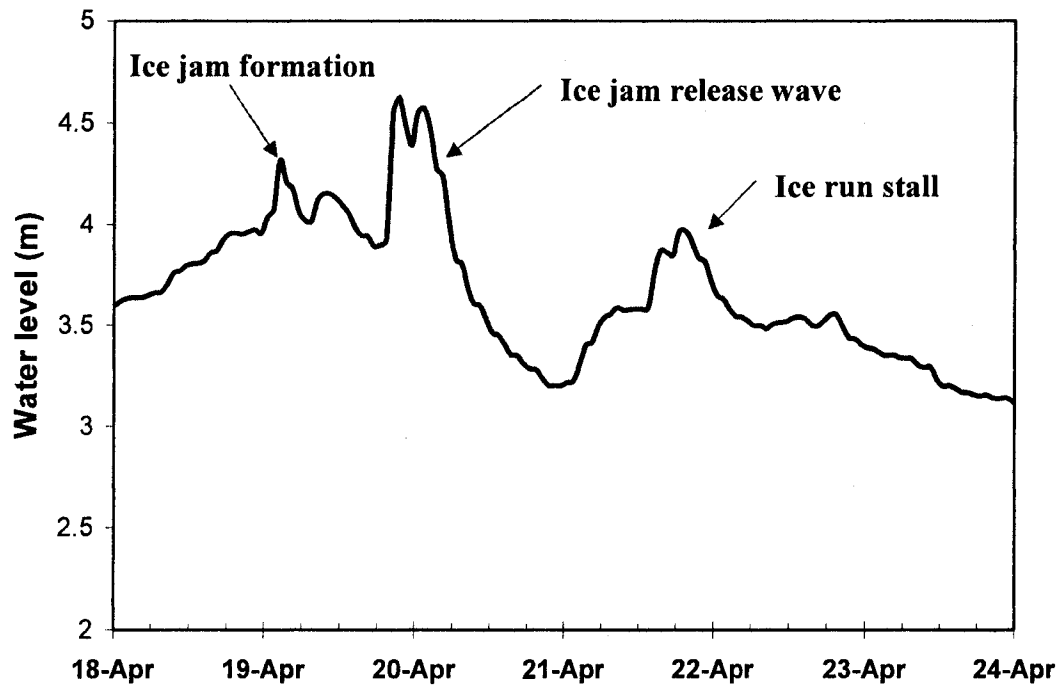


Figure 2.13 Recorded water levels at the WSC gauge below Fort McMurray, during the 2007 breakup period.

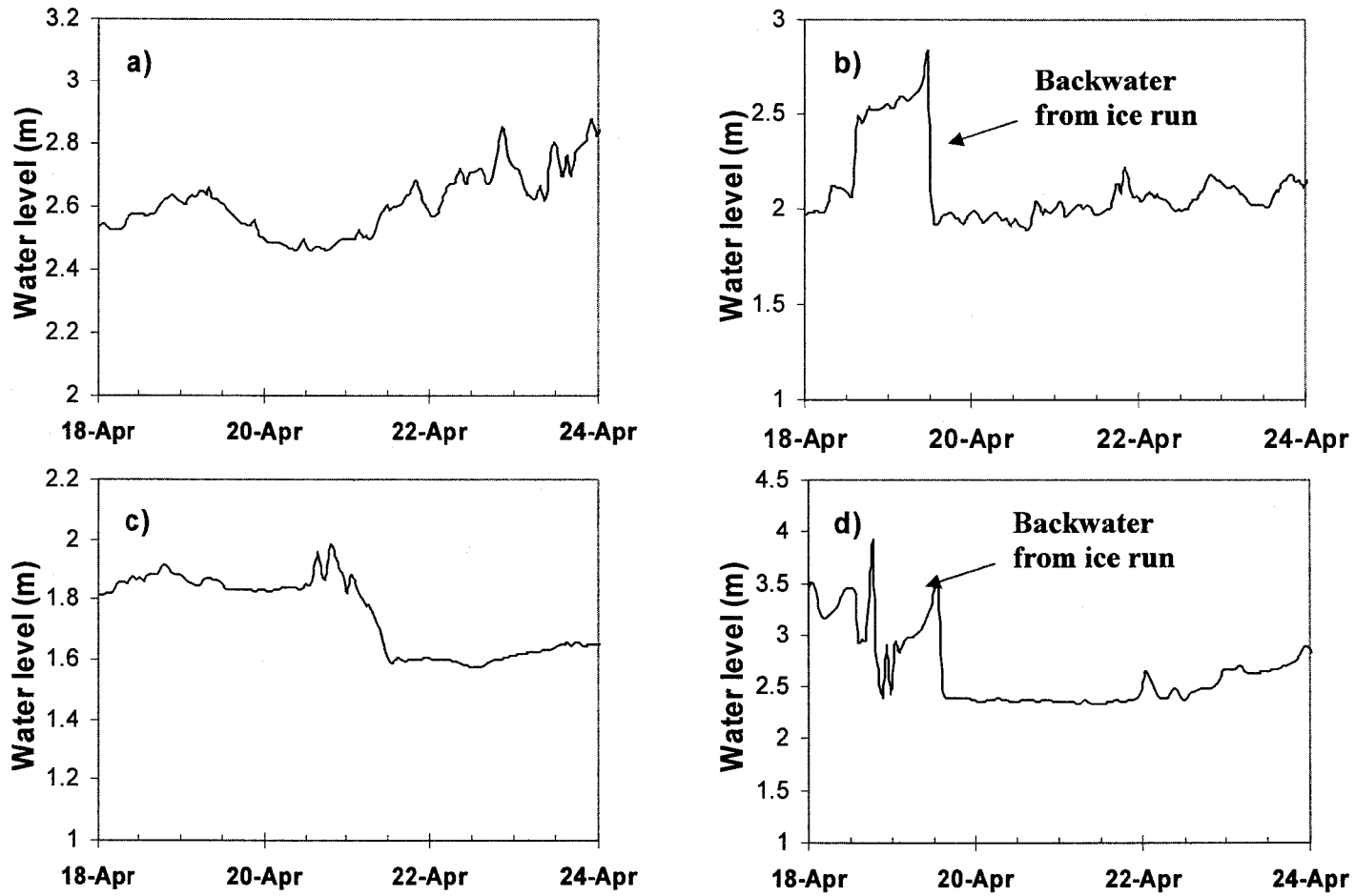


Figure 2.14 2007 breakup water levels recorded at a) Beaver River above Syncrude, b) Steepbank River near Fort McMurray, c) Muskeg River near Fort MacKay and d) MacKay River near Fort MacKay.

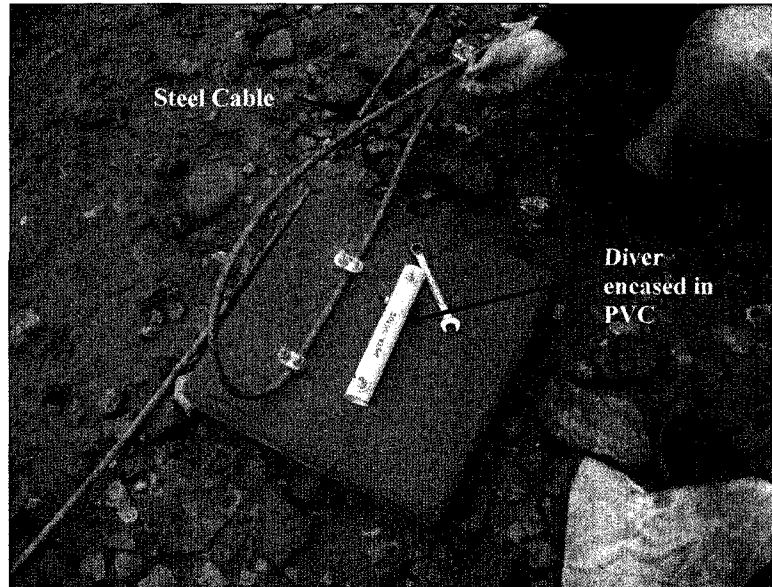


Figure 2.15 Setup used for Diver[®] installation in the field - September 2006.

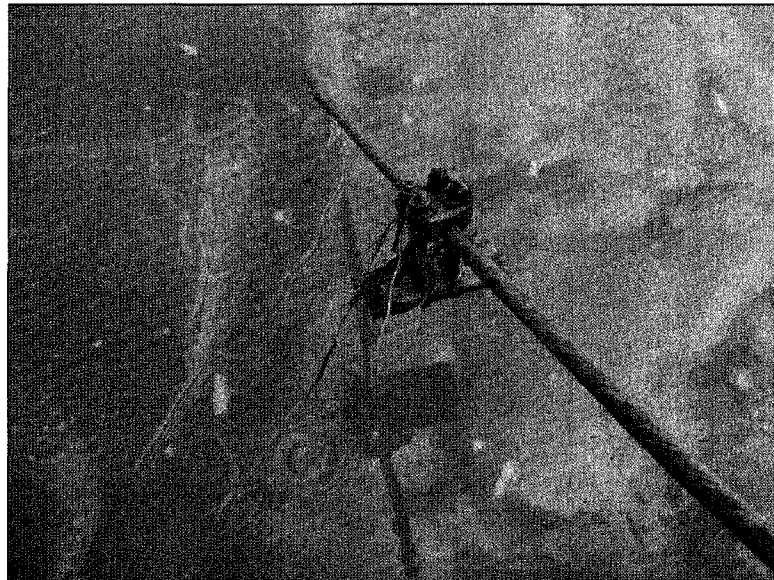


Figure 2.16 Remaining cable-clamps as they were detached from the concrete pad - May 2007.

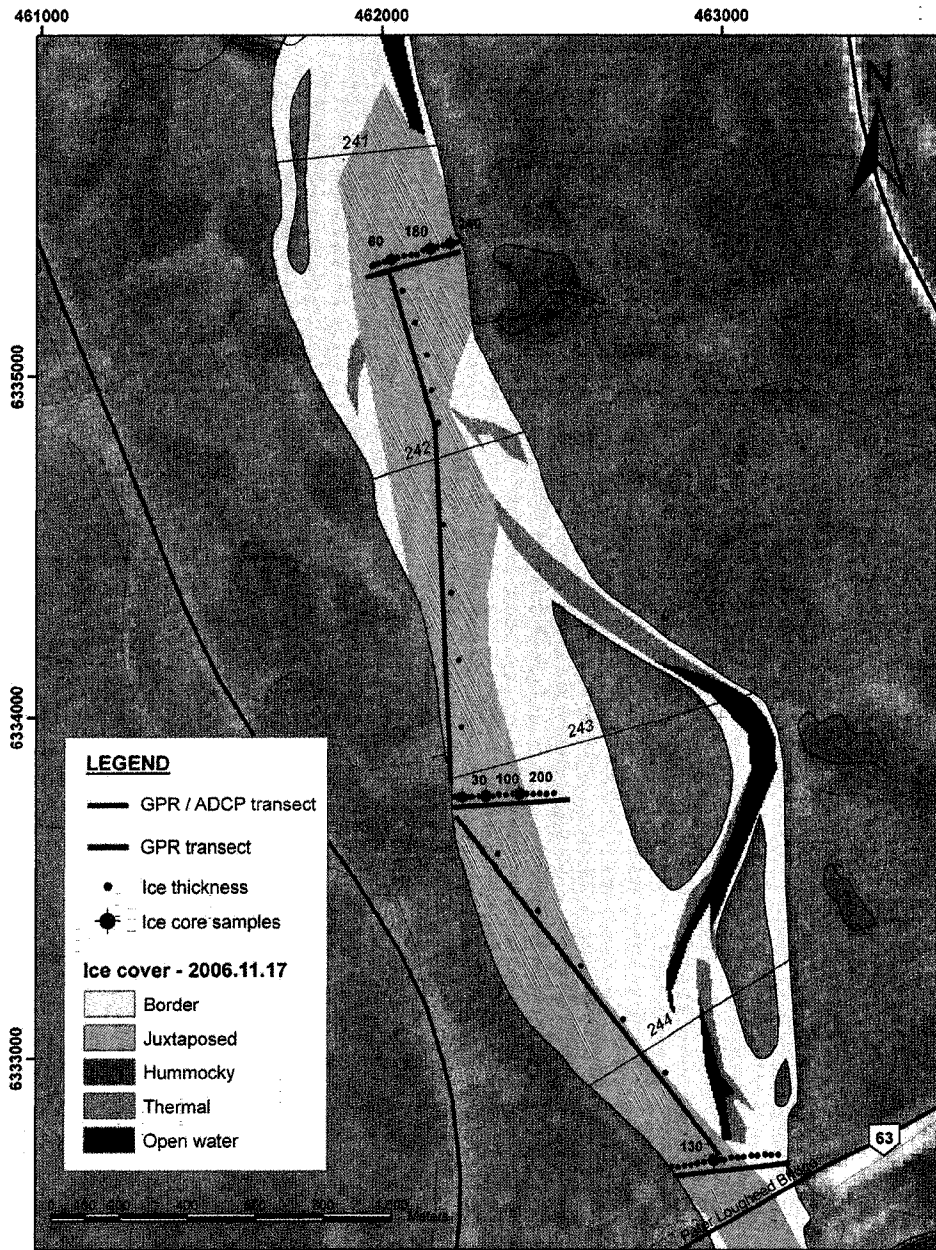


Figure 2.17 Location of ADCP, GPR, ice core samples and ice cover thickness measurements at CEMA Reach 1 – March 2007.

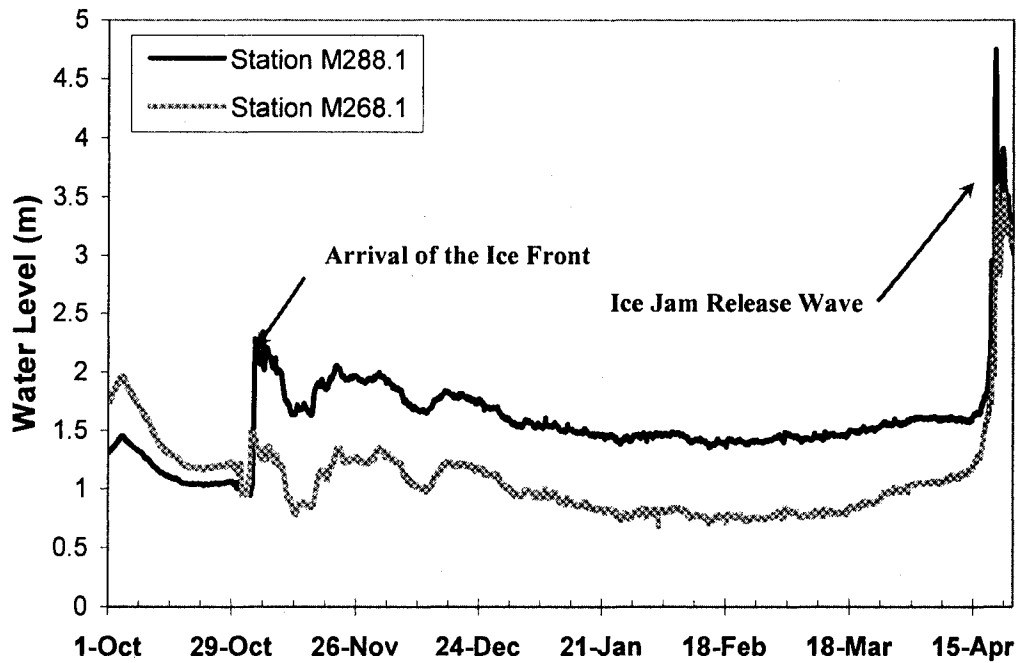


Figure 2.18 Measured Water Levels at Stations M288.1 and M268.1 – October 2006 to April 2007.

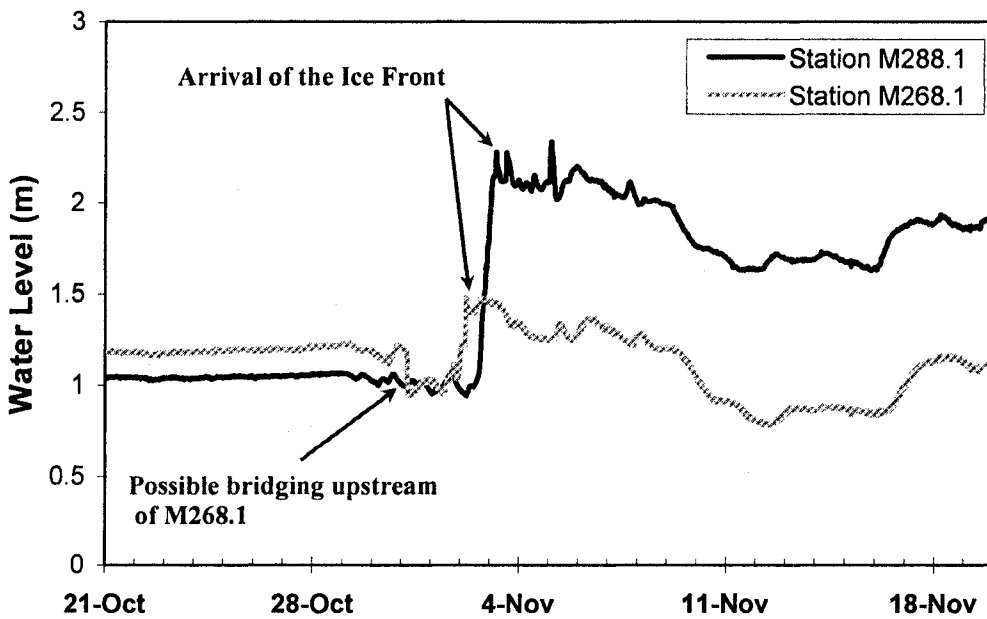


Figure 2.19 Measured water level fluctuation during ice cover formation at stations M288.1 and M268.1.

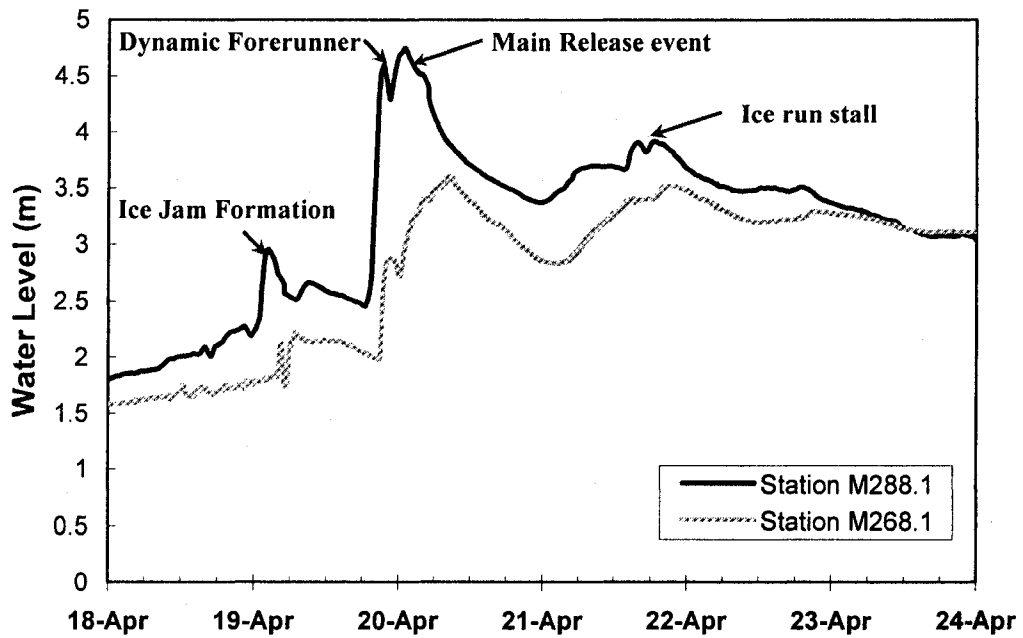


Figure 2.20 Measured ice jam release waves at stations M288.1 and M268.1 - April 2007.

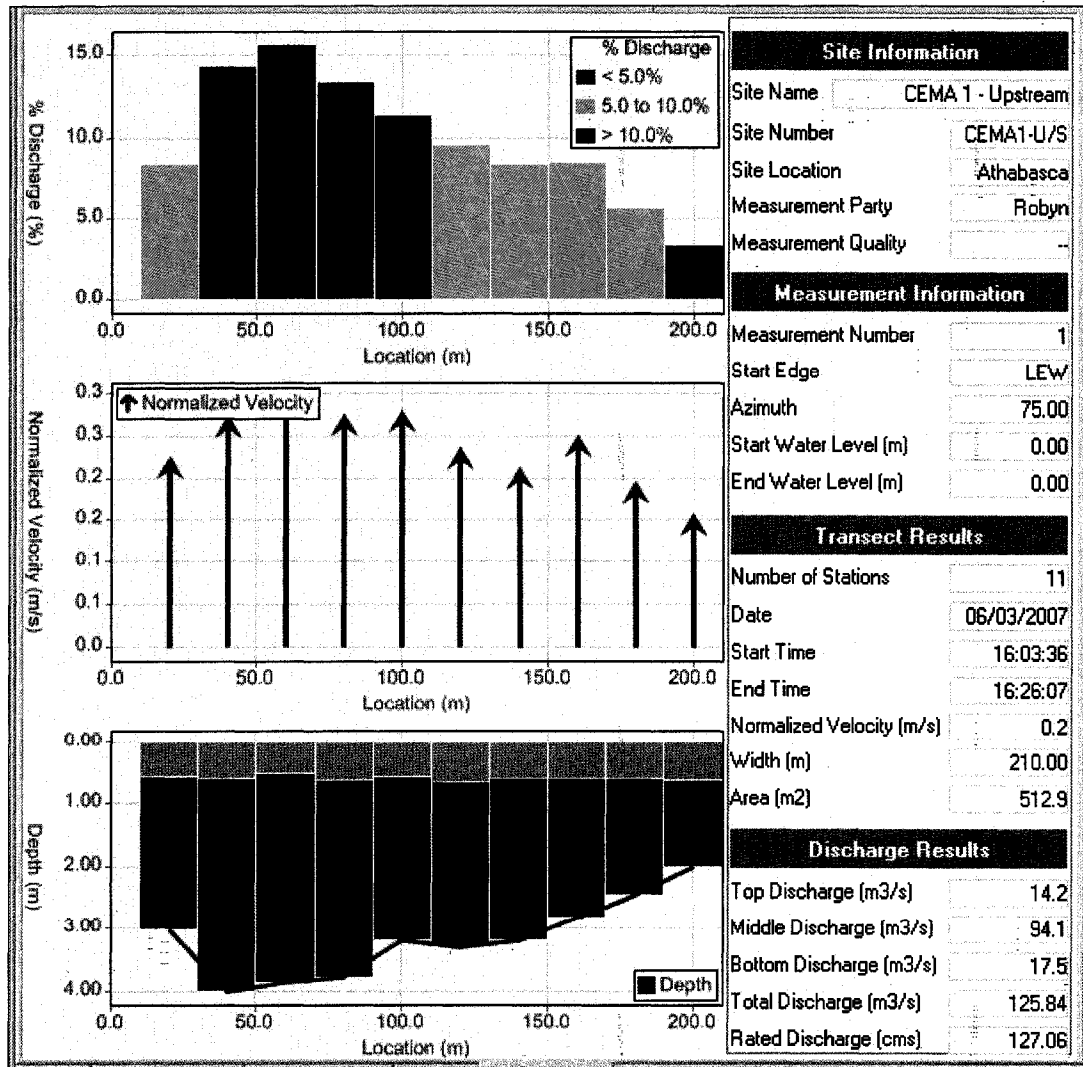


Figure 2.21 Discharge and velocities recorded with the ADCP at the upstream boundary of CEMA Reach 1 on March 6, 2007.

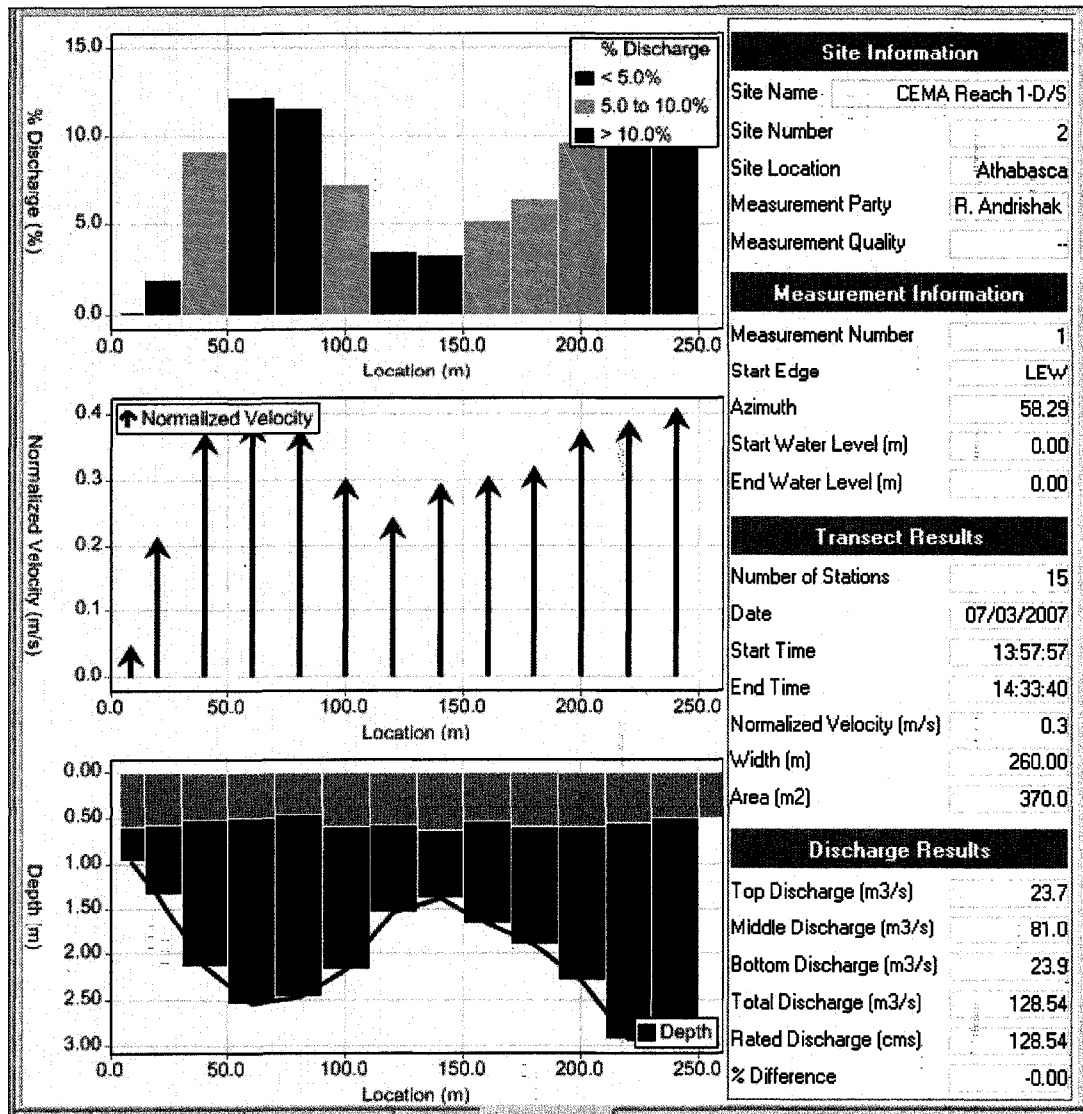


Figure 2.22 Discharge and velocities recorded with the ADCP at the downstream boundary of CEMA Reach 1 on March 6, 2007.

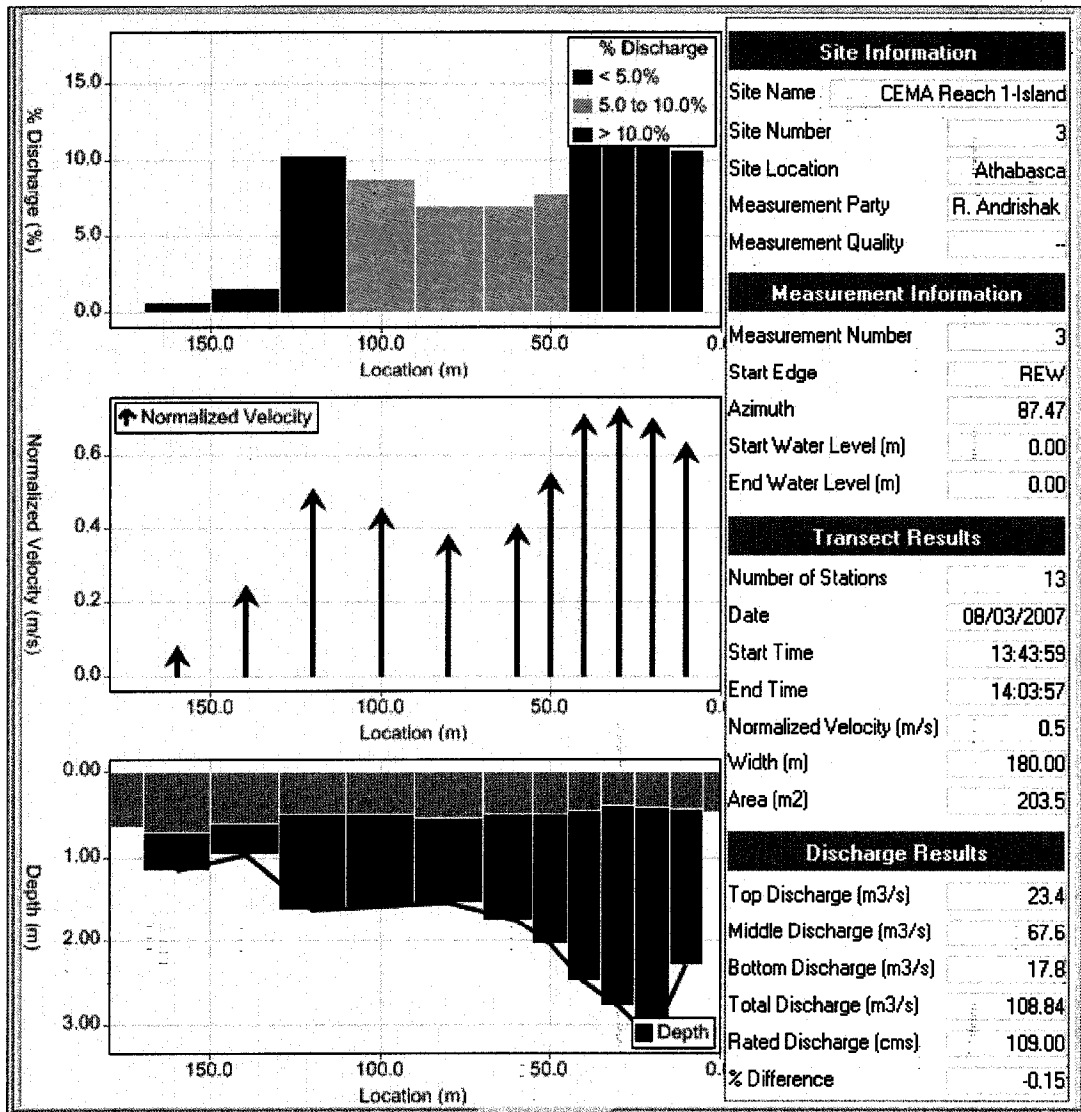


Figure 2.23 Discharge and velocities recorded with the ADCP at the island split section of CEMA Reach 1 on March 6, 2007.

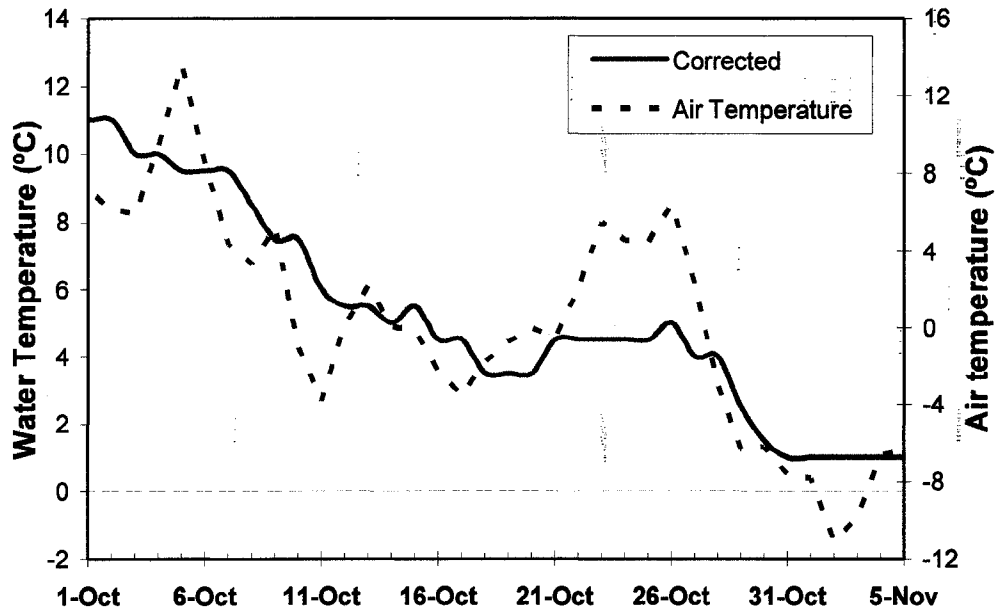


Figure 2.24 Water temperature variation during the 2006 freeze-up period recorded at the Town of Athabasca.

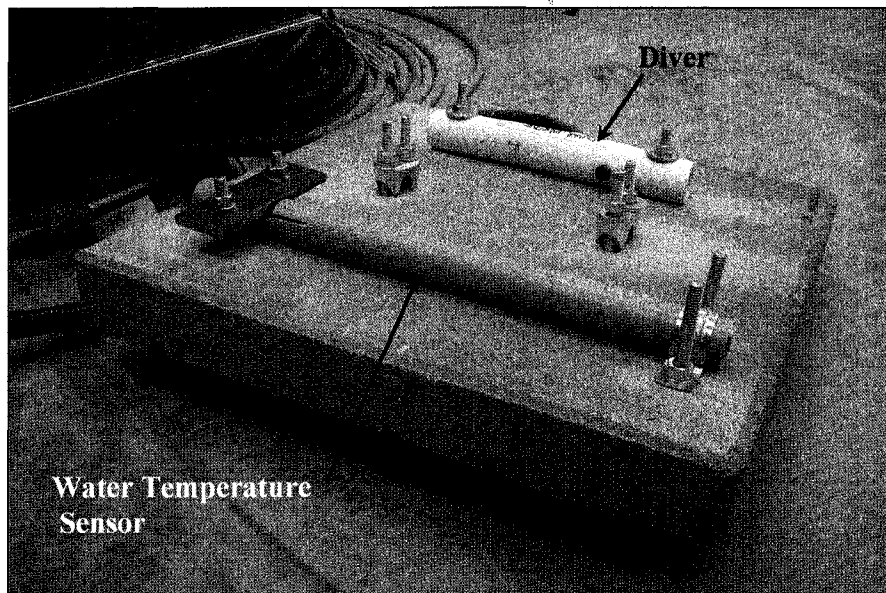
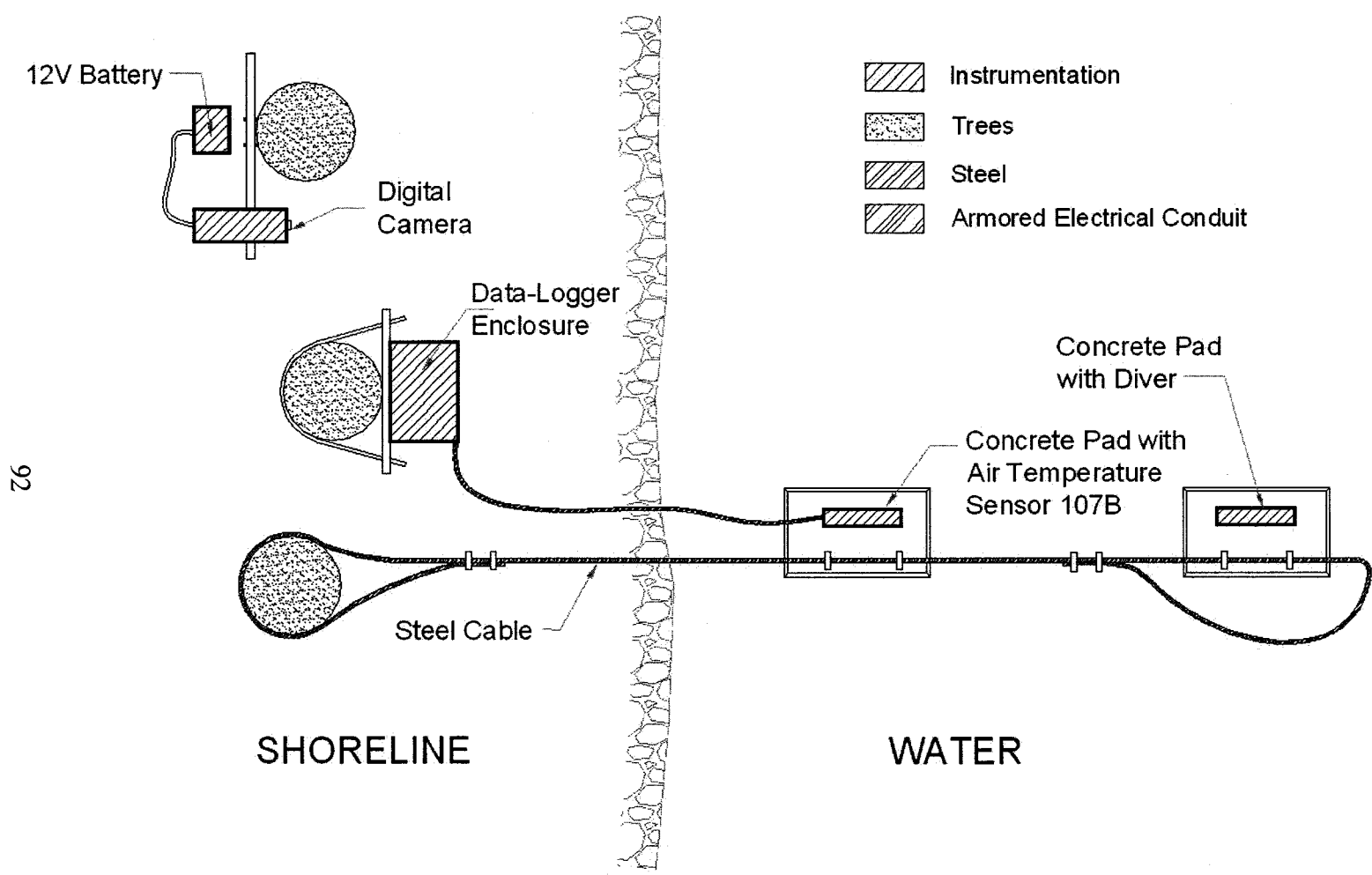


Figure 2.25 Concrete pad holding the air temperature sensor and the Diver prior to station installation.



92

Figure 2.26 Conceptual diagram of the typical monitoring station installation (separate concrete pads).

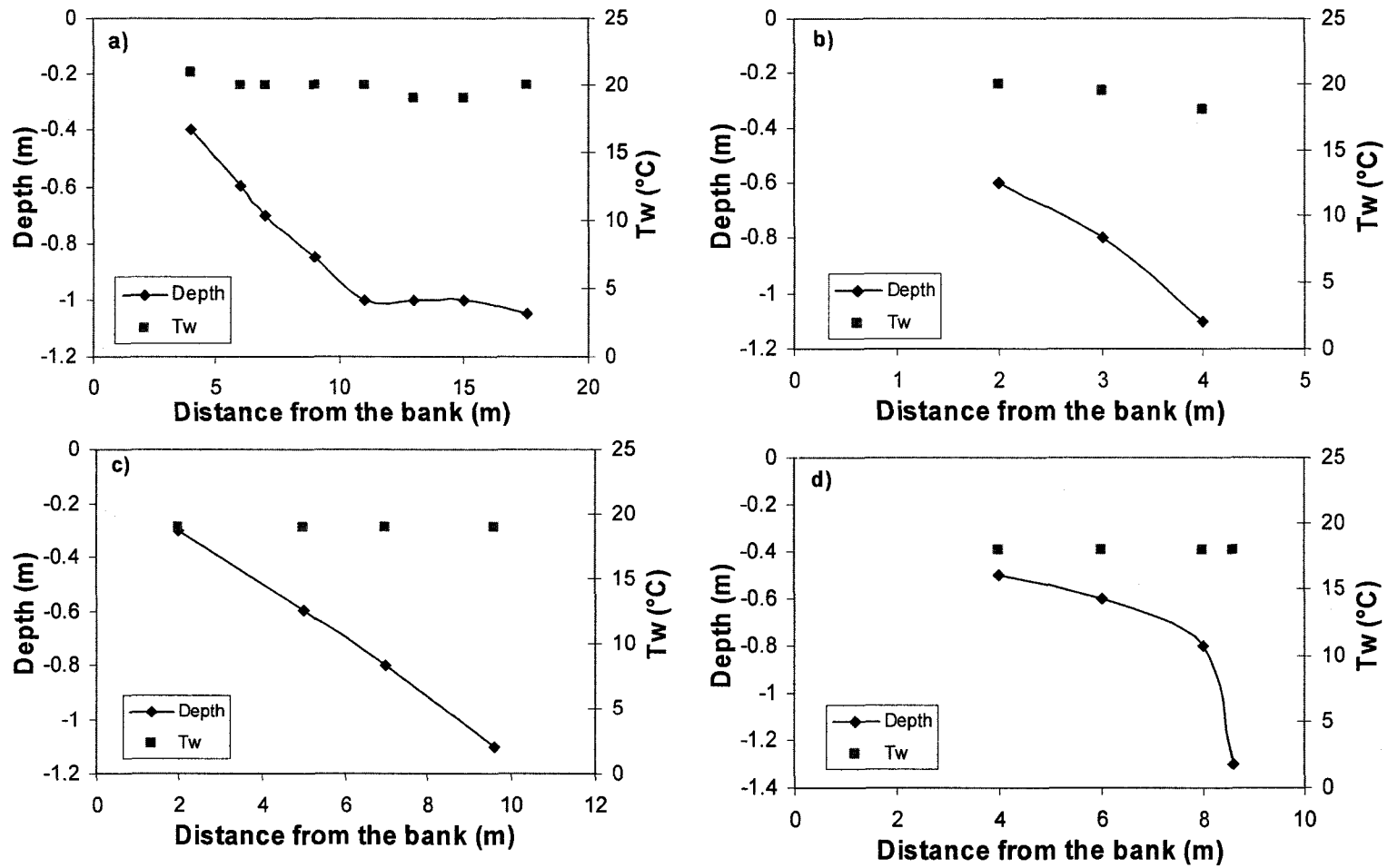


Figure 2.27 Manual water temperature measurements at stations a) M288.1, b) M268.1, c) M245.6 and d) 216.7 obtained in September 2006, prior to station installation.

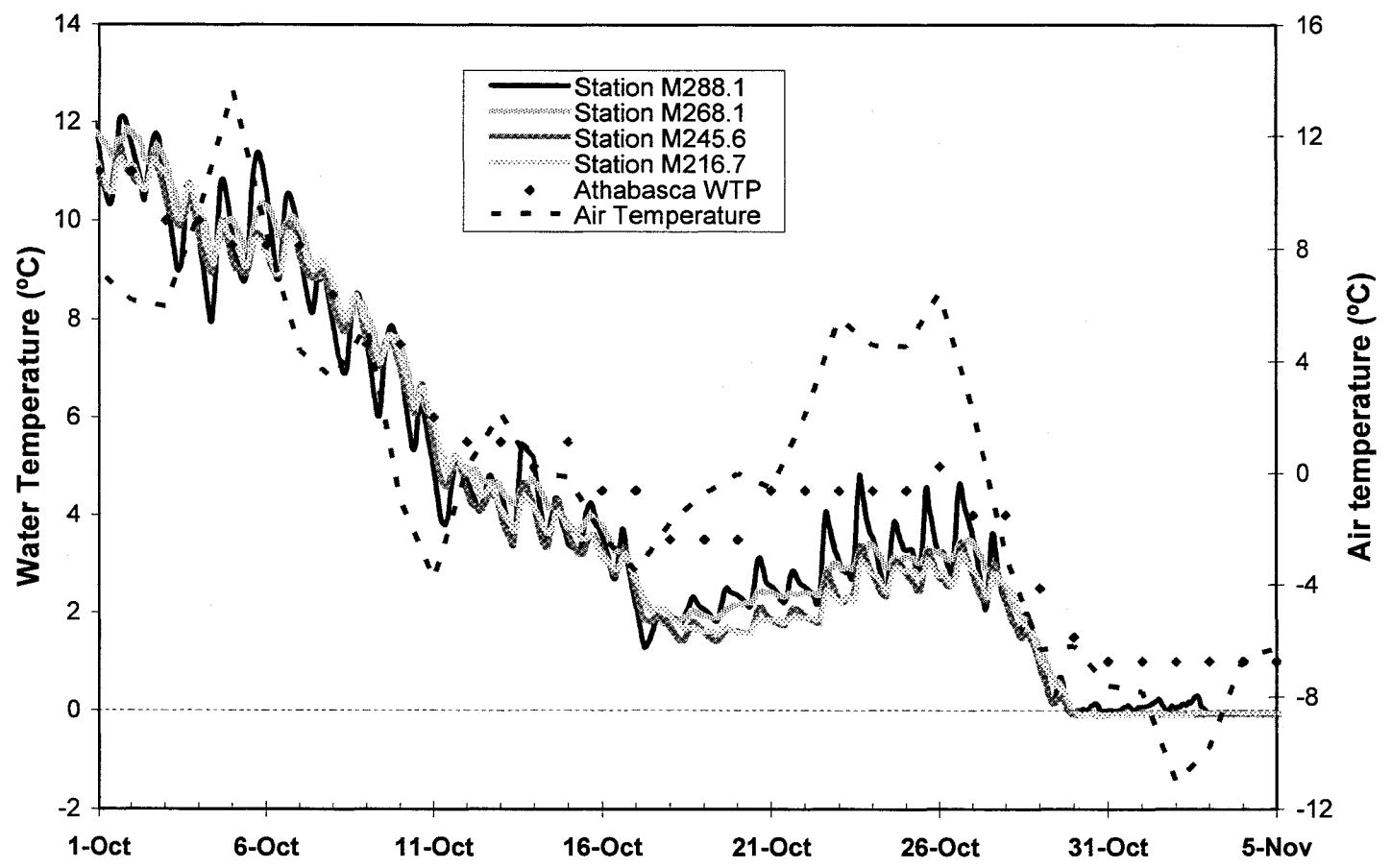


Figure 2.28 Water temperature variation data collected by the automated stations during the 2006 freeze-up period.

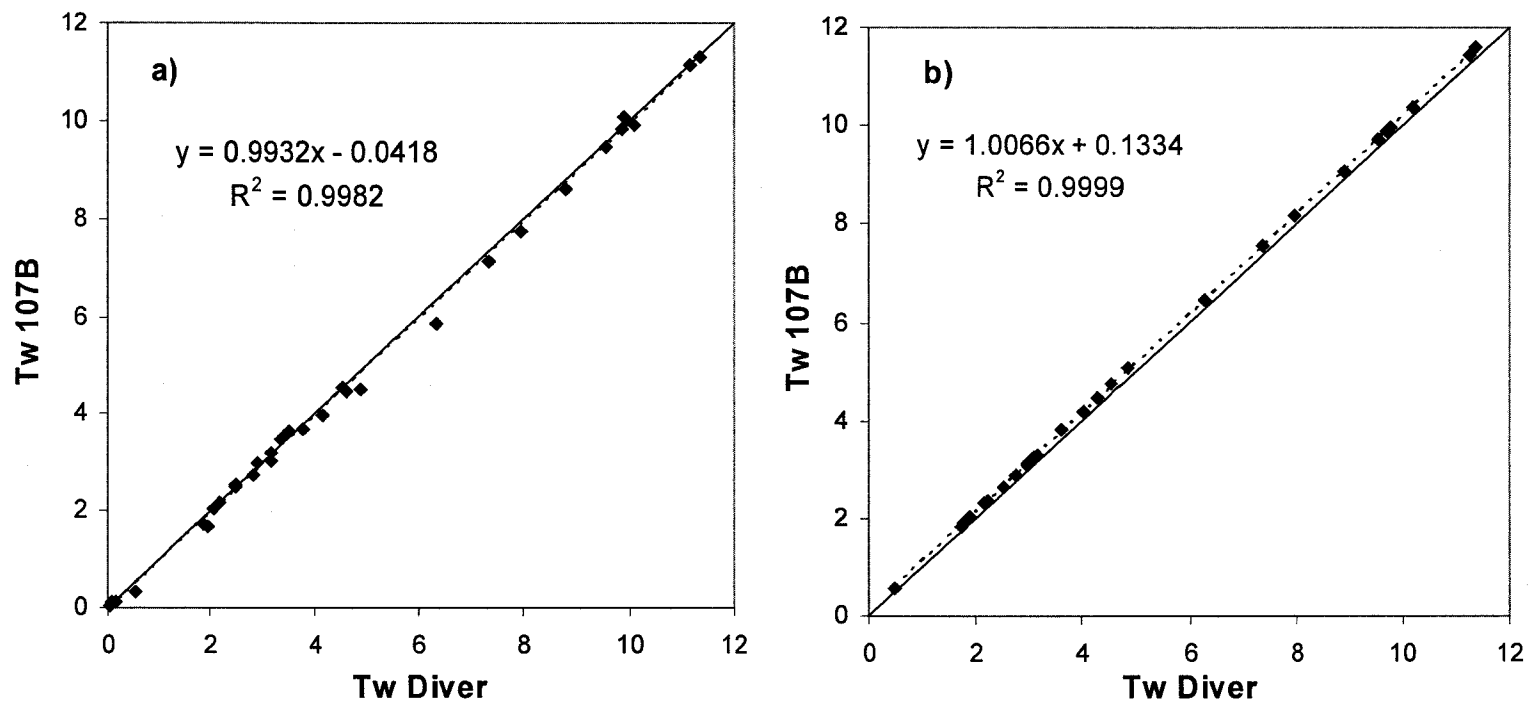


Figure 2.29 Mean daily water temperature recorded at a) station M288.1 and b) station M268.1 using Campbell Scientific 107B soil/water temperature probes and Van Essen Instruments Divers .

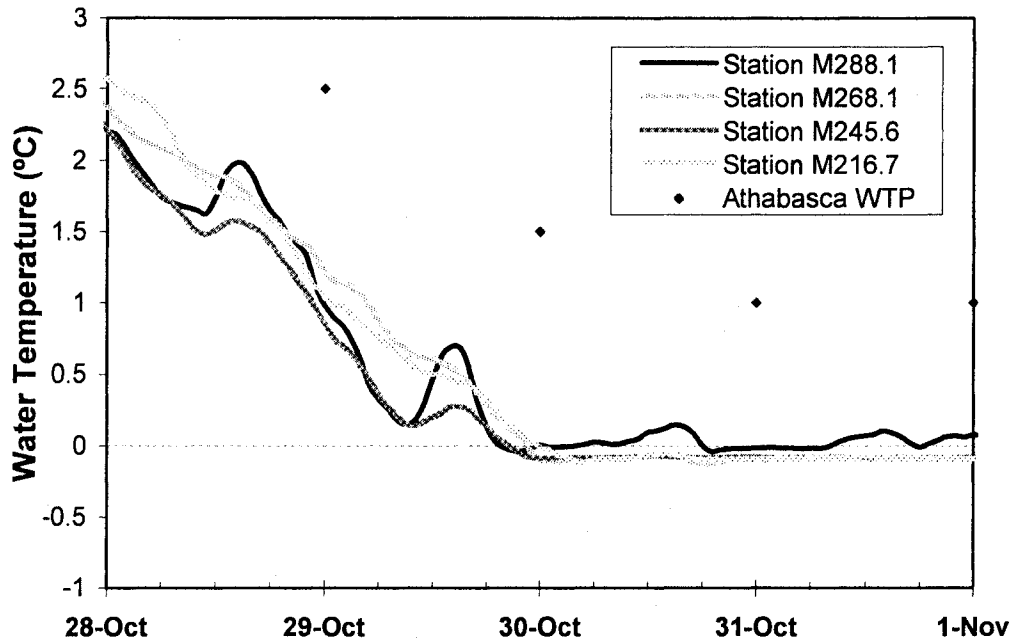


Figure 2.30 Arrival of the zero degree isotherm measured at all four monitoring stations.

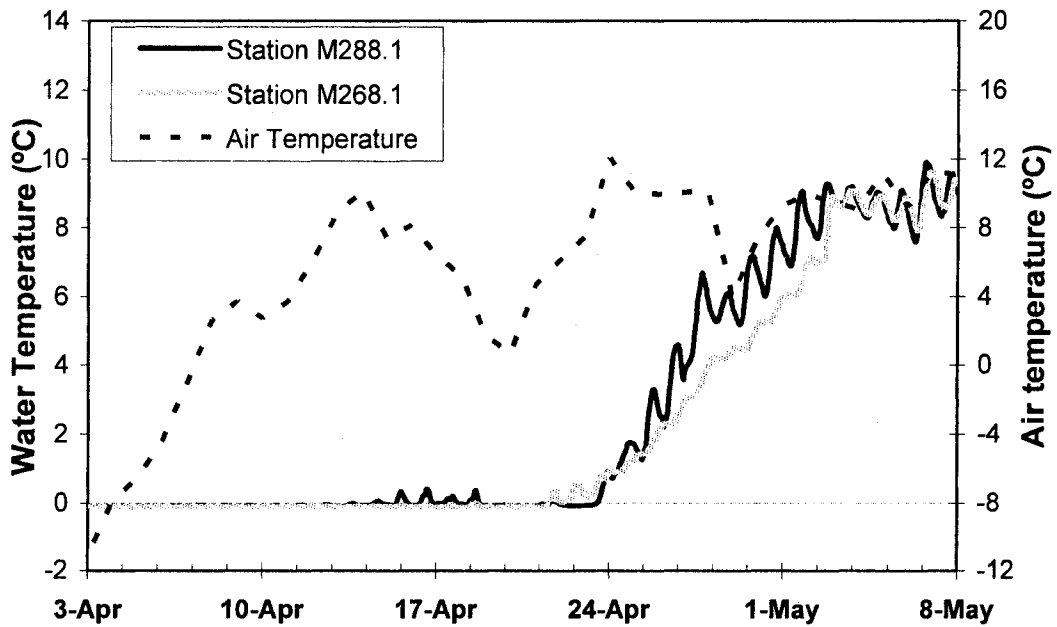


Figure 2.31 Water temperature variation data collected before, during and after breakup 2007 by station M288.1 and M268.1.

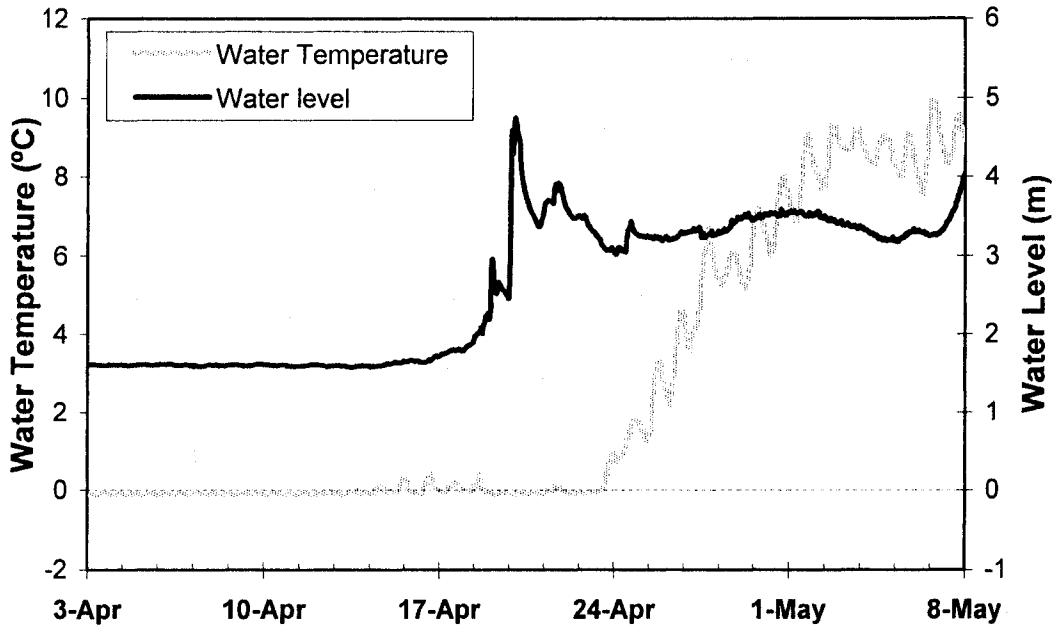


Figure 2.32 Water temperature and water level variation before, during and after breakup at river station M288.1.

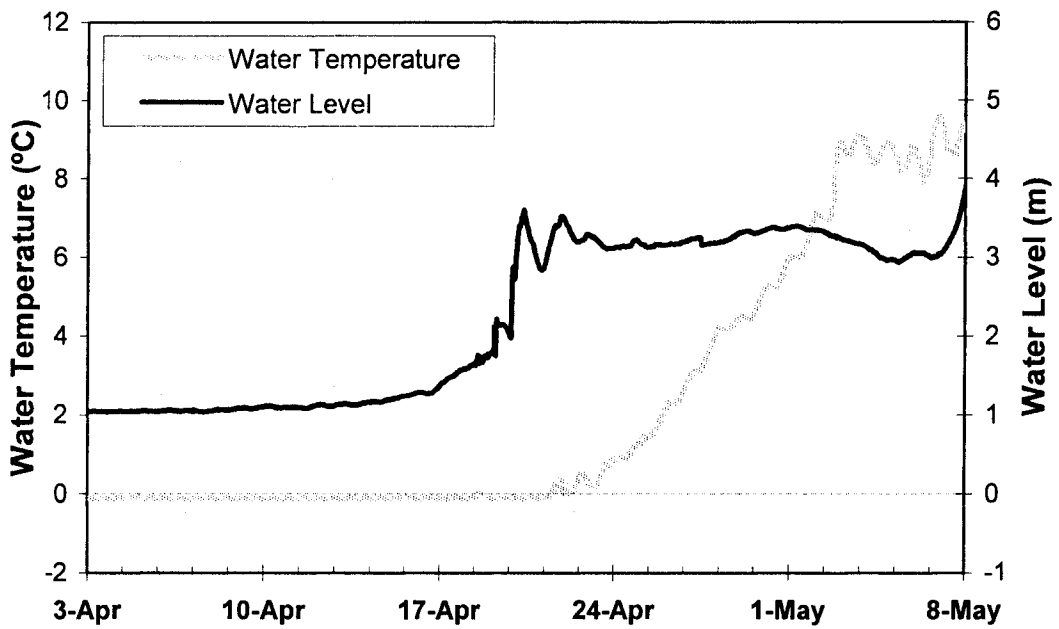


Figure 2.33 Water temperature and water level variation before, during and after breakup at river station M268.1.

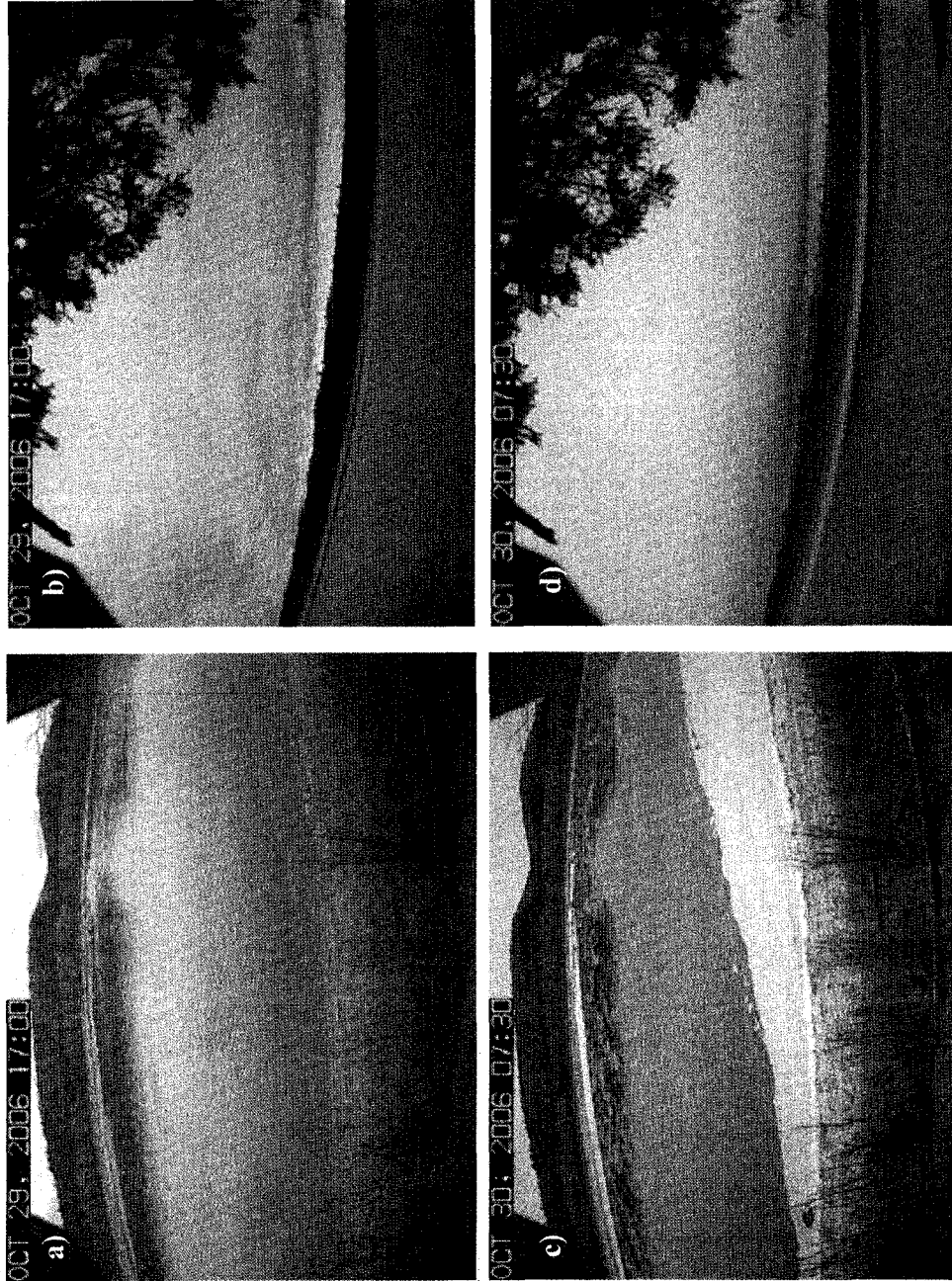


Figure 2.34 Overnight appearance of border ice and frazil floes as captured by the surveillance cameras at Stations M288.1 (a,c) and M216.7 (b,d).

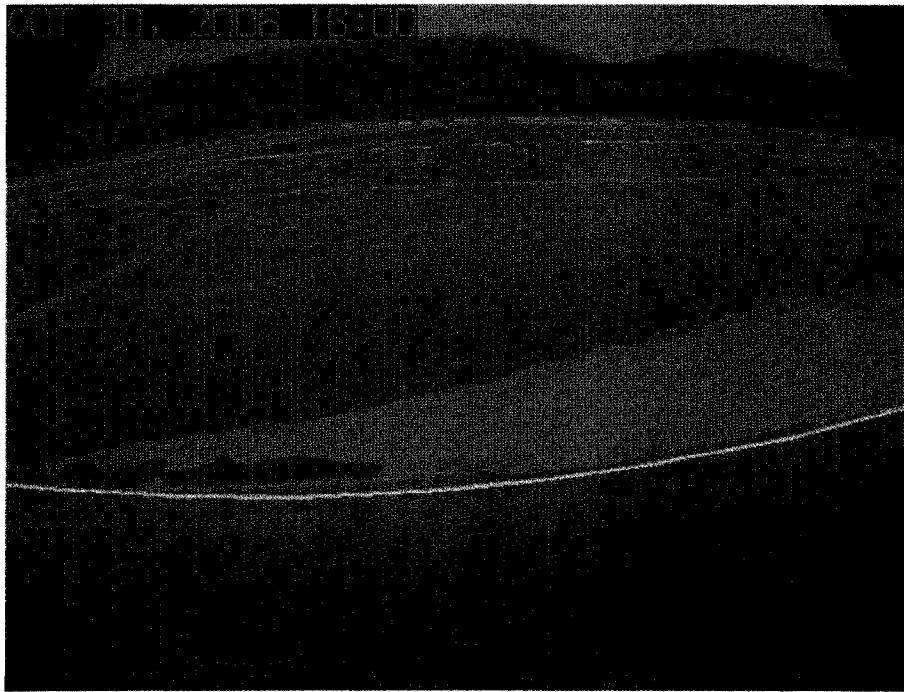


Figure 2.35 Superimposed grid created in CAD software to determine surface ice concentrations at station M288.1

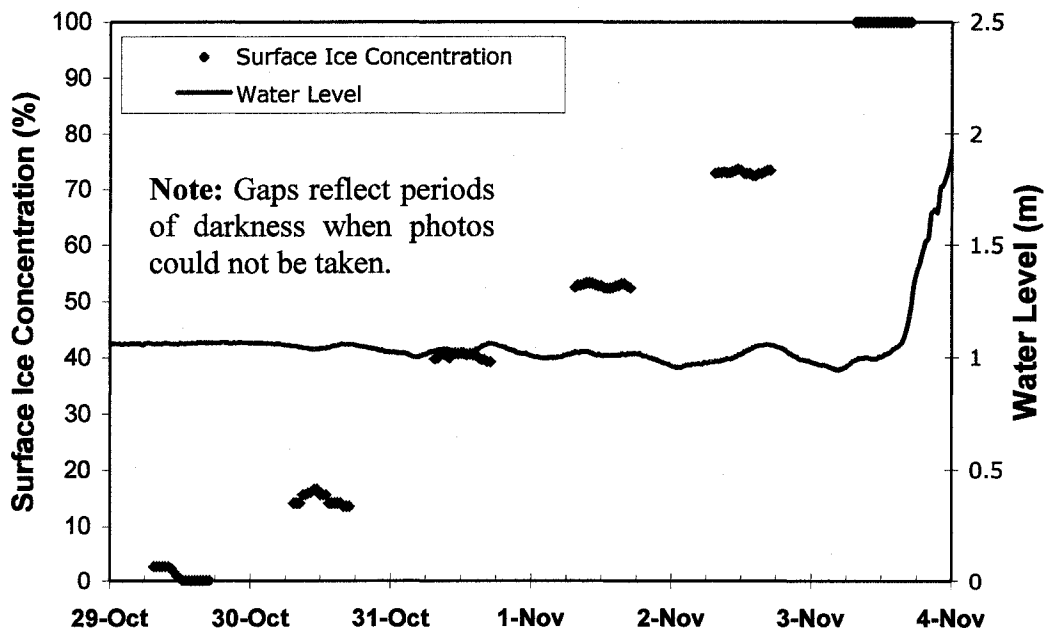


Figure 2.36 Surface ice concentration data at Station M288.1, as obtained from images captured by the surveillance camera.

100

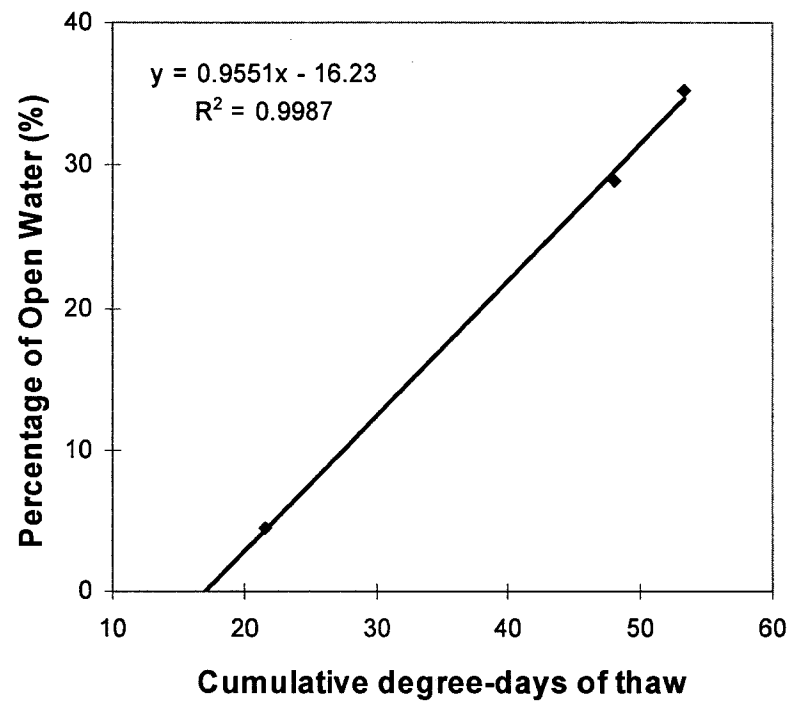
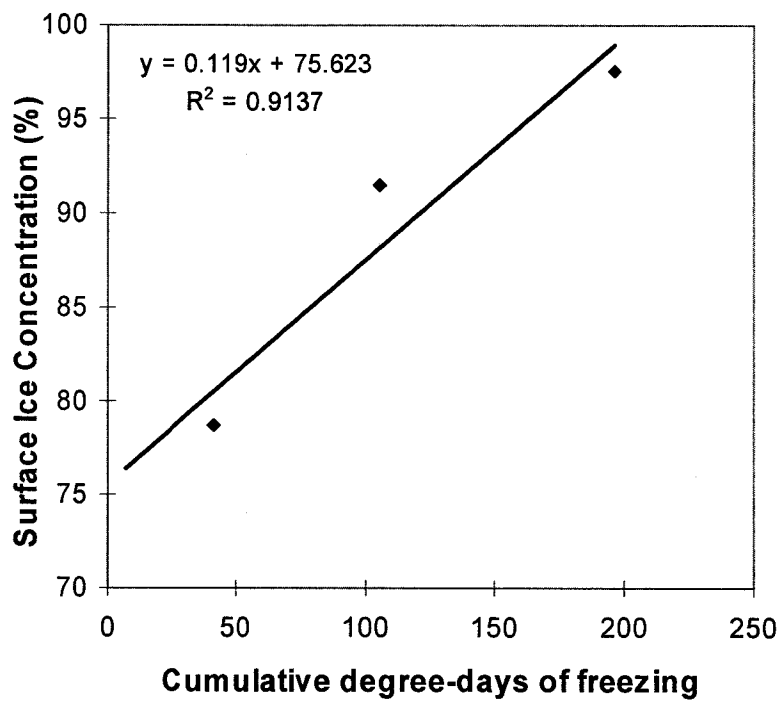


Figure 2.37 Relationship of cumulative degree-days of freezing and thaw, with percentage of surface ice concentration and open water, respectively.



Figure 2.37 Open leads in the vicinity of Willow Island as seen on November 5, 2006.



Figure 2.38 Open lead resulting from a warm water outfall near the Suncor Bridge, as seen on November 5, 2006.



Figure 2.39 **Appearance of frazil ice pans in an open lead. Thermal growth formations around islands and sand bars. November 5, 2006.**

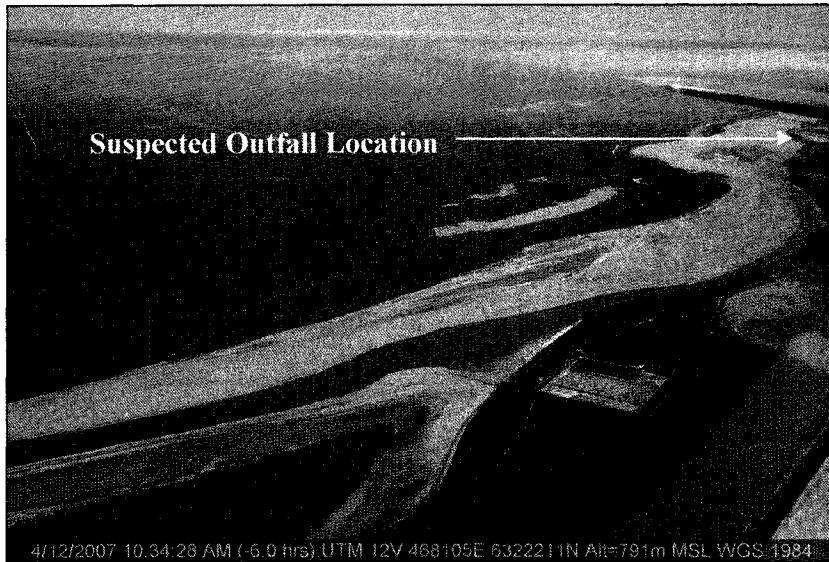


Figure 2.40 **Open lead generated downstream of Suncor Bridge. Thermal deterioration of the ice cover during breakup. April 12, 2006.**

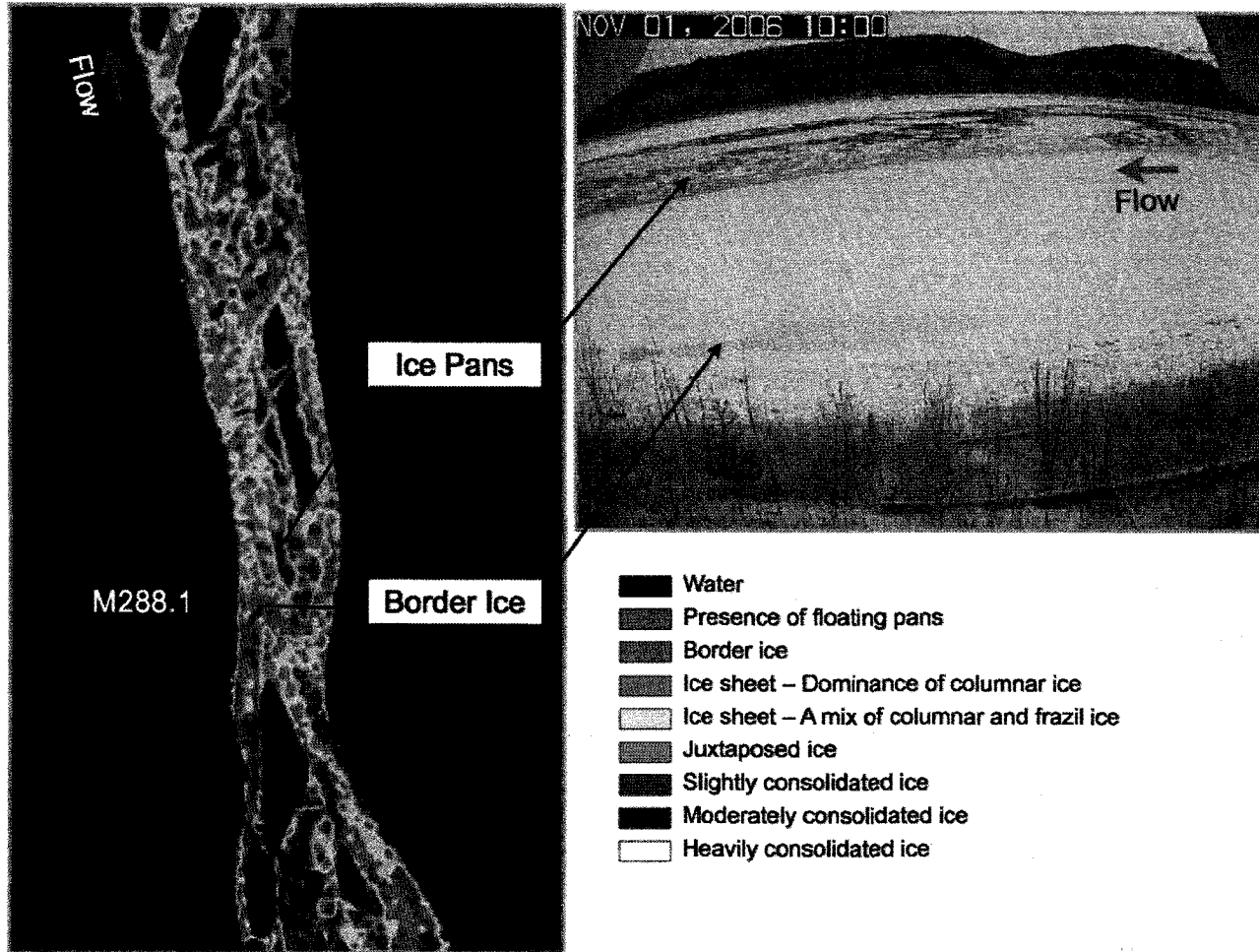


Figure 2.42 Ice cover classification of the RADARSAT SAR image taken on 1-Nov-06 (km 290 to 285) compared to the image recorded by the digital camera at station M288.1.

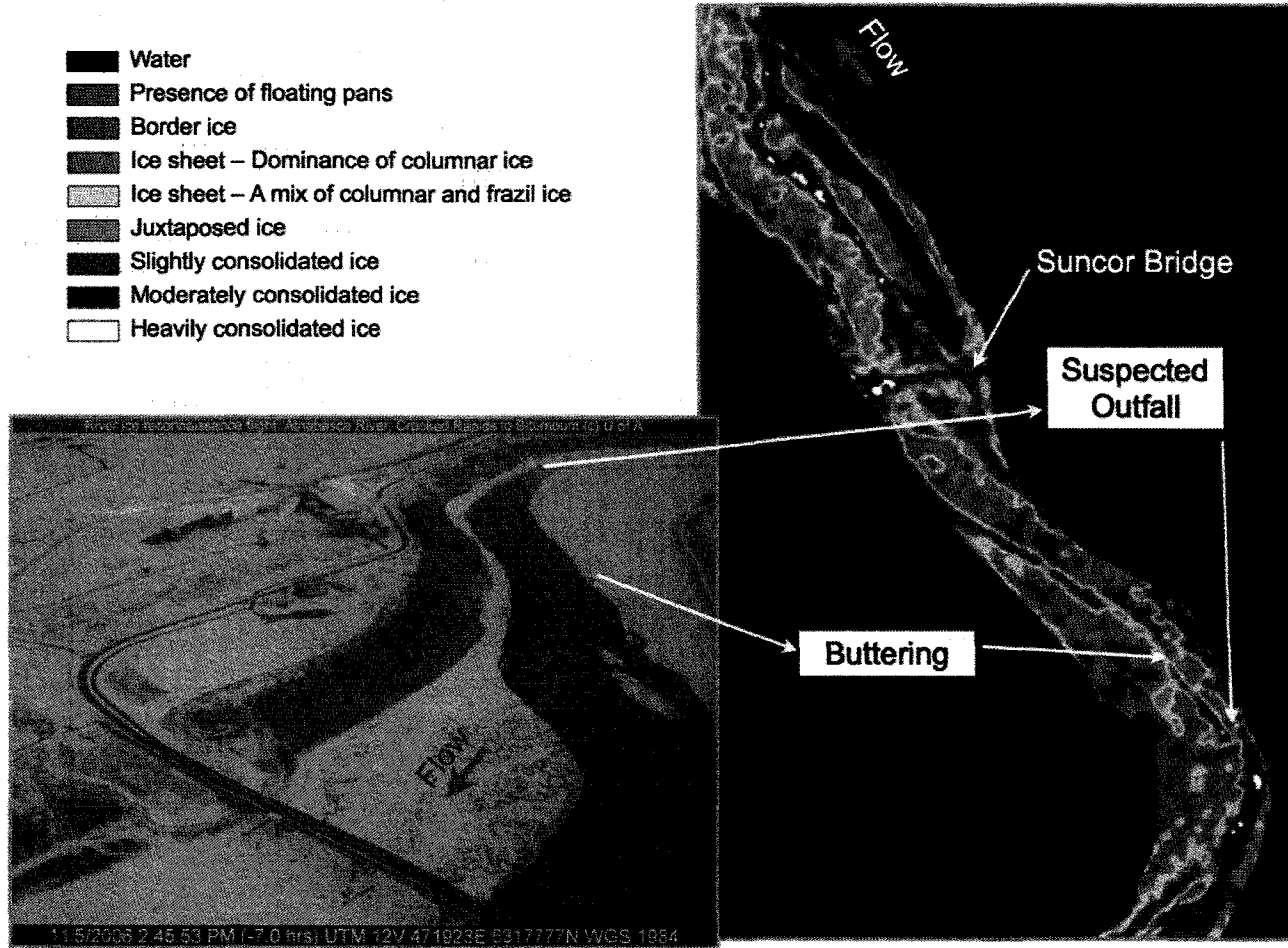


Figure 2.43 Ice cover classification of the RADARSAT SAR image taken on 01-Nov-06 (upstream of the Suncor Bridge), compared to observations during the surveillance flight undertaken on 05-Nov-07.

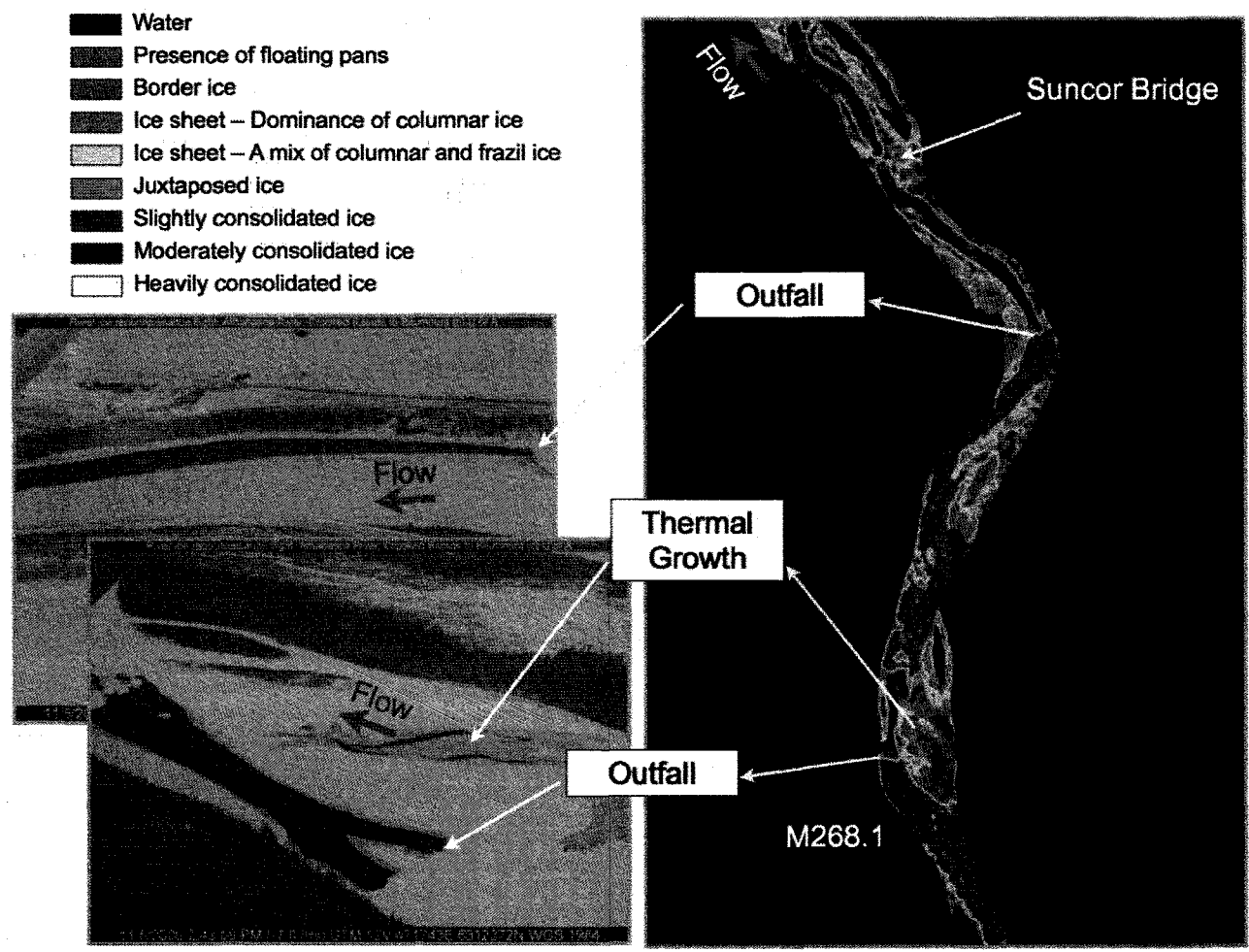


Figure 2.44 Suspected outfall locations near the Suncor Bridge seen during aerial surveillance and identified in ice cover classification of the RADARSAT SAR image taken on 05-Nov-06.

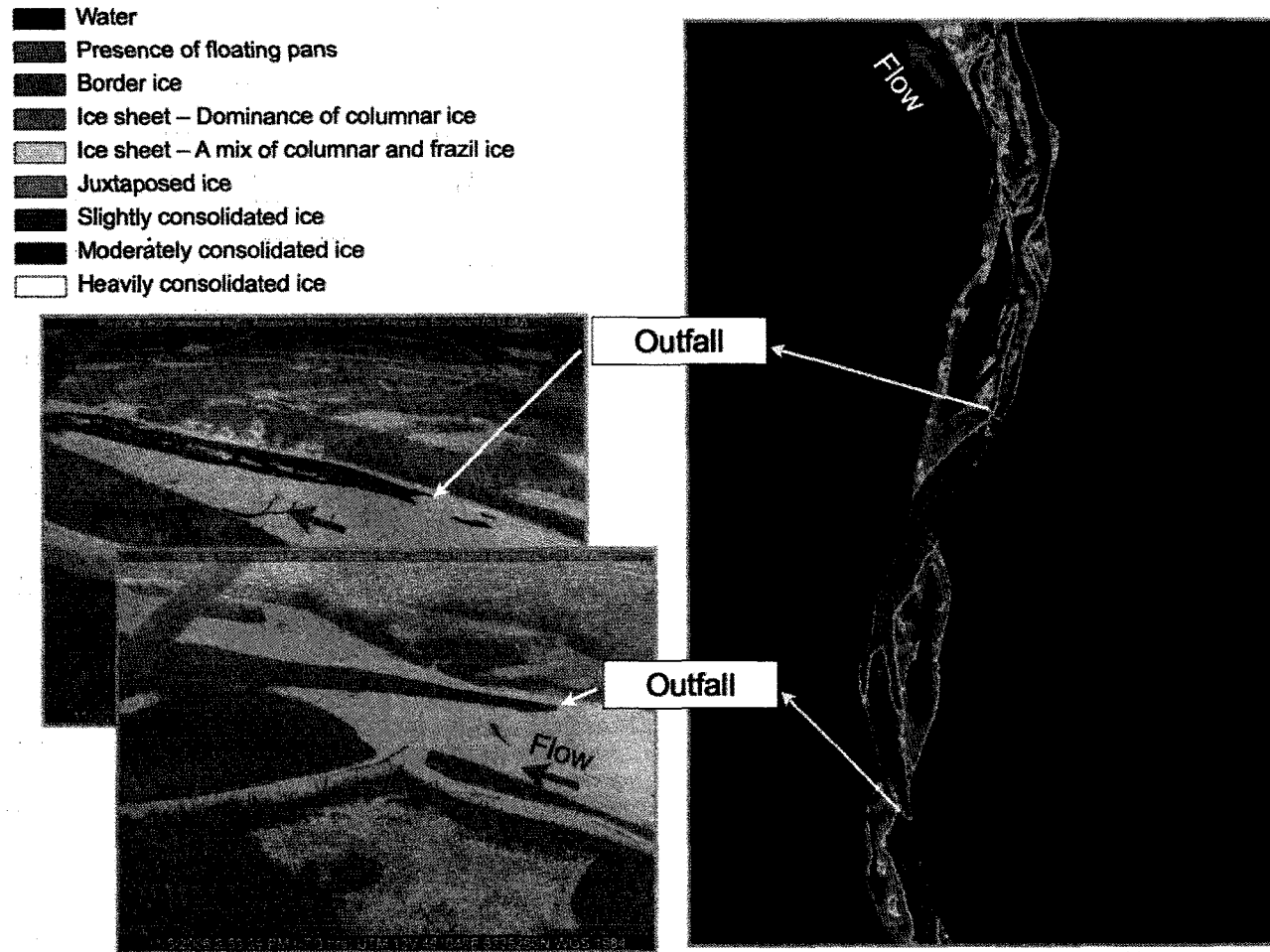


Figure 2.45 Suspected outfall locations downstream of Peter Lougheed Bridge seen during aerial surveillance and identified in ice cover classification of the RADARSAT SAR image taken on 05-Nov-06.

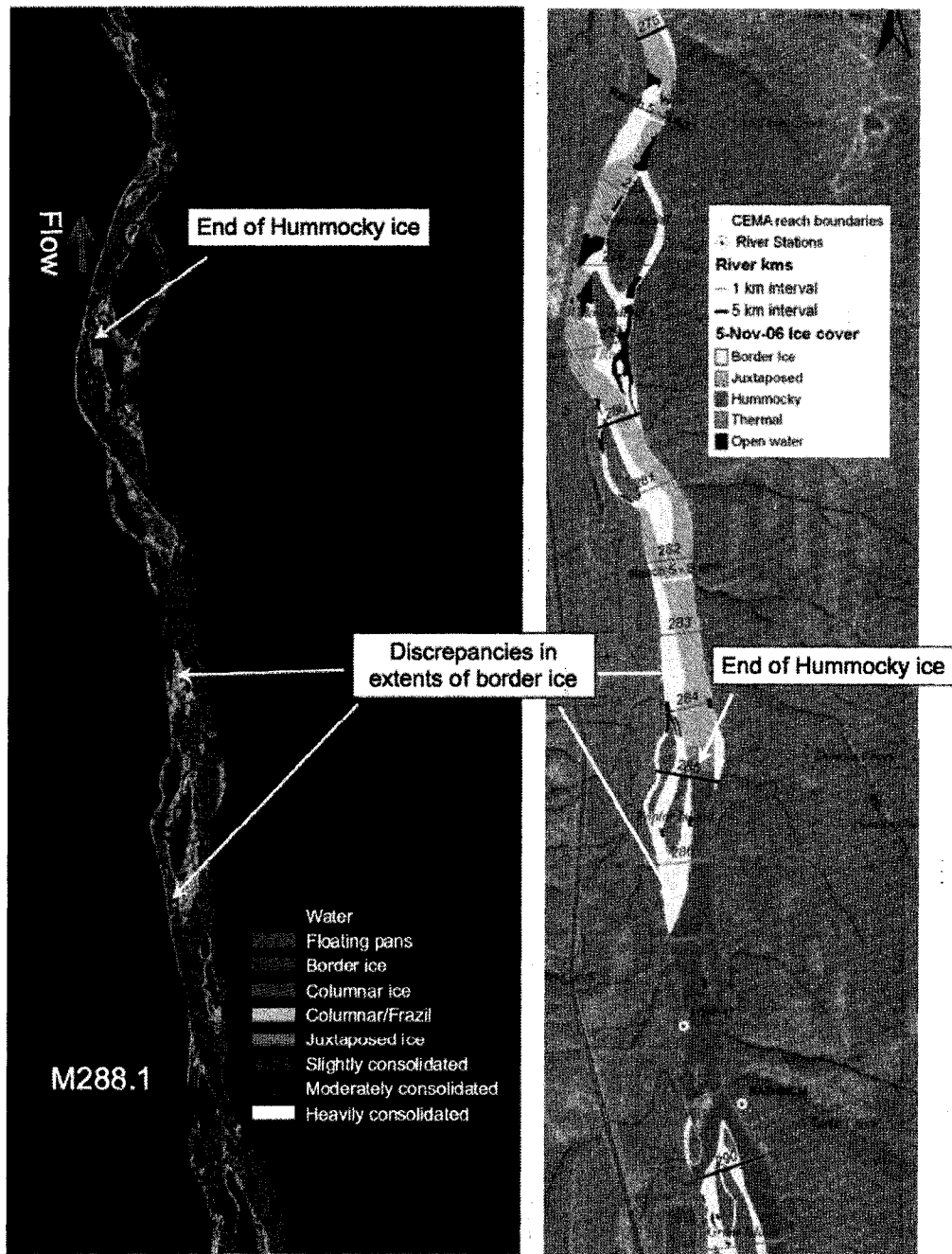


Figure 2.45 Discrepancies in ice cover classification near station M288.1, between satellite imagery (left) and aerial surveillance (right) – 05-Nov-06.

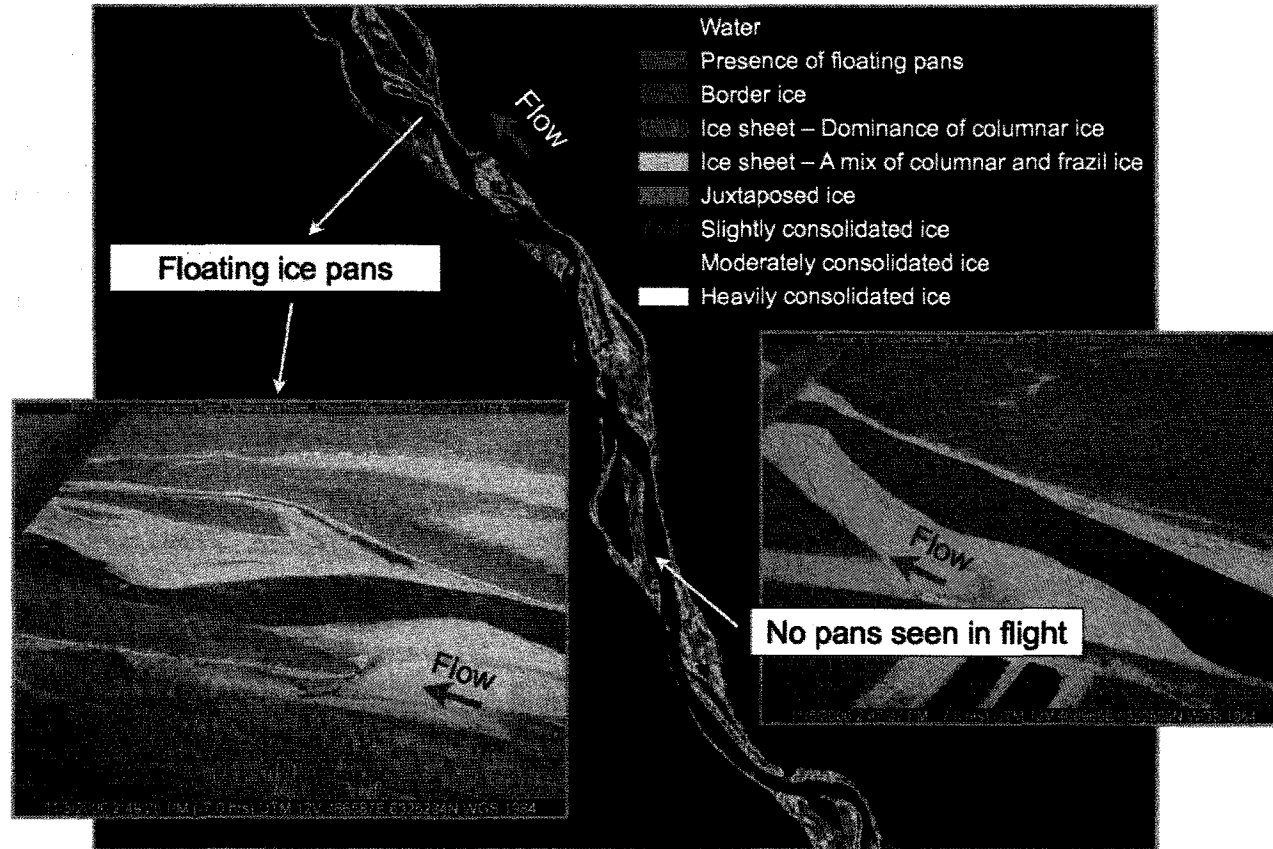


Figure 2.47 Presence of floating ice pans identified during aerial surveillance, compared to the RADARSAT SAR image taken on 05-Nov-06 (km 261 to 253).

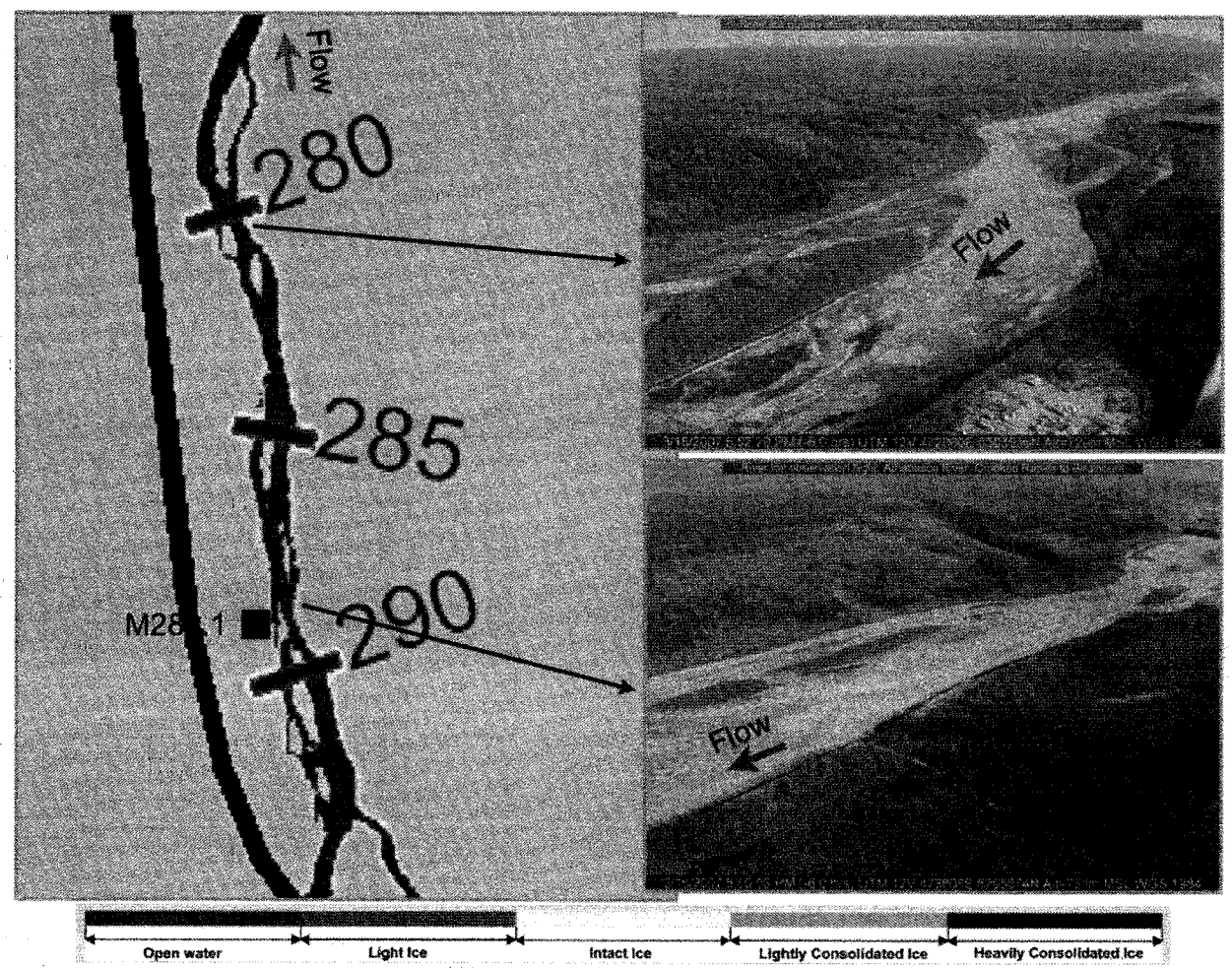


Figure 2.48 Ice cover classification of the RADARSAT SAR image taken on 15-Apr-07 (km 293 to 276), compared to observations during the surveillance flight undertaken on 16-Apr-07.

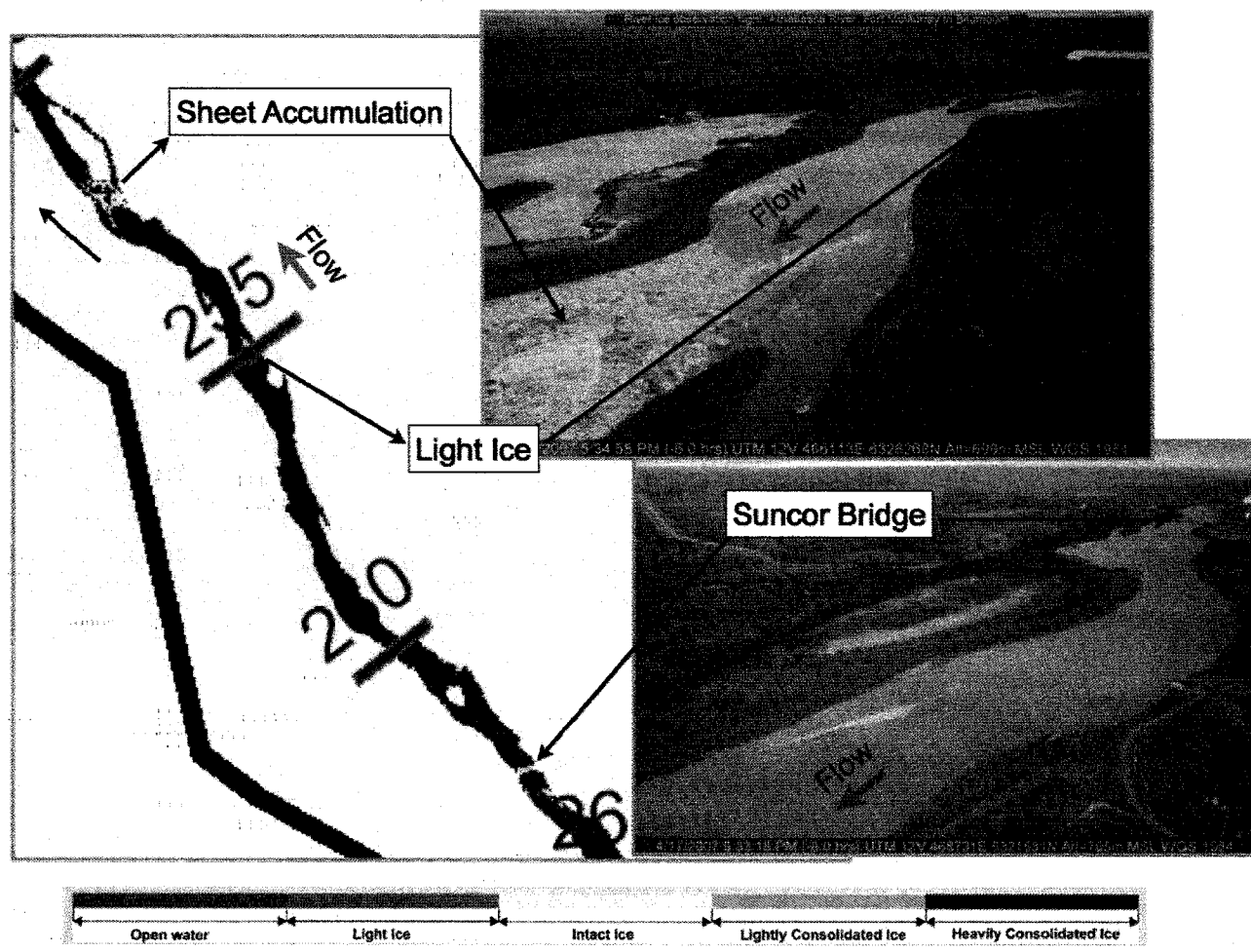


Figure 2.49 Ice cover classification of the RADARSAT SAR image taken on 18-Apr-07 (km 265 to 250), compared to observations during the surveillance flight undertaken on 17-Apr-07.

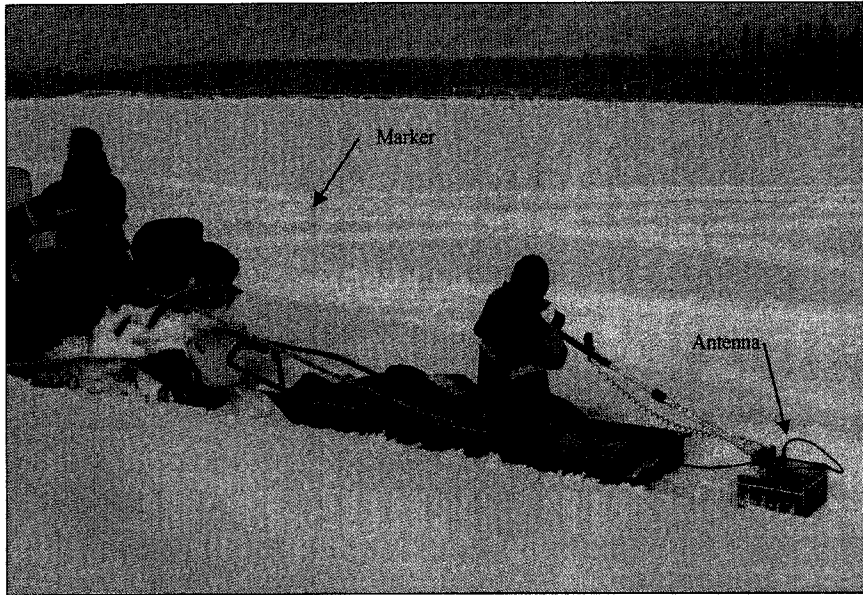


Figure 2.49 Use of a snowmobile to tow the GPR antenna along the ice cover.

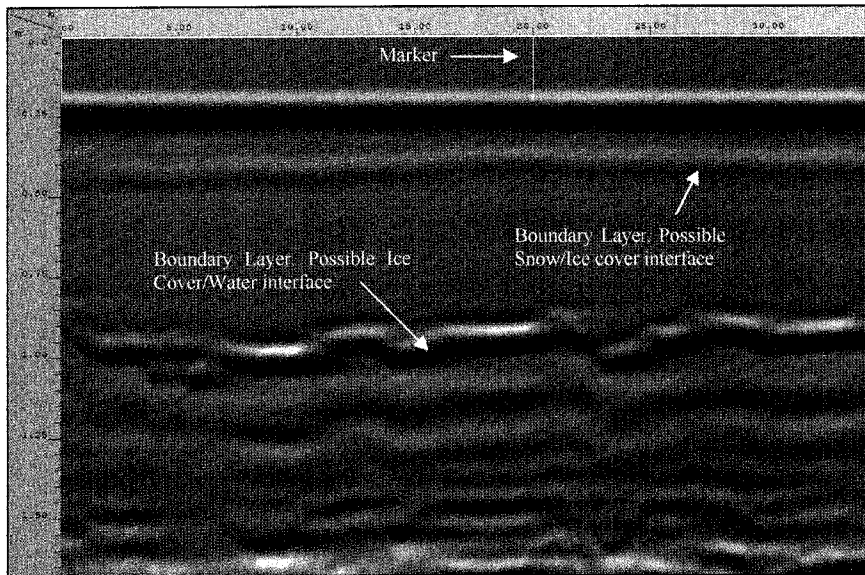


Figure 2.50 2-D scan display line acquired at the downstream boundary of CEMA Reach 4 - 900 MHz antenna.

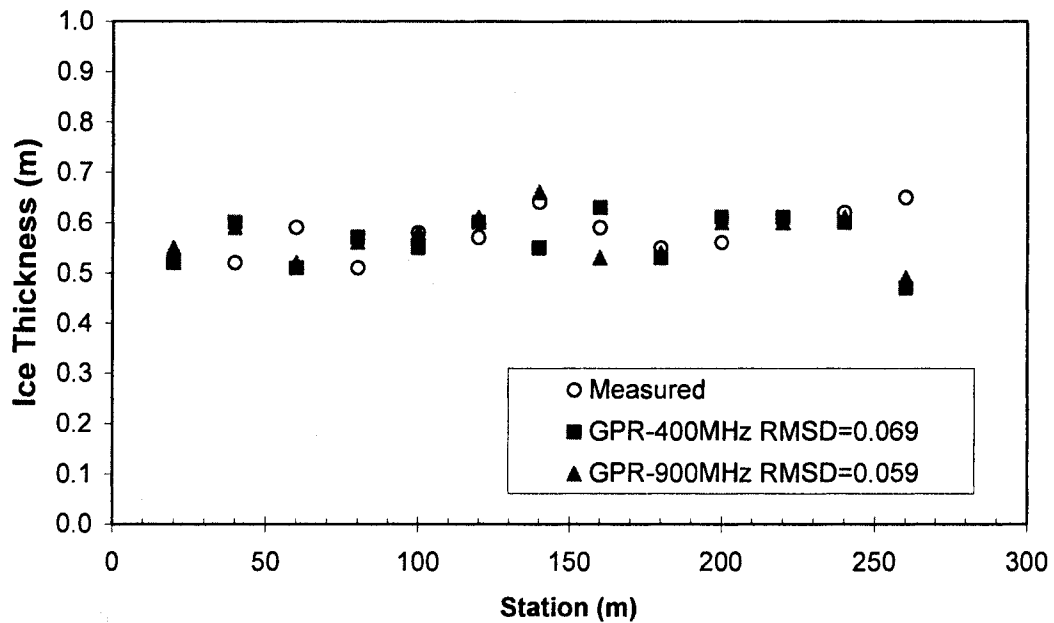


Figure 2.52 Thickness of the ice cover as obtained from GPR scans compared to measured values at the upstream boundary of CEMA Reach 1 (Transect 1).

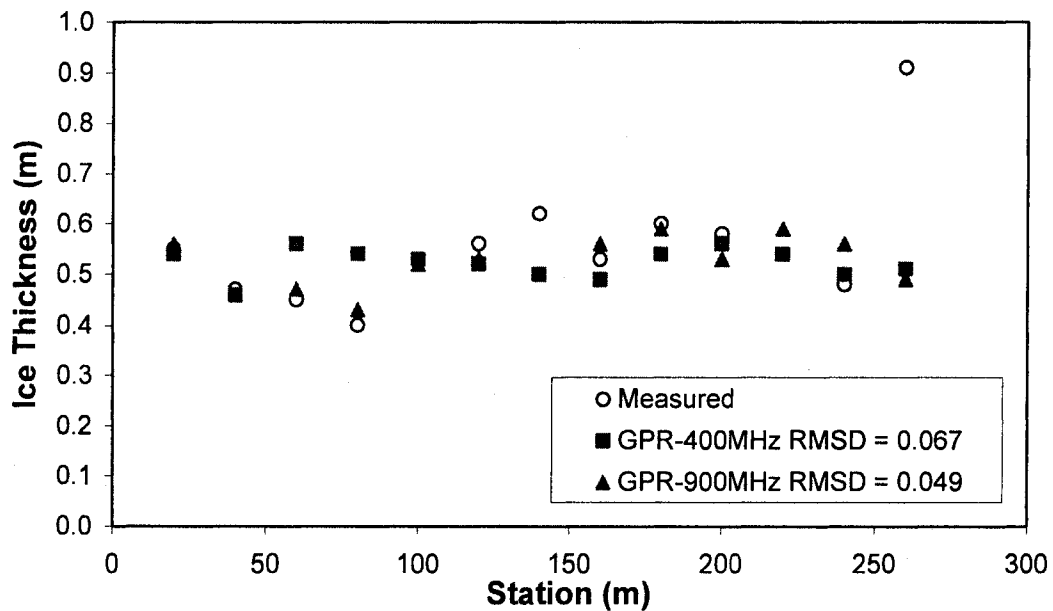


Figure 2.53 Thickness of the ice cover as obtained from GPR scans compared to measured values at the downstream boundary of CEMA Reach 1 (Transect 2).

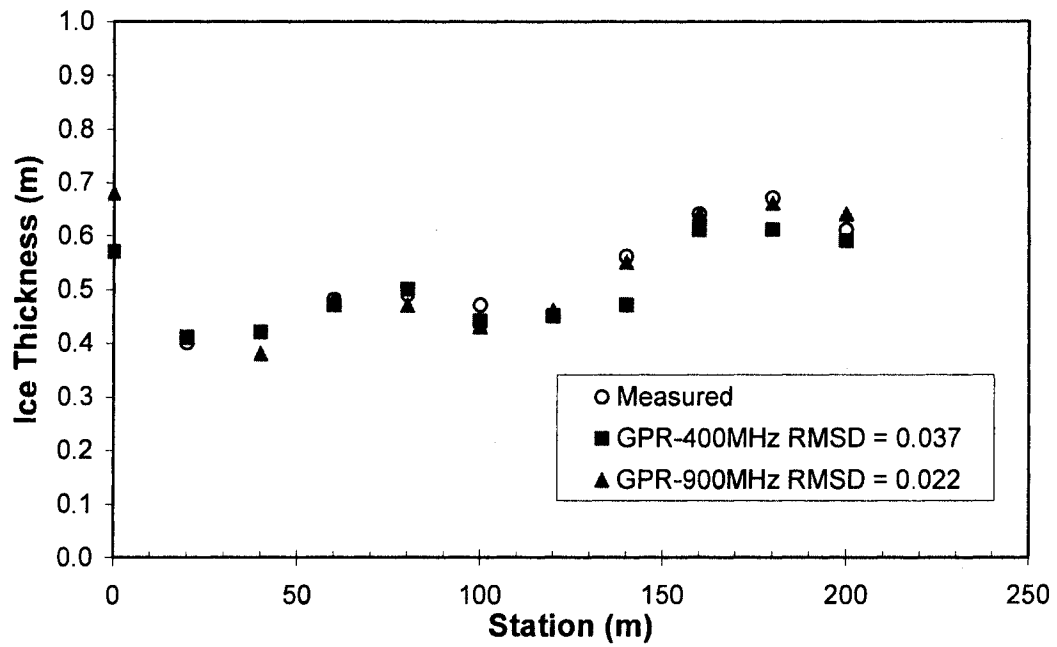


Figure 2.54 Thickness of the ice cover as obtained from GPR scans compared to measured values at the split section of CEMA Reach 1 (Transect 3).

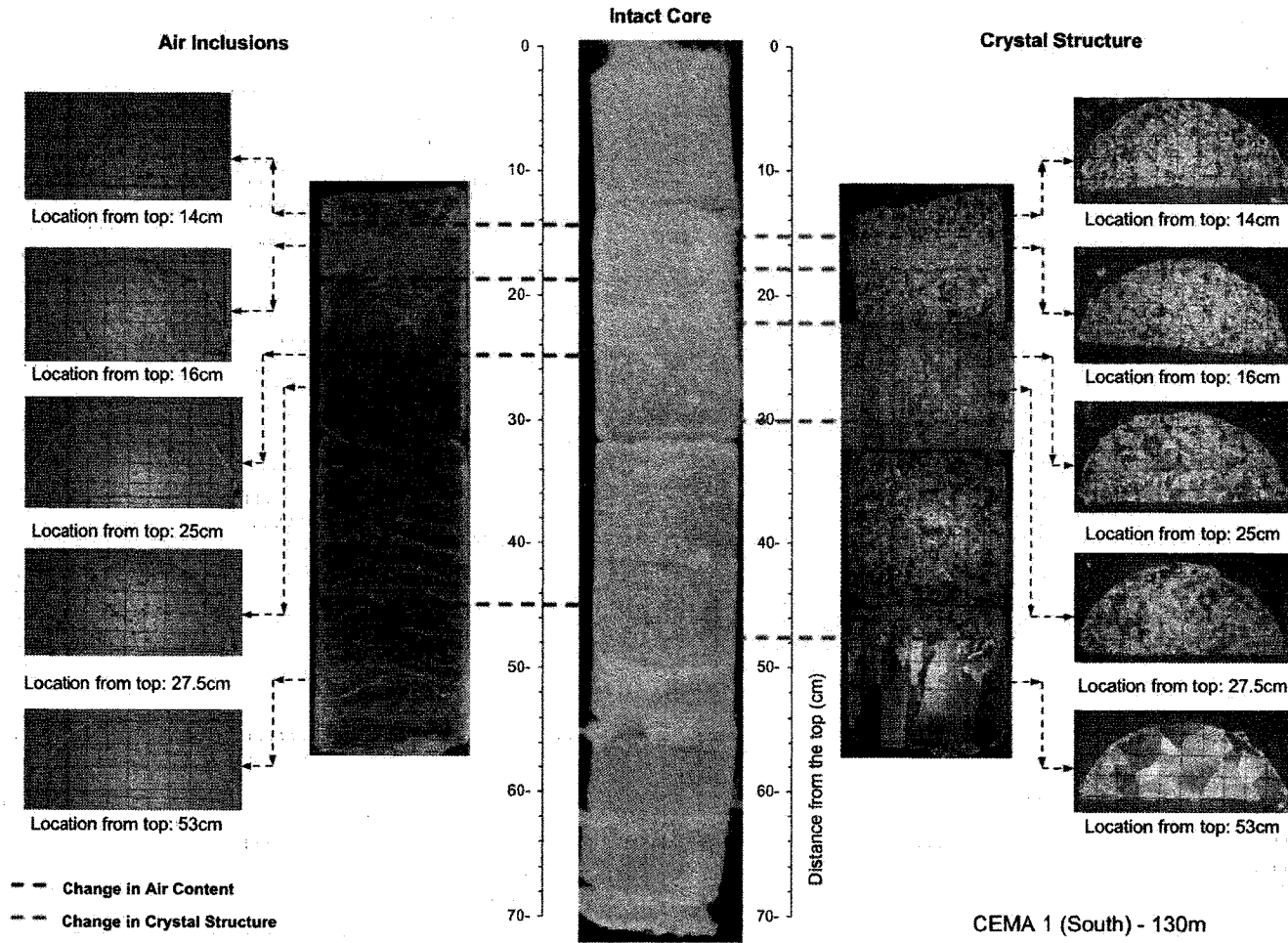


Figure 2.55 Air inclusions and crystal structure analysis of core sample obtained at the upstream boundary of CEMA Reach 1 – 130 m from the west bank.

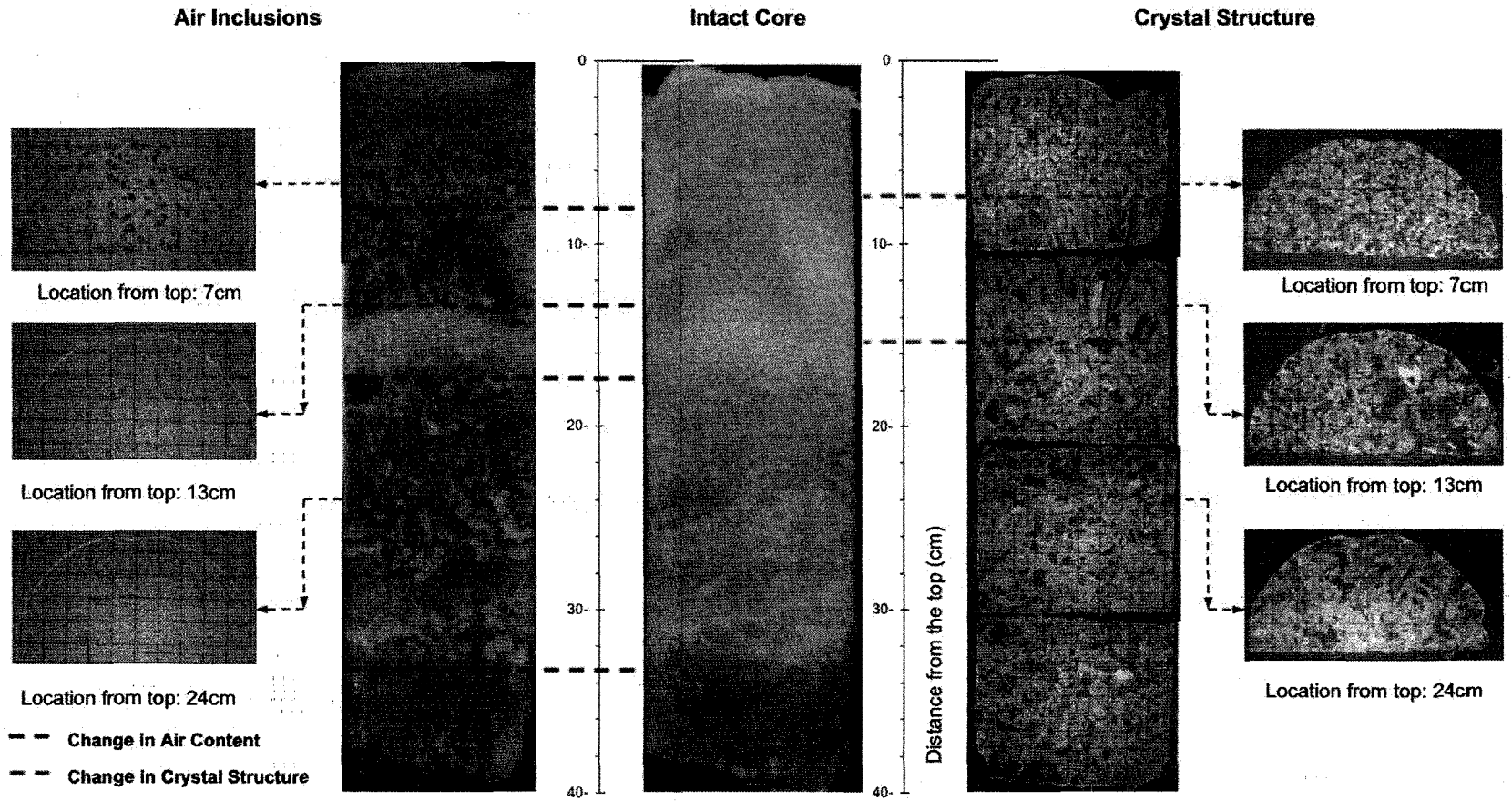


Figure 2.56 Air inclusions and crystal structure analysis of core sample obtained at the split section of CEMA Reach 1 – 30 m from the west bank.

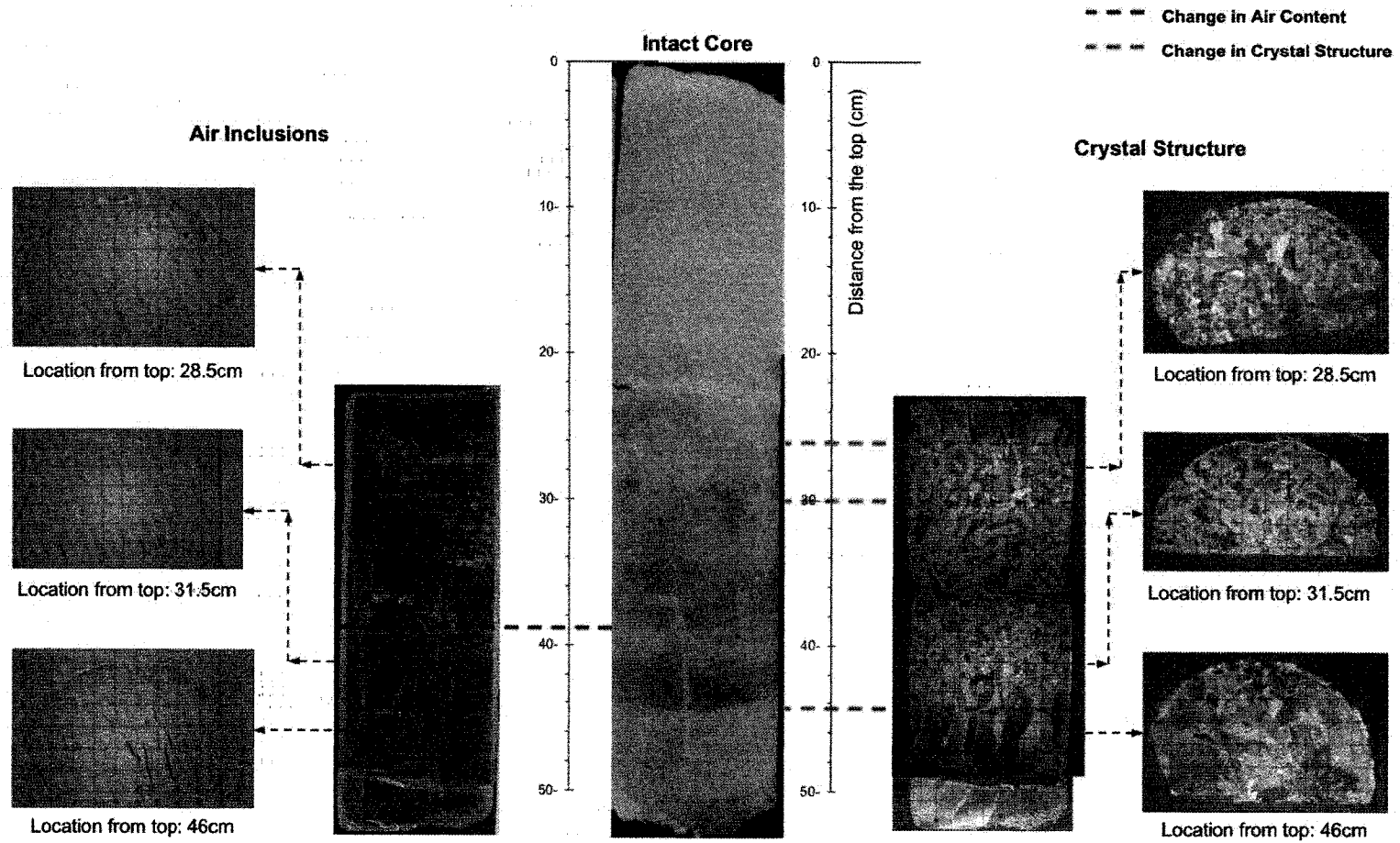


Figure 2.57 Air inclusions and crystal structure analysis of core sample obtained at the split section of CEMA Reach 1 – 100 m from the west bank.

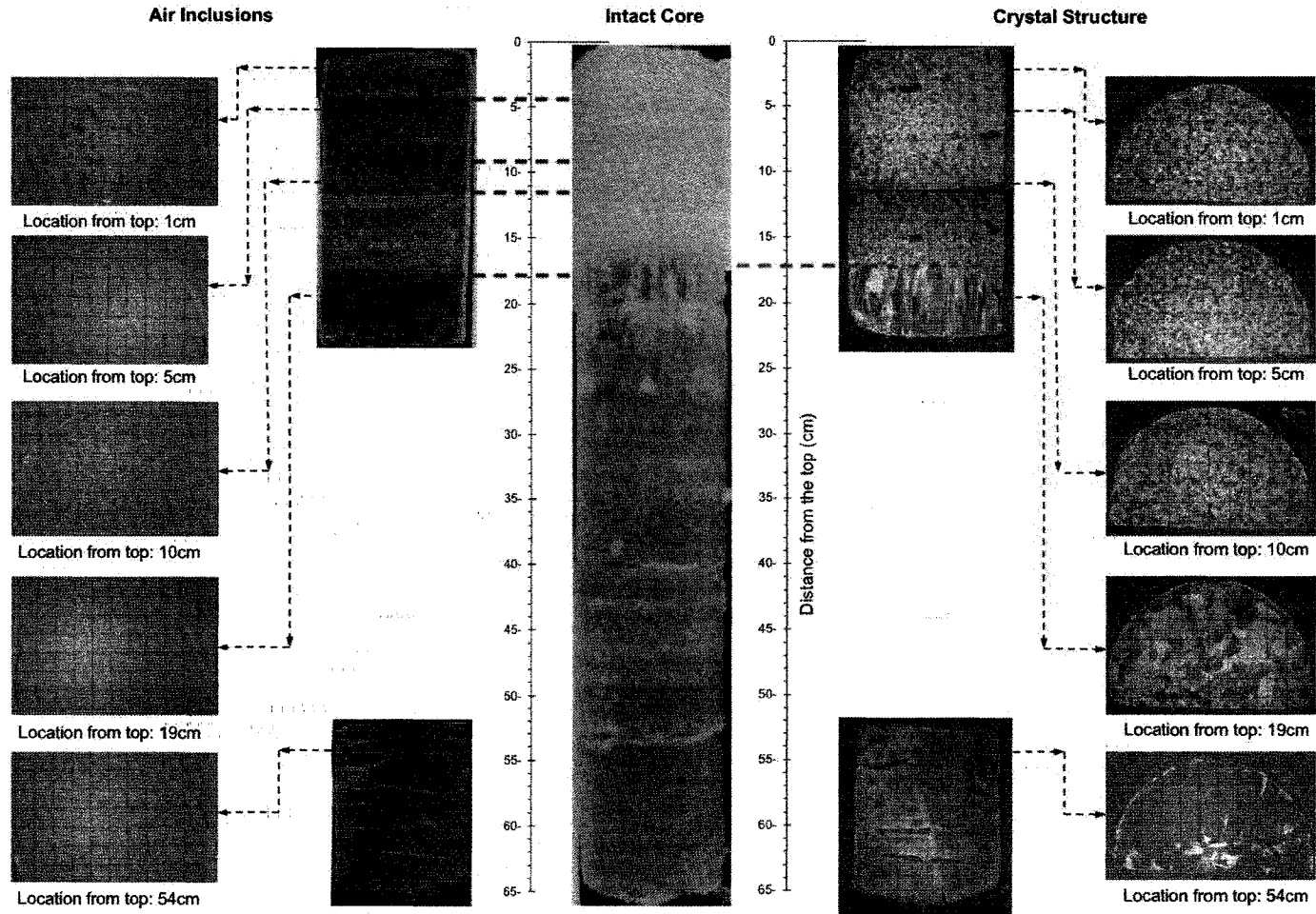


Figure 2.58 Air inclusions and crystal structure analysis of core sample obtained at the split section of CEMA Reach 1 – 200 m from the west bank.

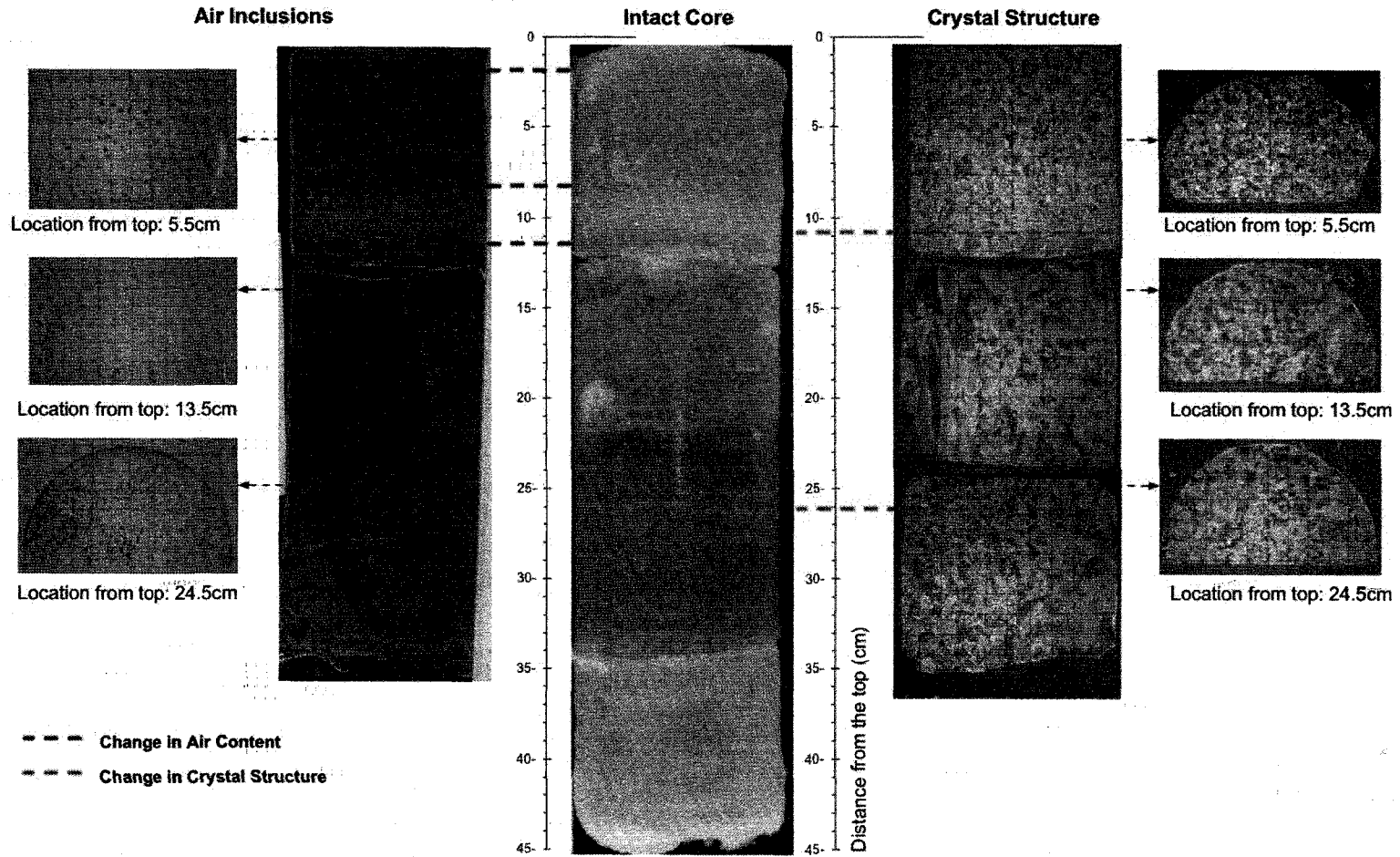


Figure 2.59 Air inclusions and crystal structure analysis of core sample obtained at the downstream boundary of CEMA Reach 1 – 60 m from the west bank.

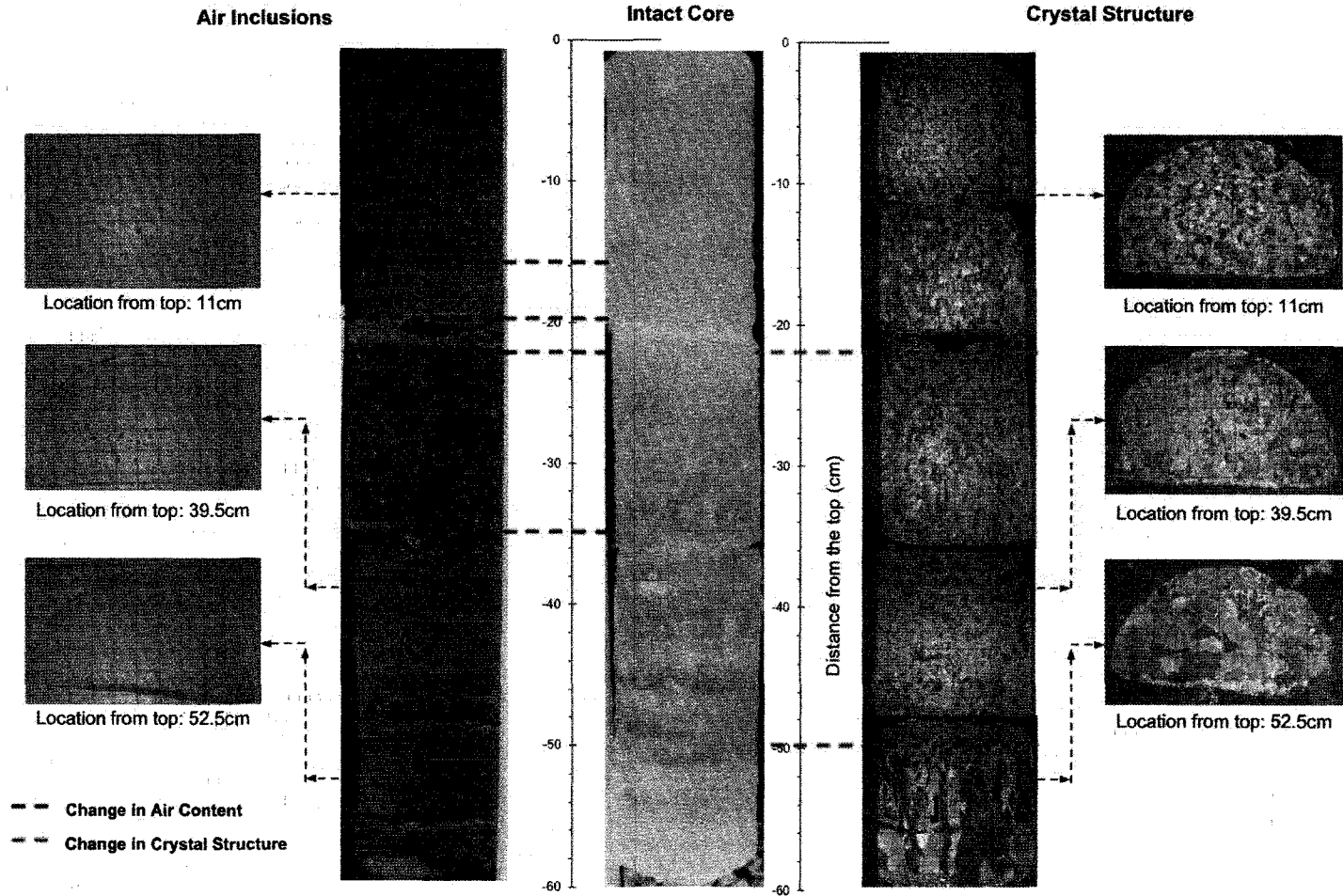


Figure 2.60 Air inclusions and crystal structure analysis of core sample obtained at the downstream boundary of CEMA Reach 1 – 180 m from the west bank.

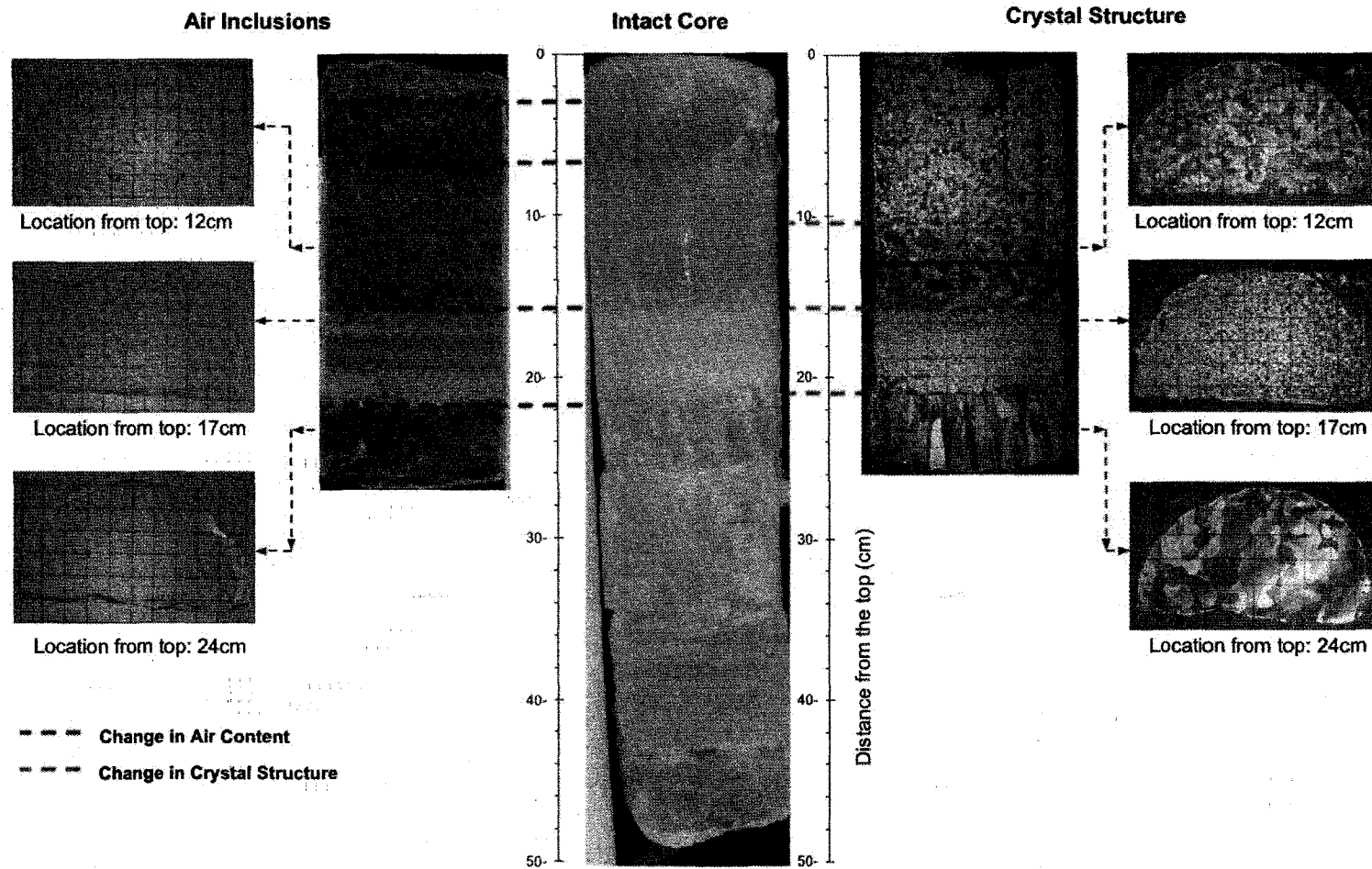


Figure 2.61 Air inclusions and crystal structure analysis of core sample obtained at the downstream boundary of CEMA Reach 1 – 240 m from the west bank.

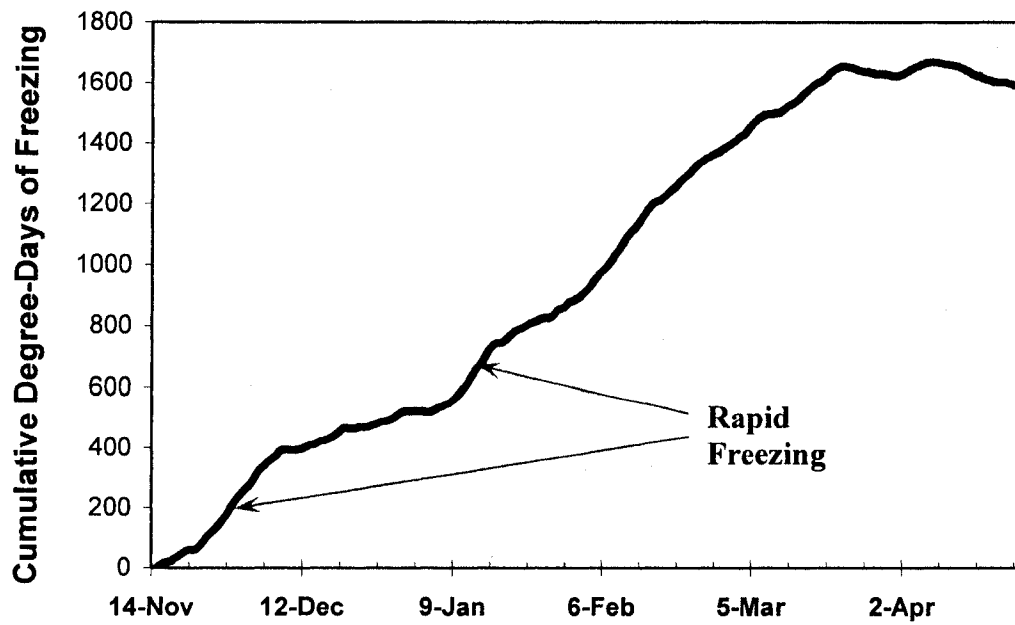


Figure 2.62 Cumulative freezing degree-day records for the 2006/07-winter season, obtained from Ta records at Fort McMurray.

CHAPTER 3 THERMAL AND HYDRAULIC MODELING

3.1. ONE-DIMENSIONAL MODELING

Data records obtained for the 2006/07-winter season allowed for a preliminary implementation of the *River1D* numerical model to the study reach. However, exhaustive calibration of all modeling parameters requires a much more comprehensive data record than the one obtained during this 8-month monitoring program. In addition, the lack of adequate historical records discards any possibility of model validation at this point. Table 3.1 contains an assessment of the adequacy of available data for one-dimensional modeling.

As discussed in Section 2.6, the winter regime of the study reach was observed to be highly two-dimensional. As a result, the accuracy of one-dimensional simulations is compromised by the inability of the model to account for a series of processes that take place in this particular reach during ice cover formation (i.e. the influence of islands and sand bars on border ice formations and ice pan conveyance). Additional inaccuracies result from limitations of the present version of the model (Section 3.11), such as the inability to account for multiple bridging points. The following sections discuss the implementation of *River1D* for thermal and hydraulic modeling of the study reach using the data record obtained during the 2006/07-winter period.

3.1.1. Model Description

River1D is a hydraulic flood routing model developed at the University of Alberta, which uses the *Characteristic-Dissipative-Galerkin* (CDG) finite element method to solve a conservation formulation for the Saint-Venant equations for rectangular channels of varying width (Hicks and Steffler, 1990, 1992). The model currently supports natural channel geometry. However, river flow routing can be accurately modeled based on limited field data, by replacing this data with information derived from topographic maps (Hicks, 1996) and digital elevation models.

Conservation of water mass and momentum equations, as solved by the model are:

$$\frac{\partial A}{\partial t} + \frac{\partial Q}{\partial x} = 0 \quad [1]$$

$$\frac{\partial Q}{\partial t} + \frac{\partial QU}{\partial x} + \frac{\partial}{\partial x} \left(\frac{gAH}{2} \right) - \frac{gAH}{2B} \frac{\partial B}{\partial x} = gA(S_o - S_f) \quad [2]$$

where

- A = cross sectional flow area (m^2)
- Q = discharge (m^3/s)
- U = cross sectional average longitudinal velocity (m/s)
- g = acceleration due to gravity (m/s^2)
- H = depth of flow (m)

- B = width of the rectangular cross section (m)
- S_o = longitudinal channel bed slope (*dimensionless*)
- S_f = Longitudinal boundary friction slope (*dimensionless*)

Version 1.11 of the *River1D* model incorporates thermal ice related processes. This includes water temperature, suspended and surface frazil ice, surface ice concentrations and solid surface ice, as well as ice front location. Developed from a control volume principle in an Eulerian frame of reference, the model solves thermal process equations, which can be written in the general form:

$$\frac{\partial}{\partial t}(\Phi) + \frac{\partial}{\partial x}(U\Phi) = \Sigma F \quad [3]$$

- where
- x, t = longitudinal and temporal coordinates (s, m)
 - Φ = the solution variable of interest
 - U = the applicable mean or surface ice velocity (m/s)
 - ΣF = the sum of the applicable mass or energy fluxes per unit distance in the longitudinal direction

Each component of the thermal process is expressed in terms of the finite element method based on this general form. Detailed equation formulation and solution methodology can be found in Andrishak (2006). A decoupled solution of the total mass and momentum conservation equations is followed by the solution of the water temperature and ice mass conservation equations for each time step in the

transient solution. It is important to note however, that the present version of the model assumes the drifting ice and the surface water velocity are the same, and only when the ice is arrested, are the corresponding resistance effects considered.

The current version of the model has several limitations worth mentioning. The model is currently incapable of handling multiple bridging points and only one station along the modeled reach is considered as a point of ice arrest (modeling results are highly dependent on an accurate estimation of the bridging date at this location). Andrishak (2006) states that the model presently neglects the formation of border ice, which could yield lower surface ice concentration values. However, the author mentions the effects are minimal, as border ice formation zones in the natural channel usually lie outside the rectangular approximation. The insulating effects of snow are not taken into consideration in the present version of the model, which may result in thicker simulated ice covers. Ice cover consolidation is also neglected, which may affect not only simulated ice cover thicknesses, but also simulated water levels and ice front locations.

3.1.2. Model Implementation

The parameters outlined below were used for all *River1D* simulations presented in this chapter. This includes the model domain, time step, Courant number, upwinding coefficient, numerical implicitness and boundary conditions. These general solution parameters were based mostly on the experiences of Andrishak (2006) who developed and evaluated the thermal component of the

River1D model on an 829-kilometer reach of the Peace River in Northern British Columbia and Alberta.

Previous simulations of the Athabasca River were conducted at the university of Alberta in *cdg-1D*, which is the precursor of the *River1D* model. That model, which spanned 1038 km from Whitecourt to Embarras, consisted of a rectangular channel approximation composed of 1126 computational nodes, spaced equally at 1 km intervals. Variations in channel width and slope for this model were adapted from National Topographic Series (NTS) maps and Kellerhalls *et al.* (1972) respectively. Manning's channel resistance was calibrated at a value of 0.035 using data from the Water Survey of Canada database.

The domain for the present study was adapted from the aforementioned model. However, it was observed that drastic variations in river width occurring along the 1-kilometer spacing between cross sections resulted in instabilities in the simulated hydraulics. As a result, the model domain was refined with interpolated cross sections, resulting in 143 computational nodes spaced at 500 meter intervals, which represents the 71 km reach spanning from station M288.1 to M216.7. It is worth mentioning that this domain corresponds to the thermal component of the model, and refinement was done only along the 71 km reach of interest. The hydraulic component is comprised of a total of 360 nodes, spanning from station M288.1 to Embarras, which is located 222 km downstream of station M216.7.

As mentioned in Chapter 1, Kellerhalls et al. (1972) and Van der Vinne (1993) found Manning's roughness coefficient to range from 0.017 to 0.030 in the study reach. However, roughness values can increase significantly under conditions of lower discharges because the form roughness of the channel increases in relation to the flow depth (Chow, 1959). As a result, the calibrated value of 0.035 was found appropriate for the present model, as records indicate that winter is a period of extreme low flow in the study area (Figure 1.1).

A time step of twelve minutes (720 seconds) was used for all hydraulic, water temperature and ice computations. Andrishak (2006) states that in order to improve the accuracy of the simulations, the value of the Courant number should be kept below one. For average discharge conditions of 450 m³/s, the selected domain discretization and time step yield a Courant number of 0.67 for the present model. In a similar manner, based on Andrishak (2006), an upwinding coefficient ' ω ' of 0.25 was used, as it improves the solution of convection dominated problems. A numerical implicitness ' θ ' of 0.5 was used for all simulations, which represents optimal (second order) accuracy (Hicks, 1990).

A series of boundary conditions must be specified to run hydraulic and thermal simulations. The hydraulic component requires inflow discharge at the upstream boundary and a specified water level at the downstream boundary. The discharge hydrograph based on the mean daily flow release, obtained from the WSC gauge at Fort McMurray (Section 2.4.1), was used at the upstream boundary and a constant water depth of 2 meters was adopted downstream. Even though this value

constitutes an approximation, the downstream boundary of the hydraulic component is located far enough from station M216.7 (222 km), and the results of the simulation are not affected by inaccuracies in this estimation.

The thermal component only requires upstream boundary conditions, as the model uses the applicable “natural” conditions for water temperature and ice at the downstream boundary (Andrishak, 2006). Water temperature, suspended frazil concentration, surface ice concentration, frazil and solid ice thicknesses must be known variables at the upstream boundary. This is particularly limiting, as most of these variables are rather difficult to quantify in the field. It is worth mentioning, that if the water temperature at the upstream boundary location remains above 0°C (i.e. industrial outfall), all four ice conditions could be set equal to zero. However, for this particular study area, the upstream boundary freezes in a similar manner as the rest of the reach; thus, all ice conditions must be known. As mentioned in Chapter 2, mean daily water temperature and surface ice concentration records at the upstream boundary were considered adequate for modeling. However, the lack of reliable methods for quantifying the remaining three variables results in an important limitation on current modeling capacity.

3.1.3. Discussion of Results

Model calibration is a multi-step process that involves the adjustment of several parameters that are characteristic of the reach being simulated, and depends highly on the amount of available data for comparison (Andrishak, 2006). Data

records for modeling of this particular reach have only started to be developed as a result of the monitoring program undertaken during the 2006/07-winter season. As a consequence, only preliminary calibration of the model can be achieved at this point, and only for certain parameters due to the present limitations of the model, as discussed in Section 3.1.1.

The most deterministic approach for calculating the net heat flux to/from the water surface would involve the calculation of a full energy budget, including accounting for net incoming solar radiation into the water (heat gain), long-wave radiation emission (heat loss), evaporation or condensation (heat gain or loss), convective heat transfer, and other minor heat fluxes. However, this approach is very data intensive (e.g. needs air temperature, water temperature, wind speed, relative humidity, and barometric pressure over the modeled reach), and still requires empirical equations for some heat components (e.g. the convective heat transfer. A simplified approach, often used in ice process modeling is the linear heat transfer approach, which lumps the temperature dependent terms. Usually, the solar radiation is considered explicitly, resulting in an equation of the form (Ashton, 1986):

$$\phi_{wa} = h_{wa}(T_w - T_a) + k_{wa} - \phi_R \quad [4]$$

where ϕ_{wa} = net rate of heat exchange per unit area between water and air
 (W/m^2)
 h_{wa} = linear heat transfer coefficient, normally used to account for

site specific conditions, such as wind or valley wall effects

$(W/m^2/^\circ C)$

T_w = water temperature ($^\circ C$)

T_a = air temperature ($^\circ C$)

k_{wa} = linear heat transfer constant (W/m^2)

ϕ_R = net rate shortwave solar radiation reaching the water surface

(W/m^2)

It is important to note that the relationship between temperature and heat flux is generally non-linear. However, Hicks *et al.* (1997) found that the non-linearity was not pronounced over the range of temperature differences ($T_a - T_w$) typical of ice process modeling. Furthermore, because of the empirical approximations required by the full energy budget, and its extensive data requirements, Hicks *et al.* (1997) found that more consistent model predictions could actually be obtained with the simplified linear heat transfer approach.

In this study, for freeze-up modeling, the heat input from solar radiation had to be neglected, since the instrument measuring this was out for servicing during a portion of the freeze-up period. However, this was not considered a significant limitation, since the heat input from the solar radiation during the day, is comparable to the heat lost due to long-wave radiation emission. Solar radiation would be significant at breakup though. Here also, the linear heat transfer constant was set to zero, since there was insufficient data with which to determine it.

Water temperature is calibrated by adjusting the linear heat transfer coefficient ' h_{wa} ' and constant ' k_{wa} ', until simulated results agree consistently with the collected data. Agreement on the arrival of the zero degree isotherm at each of the monitored locations was considered to be an important criterion for calibration, as this condition governs the initiation of ice formation processes in the model.

Andrishak (2006) states that for the Peace River in British Columbia and Alberta, typical values of h_{wa} range between 10 and 20 W/m²/°C and the constant k_{wa} can be neglected or set equal to zero. Simulations for the Peace River study resulted in a calibrated heat transfer coefficient of 15 W/m²/°C. Given that no previous studies on heat transfer processes in the Lower Athabasca River were found as a result of this investigation, values adopted by Andrishak (2006) were also used for the present model, as both rivers are subjected to similar atmospheric conditions.

Simulations were run for h_{wa} equal to 10, 15 and 20 W/m²/°C. Figures 3.1 to 3.3 show simulated water temperatures during the month of October of 2006, as compared to actual measured values at stations M268.1, M245.6 and M216.7. A heat transfer coefficient of 10 W/m²/°C appears to be the most appropriate for the modeled reach, as it shows the best agreement in the arrival of the zero degree isotherm at all three locations. The use of multiple coefficients along the reach was deemed unjustifiable, as air temperature records show that atmospheric conditions are similar for the entire study area. This is supported by the fact that water temperature decreases uniformly at all four monitoring stations. However, the effects of warm water outfalls to which the river is subjected to, appear to affect the overall

assessment of the coefficient. This resulted in a lower heat transfer coefficient value for this reach, comparatively to the coefficient calibrated for the Peace River by Andrishak (2006), which, as mentioned earlier, is subjected to similar atmospheric conditions. In other words, under equal atmospheric conditions, water temperature in the Lower Athabasca River decreases at a slower rate, as industrial outfalls maintain the water in the river slightly warmer.

Examining the results of simulated water temperature more closely, it is observed that the model appears to over-predict water temperatures during the recovery period taking place from October 19th to October 28th at all three stations. This might be attributable to error induced by the rectangular channel approximation of the river, which might be inaccurate at some locations. However, overall agreement of simulated water temperature appears to be adequate. Figures 3.4 to 3.6 show additional simulations conducted using hourly input records for flow and water temperature. Even though the results show the model is able to capture diurnal water temperature fluctuations (not achieved using mean daily input data), the overall tendency to over-predict remains consistent; the model greatly over-predicts diurnal fluctuations as well. The arrival of the zero degree isotherm slightly improves at station M268.1. However, it is important to note that the use of hourly input data is limited by the model's present limitation of 1000 points in any time series.

Note that the model does not completely capture the diurnal fluctuations in water temperature, even when hourly temperature data is used. Since the solar radiation heat input is not provided, its effect is being implicitly incorporated into the

linear heat transfer coefficient, and thus this parameter would therefore actually be different during daylight and darkness. However, this sort of empirical adjustment to the linear heat transfer coefficient was not considered appropriate or warranted in this modeling effort. In future, with solar radiation data, this can be investigated more rigorously.

Most physical ice modeling parameters required by the model were adopted from Andrishak (2006); these are summarized in Table 3.2. As mentioned earlier, surface ice concentration and inflow water temperature records were considered adequate. However, the remaining thermal boundary conditions (suspended frazil concentration, frazil and solid ice thickness) were obtained qualitatively from ice core samples and preliminary simulations of thermal processes using the Town of Athabasca as an upstream boundary, where all four thermal conditions can be set equal to zero due to the presence of a warm water discharge produced by the Al-Pac pulp/paper mill. It is important to note, that the results of this preliminary simulation provide only a useful guideline into thermal boundary conditions at Station M288.1. Suspended frazil concentrations at station M288.1 as obtained from this simulation are shown in Figure 3.7.

Figure 3.8 shows simulated surface ice concentrations at stations M268.1, M245.6 and M216.7 as compared to concentrations observed during aerial surveillance. Given the limitation in the current version of the model, noted above, especially the fact that the model does not yet consider border ice, these results are encouraging. The model over-predicts surface ice concentrations at Station M216.7,

which is located downstream of several water outfalls that are suspected to issue slightly warmer water than in the river. The inability of the model to account for these outfalls as a source of inflowing warm water, results in over-predicting the formation of ice at most of the downstream half of the modeled reach. This might be attributed to the fact that simulated ice cover development in the entire reach is based greatly on input ice formation at the upstream boundary, which occurs at a significantly faster rate. This also affects the maximum surface ice concentration obtained from the simulations, which as seen in Figure 3.8, does not achieve 100% coverage at any time. The reason for this could be attributable to the model only considering heat loss over open water to lead to suspended frazil ice formation (Andrishak, 2006). Rapid development of the ice cover upstream leads to a premature decay in frazil ice production for the rest of the simulated reach. In addition, nearly 50% of the total ice in the reach consists of large border ice formations along the banks and around islands and sand bars. The inability of the model to account for border ice formation yields significantly lower surface ice concentrations.

Simulations were conducted for four suspended frazil ice concentration conditions at the upstream boundary. These conditions were obtained by increasing the predicted suspended frazil ice concentrations at station M288.1 (obtained from simulations run from the Town of Athabasca), by 30, 60 and 90%. The resulting simulated surface ice concentrations at the remaining stations did not vary in any of the cases. This shows that the model is not particularly sensitive to this inflow boundary parameter. This can likely be explained by the fact that suspended frazil

generation within the entire reach (which occurs as a result of the exposed water surface) has a much greater influence than any frazil generated just in the inflow boundary. This is because the surface area of the 80 km long reach is much larger than the inflow cross section. For 2-D modeling of a short reach, this might not be the case. However, for 1-D modeling of this reach, it appears that extensive efforts for field measurement of this parameter in the future are considered unnecessary for establishing the inflow boundary condition. However, it would be useful validation data, if it could be measured

The advancement of the ice front is simulated by specifying the date at which bridging occurs at the downstream boundary and by calibrating the parameter P_{jux} (juxtaposition parameter), that accounts for the reduction of ice velocity as pans arrive at the leading edge. Only one bridging point can be specified, and only at the downstream boundary. As discussed in Chapter 2, multiple bridging points were observed in the reach, and in addition, a significant portion of the ice cover had already formed by the time the ice front passed through the downstream boundary. In other words, a uniform upstream progression of the ice front, as simulated by *River1D*, does not occur in the study area. As a result, calibration of P_{jux} was not attempted.

3.2. TWO-DIMENSIONAL MODELING

River ice processes in the study area are observed to be highly two-dimensional. As discussed in the previous section, the limitations of one-dimensional

modeling to accurately portray ice cover development for this particular reach are significant. The need for two-dimensional modeling becomes evident, as key sites such as water intakes, industrial outfalls and areas with an important presence of islands and sand bars, demand a much more detailed analysis than that of a one-dimensional rectangular channel approximation.

The disadvantage of 2-D modeling is the high demand for collected field data. Depth average models, such as *River2D*, require detailed bathymetric information, not only as model input, but also if any calibrations or validations are to be attempted. Furthermore, if any modeling is to be conducted under ice-covered conditions, even greater amounts of data are required. This includes winter bathymetry and ice cover characterization, which as discussed in previous sections, can be challenging and time consuming to acquire, especially under a hostile winter environment.

As part of an assessment of ecological health of the reach in the vicinity of the oil sands mining operations, CEMA acquired detailed bathymetric information of five river reaches of the Lower Athabasca River, during the summer and winter months of 2001 through 2005. Three of these reaches lie within the study area; their location was shown earlier in Figure 1.1. The collected bathymetric data was provided by CEMA for this study, and includes water surface and bed elevations, snow depth, ice cover thickness and flow velocity at hundreds of locations within these reaches, spaced an average of 20 m apart. In later years, Katopodis and Ghamry (2005) of the Department of Fisheries and Oceans conducted *River2D*

modeling of these reaches, for which bed and ice roughness values were calibrated; these models were also provided for this study.

As two-dimensional modeling in *River2D* will constitute an important effort in future years, a preliminary evaluation of the calibrated model of CEMA Reach 1 was accomplished. As discussed in Chapter 2, discharge measurements at this reach were taken on March 2007 using an Acoustic Doppler Current Profiler. Ice core samples and ice cover thickness measurements also took place. This allowed for an evaluation of the accuracy of the model to portray flow under ice-covered conditions at this reach. Unfortunately, due to time constraints, data was only collected at this one location, which excludes the possibility of evaluating the remaining CEMA reach models.

3.2.1. Model Description

River2D is a two-dimensional, depth averaged finite element model intended for use in natural streams and rivers. The model provides an accelerated convergence to steady-state conditions, even though it is a transient model. The hydrodynamic component of the model is based on a conservative form of the Saint Venant equations, representing the conservation of mass and two components of the momentum vector. The dependent variables solved are the depth and discharge in the two coordinate directions. Conservation of mass is represented by the following equation:

$$\frac{\partial H}{\partial t} + \frac{\partial q_x}{\partial x} + \frac{\partial q_y}{\partial y} = 0 \quad [5]$$

where H = depth of flow (m)

q_x, q_y = discharge intensity in the x- and y-directions (m^3/s)

Conservation of momentum in the x- and y-directions are represented by:

$$\begin{aligned} \frac{\partial q_x}{\partial t} + \frac{\partial}{\partial x}(Uq_x) + \frac{\partial}{\partial y}(Vq_x) + \frac{g}{2} \frac{\partial}{\partial x} H^2 \\ = gH(S_{0x} - S_{fx}) + \frac{1}{\rho} \left(\frac{\partial}{\partial x}(H\tau_{xx}) \right) + \frac{1}{\rho} \left(\frac{\partial}{\partial y}(H\tau_{xy}) \right) \end{aligned} \quad [6]$$

$$\begin{aligned} \frac{\partial q_y}{\partial t} + \frac{\partial}{\partial x}(Uq_y) + \frac{\partial}{\partial y}(Vq_y) + \frac{g}{2} \frac{\partial}{\partial y} H^2 \\ = gH(S_{0y} - S_{fy}) + \frac{1}{\rho} \left(\frac{\partial}{\partial x}(H\tau_{yx}) \right) + \frac{1}{\rho} \left(\frac{\partial}{\partial y}(H\tau_{yy}) \right) \end{aligned} \quad [7]$$

where H = depth of flow (m)

q_x, q_y = discharge intensity in the x- and y-directions (m^3/s)

U = depth averaged velocity in the x-direction (m/s)

V = depth averaged velocity in the y-direction (m/s)

g = acceleration due to gravity (m/s^2)

ρ = density of water (kg/m^3)

S_{0x}, S_{0y} = bed slope in the x- and y-directions (*dimensionless*)

S_{fx} S_{fy} = friction slope in the x- and y-directions (*dimensionless*)

τ_{xx} τ_{xy} τ_{yx} τ_{yy} = components of the horizontal turbulent stress tensor (N/m^2)

Basic assumptions of the model include a hydrostatic pressure distribution, a constant distribution of the horizontal velocities over the depth and negligible Coriolis and wind forces.

The model currently does not predict thermal ice related processes. However, recent developments funded by CEMA resulted in improving the model by allowing it to simulate flows under a floating ice cover with known geometry. In other words, ice cover characteristics such as thickness and roughness must be known. When an ice cover is input, the model changes the aforementioned momentum equations to account for the roughness of the bottom of the ice cover and increases in the area on which shear stress operates, both of which result in a reduction of the average flow velocity and an increase in water surface elevation. The continuity equation however, remains unchanged.

3.2.2. Evaluation of the CEMA Reach 1 *River2D* Model

The Athabasca River at CEMA Reach 1 has an average width of 500 m and a slope of 0.0002 (Katopodis and Ghamry, 2005). Figure 3.9 shows an aerial photograph of the river at this reach. The figure illustrates a set of three islands, the larger of which is named Alexander Island. A persistent open lead forms to the east of this island, and is presumed to remain open through the entire winter season. The

total width of the river at this point is approximately 870 m. Trillium Engineering and Hydrographics Inc., who was responsible for conducting the hydrometric surveys of the reach in 2002, describes the bed material as being mostly comprised of sand with little scattered silt, gravel and cobble. Average ice cover thicknesses measured during the 2002 survey are very similar to those found on 2007, ranging between 0.50 m for areas of juxtaposed ice, to 0.70 m for zones of thermal growth.

As mentioned earlier, Katopodis and Ghamry (2005) performed hydrodynamic simulations of this reach using *River2D*. All model components, which include calibrated bed, mesh and ice files, were provided for this study. According to Katopodis and Ghamry (2005), computational meshes were created and refined based on topographic matching, by overlying the entire reach with uniformly spaced nodes and adding additional nodes around specific channel features. Subcritical inflow and outflow boundaries were defined based on discharges reported by WSC for the period of field data collection. Boundaries of no-flow across side vertical walls were determined on areas where the elevation was above high water levels associated with the applied discharges. As illustrated in Figure 3.10, this includes two internal boundaries, one corresponding to Alexander Island and the other presumably to a sand bar of considerable size, as no other islands were seen in the reach during aerial surveillance (Figure 3.9).

Calibration of the model, as described by Katopodis and Ghamry (2005) was a multi-step process. Initial bed roughness heights were assumed from descriptions of grain size and distribution of the bed material, provided in the initial collected

data. Bed channel roughness was then calibrated for open water conditions using the hydrometric record corresponding to the ice-free period. Final calibration of the combined roughness (bed and ice) was achieved by adjusting the parameter and comparing simulated versus surveyed water levels and velocities, until good agreements were found for the ice covered surveyed discharges.

This calibrated version of the model was implemented for the flow conditions obtained with the ADCP during the 2007 winter survey. As mentioned in Chapter 2, ADCP measurements showed that 85% of the total flow diverted to the west of Alexander Island. Figure 3.10 shows the cumulative discharge resulting from steady solution runs performed by *River2D*. It is observed in the figure that a total of 42 m³/s diverted to the east of Alexander Island, which, from a total of 127 m³/s, translates into only 66% of the total flow diverting to the west. This discrepancy might be attributable to a number of things, including inaccurate discharge results from the ADCP measurements. However, it is suspected that most of the error originates in an inappropriate definition of internal boundaries. The current configuration of the bed might not be correctly portrayed by what was measured in 2002, due to sediment transport in the reach. As a result, what was defined as a no-flow internal boundary for the 2002 data model, might in fact currently be an area where some flow is present underneath the ice cover. This might be particularly true for the eastern most internal boundary, where no sand bar was seen during the 2006 surveillance flights. However, the extent of the boundary representing Alexander Island might also be inaccurate, as it seems to also account for the small adjacent island to the east of it, discarding any possibility of flow in between.

It is equally possible that the characteristics of the ice cover might also be a source for the discrepancy. Ice cover thickness measurements conducted on March 2007 were limited to the west of Alexander Island, and no measurements were conducted on the east side. As a result, it was not possible to verify whether the thickness of the ice cover on the east side of the island was underestimated during the simulations. If a significant amount of ice grounding occurred on the east of Alexander Island, flow underneath the ice cover would be considerably lower at this location.

3.3. SUMMARY

Preliminary one-dimensional numerical modeling of thermal river ice processes was conducted in *River1D*, for the 2006 freeze-up period. The model domain was adapted from a previous flood routing model of the Athabasca River, and was refined due to unstable hydraulic solutions resulting from drastic variations in river width. Input and calibration data was based on records collected during the 2006/07 monitoring program.

Sensitivity analyses showed that the model is particularly responsive to changes in water temperature and surface ice concentration at the upstream boundary. As a result, improvements on surface ice concentration data collection techniques are highly recommended. The present technique resulted in inaccurate estimations of mean daily concentrations, as no data was collected during low visibility conditions. Changes in suspended frazil ice concentrations have very little

influence over the results of the simulations, and can be estimated from simulations run from the Town of Athabasca, where the only required thermal condition is the inflow water temperature time series. Additional runs were conducted using both hourly and mean daily input records, and the results agreed reasonably well for both conditions. Model results from hourly input records show minor improvements in the simulated arrival of the zero degree isotherm. However, the model greatly over-predicts daily fluctuations in water temperature and is also currently unable to handle more than 1000 points per inflow time series. As a result, the use of hourly data is unjustifiable and considered unnecessary.

Water temperature calibration was accomplished by varying the heat transfer coefficient (h_{wa}). A value of 10 W/m²/°C showed the best agreement of simulated versus measured water temperature variations at stations M268.1, M245.6 and M216.7. Calibration of the juxtaposition parameter, which controls the rate of advancement of the ice front was not accomplished, as the model is currently incapable of handling multiple bridging points, occurring within the study reach. Further enhancements of the model should be directed to address this limitation.

The model over-predicts surface ice concentrations at station M216.7, possibly due to the presence of warm water outfalls, which results in the water cooling down at a slower rate at this location. Additionally, given the ice cover develops at a much faster rate at the upstream boundary than the rest of the simulated reach, a decrease in frazil production results in a premature decline of ice formation at downstream locations. As a consequence, surface ice concentrations never reach

100% at any of the downstream monitoring stations. The inability of the model to account for border ice formation, also contributes to this under-prediction of surface ice concentrations. This, along with the inability to account for multiple water temperature inputs, should also be addressed in future model developments.

A calibrated *River2D* model of CEMA Reach 1 was implemented for the flow conditions obtained with the ADCP during the 2007 winter survey. Simulated flows, at either side of an island of considerable size present in the reach, disagree with the collected data by nearly 20%. This discrepancy might be attributable to changes in bed characteristics from the time the bathymetry in the reach was completed in 2002, to the time flow was measured in 2007, which affects the definition of internal boundaries. It can also be a result of dissimilar grounding conditions of the ice cover for the different winter periods.

Table 3.1 Summary of available records for *River1D* model implementation and calibration, obtained for the 2006/07-winter season.

Data Record	Overall Adequacy	Assessment
Air Temperature*	Good	Complete record at upstream and downstream boundaries. Adequate to cover entire modeled reach.
Solar Radiation*	Good	Complete record at upstream boundary. Good spatial correlation for entire modeled reach.
Water Temperature	Good	Complete record at four locations along the modeled reach.
Discharge*	Fair	Adequate records prior to ice cover formation. Crude estimations through linear interpolation for the months of November to April.
Surface Ice Concentration	Fair	Adequate record at the upstream boundary, with gaps during nighttime. Records for the entire reach only on November 4,5,10 and 17.
Ice Front Location	Weak	No record for initial 35 km of reach. Downstream record available only for November 4, 5, 10 and 17.
Suspended Frazil Concentration*	Non Existent	No appropriate technique for field measurements.
Initial Frazil Pan Thickness	Poor	No field measurements. Estimated from ice core sample analysis.

* Only required for model input; not required for model calibration.

Table 3.2 Summary of ice modeling parameters adopted from Andrishak, 2006 for *River1D* model implementation.

Modeling Parameter	Adopted Value
Frazil Floe Porosity, e_f	0.5
Initial Frazil Pan Thickness, t_f	0.35 m
Frazil Rise Parameter, n	0.0001 m/s
Manning's n for Ice Cover	0.020
Ice Water Heat Exchange Coefficient, aiw	1187 W.s ^{0.8} /m ^{2.6} /oC

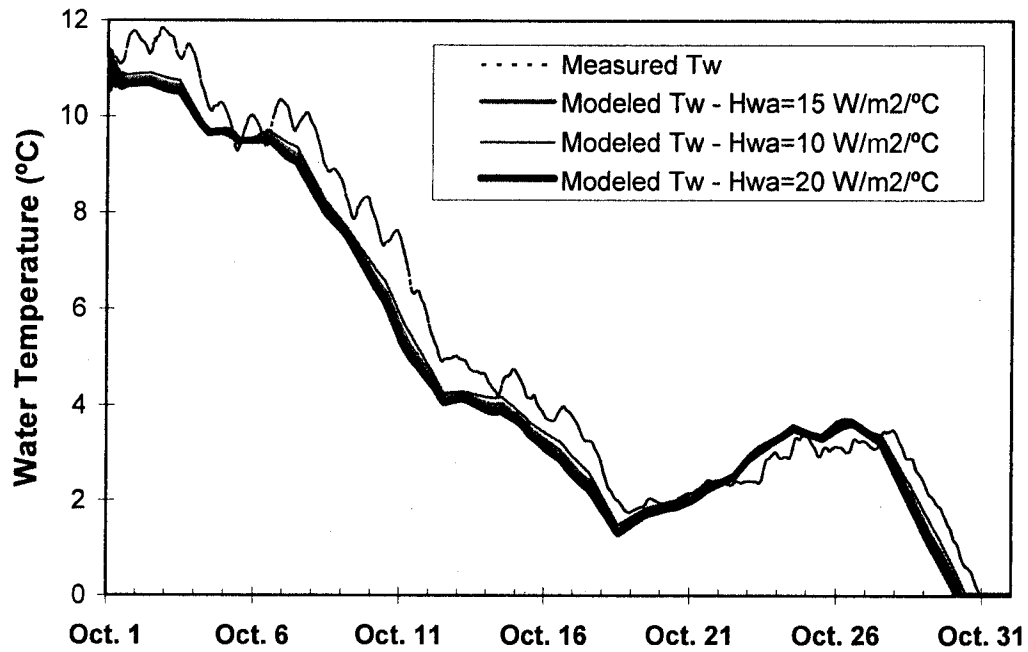


Figure 3.1 River1D water temperature calibration to measured values at Station M268.1.

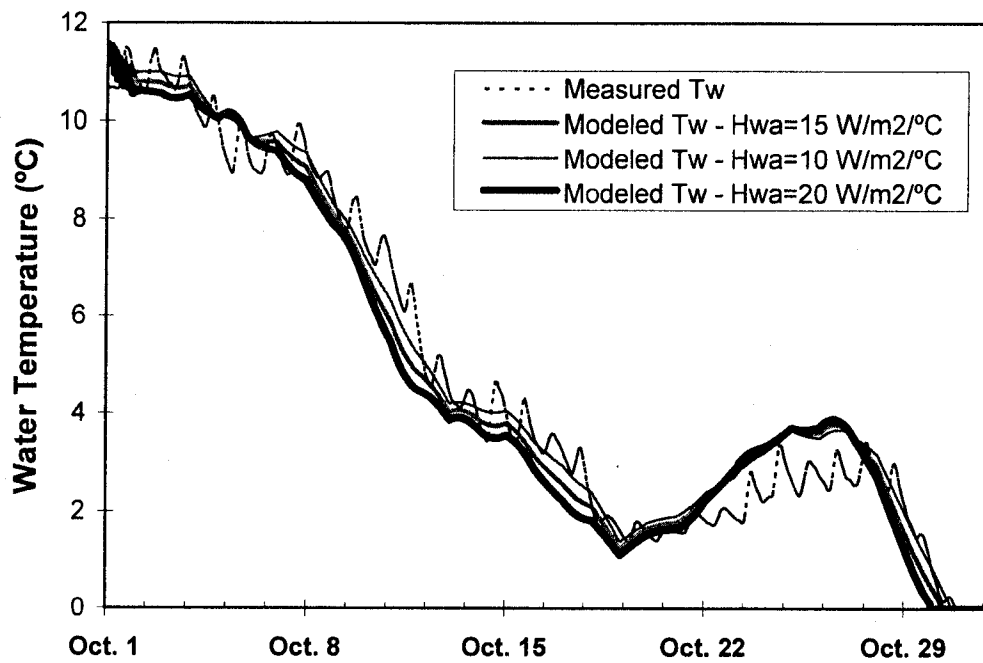


Figure 3.2 River1D water temperature calibration to measured values at Station M245.6.

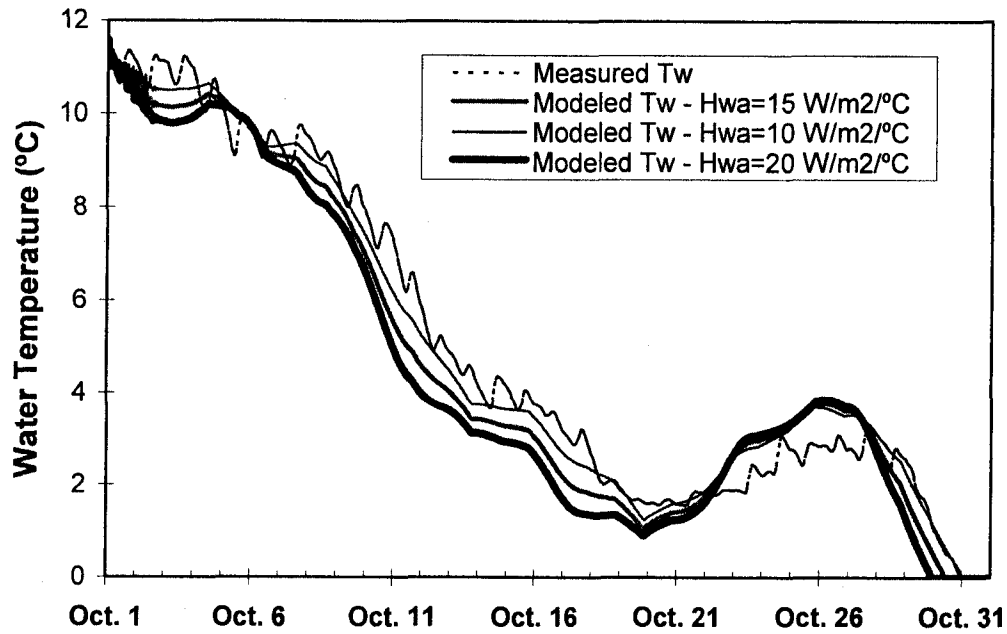


Figure 3.3 River1D water temperature calibration to measured values at Station M216.7.

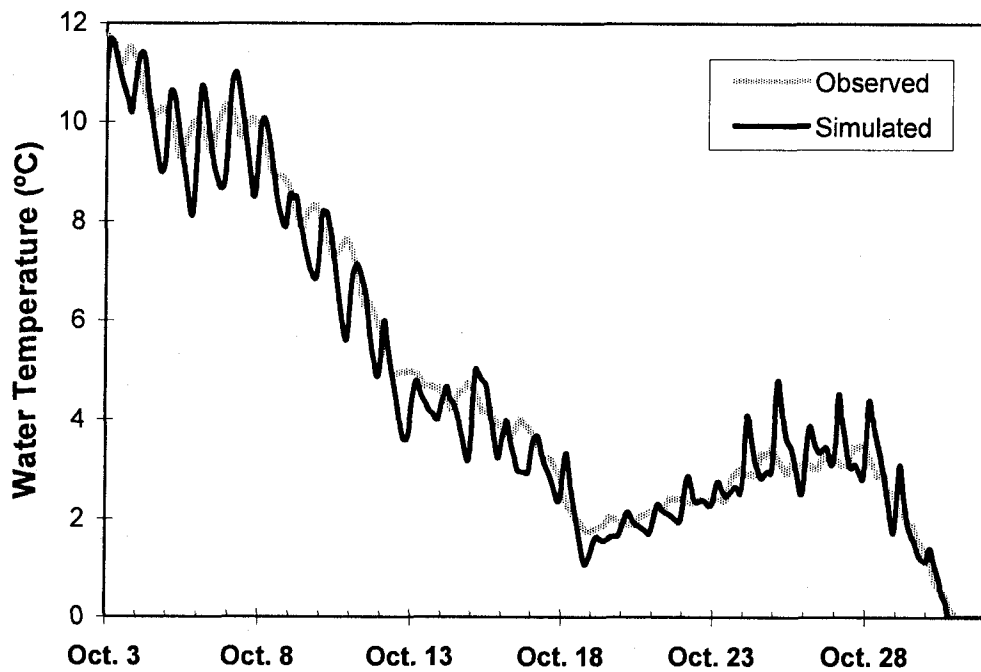


Figure 3.4 River1D water temperature simulation using hourly input data at Station M268.1 – $H_{wa} = 10 \text{ W/m}^2/\text{°C}$

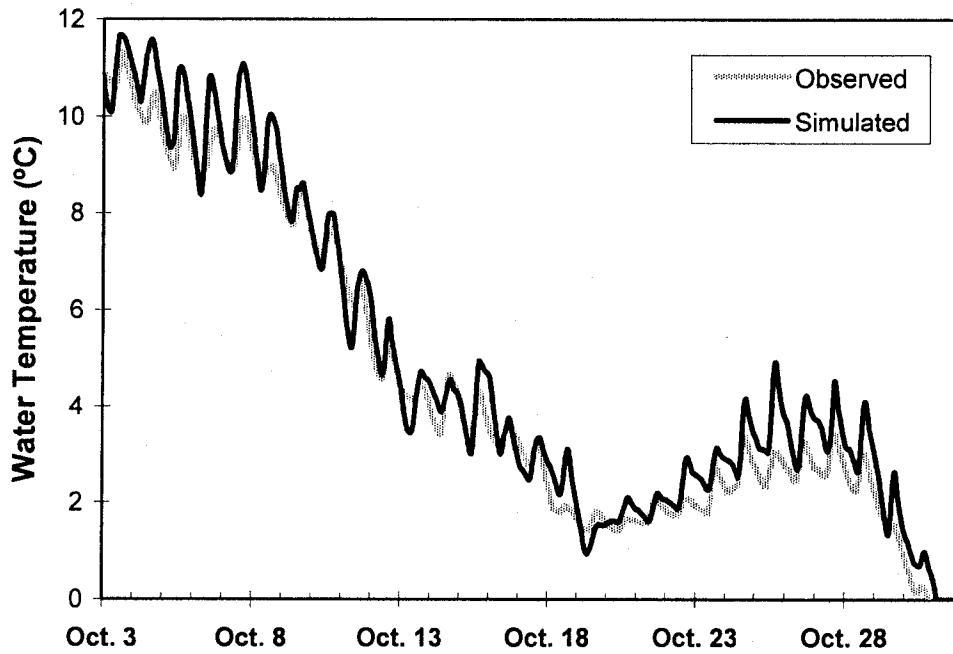


Figure 3.5 River1D water temperature simulation using hourly input data at Station M245.6 - $H_{wa} = 10 \text{ W/m}^2/\text{°C}$

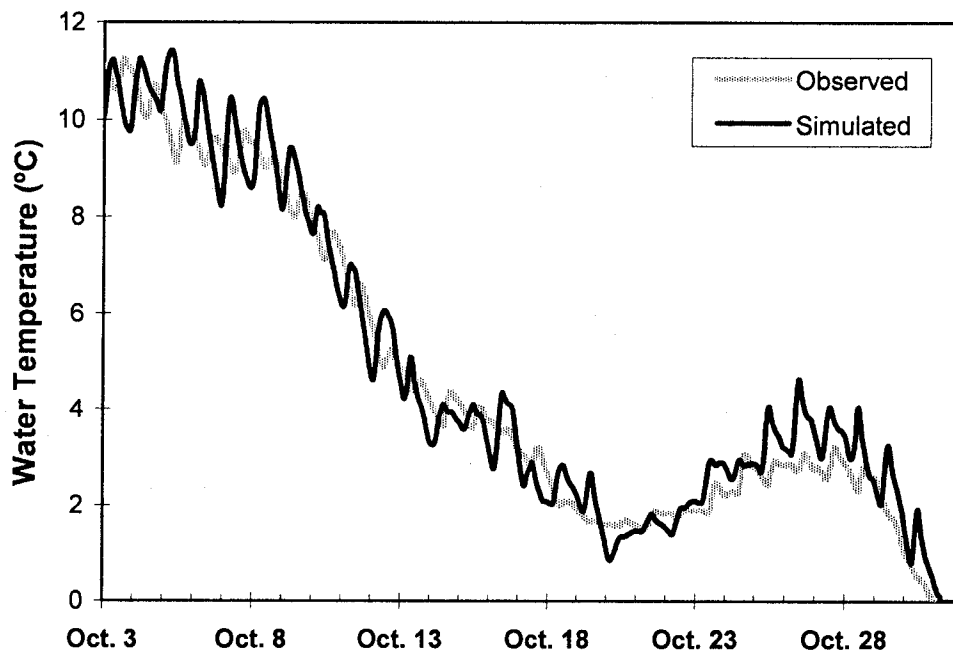


Figure 3.6 River1D water temperature simulation using hourly input data at Station M216.7 - $H_{wa} = 10 \text{ W/m}^2/\text{°C}$

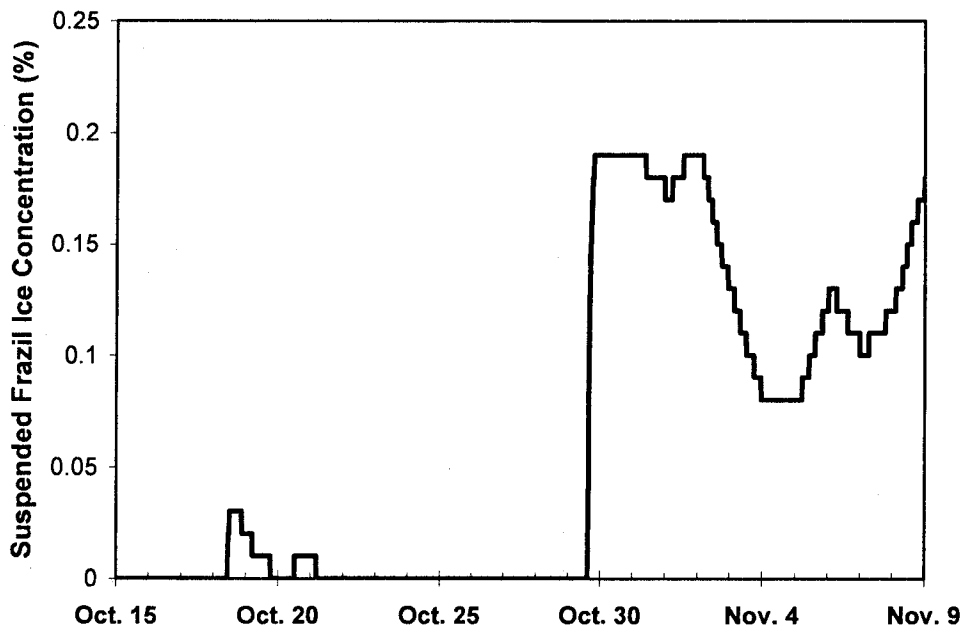


Figure 3.7 Suspended frazil ice concentrations at station M288.1 as obtained from simulations run from the Town of Athabasca.

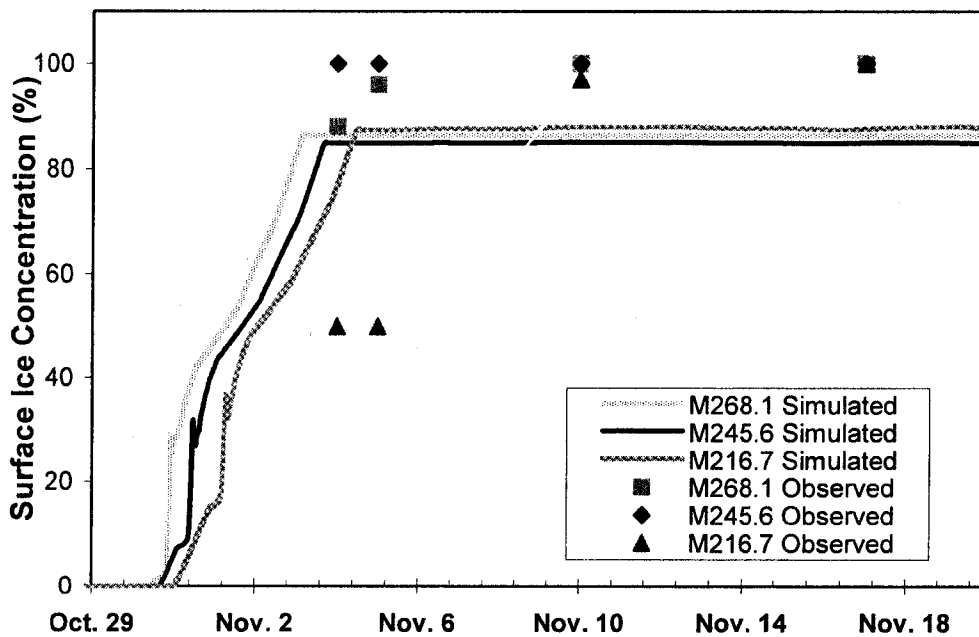


Figure 3.8 Observed vs. River1D simulated surface ice concentration at stations M268.1, M245.6 and M216.7

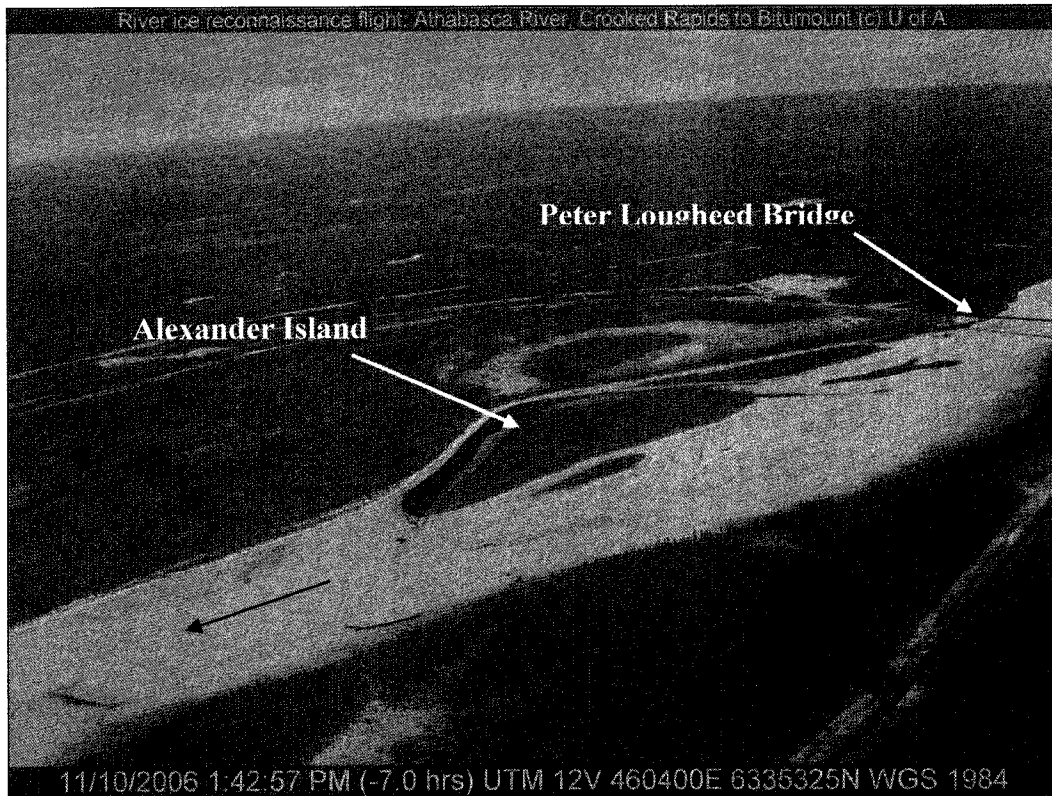


Figure 3.9 Aerial Photograph of CEMA Reach 1 – November 10th, 2006.

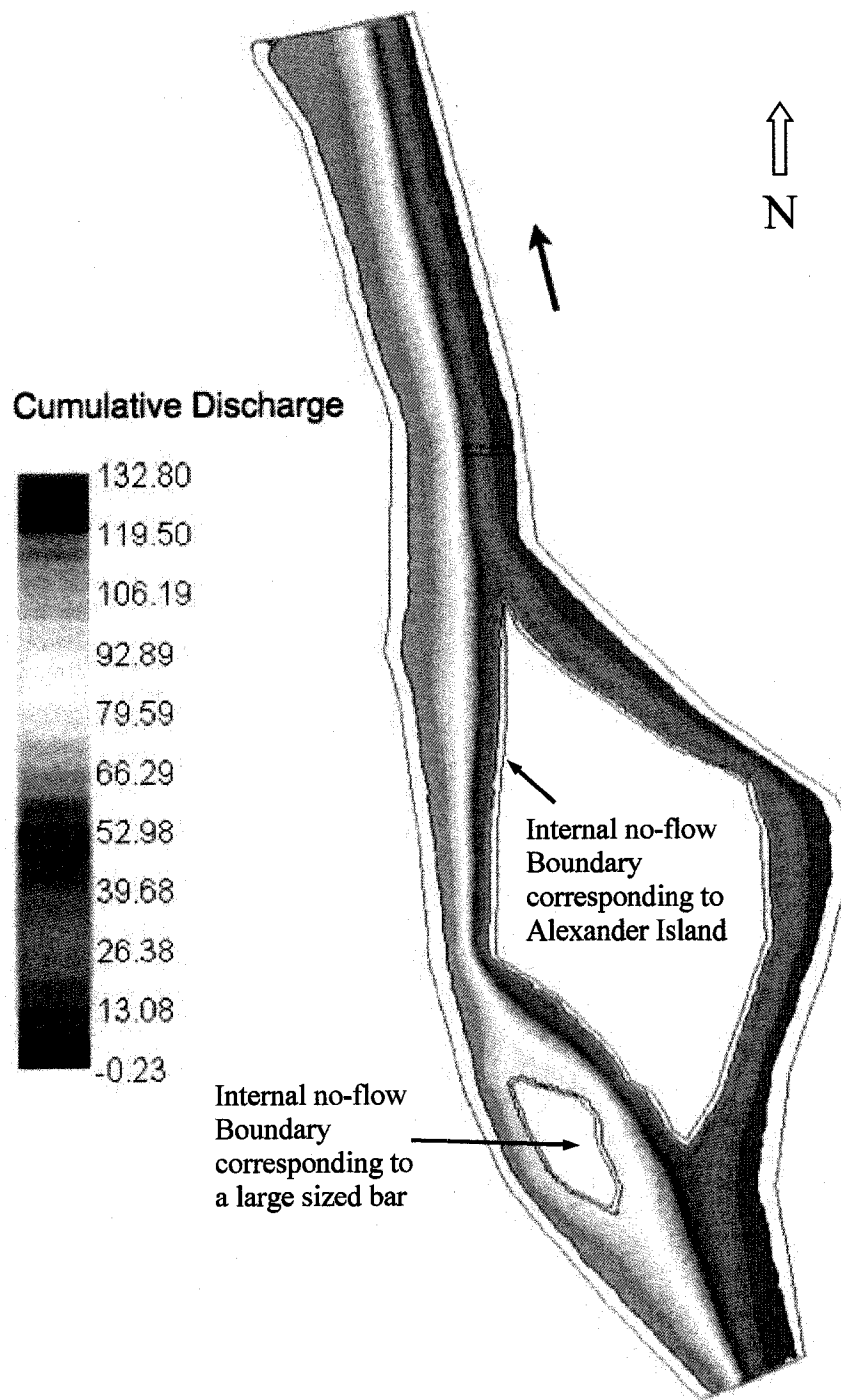


Figure 3.10 Cumulative Discharge at CEMA Reach 1 obtained from *River2D* simulations.

CHAPTER 4 SUMMARY AND RECOMMENDATIONS

Rapid expansion of the oil sands mining operations at Fort McMurray, Alberta, will increase significantly the rate of water withdrawals from the Lower Athabasca River. As a consequence, river ice processes may be altered, resulting in thicker ice covers and even less availability of liquid water during the winter period of low flow. This constitutes an important issue that could affect the sustainability of the mining projects. These potential impacts can be evaluated with the appropriate modeling tools, but requires hydrometeorological and ice cover characterization data for calibration and validation purposes. Historical data regarding ice cover formation and deterioration processes in this reach are limited, and most of the previous studies in the area have focused on evaluating the river from an ecological perspective. The purpose of this study was to establish the main conditions describing the winter ice regime of an 80 km reach of the Athabasca River spanning from Fort McMurray to Bitumont. To achieve these goals, an eight month monitoring program of was established in September 2006. Additionally, preliminary simulations in *River1D* and *River2D* were conducted to provide a guideline to direct the field monitoring program and model development plans for future years.

A comprehensive historical record of hydrometeorological data was established using existing monitoring stations. This record was complemented for the 2006/07-winter season through the installation of four automated stations along the study reach, which took place in September 2006. These stations recorded water temperature, water level and air temperature data continuously throughout the entire

season, and each data record was analyzed independently to place the season within a historical context. Air temperature records showed the 2006/07 winter season was warmer in average (approximately 2°C), with respect to the records from 1944 to 1997, but maintaining a comparable range of temperatures during the breakup season. However, freeze-up was significantly colder than the past decade, by an average of 7°C. Air temperature records were obtained from three distinct sources, two of them located within the city of Fort McMurray and one of them at river level. A discrepancy between these records, particularly for temperatures below freezing, suggests that the stations located at Fort McMurray might not be completely representative of the study reach. As a result, it is recommended that additional air temperature sensors be installed at river level. Discharge records showed that flows were approximately 23% lower in average during the 2006/07 winter season, with respect to the records from 1957 to 2005. Recorded water temperature data showed that the reach cooled down at the same rate at all four monitoring stations, reaching supercooling conditions practically simultaneously at all locations.

Ice cover formation and deterioration processes were monitored through aerial surveillance, satellite imagery and ice core sampling, all of which combined, provided a complete vision of the current state of the ice regime of the river. River ice processes in the reach were observed to be highly two-dimensional, with approximately 65% of the ice cover being formed through thermal growth, which occurred along the banks and in the vicinity of the numerous islands and sand bars present in the reach. Most of the remaining ice cover was formed through juxtaposition, with hummocky ice developing only in the uppermost 8.5 km of the

study reach, near the Fort McMurray area. Natural constrictions created by border ice encroachment resulted in numerous bridging points and small open leads that froze in place over the course of the winter. Very few dynamic processes took place during the breakup period, and most of the ice cover deteriorated thermally. However, the release of ice jams formed upstream of Fort McMurray resulted in numerous ice runs passing through the reach, and it is suspected (based on water level observations) that this ice stalled and released briefly at one location at least, within the study reach.

The presence of the mining industry along the reach was observed to have an important impact over the ice regime of the river. Industrial warm water outfalls created large sized (>7 km) open leads, where ice cover development was delayed with respect to the rest of the reach. During breakup, these outfalls also contributed to a premature initiation of thermal deterioration of the ice cover, and open water areas predominantly formed downstream of these locations early in the breakup season. The exact location and characteristics of these outfalls are yet to be determined; however, this information is not publicly available. Given their importance in determining the nature of ice cover formation and deterioration in the reach, efforts should be directed to properly identify these outfalls, and obtain records of local water temperature at their positions.

Several measurement techniques were evaluated throughout the course of the 2006/07 field program. Digital cameras were placed on the bank of the river to obtain surface ice concentration data during the freeze-up period. It was noted that

distortions created by the use of short focal length lenses create complications for automating the post-processing of the images; therefore, it is recommended short focal lengths be avoided in future installations. Additionally, photographs could only be obtained during daylight hours, and so no surface ice concentration data could be obtained during the hours of darkness. For this reason, the use of thermal imaging sensors is recommended for future stages of the field program. An Acoustic Doppler Current Profiler was used in winter to obtain discharges under ice covered conditions. The results were highly comparable to data measured by the Water Survey of Canada, with a difference in discharge of only 1.5%. Ground Penetrating Radar was used as a tool for ice cover thickness characterization. 400 MHz and 900 MHz antennas were towed across the reach on foot and using snowmobiles. The ice cover in the GPR scans was identified as the area located between easily identifiable black bands, which occur as a result of drastic changes in the permittivity of the material (i.e. snow, ice, water). The 400 MHz antenna proved to be less accurate, as lower frequency antennas are capable of resolving only large subsurface features. Correlation between manual and GPR ice thickness measurements is relatively low ($R^2 = 0.5971$) and sources of error were mostly attributable to field operation techniques. However, error might also be induced by the use of an averaged dielectric constant for the ice cover, which ice core samples showed was comprised of different layers, all of which have dissimilar electrical properties.

Preliminary one-dimensional numerical modeling of thermal river ice processes in the study reach was conducted in *River1D*, for the 2006 freeze-up period. A calibrated air-water linear heat transfer coefficient of $10 \text{ W/m}^2/\text{°C}$ gave the

best agreement between simulated and measured water temperatures, particularly in terms of accurately capturing the cooling to zero degrees. Sensitivity analyses showed that the simulation results were quite sensitive to changes in surface ice concentration and water temperature input data at the upstream boundary. However, the model is not particularly sensitive to changes in suspended frazil ice concentrations. The use of hourly input data (air temperature and inflow ice and water discharges) proved to be unnecessary, as simulated results for both conditions were highly comparable..

This as the first application of the *River1D* thermal ice process model to an unregulated river reach, and it was found that the current version of the *River1D* model has several limitations which affected the overall accuracy of the results. These limitations include the inability of handling border ice formation and multiple bridging points, both of which were observed to be governing factors influencing ice cover formation in the study area. Additionally, the current version of the model is unable to account for multiple water temperature inputs and as a consequence, the influence of warm water outfalls cannot yet be considered either. It is recommended that model enhancements be undertaken to include these capabilities.

Two-dimensional modeling was performed using a calibrated version of the *River2D* model of CEMA Reach 1, provided by the Department of Fisheries and Oceans Canada. For this project, the *River2D* model of this subreach was implemented for the flow conditions obtained with the ADCP during the 2007 survey. The results showed a discrepancy in simulated versus measured flows around

an island present in the reach, by nearly 20%. The source of this discrepancy might be attributable to changes in bed and ice cover characteristics from 2002 (when bathymetric source data for the model was obtained) to 2007, where dissimilar conformation of the bed and grounding conditions of the ice cover, results in inappropriate definitions of internal boundaries of no flow. It might also be partly due to inaccuracies in mapping details of ice thickness, and/or the precise edge of the water under the ice when conducting the discharge measurements. Alternatively, this discrepancy might also be attributable, in part at least, to measurement error as well. It is recommended that additional data be obtained to investigate these possibilities.

This study offers the first data describing the details of ice formation and deterioration in this reach of the Athabasca River. It was established that even though ice processes in the reach are highly two-dimensional, one-dimensional simulations might produce sufficiently accurate results, if the present limitations of the ice process model can be addressed. Future improvements in the *River1D* modeling capabilities should be focused on enabling it to handle multiple bridging points, border ice formation, and point sources of heat and flow. This way, key factors influencing ice cover formation and decay in the reach, such as industrial warm water outfalls, as well as the presence of islands and sand bars (which constitute important areas of ice arrest and thermal growth) can be taken under consideration.

Continued and improved data collection is essential for further calibration and validation of the one- and two-dimensional ice process models of the study reach. Efforts should be directed to improve data records required by one dimensional modeling, as the high amounts of data necessary for two-dimensional models, results in costly and time consuming field data collection programs, which are most likely not viable at the present time. Given the high sensitivity of the *River1D* model to water temperature and surface ice concentration variations in the upstream boundary, special attention should be paid to field data collection of these two records.

CHAPTER 5 REFERENCES

- Andrishak, R. (2006). "Impact of Climate Change on the Winter Regime of the Peace River". A thesis submitted to the Faculty of Graduate Studies and Research in partial fulfillment of the requirements for the degree of Master of Science in Water Resources Engineering. Department of Civil Engineering, University of Alberta, Edmonton, Alberta, 146 pp.
- Chow, V.T. (1959). "Open Channel Hydraulics". McGraw Hill Company, Toronto, Ontario.
- Conly, F.M., Crosley, R.W., and Headley, J.V. (2002). "Characterizing Sediment Sources and Natural Hydrocarbon Inputs in the Lower Athabasca River, Canada", *Journal of Environmental Engineering and Science*, Volume 1, Number 3, June 2002, pp 187 – 199, NRC Research Press.
- Daniels, J. J. (2000). "Ground Penetrating Radar Fundamentals". Department of Geological Sciences, Ohio State University. U.S.EPA Region V Report, November, 2000.
- Doyle, P. F. (1977). "Hydrologic and Hydraulic Characteristics of the Athabasca River from Fort McMurray to Embarras", Report SWE 77-2, Transportation and Surface Water Engineering Division, Alberta Research Council, Edmonton.
- Drouin, H., Gauthier, Y., Bernier, M., Jasek, M., Penner, O., and Weber, F. (2007). "Quantitative Validation of RADARSAT-1 River Ice Maps". Committee on

River Ice Processes and the Environment – 14th Workshop on the Hydraulics of Ice Covered Rivers. Quebec City, Ontario, 2007.

Gauthier, Y., Weber, F., Savary, S., Jasek, M., Paquet, L-M. and Bernier, M., (2006). “A Combined Classification Scheme to Characterise River Ice from SAR Data”. EARSel. eProceedings, 5(1) : 77-88

Gherboudj, I., Bernier, M., Hicks, F.E., and Leconte, R. (2007). “Physical Characterization of Air Inclusions in River Ice”. Cold Regions Science and Technology (2007), doi: 10.1016/j.coldregions.2007.02.008.

Hicks, F. E. and Steffler, P.M. (1990). “Finite Element Modeling of Open Channel Flow”. Water Resources Engineering Report No. 90-6. Department of Civil Engineering, University of Alberta. Edmonton, Alberta.

Hicks, F. E. and Steffler P.M. (1992). “A Characteristic-Dissipative-Galerkin Scheme for Open Channel Flow”. ASCE Journal of Hydraulic Engineering, Vol. 118, No. 2, 337-352.

Hicks, F.E. (1996). “Hydraulic Flood Routing with Minimal Channel Data: Peace River, Canada”. Canadian Journal of Civil Engineering, Vol.23, No. 2, 524-535.

Hicks, F.E., Cui, W., and Andres, D. (1997). “Modeling Thermal Breakup on the Mackenzie River at the Outlet of Great Slave Lake, NWT”, Canadian Journal of Civil Engineering, 24(4): 570 - 585.

- Katopodis, C., and Ghamry, H. (2005). "Ice-covered hydrodynamic simulation: model calibration and comparisons for three reaches of the Athabasca River, Alberta, Canada". CGU HS Committee on River Ice Processes and the Environment – 13th Workshop on the Hydraulics of Ice Covered Rivers. Hanover, NH, September 15-16, 2005.
- Kellerhals, R., Neil, C.R., and Bray, D.I. (1972). "Hydraulic and Geomorphic Characteristics of Rivers in Alberta". River Engineering and Surface Hydrology Report 72-1. Alberta Research Council, Edmonton, Alberta.
- Kowalczyk, C., and Hicks, F.E. (2007). "Observations of Ice Jam Release Events on the Athabasca River near Fort McMurray, AB". Canadian Journal of Civil Engineering. 34 (4)473-484.
- Michel, B. (1971). "Winter Regime of Rivers and Lakes". Cold Regions Science and Engineering Monograph III-B1a, Cold Regions Research and Engineering Laboratory, U.S. Army, Hanover, New Hampshire, 131 pp.
- Moldoveanu-Constantinescu, M., and Stewart, R. (2004). "3D Ground Penetrating Radar Surveys on a Frozen River Lagoon". Canadian Society of Exploration Geophysicists – Recorder Committee. November, 2004.
- Moorman, B.J., and Michel, F.A. (1998). "The Application of Ground Penetrating Radar to the study of Glacial Hydrology". GPR '98: Seventh International Conference on Ground Penetrating Radar. The University of Kansas, Lawrence, Kansas, USA, May 27-30, 1998.

Pelletier, K.D., Van der Sanden, J., and Hicks, F.E. (2005). "Synthetic Aperture Radar: Current Capabilities and Limitations for River Ice Monitoring". CSCE 17th Annual Canadian Hydrotechnical Conference. Edmonton, AB, (August 17-19, 2005), 10 pp.

She, Y. *et al.* (2007). "Ice Jam Formation and Release Events on the Athabasca River, 2007". Committee on River Ice Processes and the Environment – 14th Workshop on the Hydraulics of Ice Covered Rivers. Quebec City, Ontario, 2007.

Robichaud, C. and Hicks, F.E. (2001). "Remote Monitoring of River Ice Jam Dynamics". Committee on River Ice Processes and the Environment – 11th Workshop on the Hydraulics of Ice Covered Rivers. Ottawa, Ontario, 2001.

Robichaud, C. (2003). "Hydrometeorological Factors Influencing Breakup Ice Jam Occurrence at Fort McMurray, Alberta". A thesis submitted to the Faculty of Graduate Studies and Research in partial fulfillment of the requirements for the degree of Master of Science in Water Resources Engineering. Department of Civil Engineering, University of Alberta, Edmonton, Alberta, 281 pp.

Weber, F., Nixon, D., Hurley, J. (2003). "Semi-automated classification of river ice types on the Peace River using RADRASAT-1 Synthetic Aperture Radar (SAR) imagery". *Canad. Journal of Civil Engineering*. Vol. 30, 2003: 11-27

Woynillowicz, D., and Severson-Baker, C. (2006). "Down to the Last Drop - The Athabasca River and Oil Sands", Oil Sands Paper No. 1, The Pembina Institute.

Van der Vinne, G., and Andres, D. (1993). "Winter Low Flow Tracer Dye Studies - Athabasca River. Athabasca to Bitumont, February and March, 1992 - Part I: Time of Travel". Northern River Basins Study Project Report No. 7. Edmonton, Alberta, June 1993.

- APPENDIX A -

Appendix A1 Campbell Scientific air temperature sensor (model 44212) – Specification sheet.

Appendix A. Specifications

YSI Thermilinear Network Specifications

44212	Linear Range	Linearity Deviation
	-50 to +50°C	±0.09°C

YSI Components Used in 44212 Network

44020 Thermistor	Maximum Operating Temperature	Accuracy and Interchangeability
$T_1 = 2,000 \Omega @ 25^\circ\text{C}$	55°C (131°F)	±0.1°C
$T_2 = 15,000 \Omega @ 25^\circ\text{C}$		
$T_3 = 45,000 \Omega @ 25^\circ\text{C}$		

44312 Resistor Set	Resistor Error
$R_1 = 23,100 \Omega$	±0.15°C @ -50°C, ±0.03°C @ +50°C
$R_2 = 88,200 \Omega$	
$R_3 = 38,000 \Omega$	

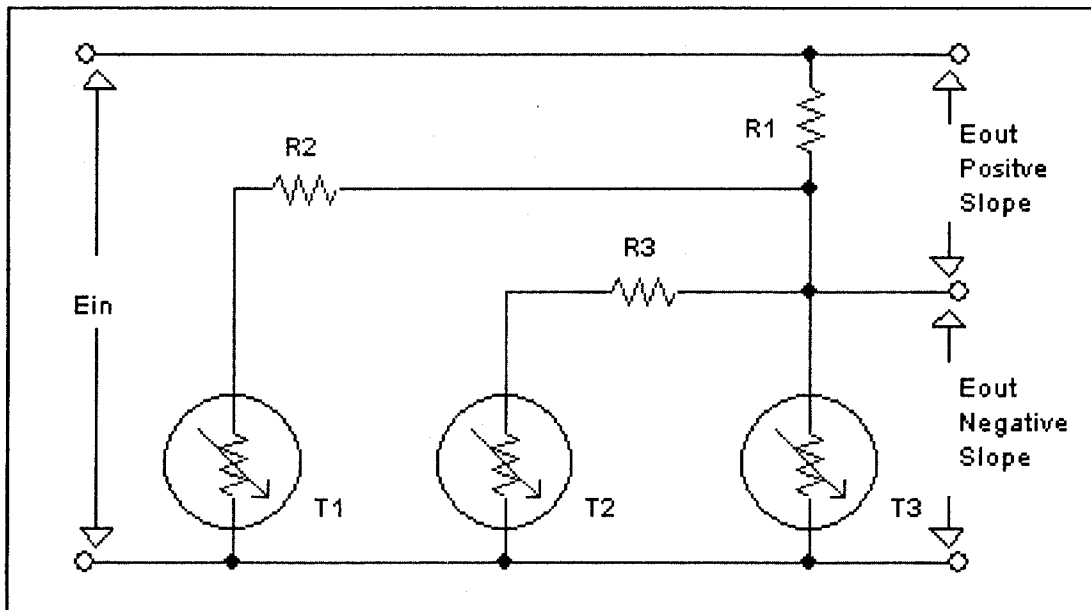


Figure A-1. YSI 44212 Thermilinear Network

Appendix A2 Van Essen Instruments Divers – Specification sheet

Mini-Diver datalogger

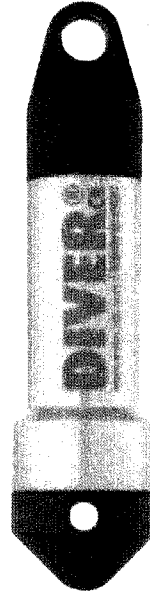


Applications:

- Monitoring projects
- Groundwater monitoring network automation

Mini-Diver: the proven concept

The Mini-Diver is based on an ingenious and proven concept and is acknowledged as the most reliable instrument for the autonomous measuring and recording of groundwater level and temperature. Its internal memory of 24,000 measurements per parameter provides sufficient capacity to perform nearly one measurement every ten minutes for six months. For each measurement, the Diver registers the date and time, groundwater level and temperature. The built-in battery has an expected lifespan of 10 years. Its compact dimensions (Ø22 mm, length 90 mm) mean that the Mini-Diver will fit into virtually any monitoring well.

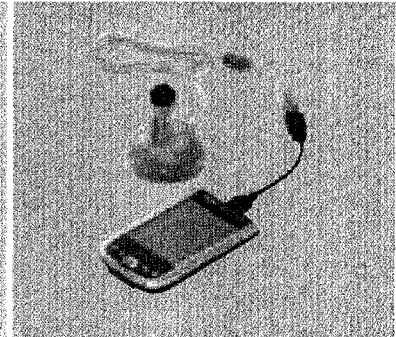


Highlights:

- 3 year warranty
- Long-term and frequent measurements
- Temperature corrected measurement
- Reliable and accurate measurement data
- Non-volatile memory
- Compact size
- Hermetically sealed in stainless steel housing
- Free of maintenance

Specifications:

Dimensions	Ø22 mm x 90 mm
Memory	24,000 measurements (non-volatile)
Sample rate	0.5 sec to 99 hours
Housing material	RVS 316L
Pressure sensor material	ceramic (Al ₂ O ₃)
Temperature range	-20 °C to 80 °C
- accuracy	±0.1 °C
- resolution	0.01 °C
- compensated range	0 °C to 40 °C
Battery life	10 years (depending on use)
Weight	70 grams



Mini-Diver® Technical specifications (pressure)

Type	DI 501	DI 502	DI 505	DI 510	DI 500 (Baro)
Range	10 m H ₂ O	20 m H ₂ O	50 m H ₂ O	100 m H ₂ O	1.5 m H ₂ O
- accuracy**	0.5 cm H ₂ O	1 cm H ₂ O	2.5 cm H ₂ O	5 cm H ₂ O	0.5 cm H ₂ O
- resolution	0.2 cm H ₂ O	0.4 cm H ₂ O	1 cm H ₂ O	2 cm H ₂ O	0.1 cm H ₂ O

** within temperature compensated range

**Appendix A3 Sontek Acoustic Doppler Current Profiler –
Specification sheet**

RiverSurveyor/RiverCAT Specifications

Velocity Data

- Range: ± 10 m/s
- Resolution: 0.1 cm/s
- Accuracy: ± 1 % of measured velocity, ± 0.5 cm/s
- Up to 100 range cells

Frequency	Profiling Range Min - Max	Minimum Cell Size
500 kHz System	2.0 - 160 m (6.6 - 330 ft)	1.0 m (3.3 ft)
1.0 MHz Mini	0.75 - 35 m (2.5 - 115 ft)	0.25 m (0.8 ft)
1.5 MHz Mini	0.5 - 25 m (1.6 - 82 ft)	0.25 m (0.8 ft)
3 MHz Mini	0.3 - 8.0 m (1.0 - 20 ft)	0.15 m (0.5 ft)

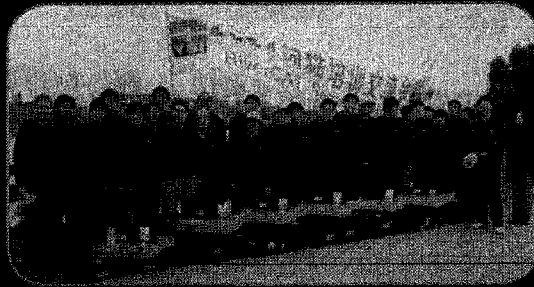
Nominal range can vary depending on environmental conditions

RiverSurveyor Hardware Features (Mini Only)

- SonTek ADP (Acoustic Doppler Profiler)
- 360° solid state TrueCompass/tilt sensor
- Temperature sensor
- RS-232 serial interface
- Bluetooth telemetry system (200m range)

Optional Features

- Pressure sensor for transducer depth corrections (not available on 1.0 MHz Mini)
- Built-in recorder (not available on 1.0 MHz Mini)
- Four-beam transducer head (500 kHz system only)
- Integrated DGPS system via ADP electronics
- 40" plastic OceanScience Catamaran/Trimaran hulls
- Premium FreeWave radio modem (over 2-km range)



China's National RiverCAT Training Course, Shanghai, China

RiverSurveyor/RiverCAT Features

RiverCAT

- 27" Aluminum catamaran (with case)
- Integrated Bluetooth telemetry
- Battery compartment with replaceable "C" cells
- Hard plastic shipping case with wheels



Convenient mobile carrying case

RiverSurveyor Software Features

- Windows 2000/NT/XP/Vista+ compatible
- Bottom-tracking (independent of GPS)
- DGPS and Echo Sounder interface
- Real-time discharge calculation
- Landmarks and navigation waypoints
- Discharge measurement options for unmeasured areas
- Professional discharge summary reports and output
- Vessel track with velocity vectors
- Bathymetric profile



Under-ice discharge measurements on the Mackenzie River, Northwest Territories, Canada

**Appendix A4 Campbell Scientific soil/water temperature probe
(model 107B) – Specification sheet**

Model 107 Temperature Probe

1. General

The 107 Temperature Probe uses a thermistor to measure temperature. The probe is designed for measuring air/soil/water temperatures. For air temperature, a 41303-5A radiation shield is used to mount the 107 Probe and limit solar radiation loading. The probe is designed to be buried or submerged in water to 50' (21 psi).

The -L option on the model 107-L Temperature probe indicates that the cable length is user specified. This manual refers to the sensor as the 107.

Lead length for the 107 is specified when the sensor is ordered. Table 1-1 gives the recommended lead length for mounting the sensor at the top of the tripod/tower with a 2 foot crossarm. Lead length can be 2 feet shorter when the sensor is mounted to the tripod mast / tower leg without a crossarm.

CM6	CM10	CM110	CM115	CM120	UT10	UT20	UT30
11'	14'	14'	19'	24'	14'	24'	37'

The 107 ships with:

- (1) Instruction Manual

1.1 Specifications

Sensor: BetaTherm 100K6A Thermistor

Temperature
Measurement Range: -35° to +50°C

Thermistor Inter-
changeability Error: Typically $<\pm 0.2^{\circ}\text{C}$ over 0°C to 60°C ; ± 0.4 @ -35°C

Temperature
Survival Range: -50°C to $+100^{\circ}\text{C}$

Polynomial
Linearization Error: $<\pm 0.5^{\circ}\text{C}$ over -35°C to $+50^{\circ}\text{C}$

Time Constant
In Air: Between 30 and 60 seconds in a wind speed of 5 m s^{-1}

Maximum Lead
Length: 1000 ft.

NOTE

The black outer jacket of the cable is Santoprene® rubber. This compound was chosen for its resistance to temperature extremes, moisture, and UV degradation. However, this jacket will support combustion in air. It is rated as slow burning when tested according to U.L. 94 H.B. and will pass FMVSS302. Local fire codes may preclude its use inside buildings.

2. Accuracy

The overall probe accuracy is a combination of the thermistor's interchangeability specification, the precision of the bridge resistors, and the polynomial error. In a "worst case" all errors add to an accuracy of $\pm 0.4^\circ\text{C}$ over the range of -24° to 48°C and $\pm 0.9^\circ\text{C}$ over the range of -38°C to 53°C . The major error component is the interchangeability specification of the thermistor, tabulated in Table 2-1. For the range of 0° to 50°C the interchangeability error is predominantly offset and can be determined with a single point calibration. Compensation can then be done with an offset entered in the measurement instruction. The bridge resistors are 0.1% tolerance with a 10 ppm temperature coefficient. Polynomial errors are tabulated in Table 2-2 and plotted in Figure 2-1.

TABLE 2-1. Thermistor Interchangeability Specification

Temperature ($^\circ\text{C}$)	Temperature Tolerance ($\pm^\circ\text{C}$)
-40	0.40
-30	0.40
-20	0.32
-10	0.25
0 to +50	0.20

TABLE 2-2. Polynomial Error

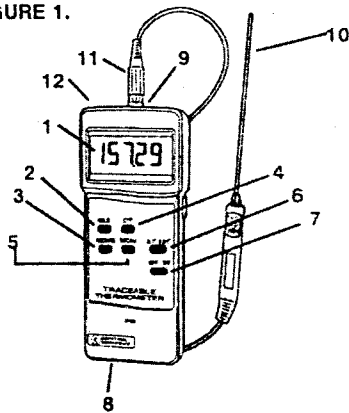
-40 to +56	$<\pm 1.0^\circ\text{C}$
-38 to +53	$<\pm 0.5^\circ\text{C}$
-24 to +48	$<\pm 0.1^\circ\text{C}$

Appendix A5 RTD Platinum Thermometer – Specification sheet

SPECIFICATIONS

- Display: LCD, 1/2" digits
- Meter Range: -328 to 1472°
(-200 to 800°C)
- Probe Range: -58 to 752°F
(-50 to 400°C)
- Accuracy: ±(0.1% + 0.2°) below 200°
and ±(0.15% + 0.5°)
- Power: 9V battery
- Size: 7 x 3 x 1-1/4 inches
- Accessories: Platinum probe, battery,
Supplied: Traceable Certificate and
instructions.

FIGURE 1.



Description:

- 1 Display
- 2 HOLD Button
- 3 Record Button
- 4 °C/°F Switch
- 5 Recall Button
- 6 0.1%/0.01° Button
- 7 Power Switch
- 8 Battery Cover
- 9 Input Socket
- 10 PT 100 ohm
Temperature Probe
- 11 Probe Plug
- 12 RS-232 output
terminal

OPERATION

1. Turn on the unit by sliding the power switch (7, Fig. 1) to the "ON" position.
2. Press the °F/°C Button to select the desired temperature unit (4, Fig. 1).
3. Select the desired resolution by pressing the 0.1%/0.01° Button (6, Fig. 1).
4. Connect the Probe Plug (11, Fig. 1) to the input Socket (9, Fig. 1). The display will show the temperature from the tip of the probe.
5. Press the HOLD button (2, Fig. 1) once to "freeze" the display at the current temperature reading. "HOLD" appears on the upper portion of the display indicating that the unit is in hold mode. Press the HOLD button again to release the reading.
6. The data record function captures the maximum and minimum readings. To begin, press the RECORD button (3, Fig. 1) once. "RECORD" appears in the upper portion of the display.
7. While in record mode, press the RECALL button (5, Fig. 1) once. "MAX" appears on the display indicating the temperature shown is the maximum value recorded.
8. Press the RECALL button a second time, and "MIN" appears on the display, indicating that this is minimum value recorded.
9. To exit the record mode, press the RECORD button once again. The display will show the current reading

RS—232 PC SERIAL INTERFACE

This unit features RS-232 output. An RS-232 OUTPUT SOCKET (12, Fig. 1) is located on the top of the unit. To utilize this feature, connect the unit to a PC with the Data Acquisition Accessory (see "ACCESSORIES" section).

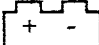
Data is displayed in a 16-digit stream: D15 through D0. Each digit indicates the following:

- D0 end word
- D1 to D8 Display Reading: D1=LSD, D8=MSD
- D9 Decimal Point (DP): 0=no DP,
1 = 1 DP, 2 = 2 DP, 3 = 3DP
- D10 Reading Polarity for the display:
0 = "+", 1 = "-"
- D11/D12 Annunciator for Display: 01=°C, 02=°F
- D13 1
- D14 4
- D15 start word

ALL OPERATIONAL DIFFICULTIES

If this thermometer does not function properly for any reason, please properly replace the battery with a new 9V battery (see Battery section, below). Low battery power can occasionally cause any number of "apparent" operational difficulties. Replacing the battery with a new fresh battery will solve most difficulties.

BATTERY REPLACEMENT

When  appears on the display, erratic readings appear, there is a faint display or no display—these are all indicators that the battery is low and needs to be replaced. To replace the battery, remove the battery cover located on the back of the unit (8, Fig. 1) by using a coin to slide the cover away from the unit. Insert a new 9V battery (alkaline). Incorrectly installed batteries may damage electronics. Replace the battery cover.

- APPENDIX B -

Appendix B1 Ice cover mapping – November 5, 2006

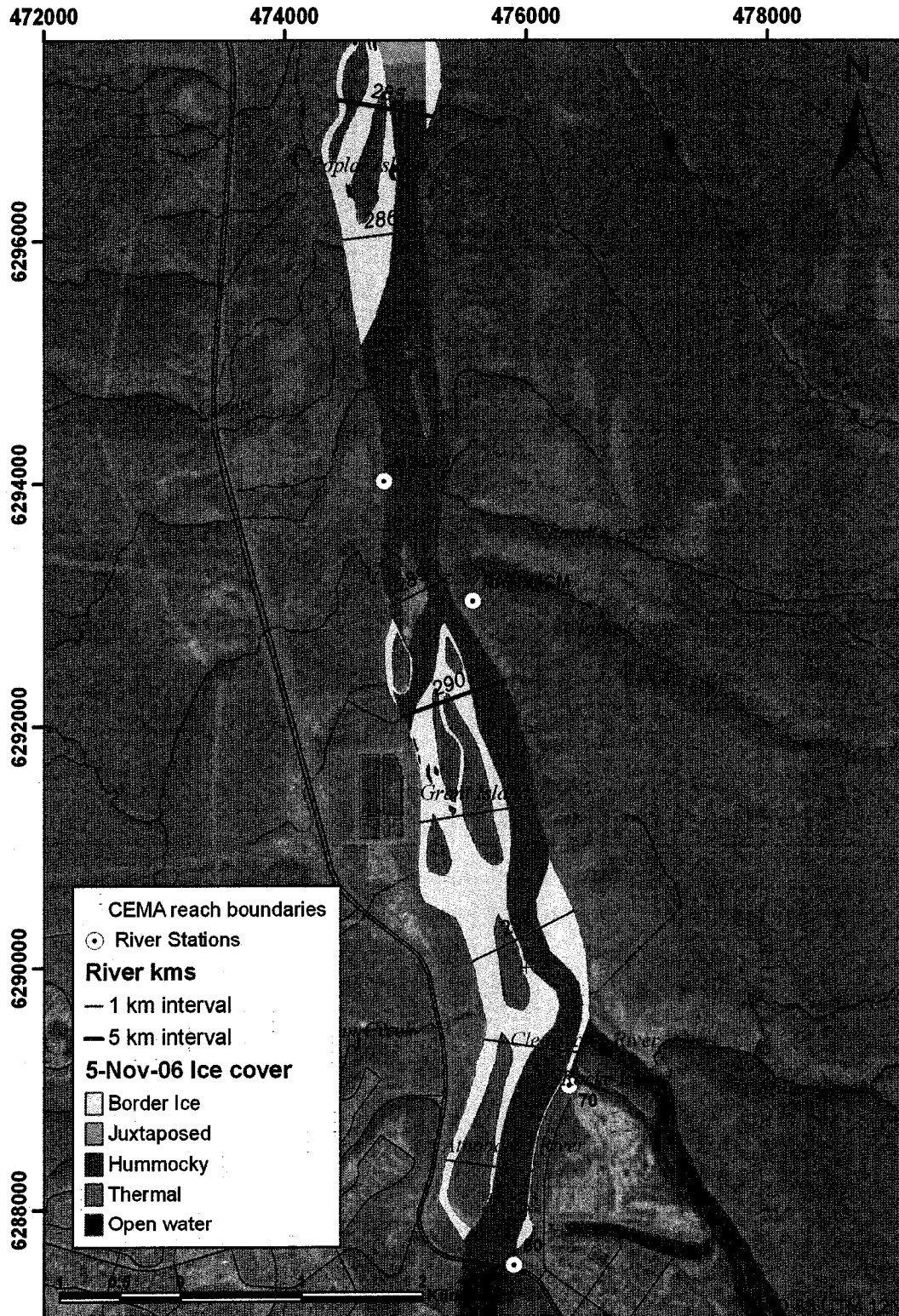


Figure B1.1 Ice cover mapping: November 5, 2006 - km 295 to 285

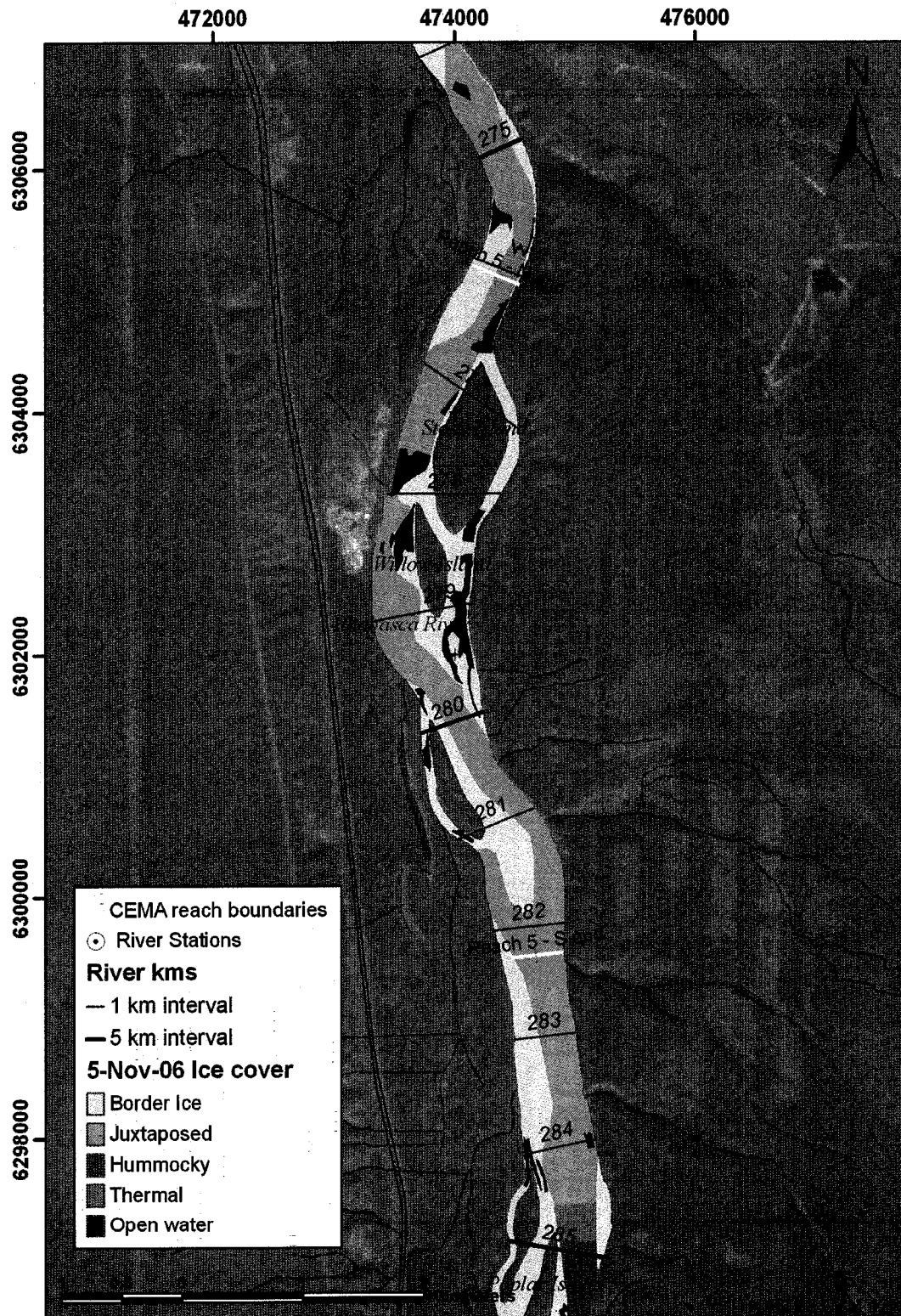


Figure B1.2 Ice cover mapping: November 5, 2006 - km 285 to 274

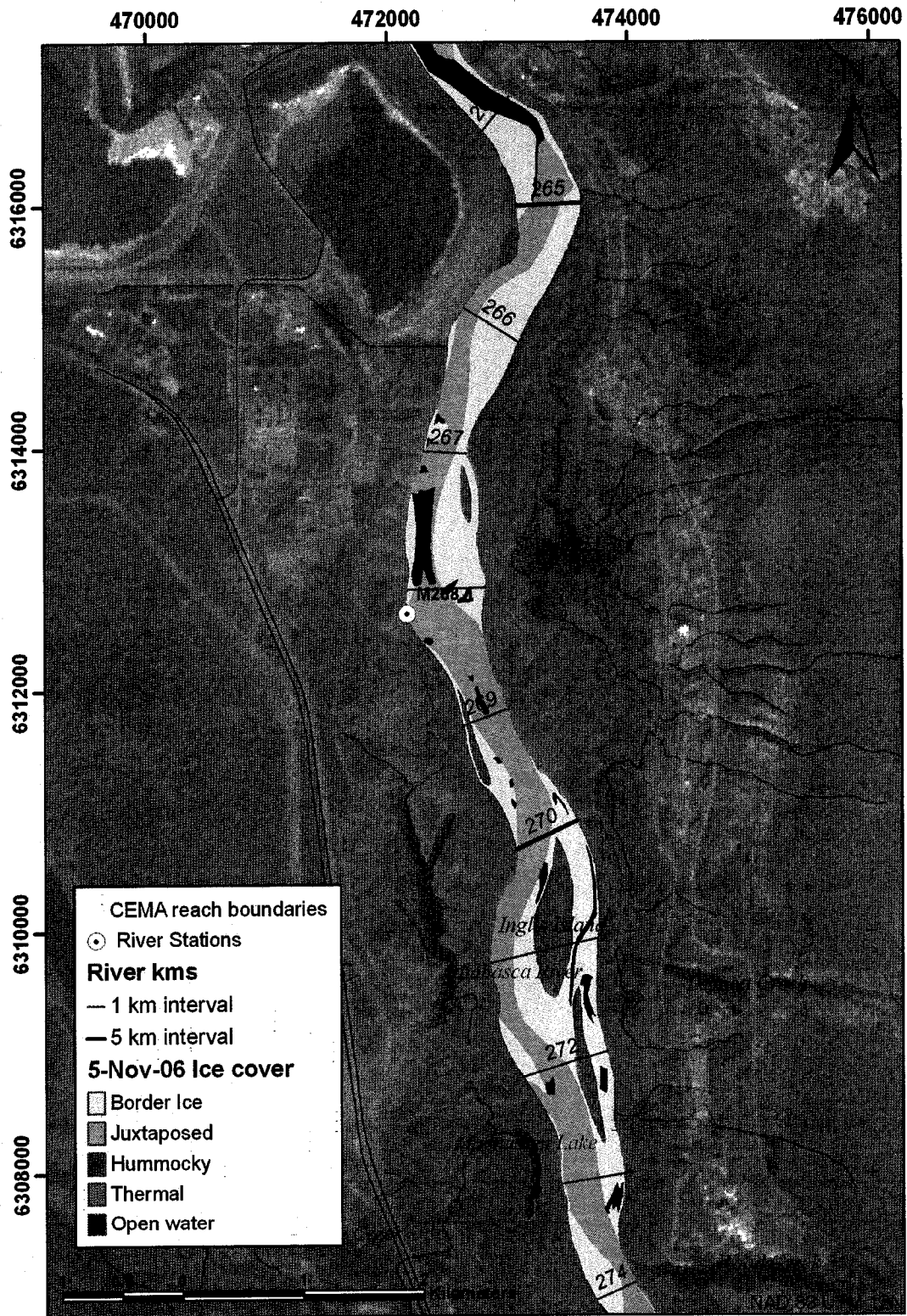


Figure B1.3 Ice cover mapping: November 5, 2006 - km 274 to 264

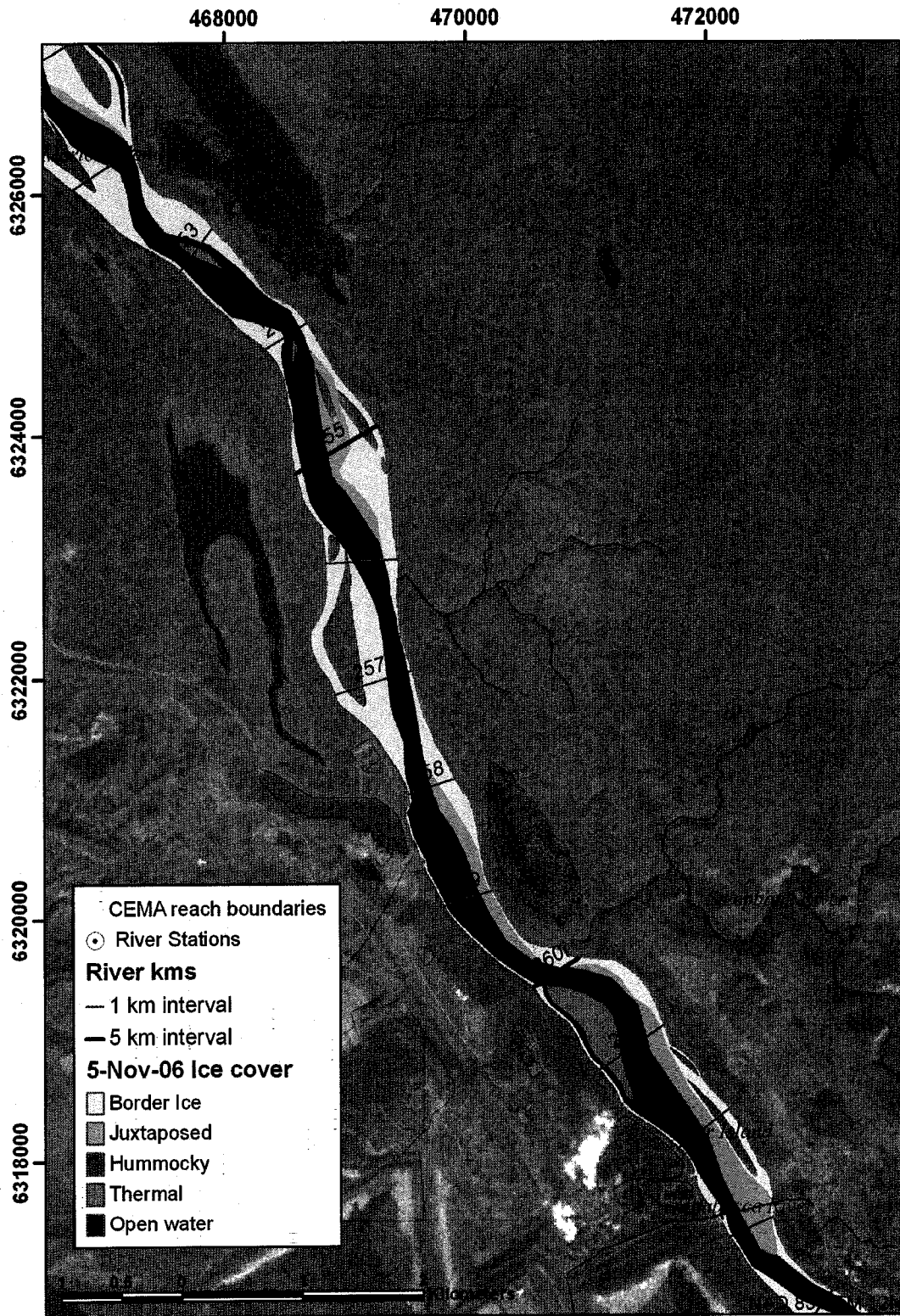


Figure B1.4 Ice cover mapping: November 5, 2006 - km 264 to 252

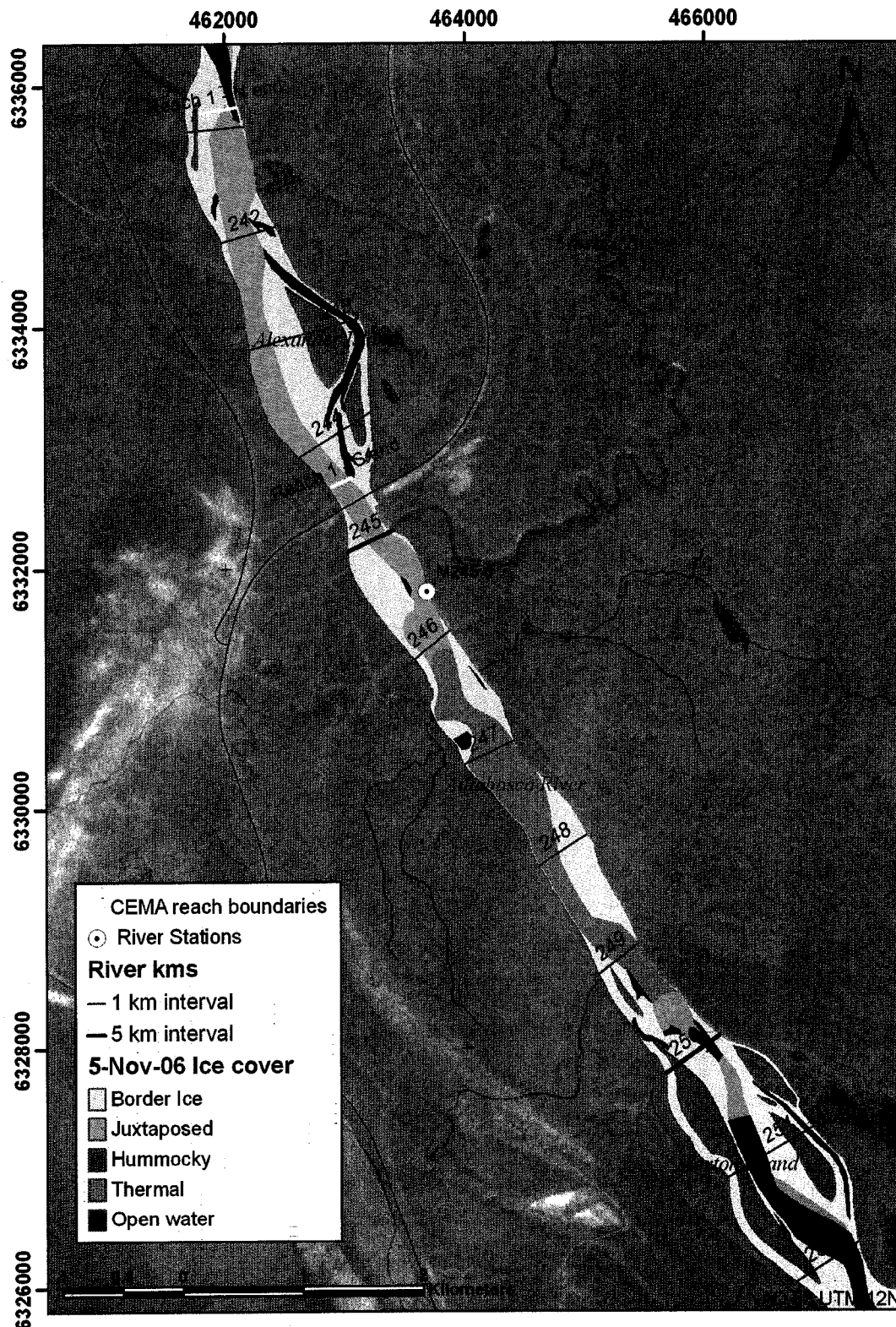


Figure B1.5 Ice cover mapping: November 5, 2006 - km 252 to 241

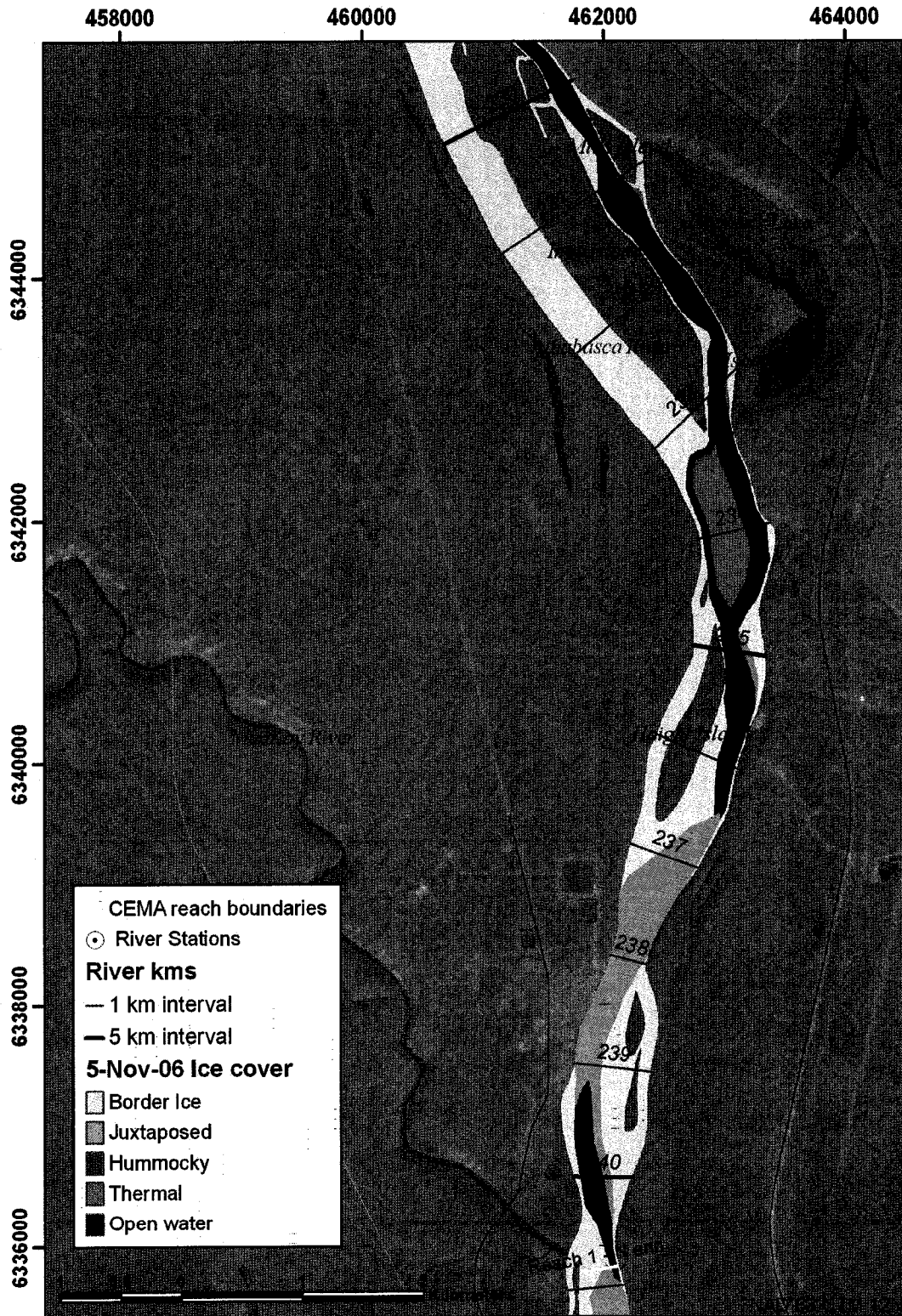


Figure B1.6 Ice cover mapping: November 5, 2006 - km 241 to 230

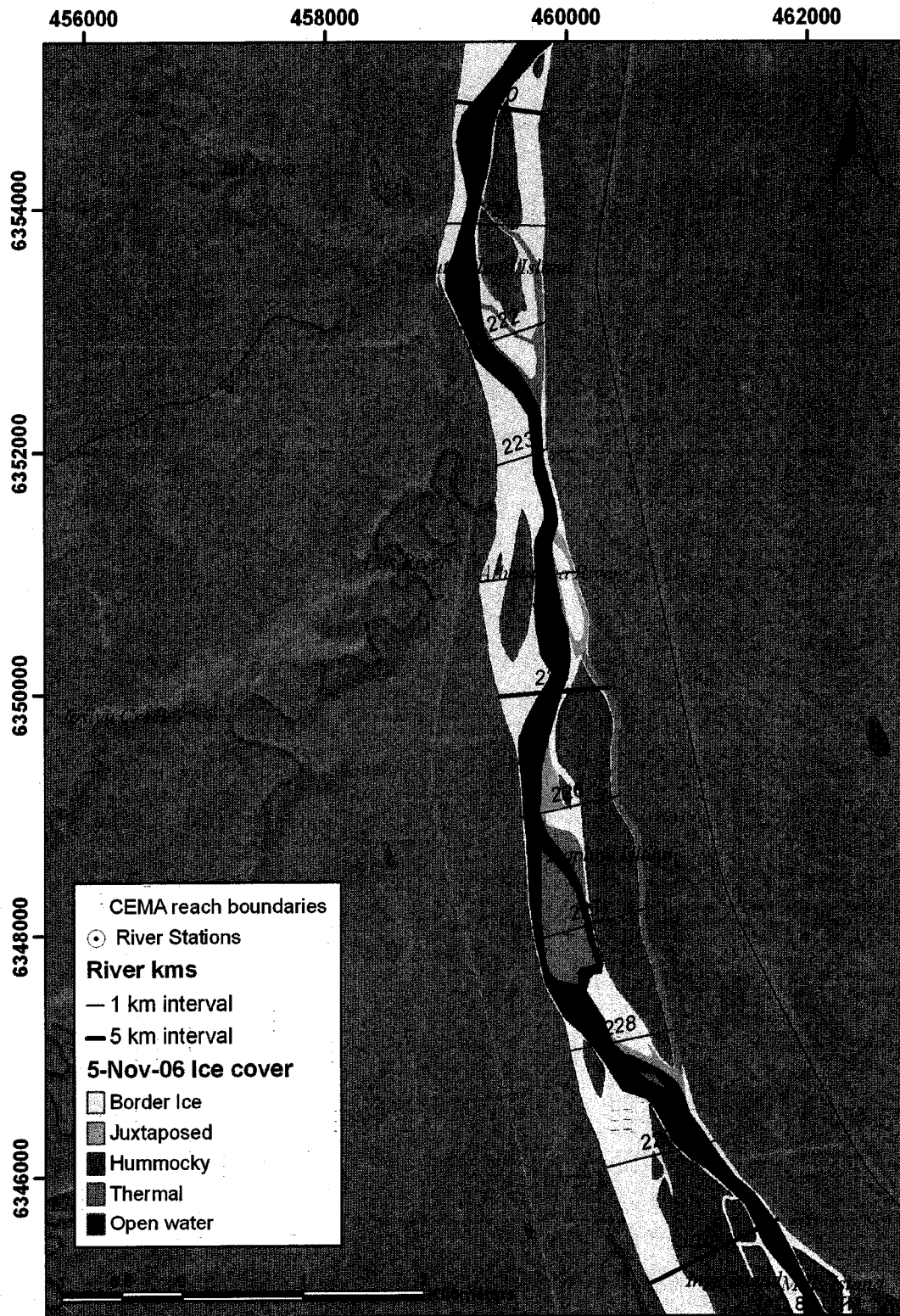


Figure B1.7 Ice cover mapping: November 5, 2006 - km 230 to 220

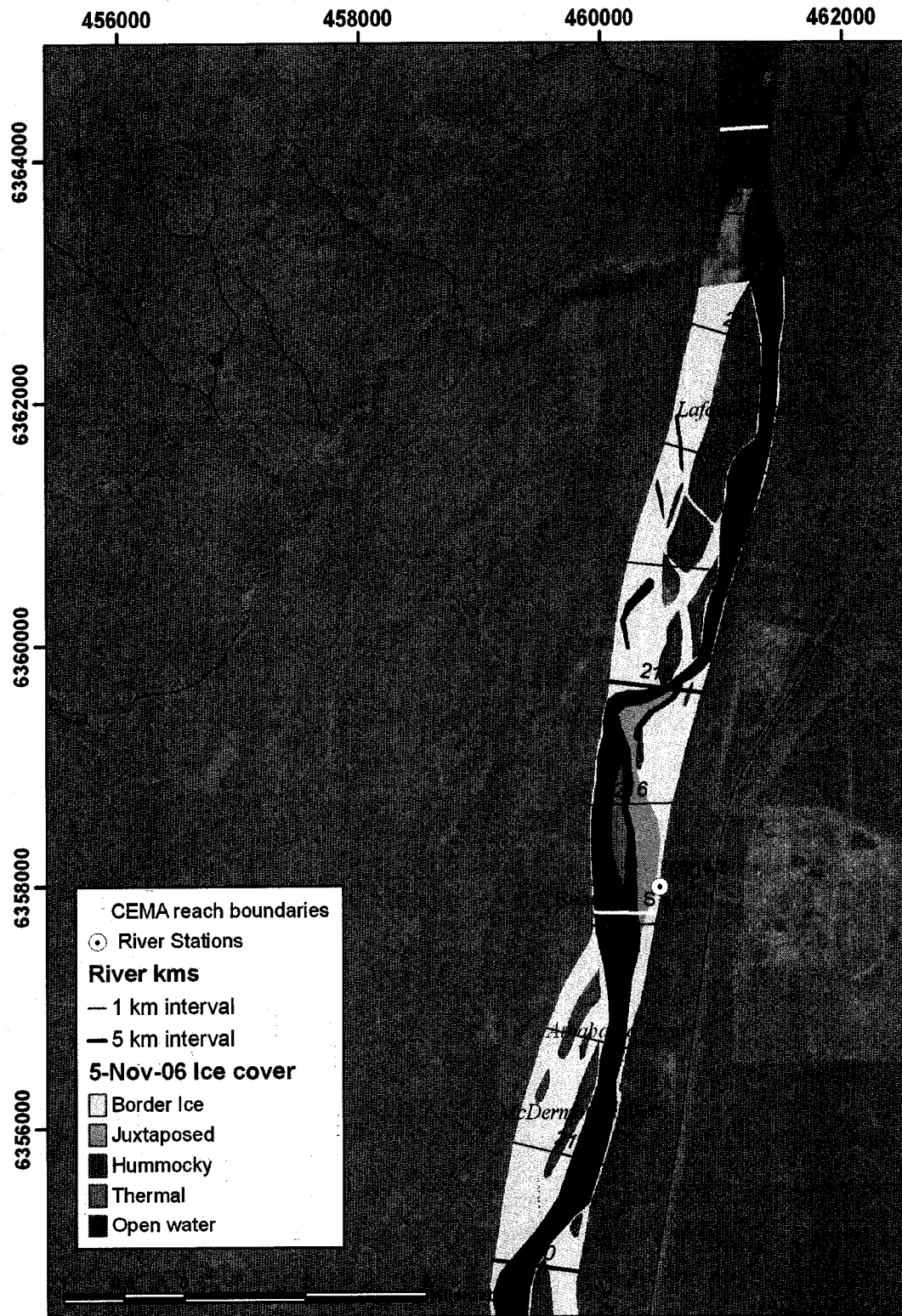


Figure B1.8 Ice cover mapping: November 5, 2006 - km 220 to 210

Appendix B2 Ice cover mapping – November 10, 2006

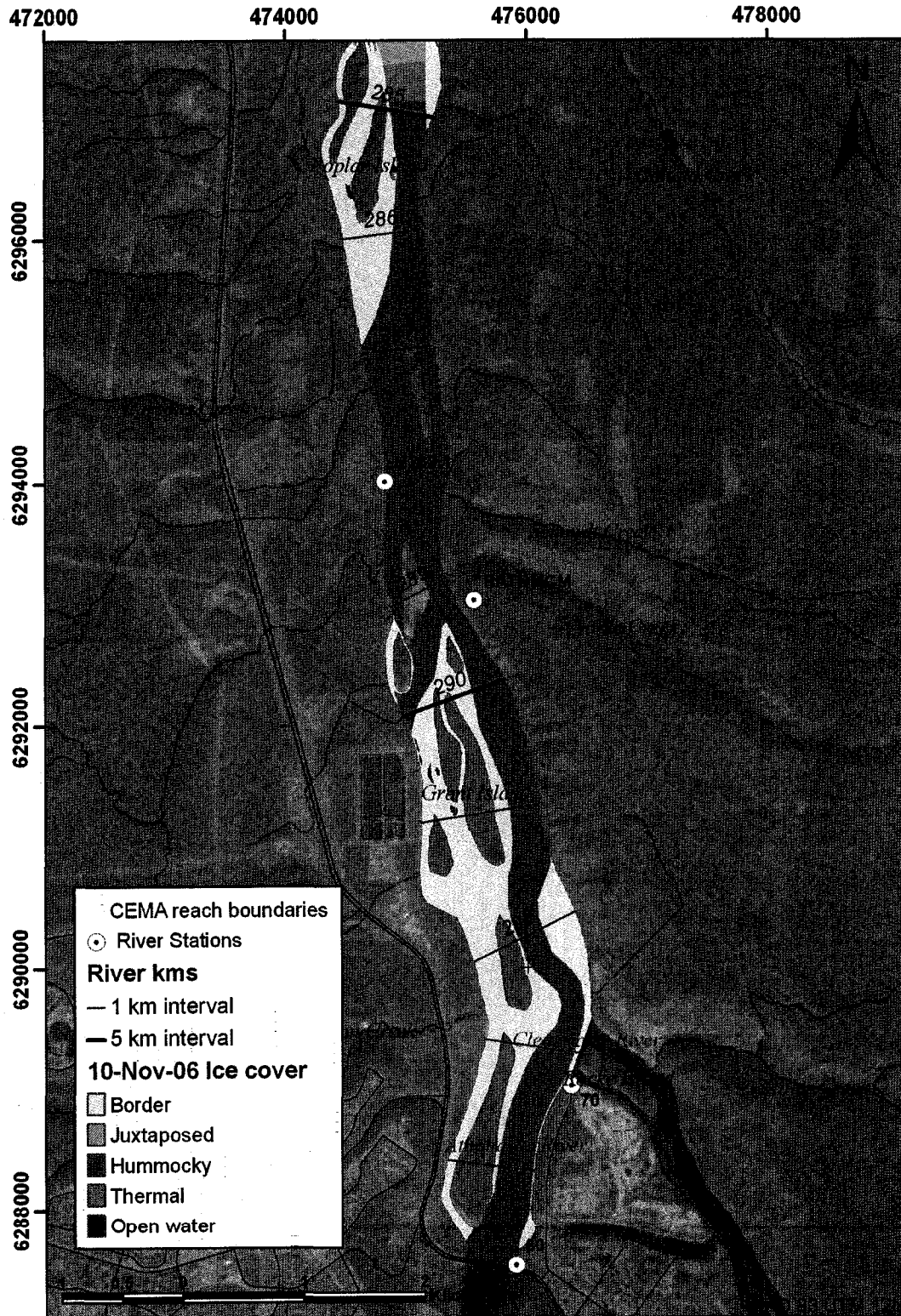


Figure B2.1 Ice cover mapping: November 10, 2006 - km 295 to 285

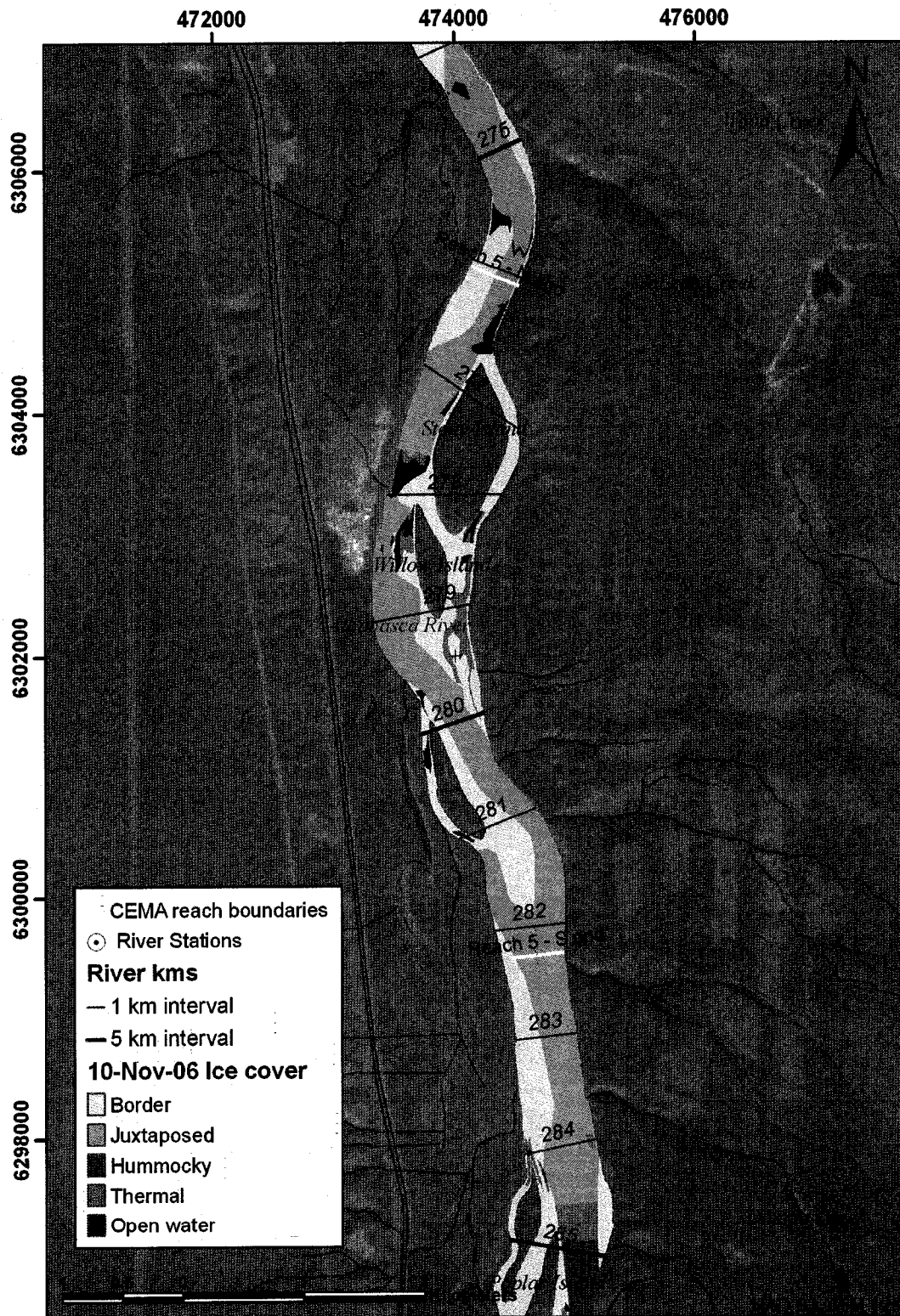


Figure B2.2 Ice cover mapping: November 10, 2006 - km 285 to 274

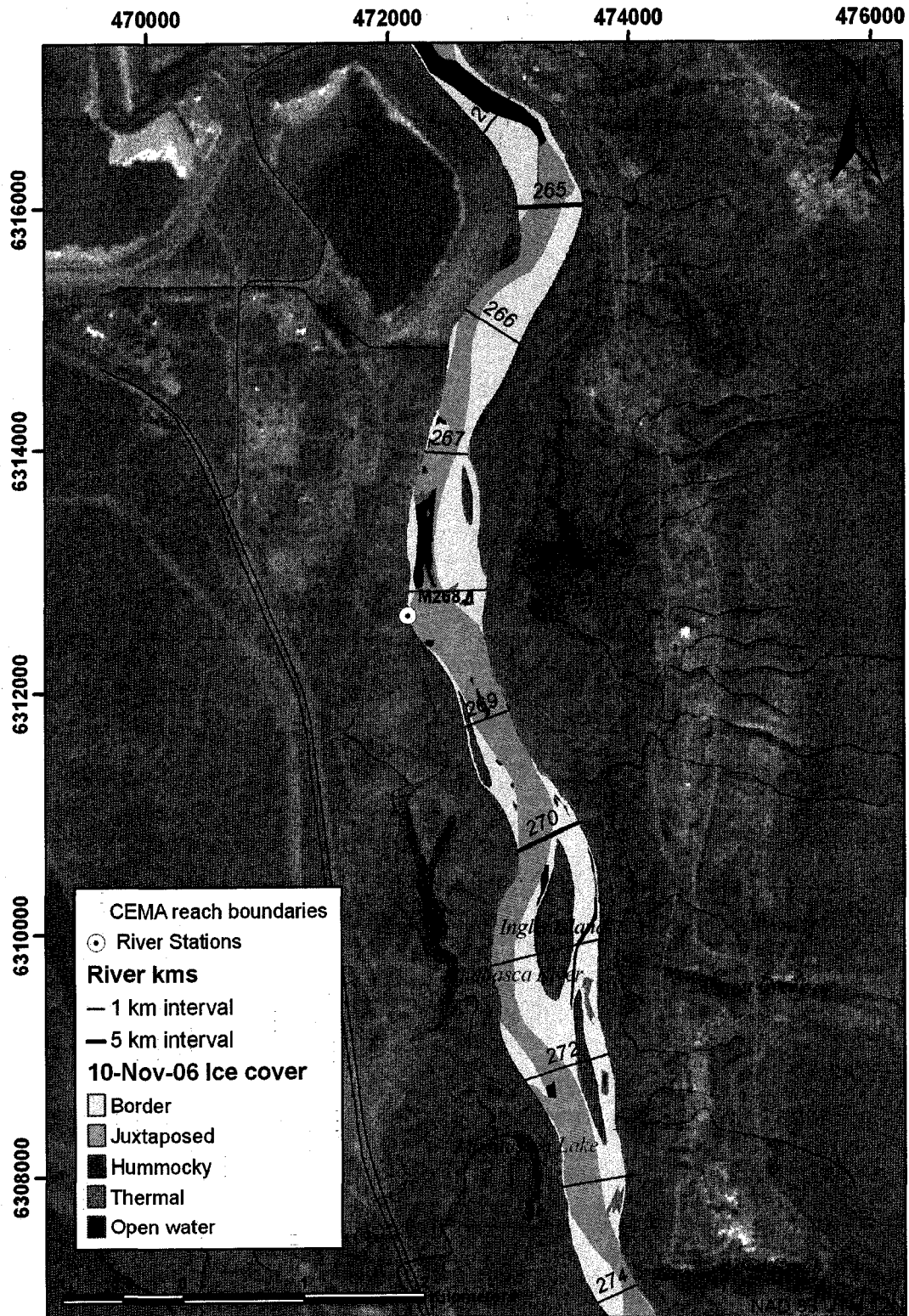


Figure B2.3 Ice cover mapping: November 10, 2006 - km 274 to 264

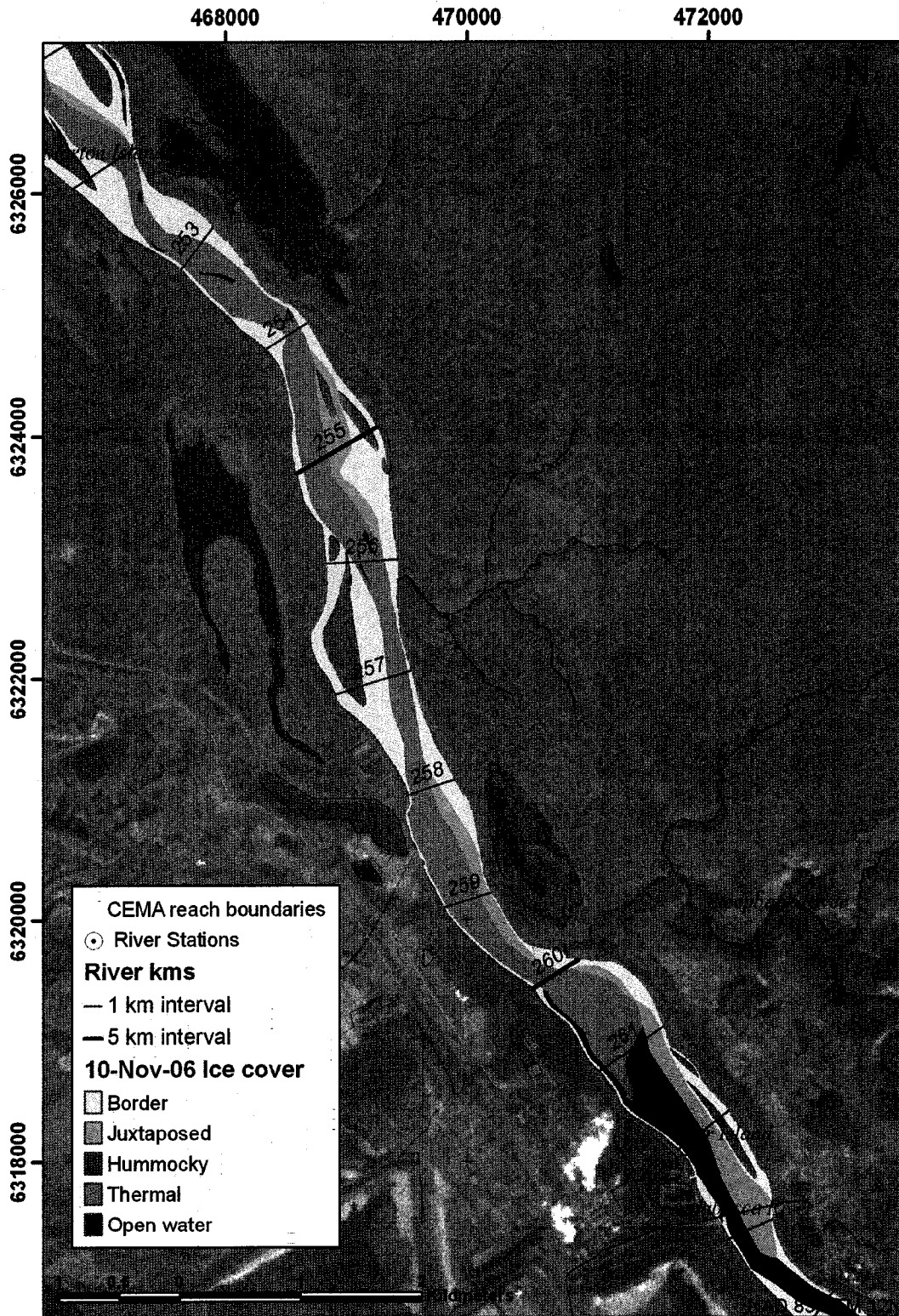


Figure B2.4 Ice cover mapping: November 10, 2006 - km 264 to 252

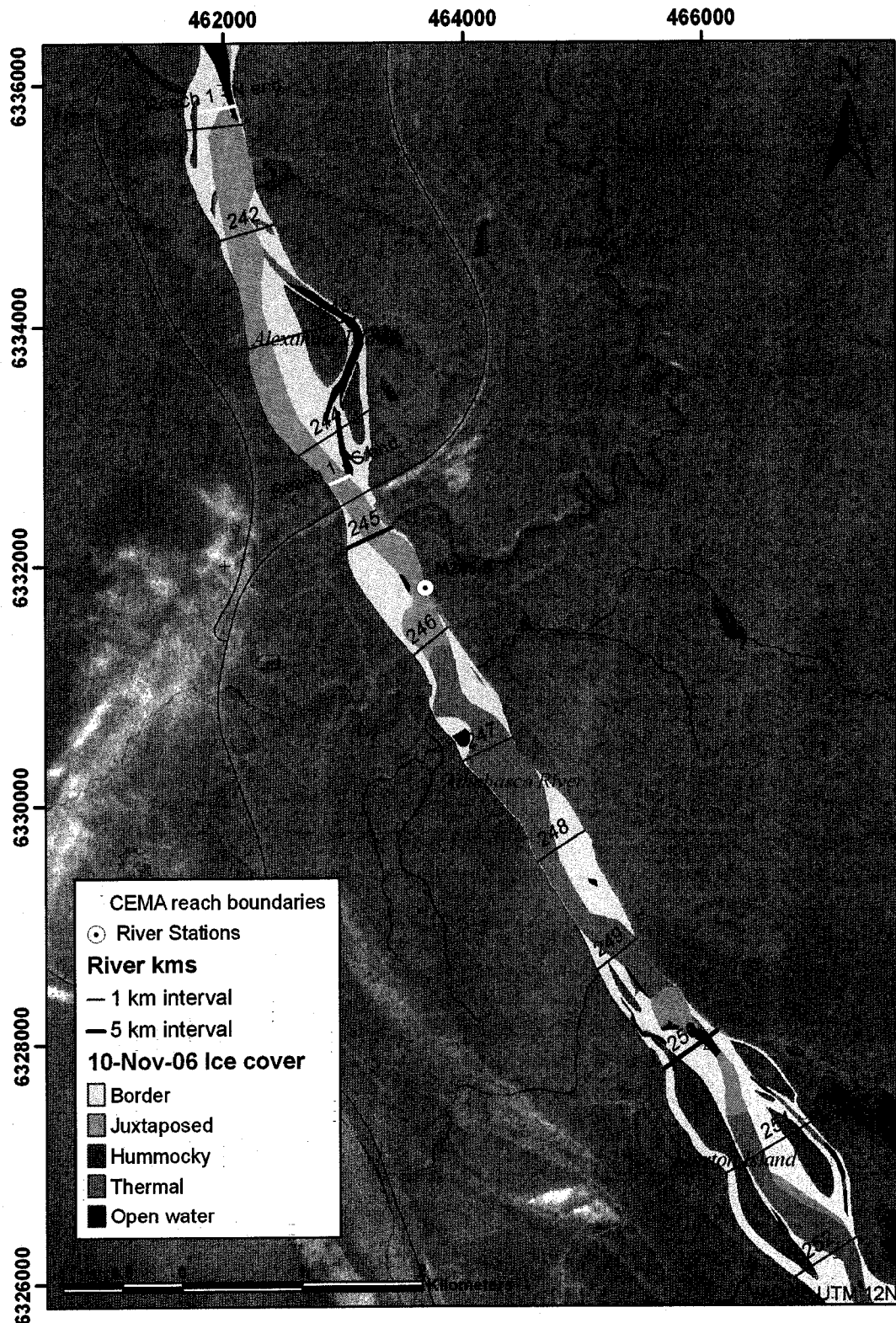


Figure B2.5 Ice cover mapping: November 10, 2006 - km 252 to 241

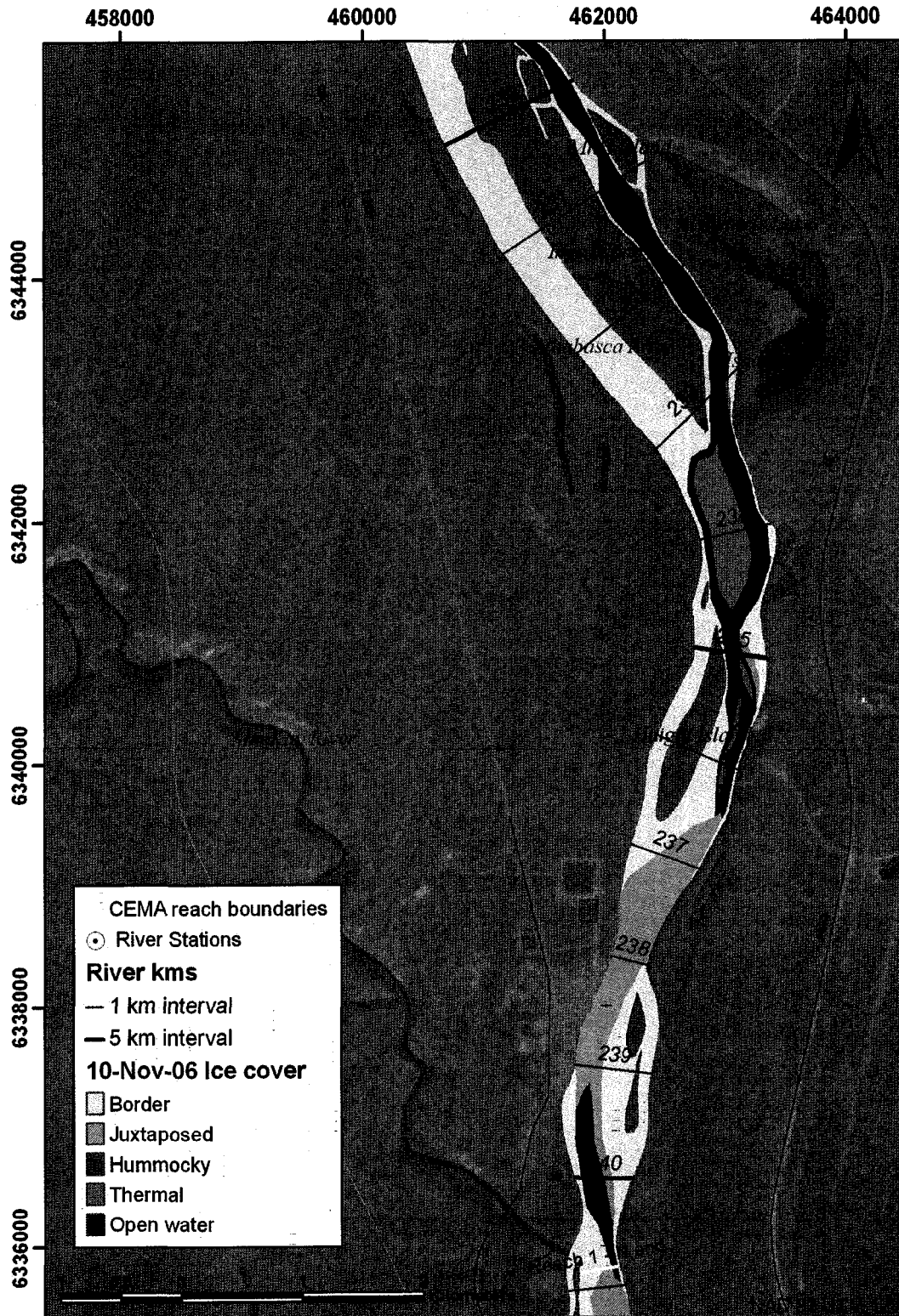


Figure B2.6 Ice cover mapping: November 10, 2006 - km 241 to 230

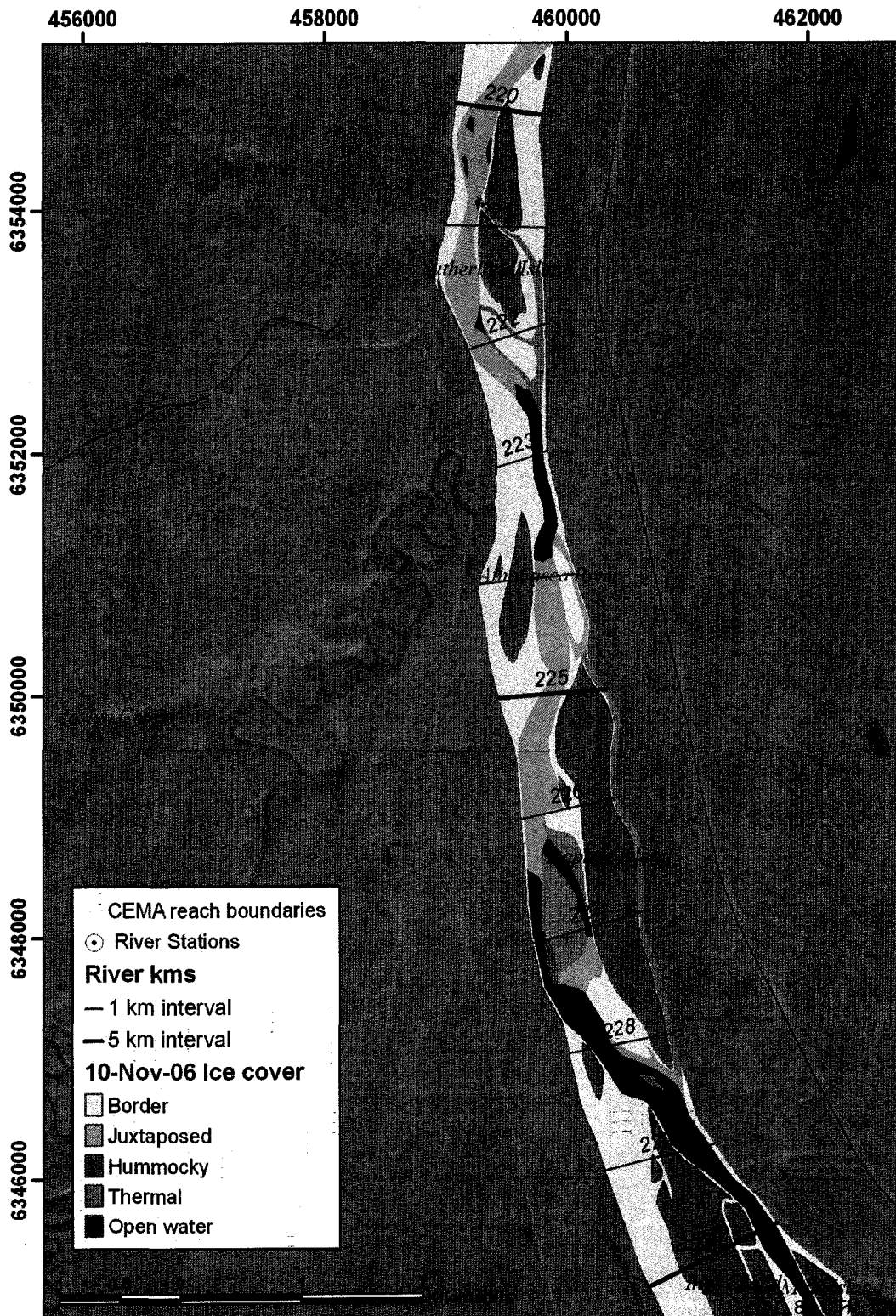


Figure B2.7 Ice cover mapping: November 10, 2006 - km 230 to 220

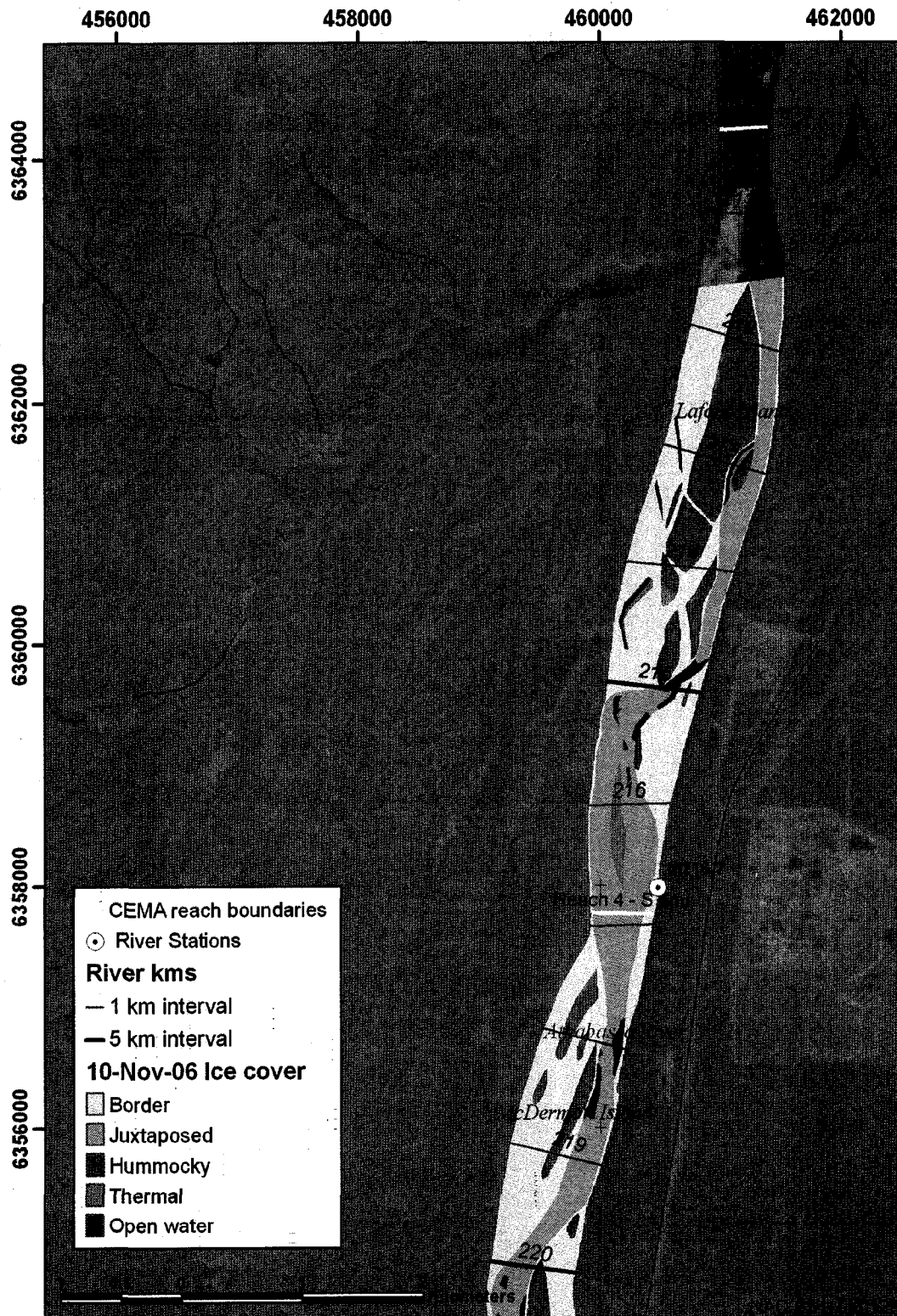


Figure B2.8 Ice cover mapping: November 10, 2006 - km 220 to 210

Appendix B3 Ice cover mapping – November 17, 2006

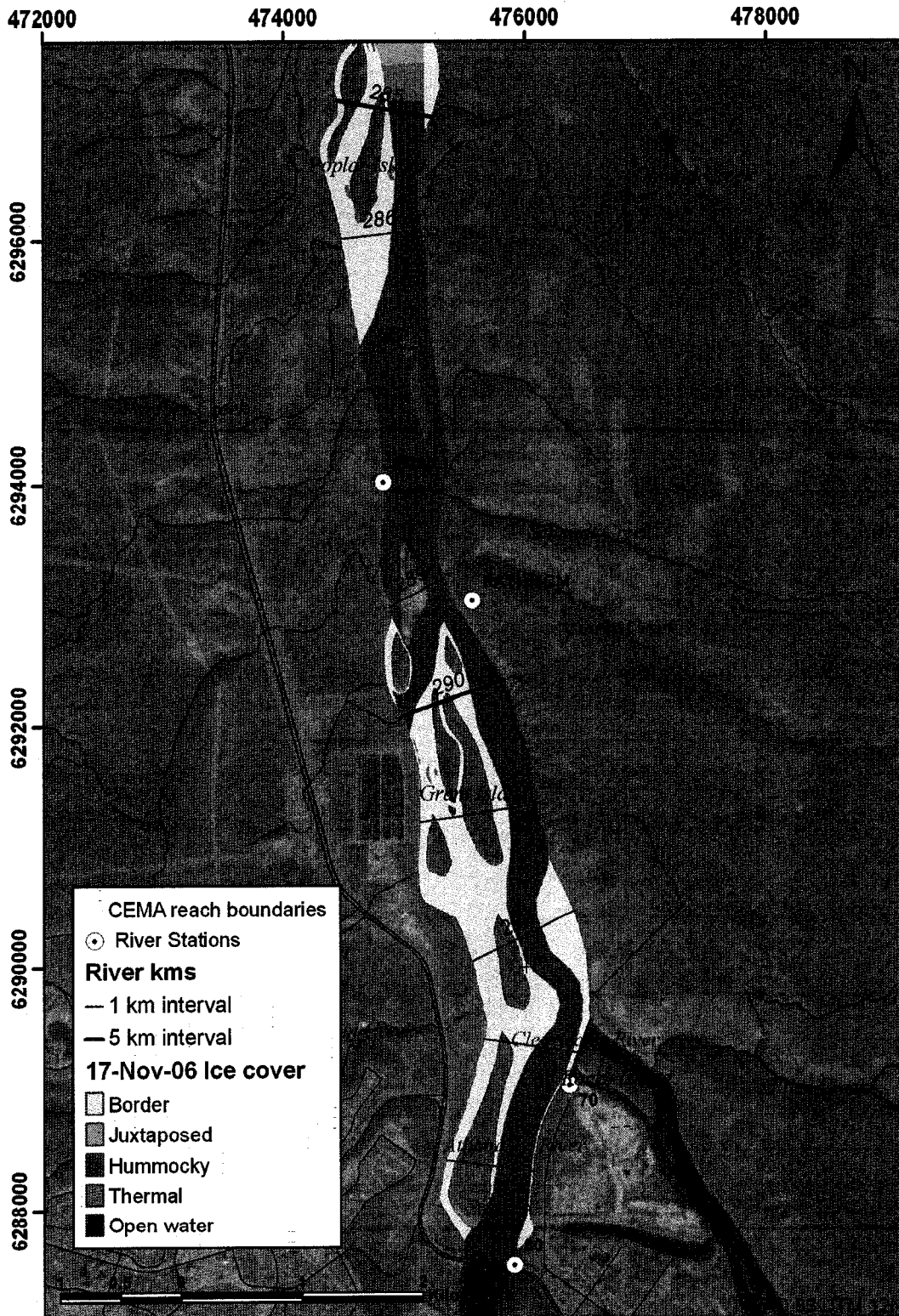


Figure B3.1 Ice cover mapping: November 17, 2006 - km 295 to 285

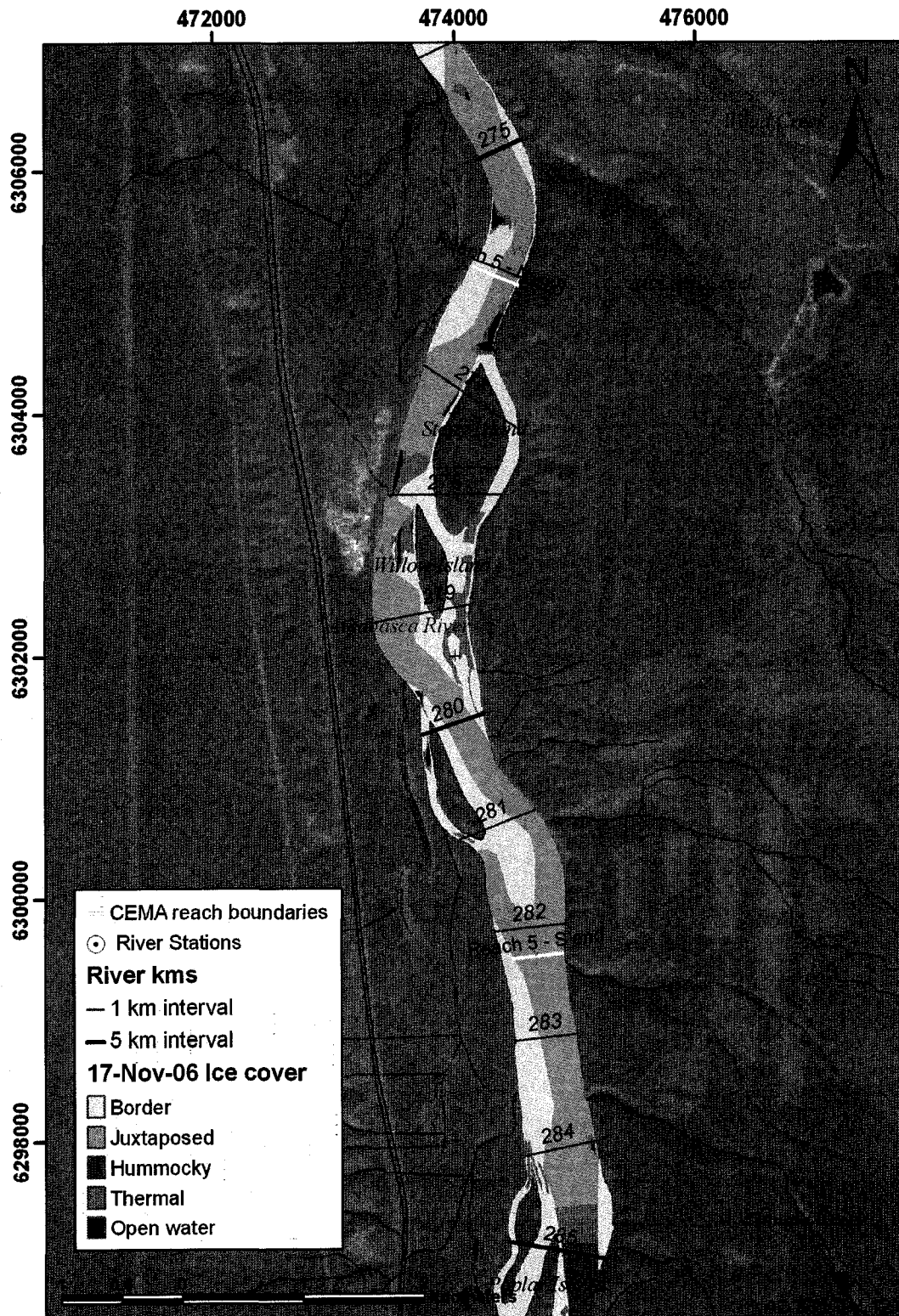


Figure B3.2 Ice cover mapping: November 17, 2006 - km 285 to 274

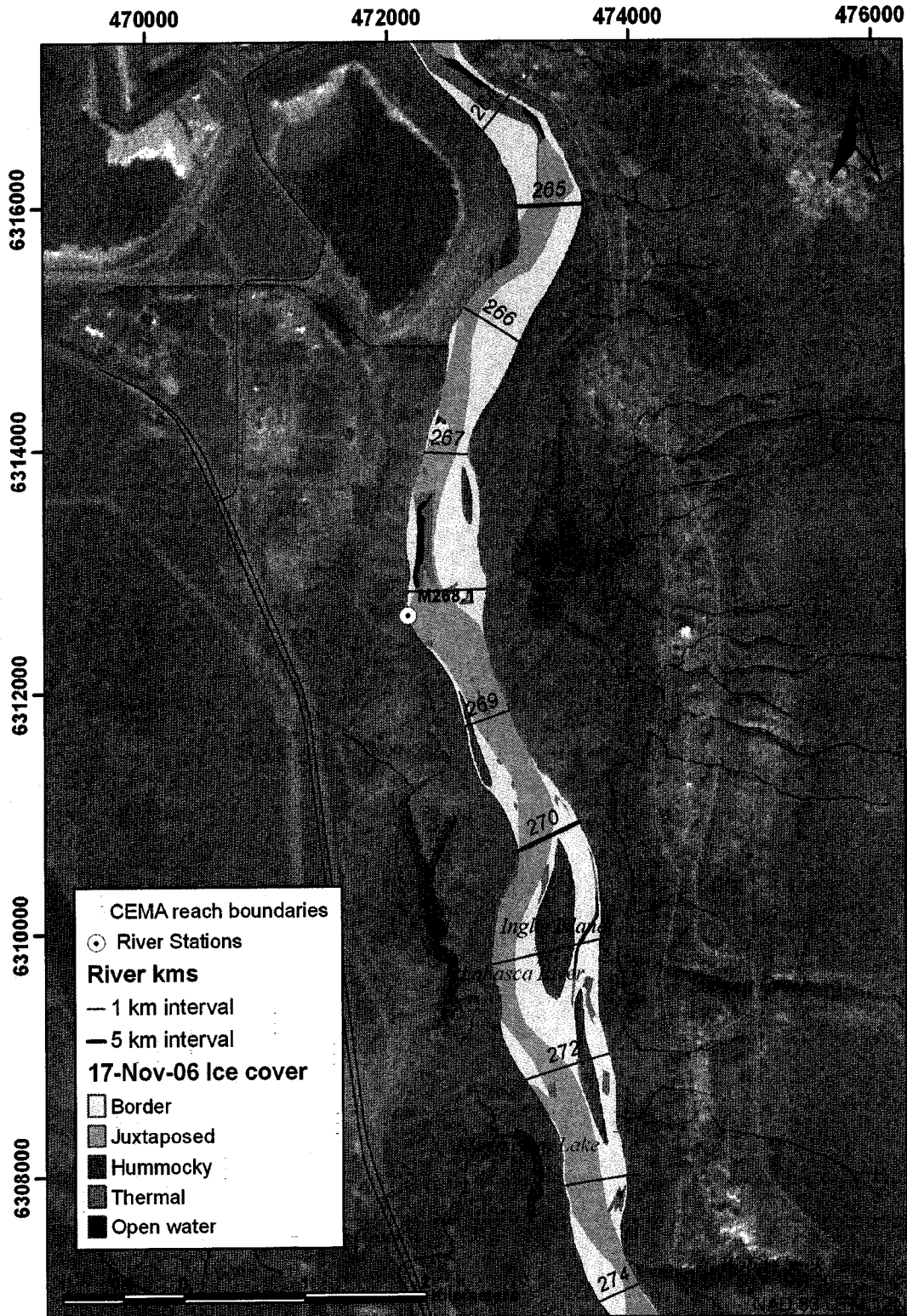


Figure B3.3 Ice cover mapping: November 17, 2006 - km 274 to 264

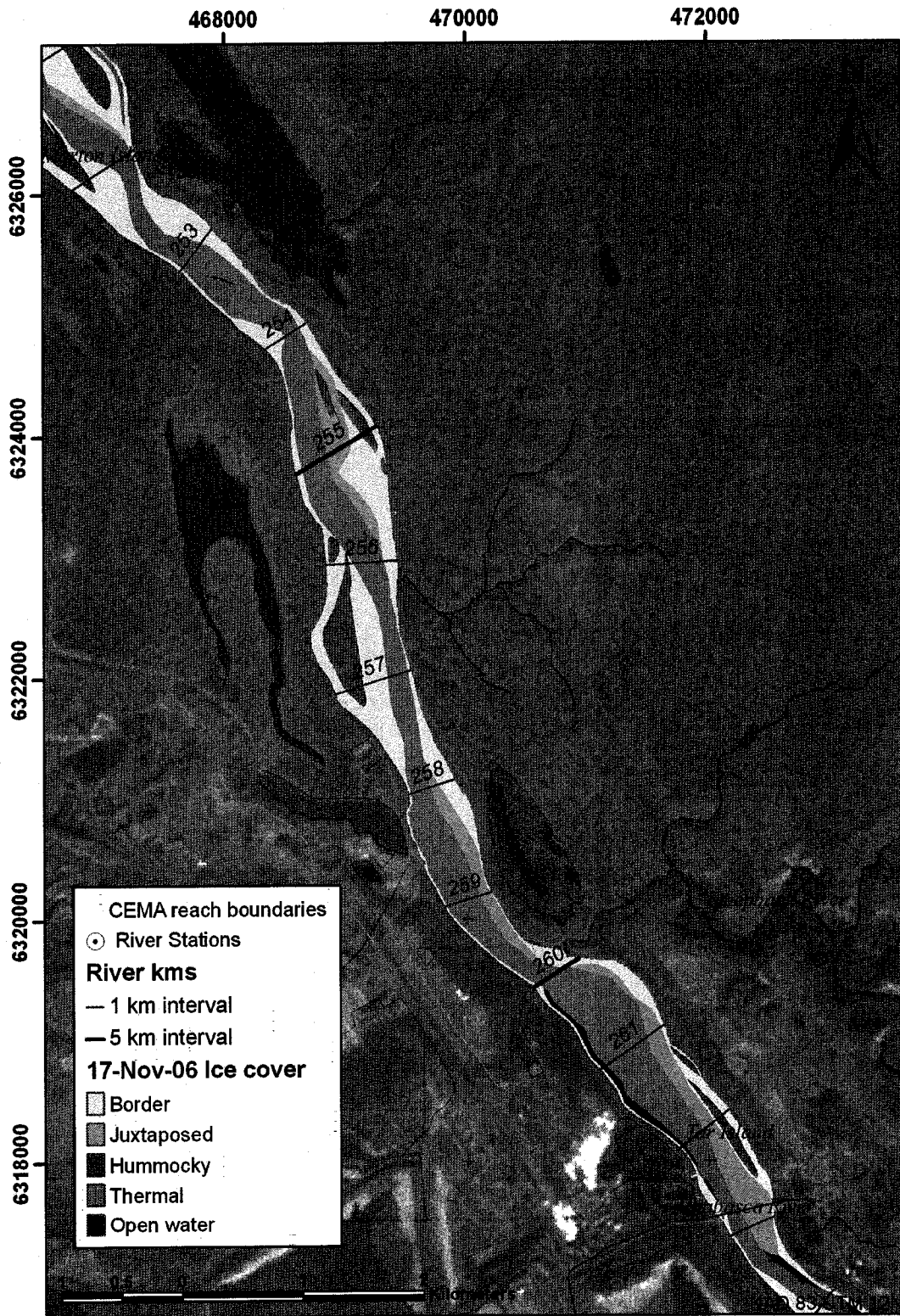


Figure B3.4 Ice cover mapping: November 17, 2006 - km 264 to 252

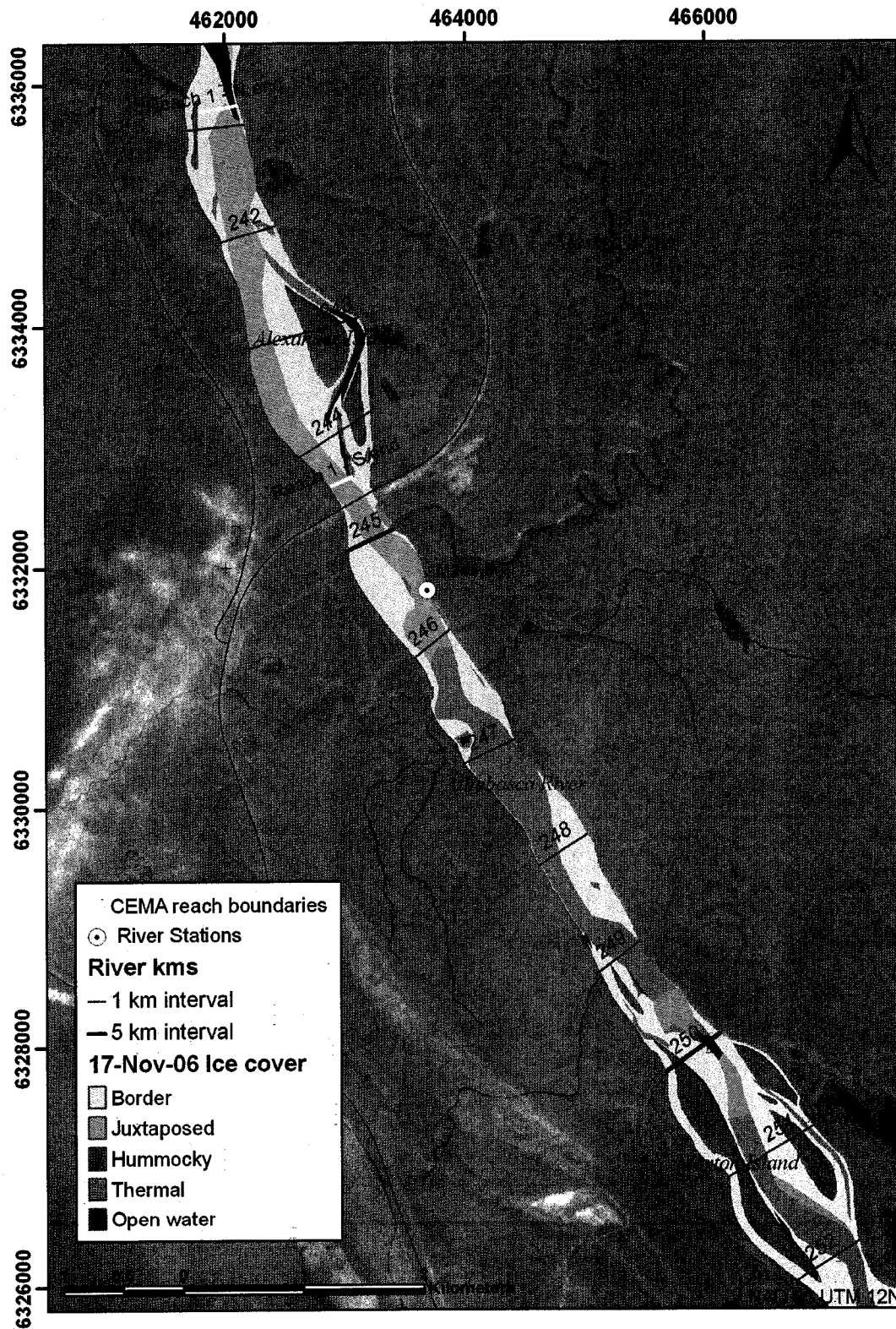


Figure B3.5 Ice cover mapping: November 17, 2006 - km 252 to 241



Figure B3.6 Ice cover mapping: November 17, 2006 - km 241 to 230

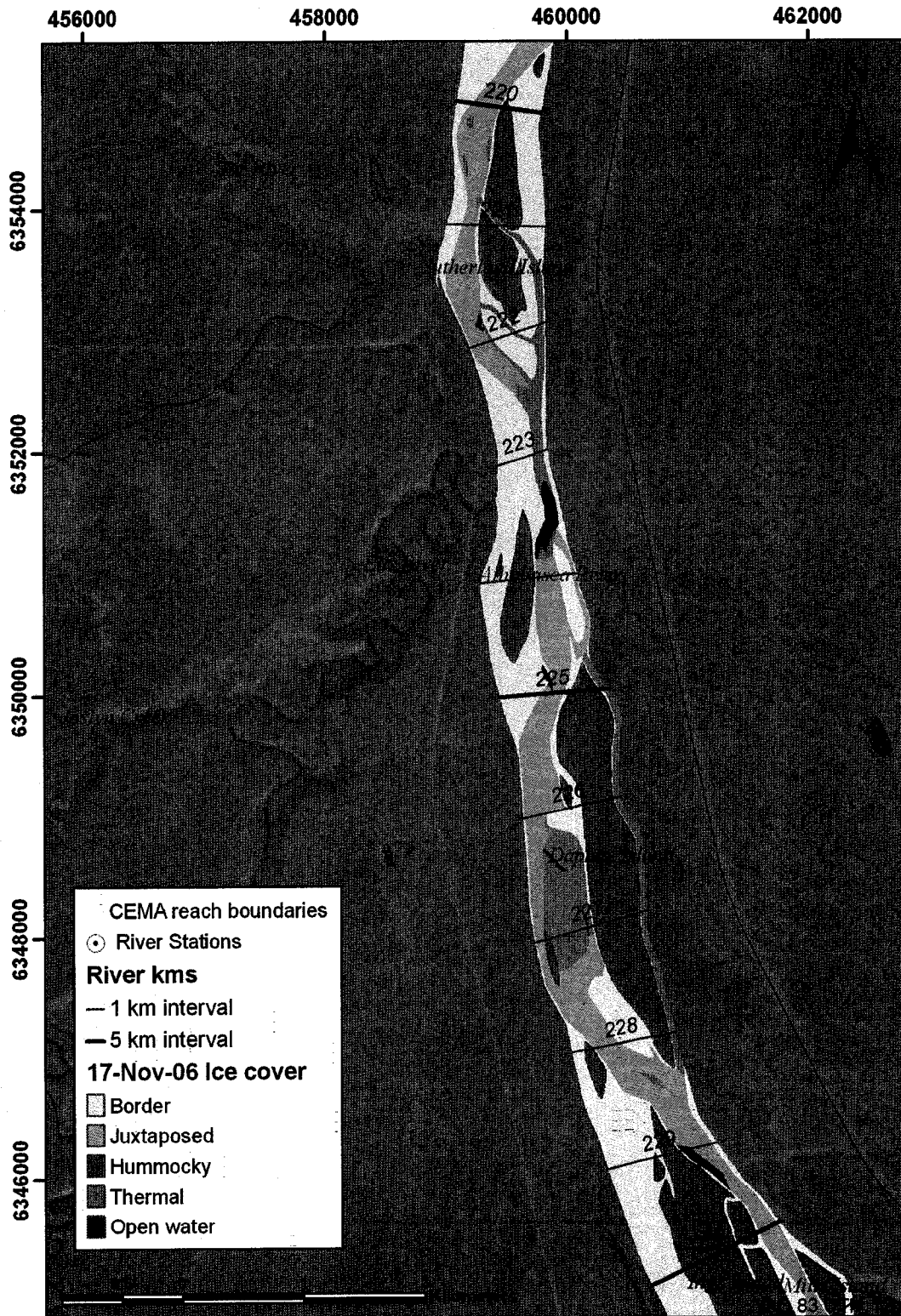


Figure B3.7 Ice cover mapping: November 17, 2006 - km 230 to 220

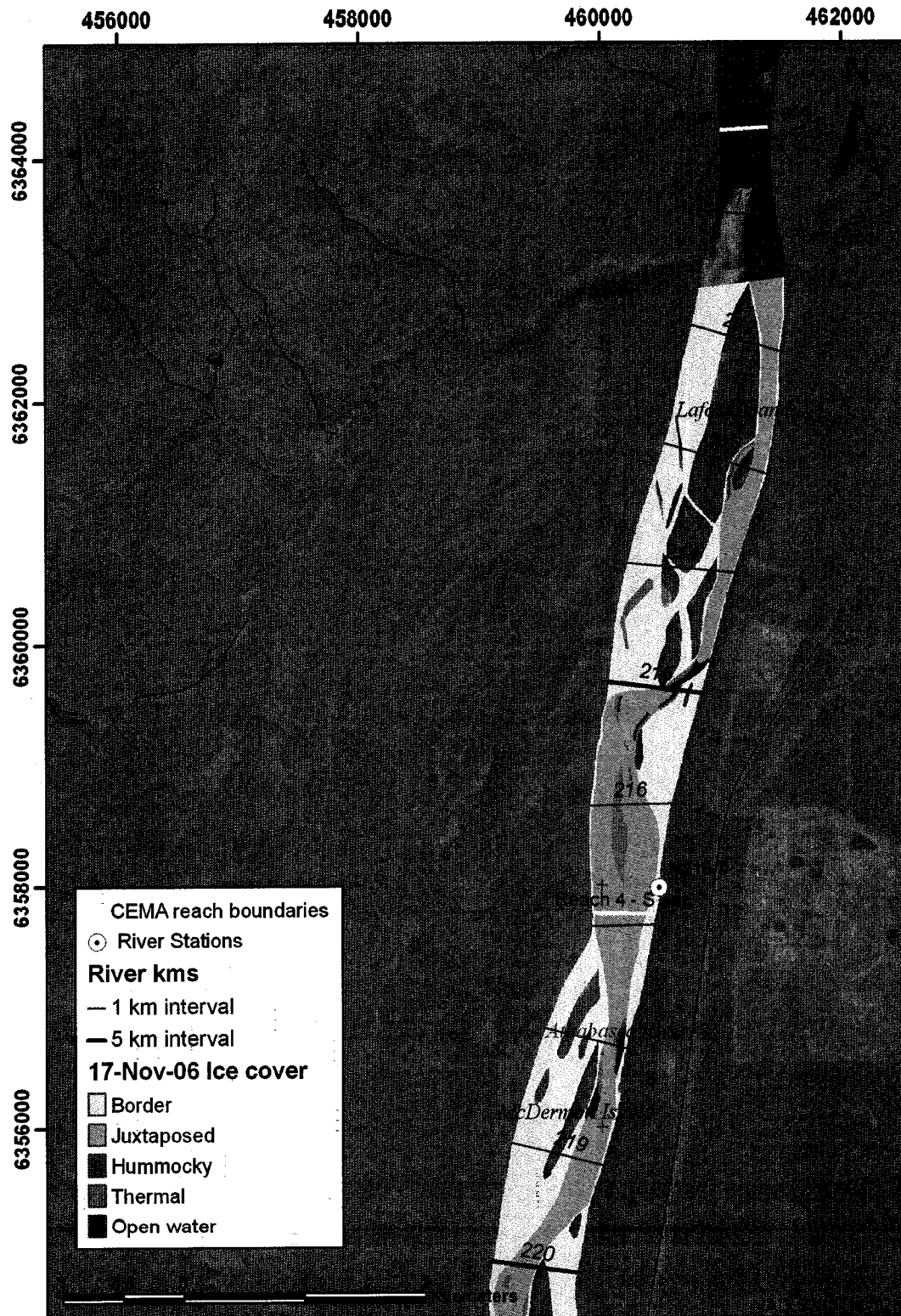


Figure B3.8 Ice cover mapping: November 17, 2006 - km 220 to 210

Appendix B4 Ice cover mapping – March 30, 2007

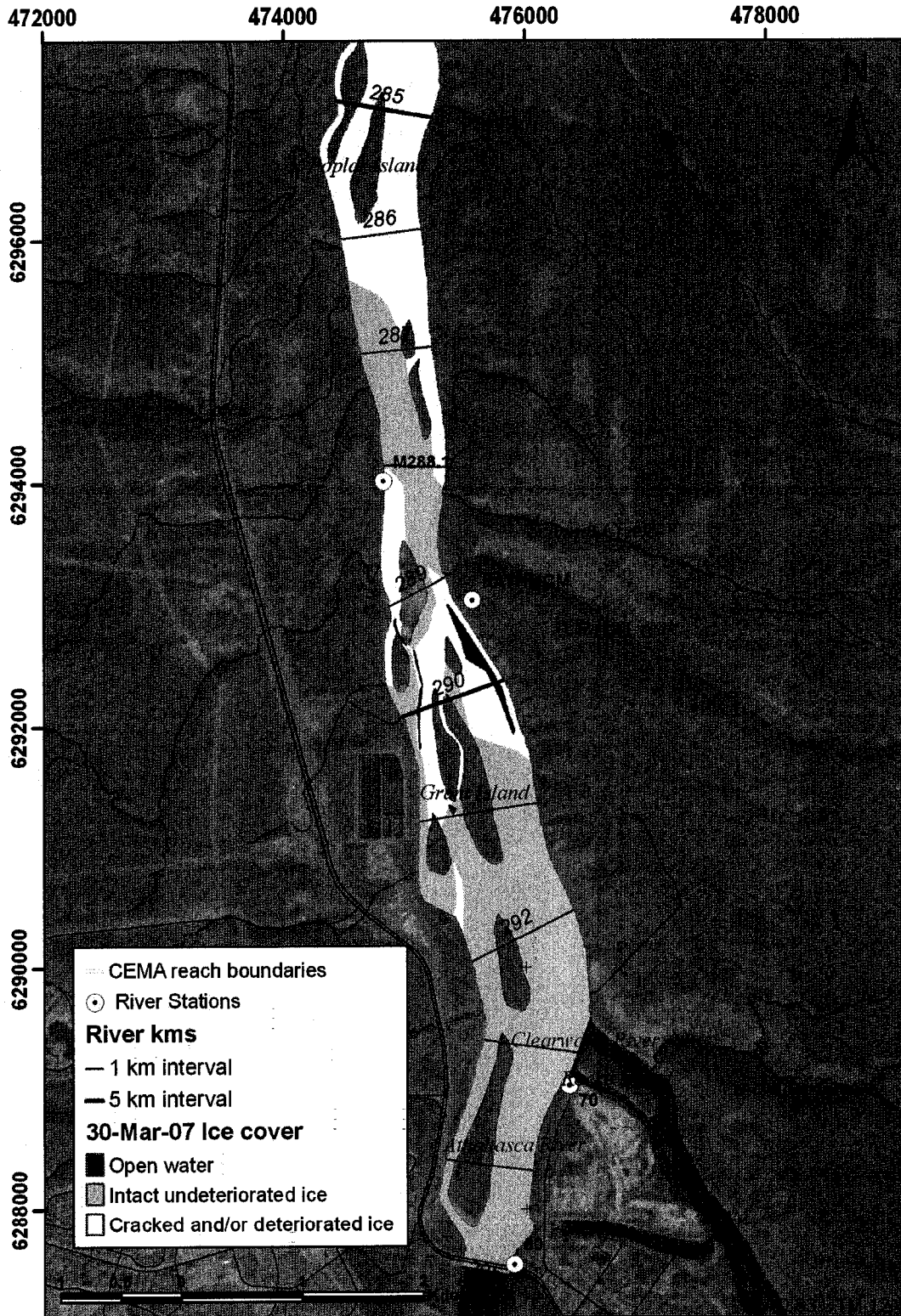


Figure B4.1 Ice cover mapping: March 30, 2007 - km 295 to 285

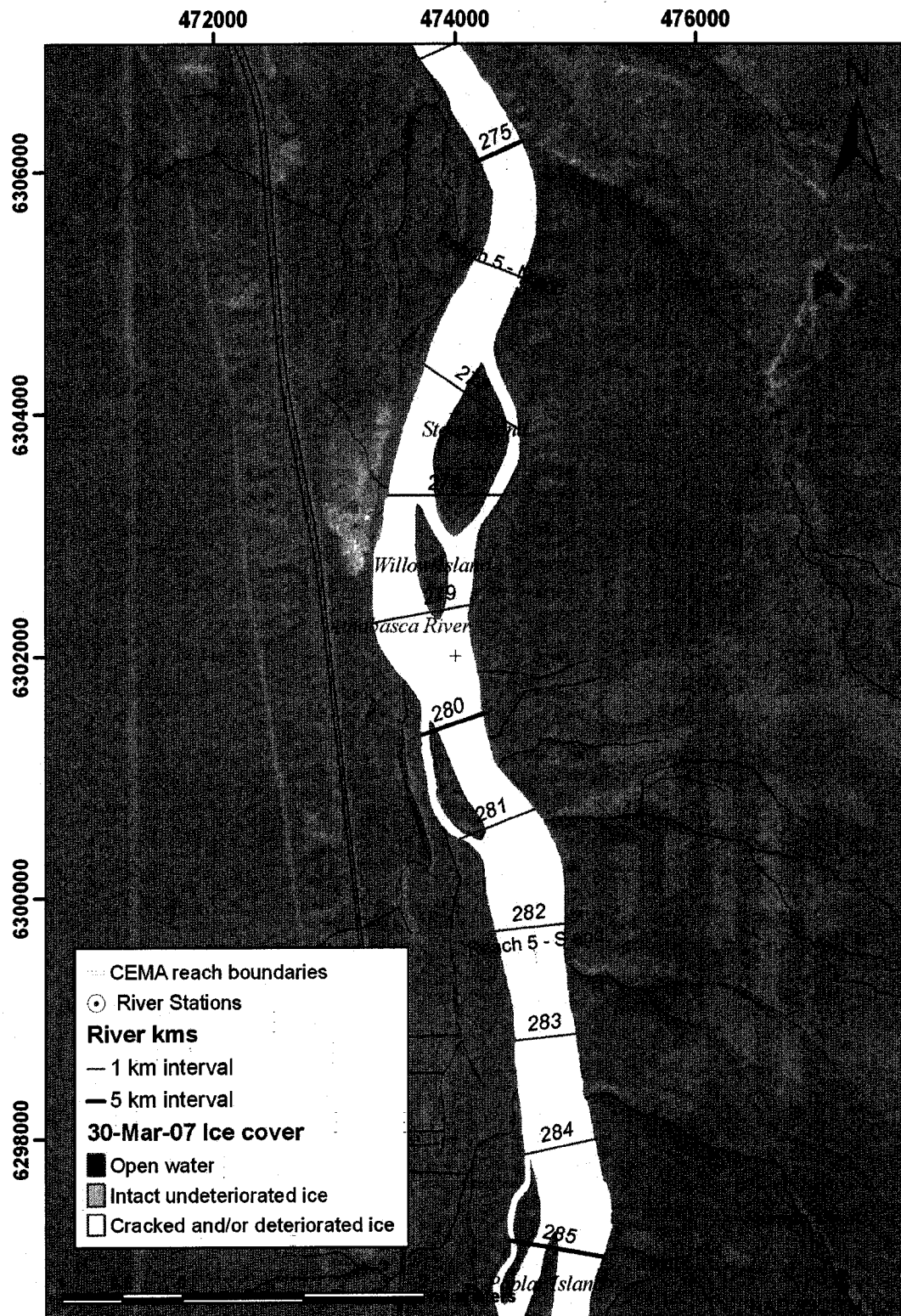


Figure B4.2 Ice cover mapping: March 30, 2007 - km 285 to 274

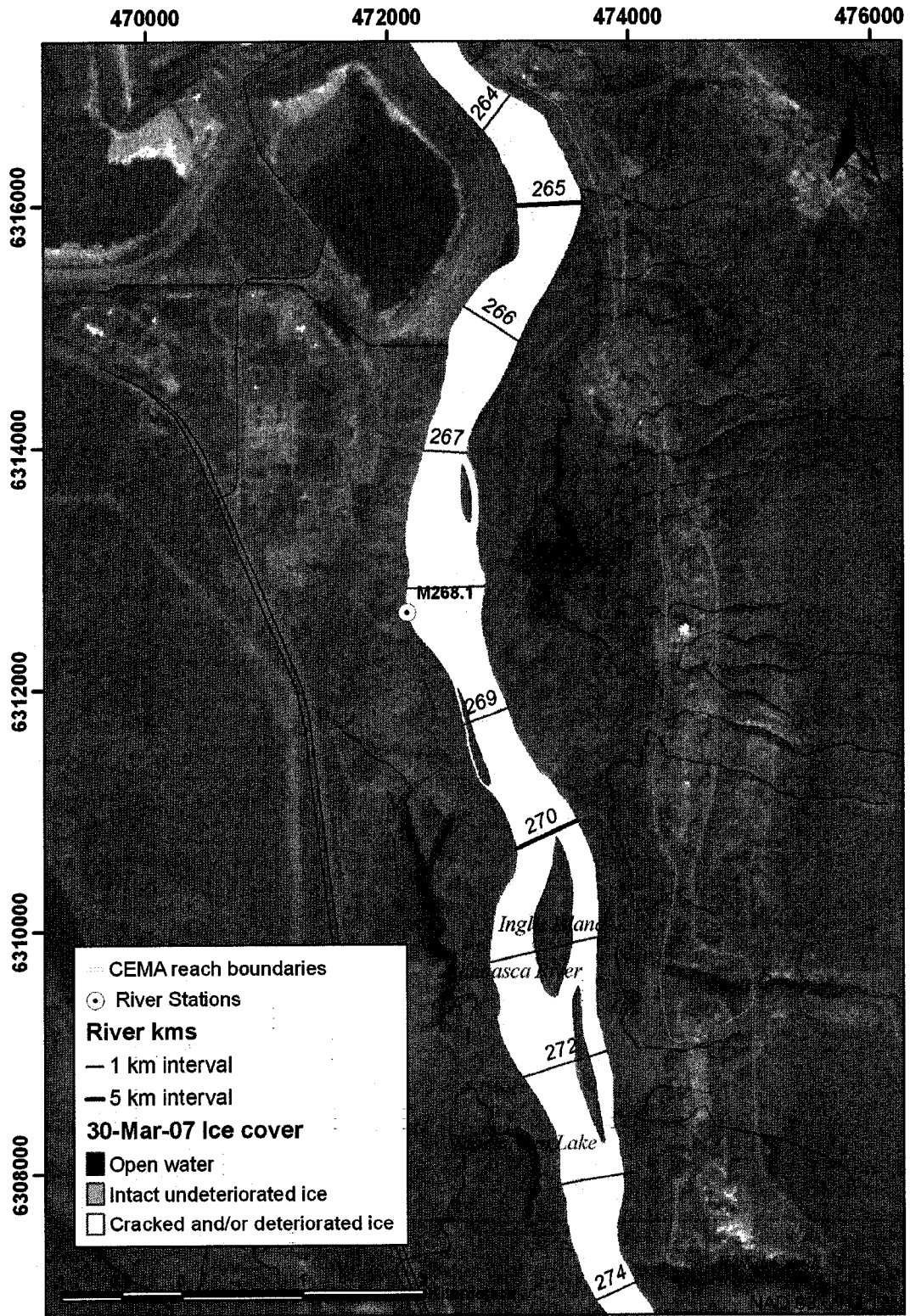


Figure B4.3 Ice cover mapping: March 30, 2007 - km 274 to 264

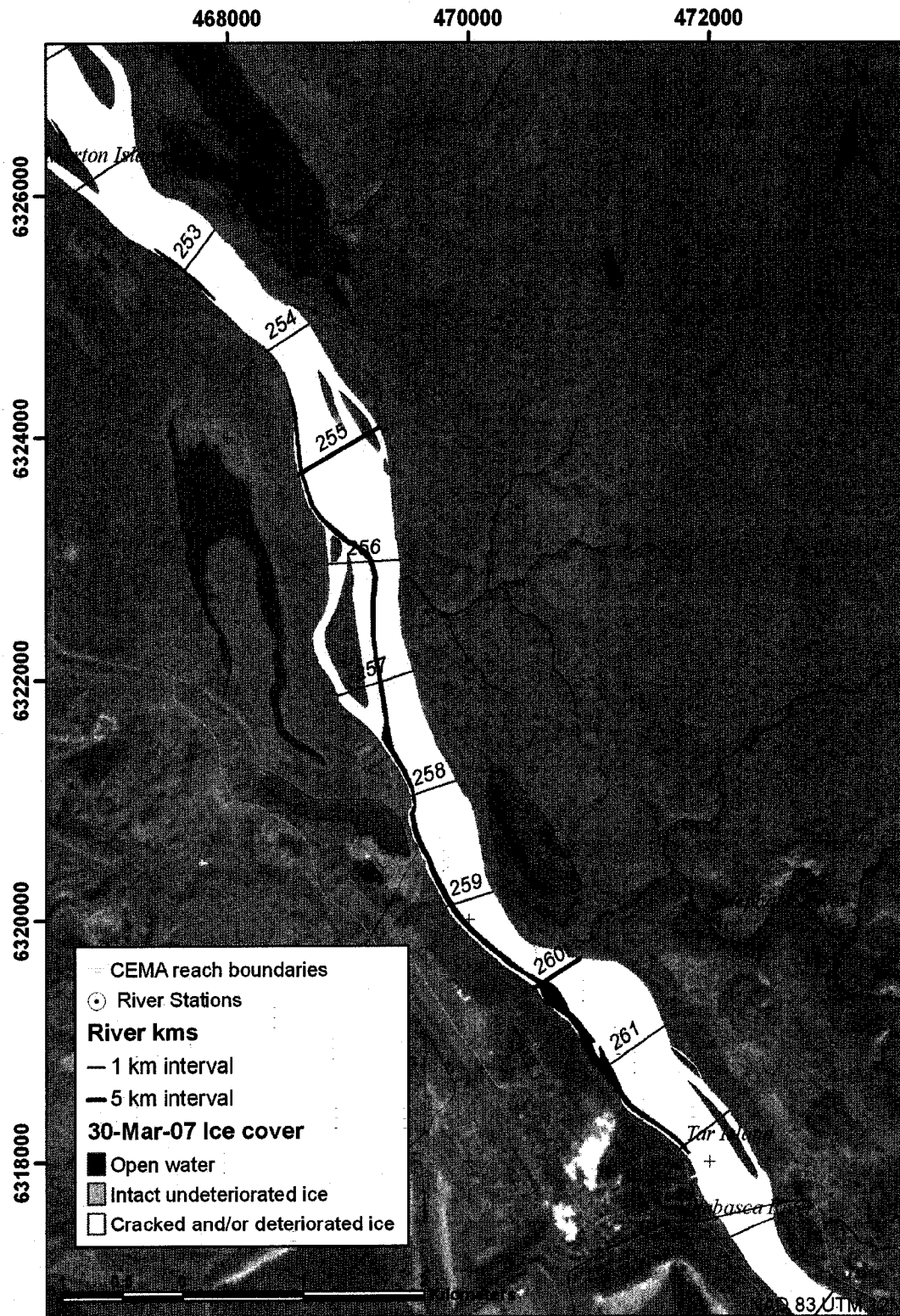


Figure B4.4 Ice cover mapping: March 30, 2007 - km 264 to 252

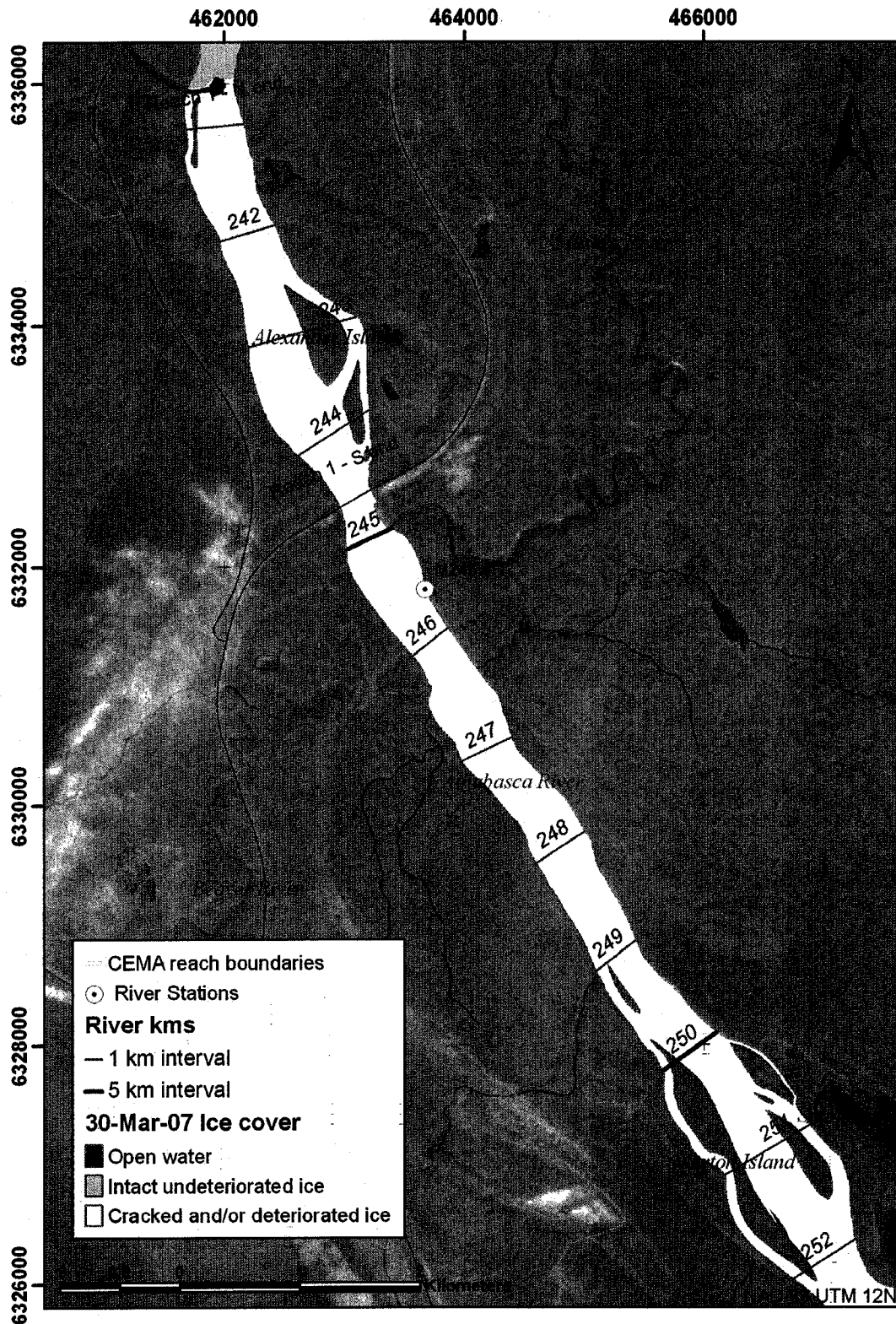


Figure B4.5 Ice cover mapping: March 30, 2007 - km 252 to 241

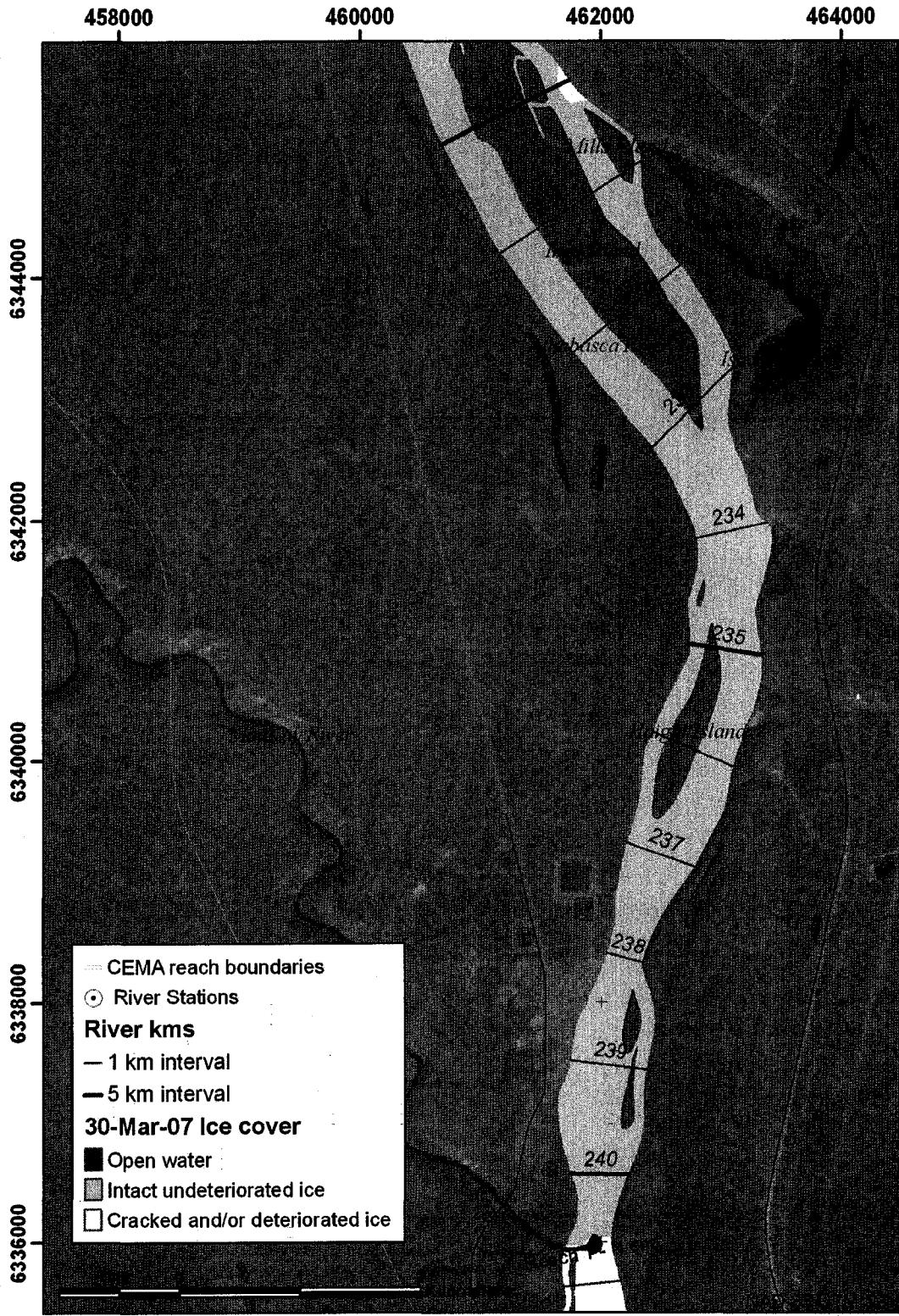


Figure B4.6 Ice cover mapping: March 30, 2007 - km 241 to 230

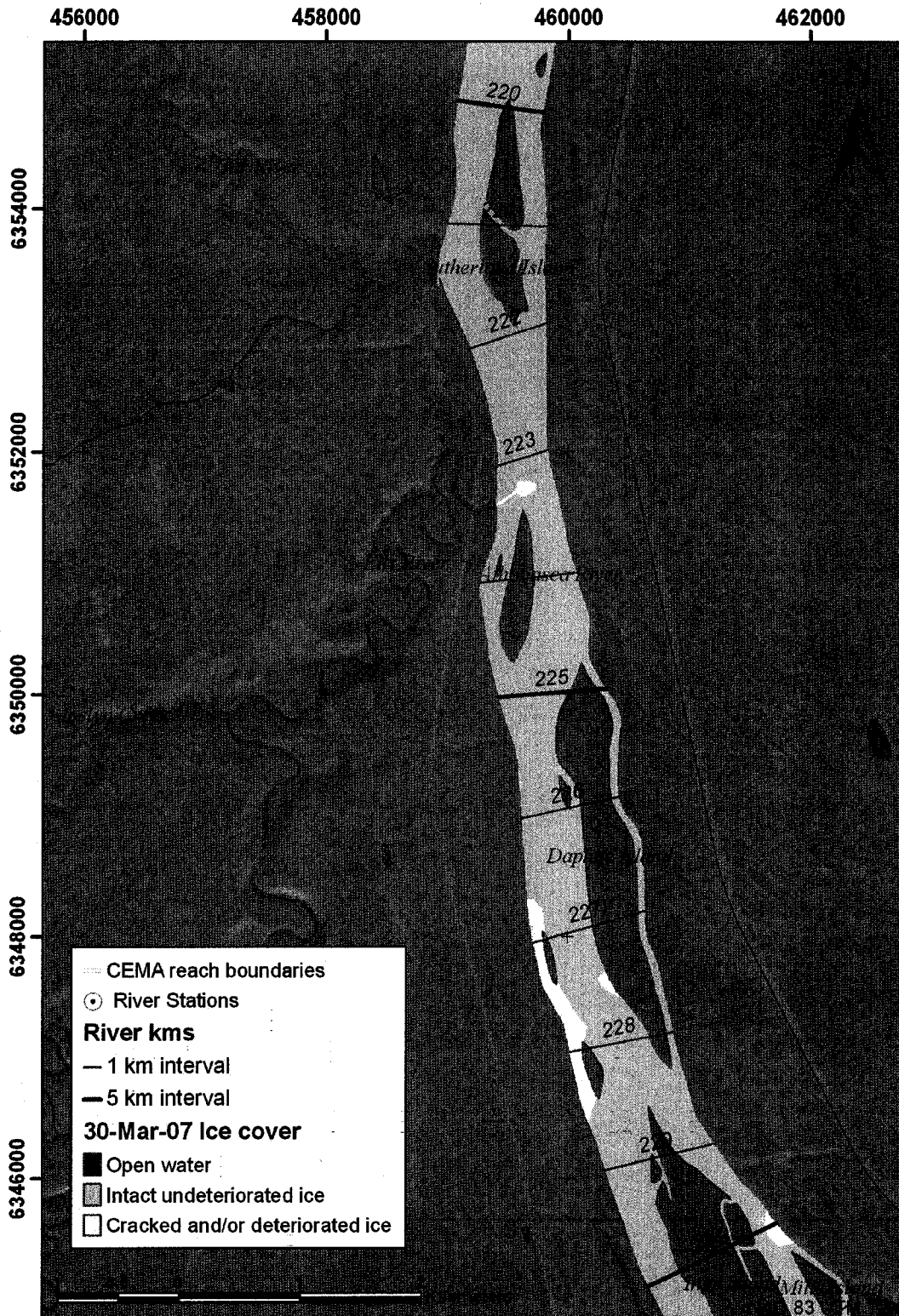


Figure B4.7 Ice cover mapping: March 30, 2007 - km 230 to 220

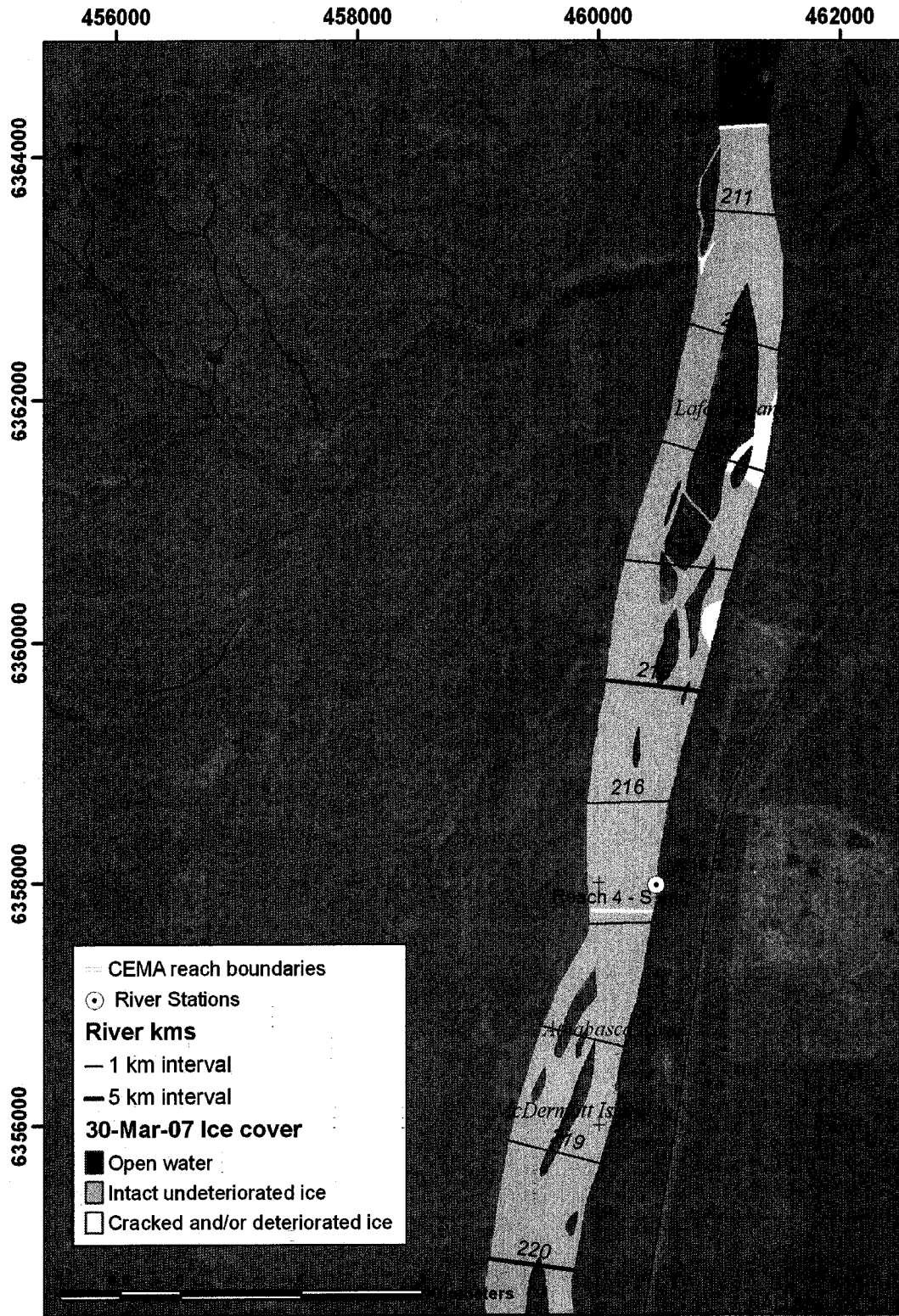


Figure B4.8 Ice cover mapping: March 30, 2007 - km 220 to 210

Appendix B5 Ice cover mapping – April 12, 2007

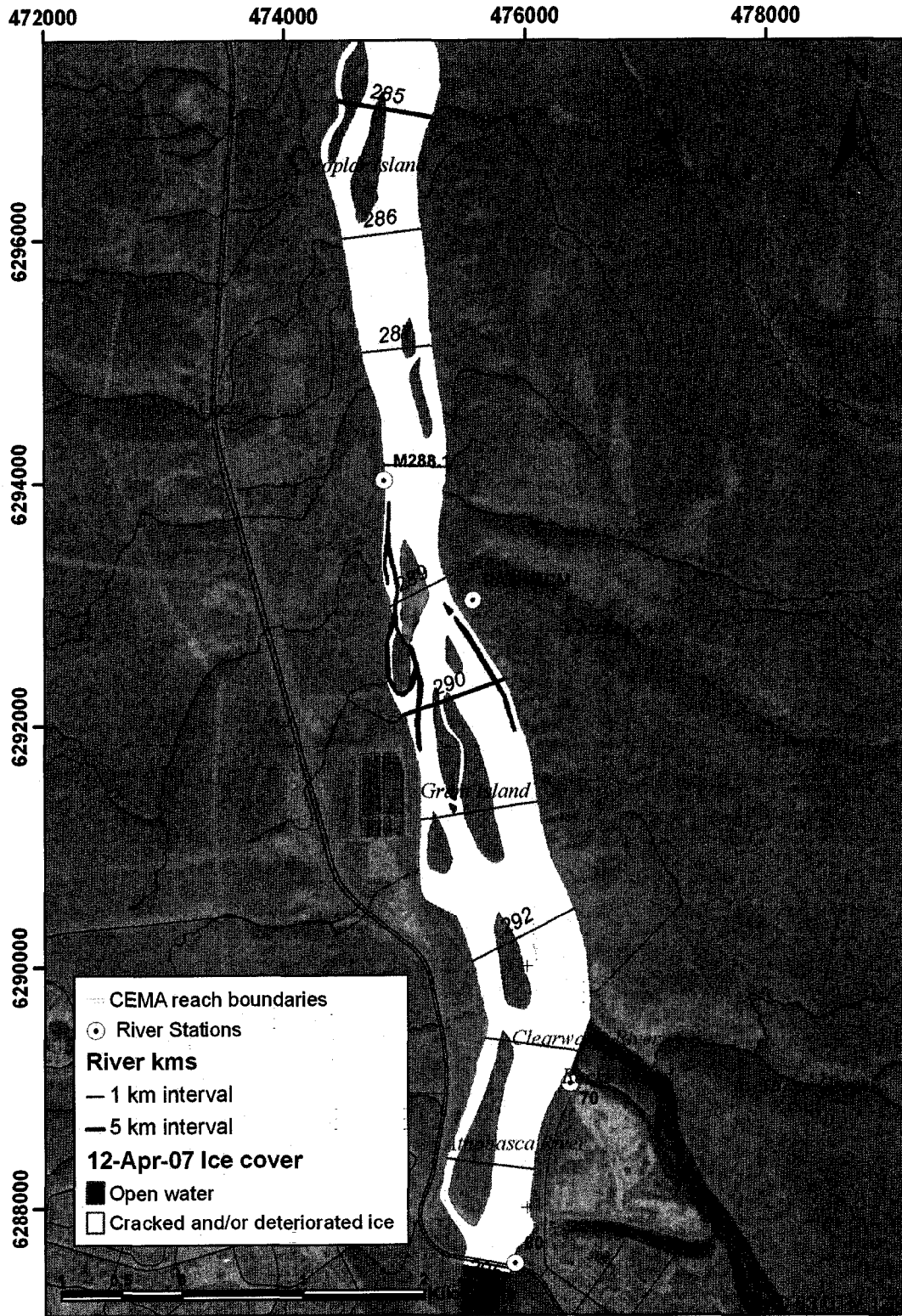


Figure B5.1 Ice cover mapping: April 12, 2007 - km 295 to 285

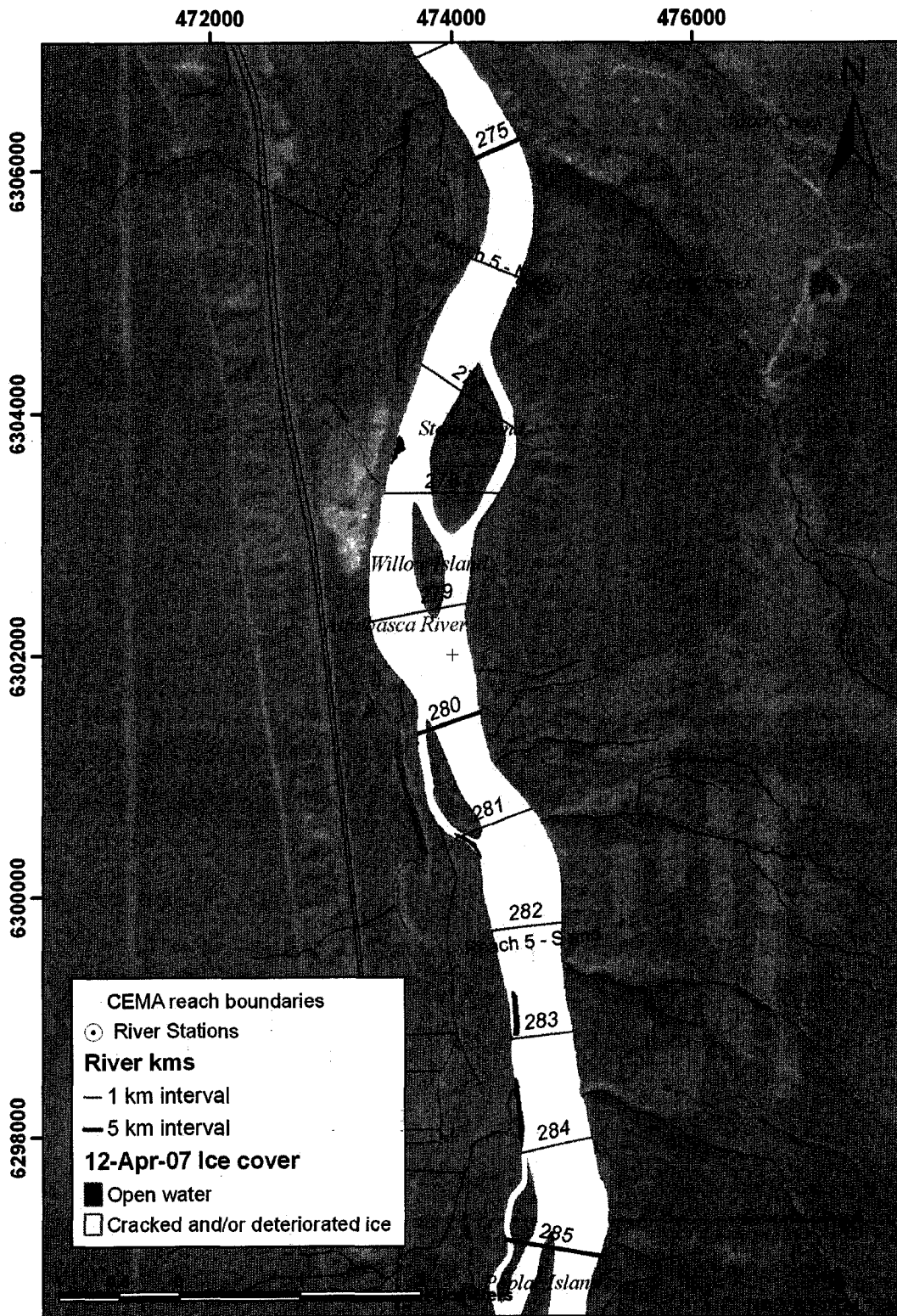


Figure B5.2 Ice cover mapping: April 12, 2007 - km 285 to 274

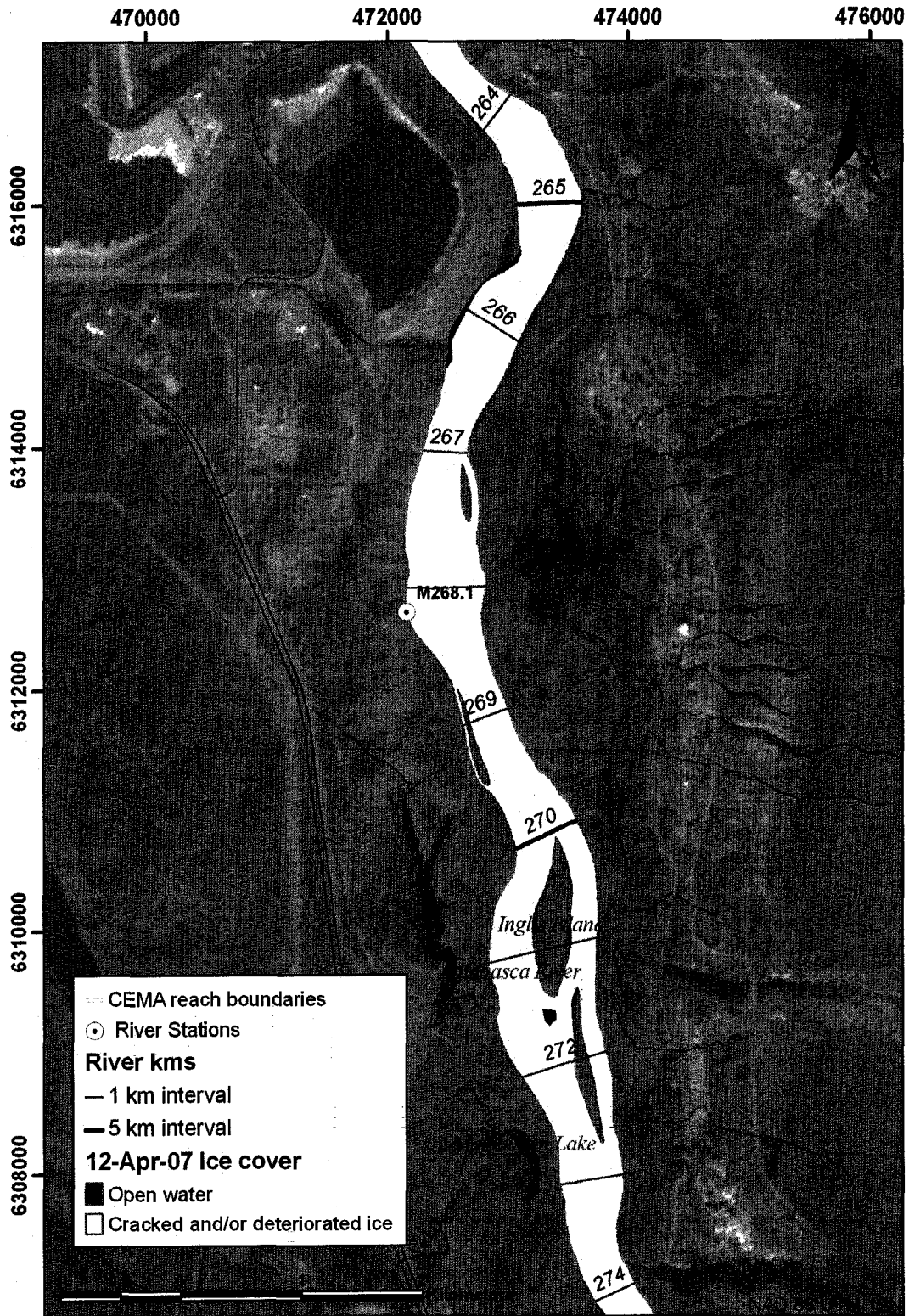


Figure B5.3 Ice cover mapping: April 12, 2007 - km 274 to 264

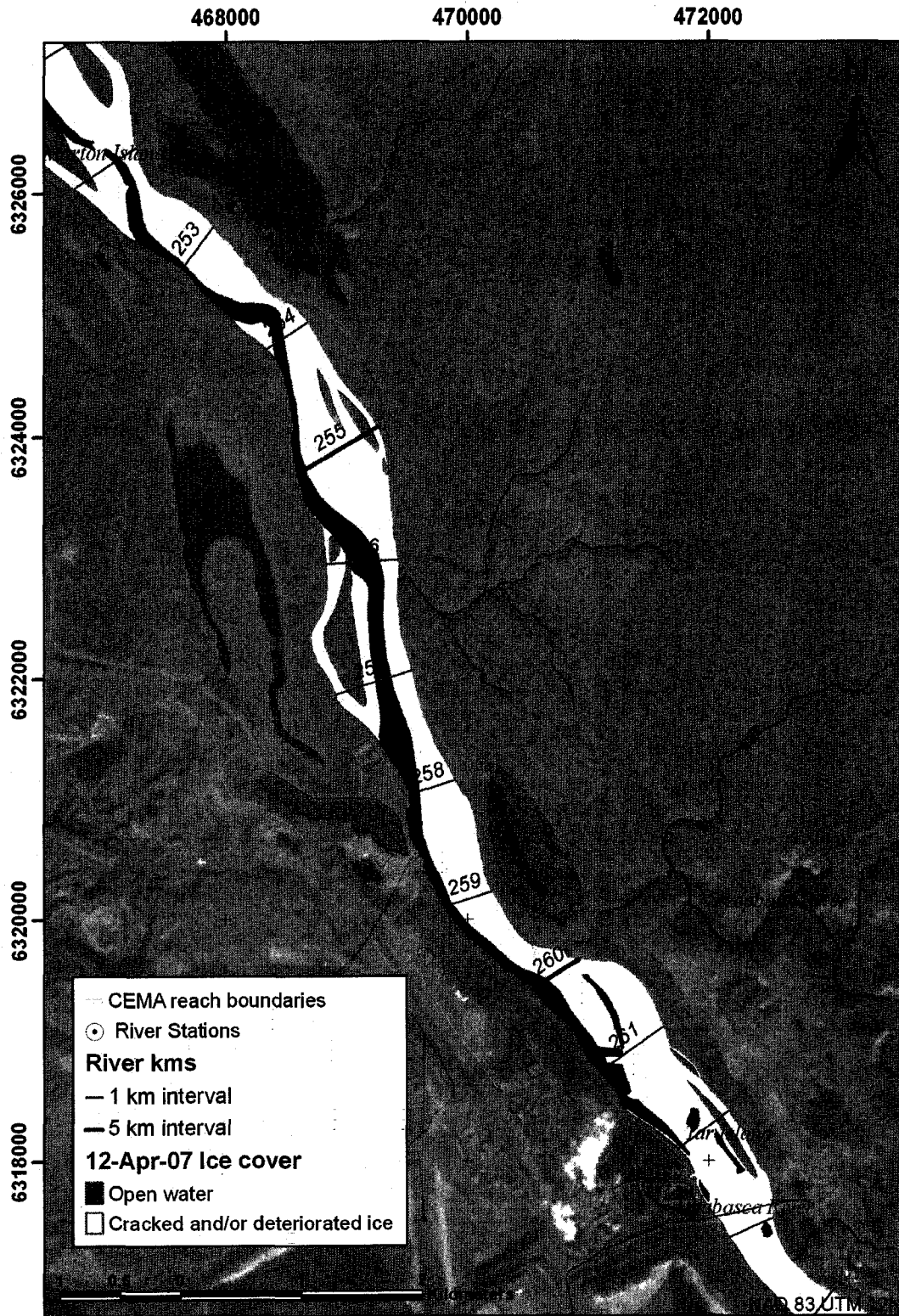


Figure B5.4 Ice cover mapping: April 12, 2007 - km 264 to 252

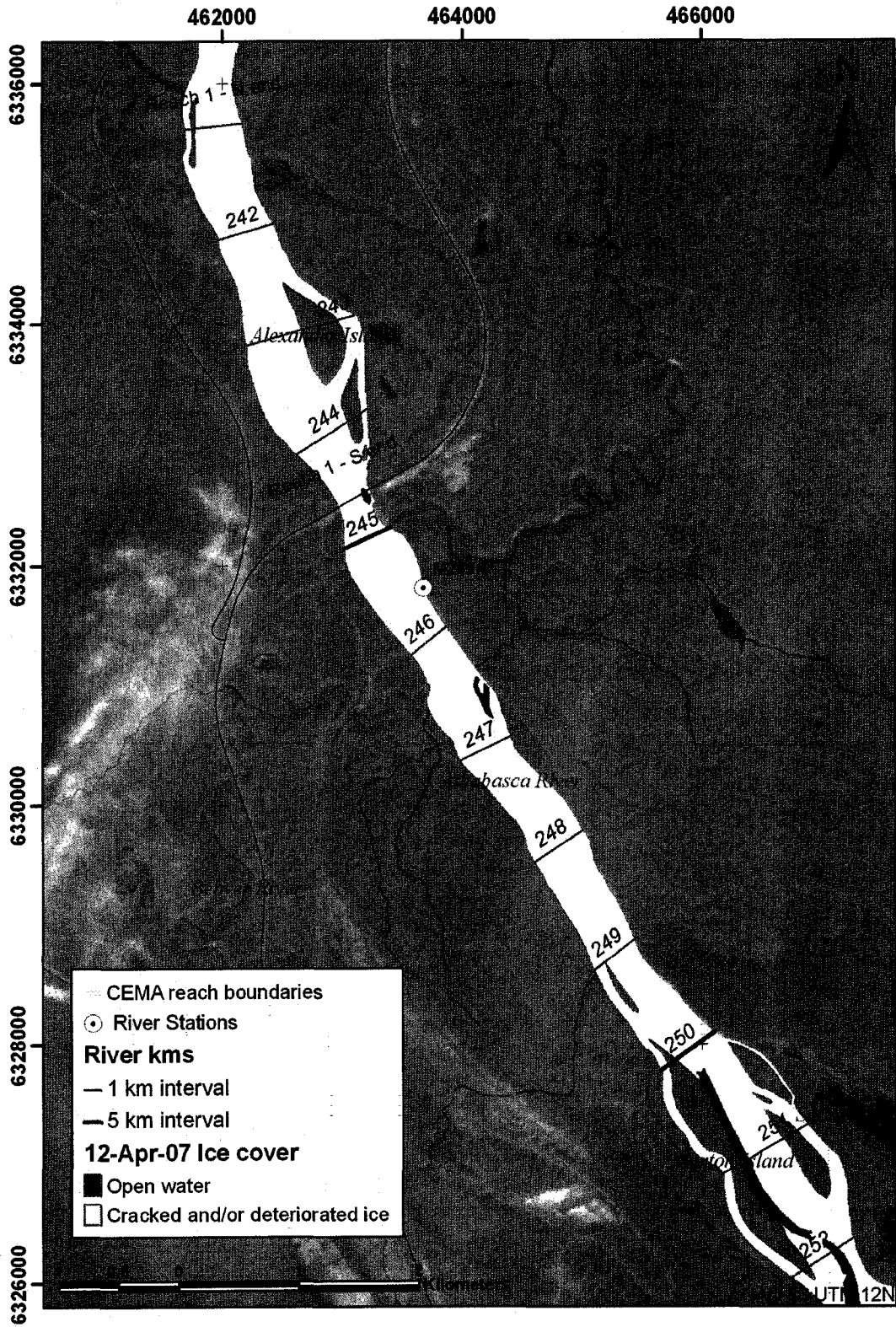


Figure B5.5 Ice cover mapping: April 12, 2007 - km 252 to 241

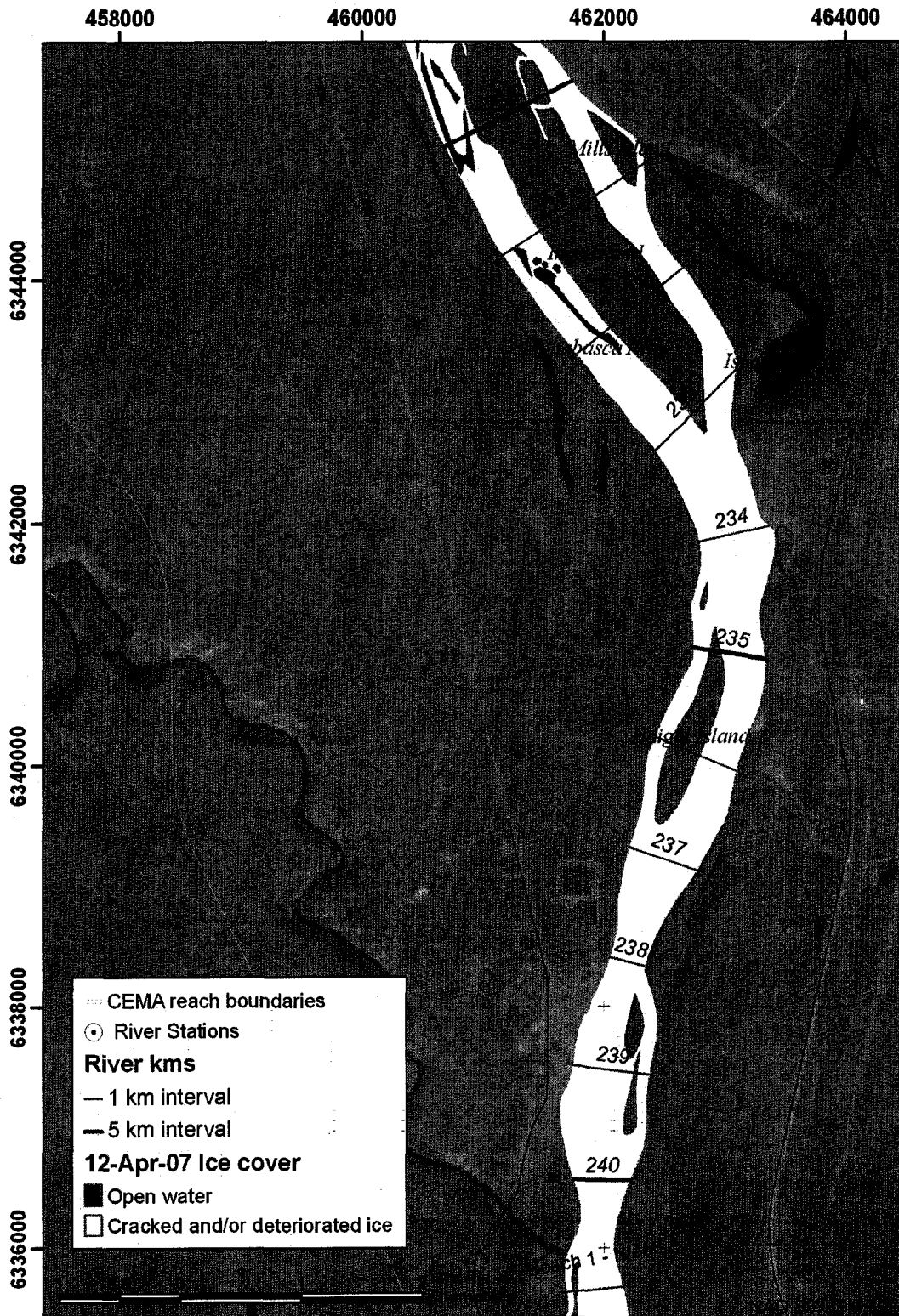


Figure B5.6 Ice cover mapping: April 12, 2007 - km 241 to 230

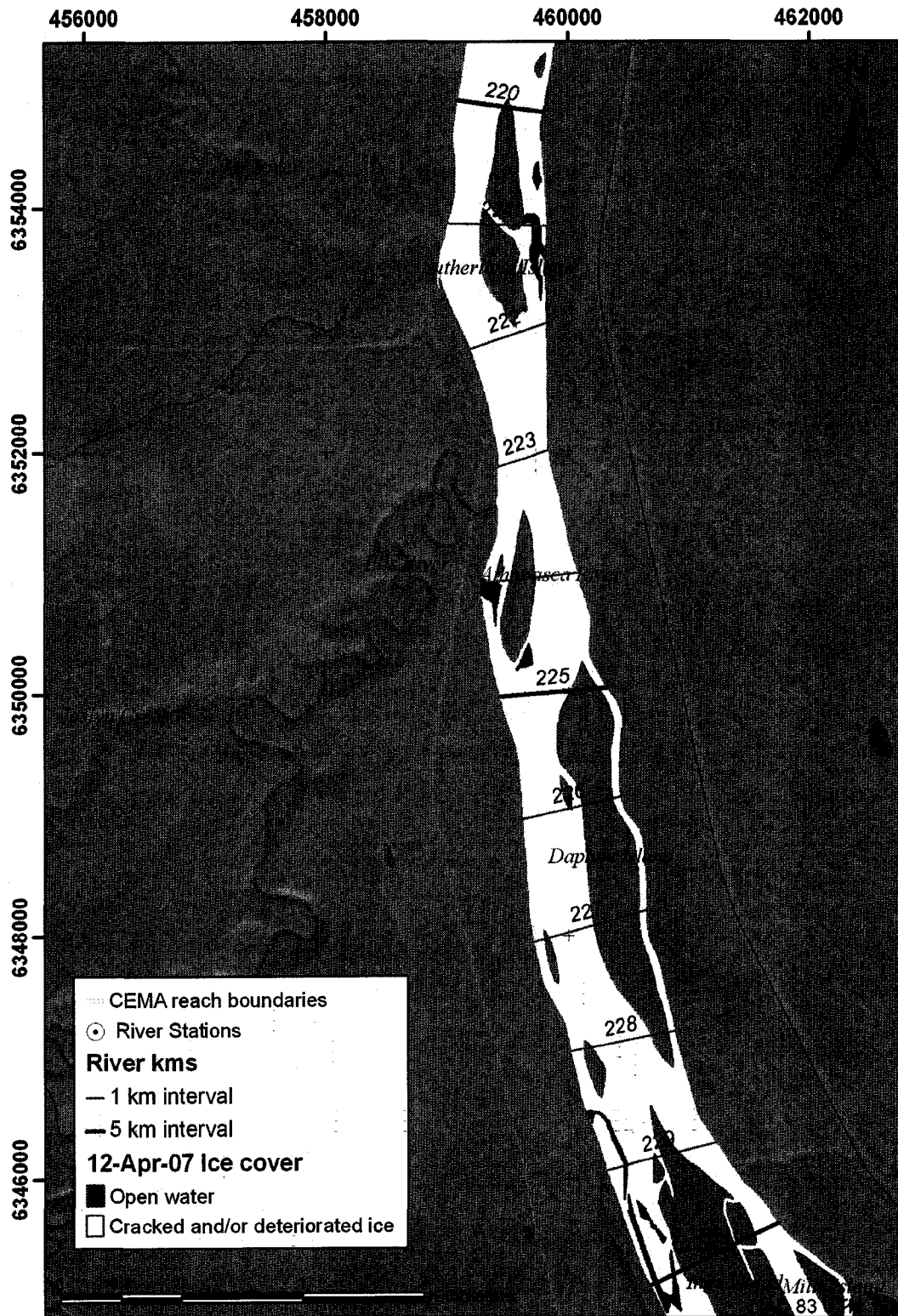


Figure B5.7 Ice cover mapping: April 12, 2007 - km 230 to 220

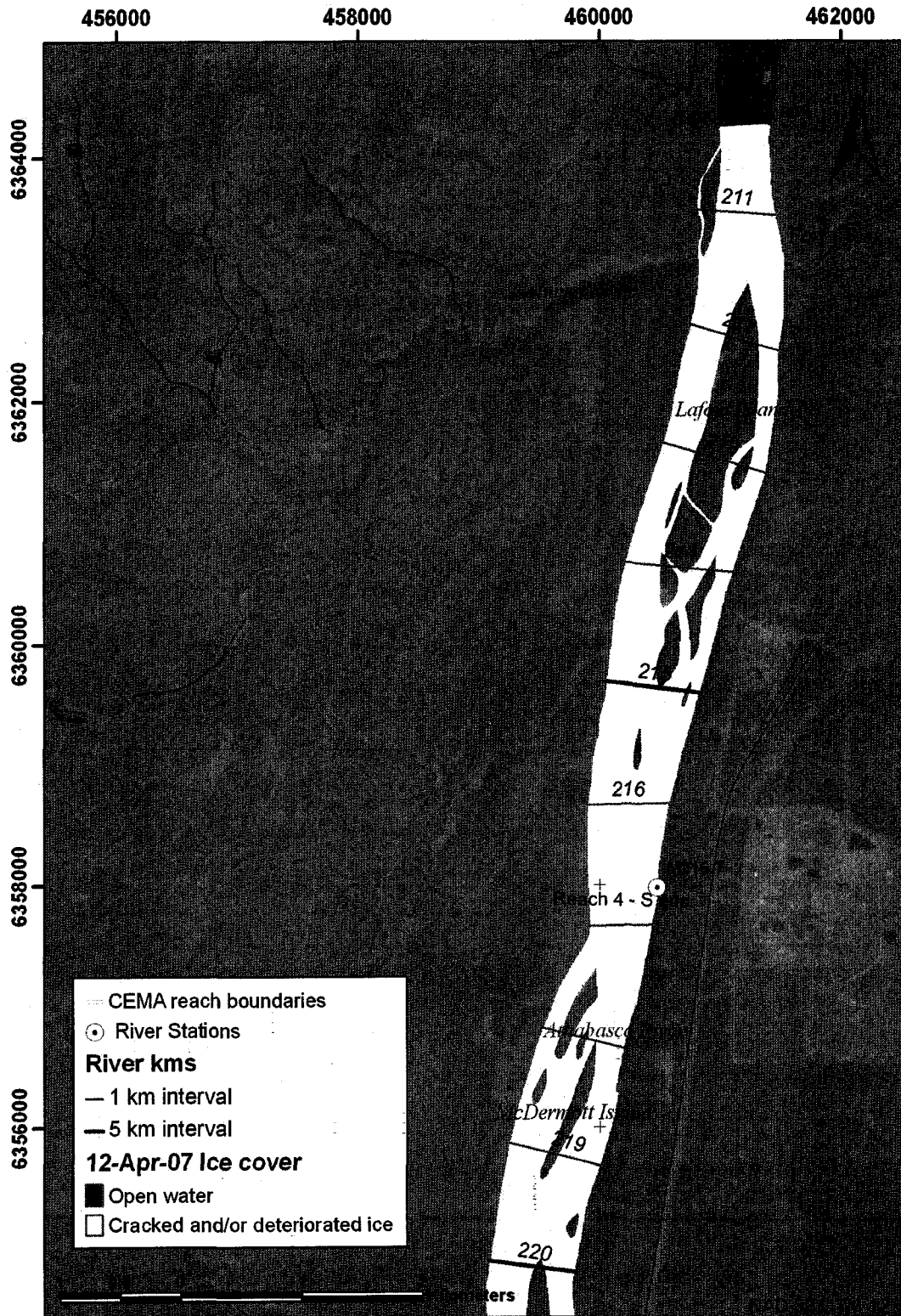


Figure B5.8 Ice cover mapping: April 12, 2007 - km 220 to 210

Appendix B6 Ice cover mapping – April 16, 2007

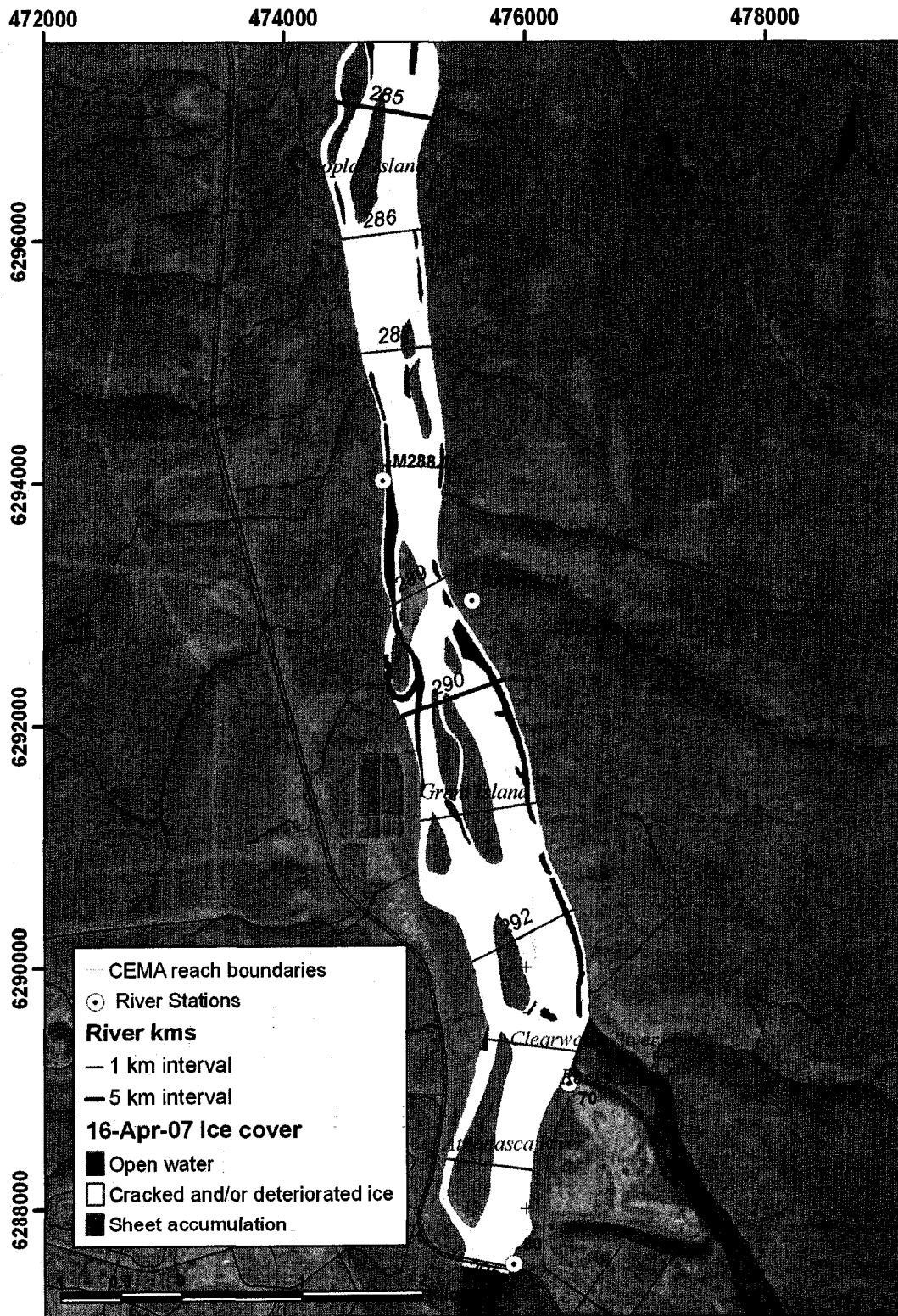


Figure B6.1 Ice cover mapping: April 16, 2007 - km 295 to 285

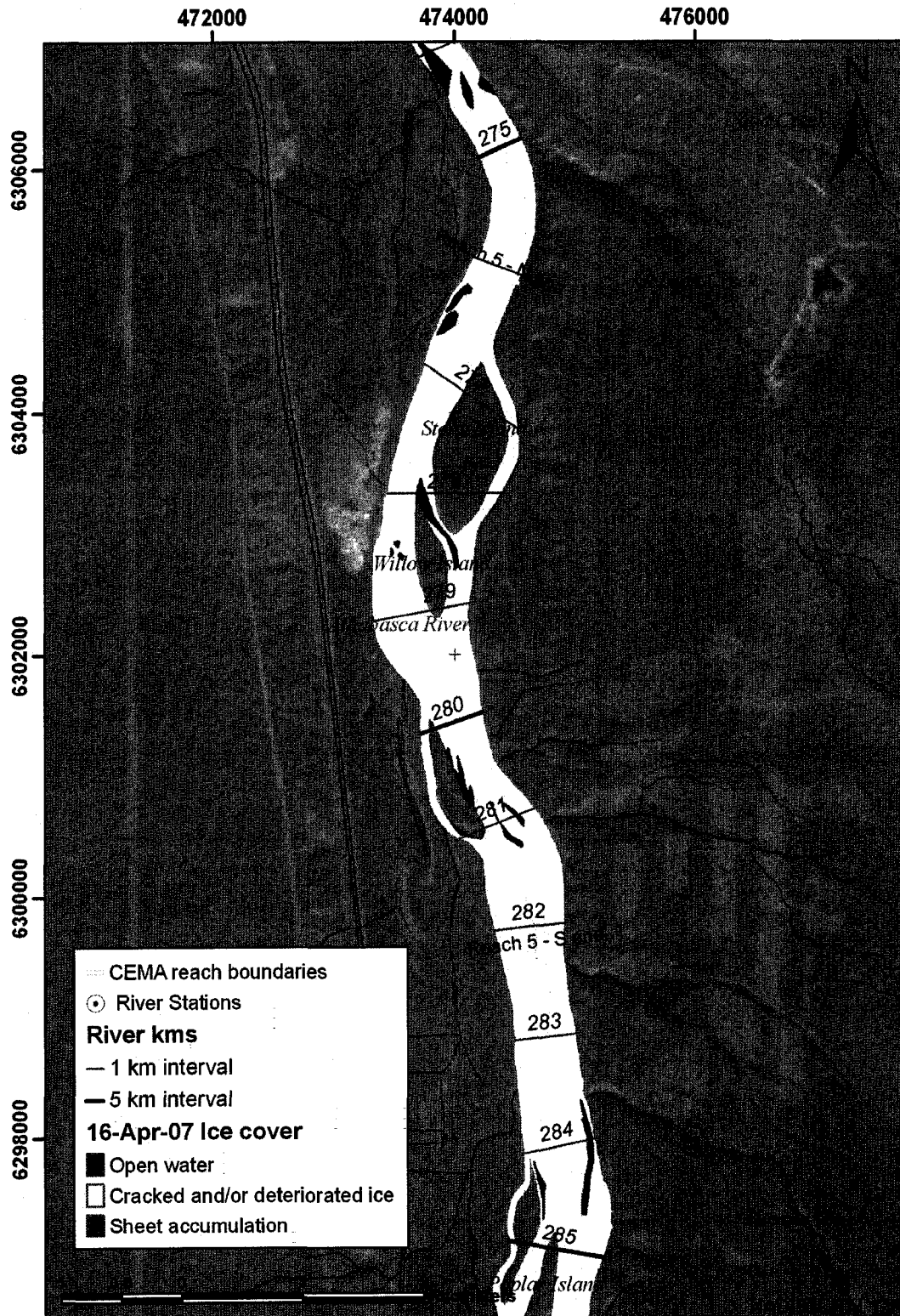


Figure B6.2 Ice cover mapping: April 16, 2007 - km 285 to 274

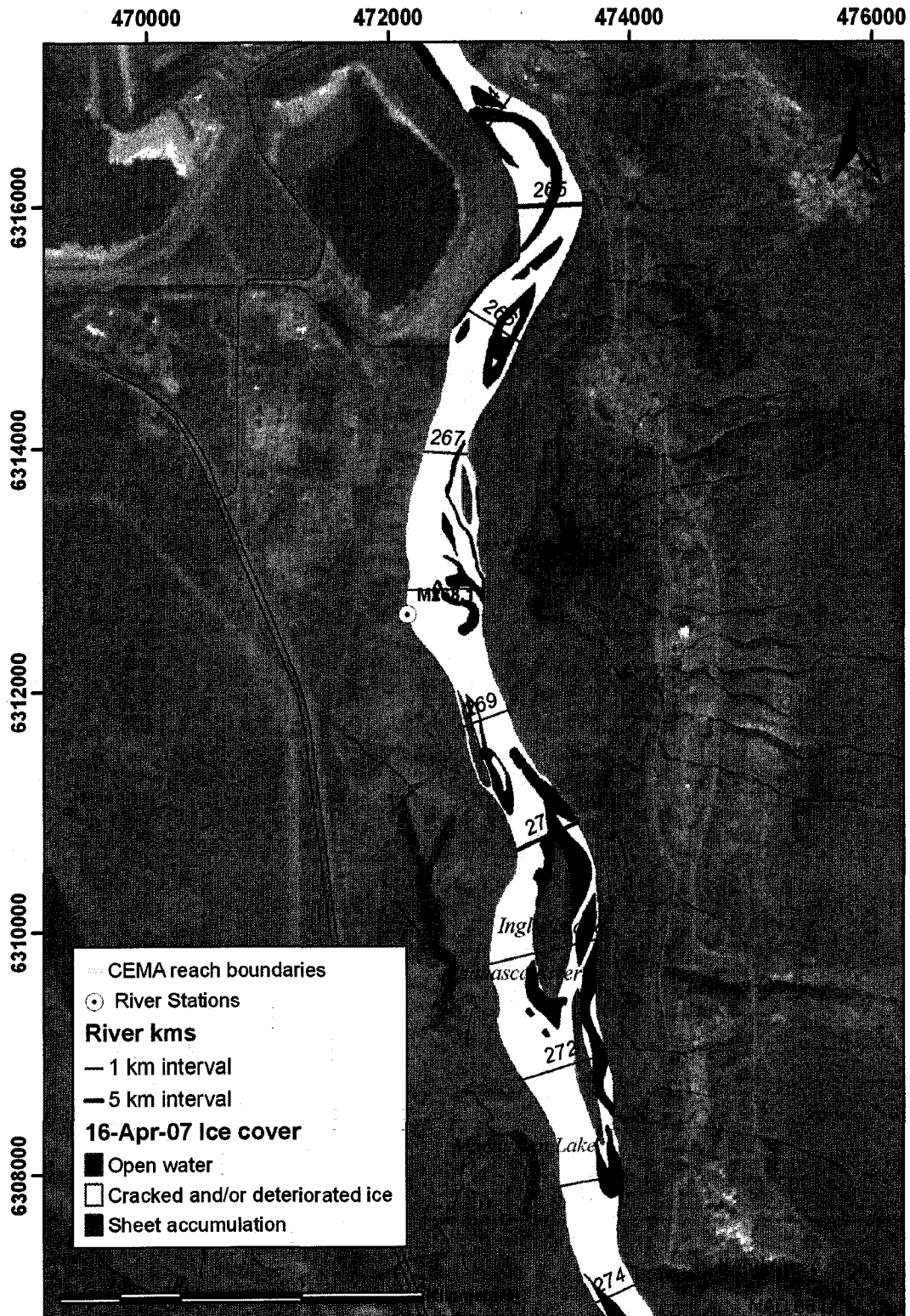


Figure B6.3 Ice cover mapping: April 16, 2007 - km 274 to 264

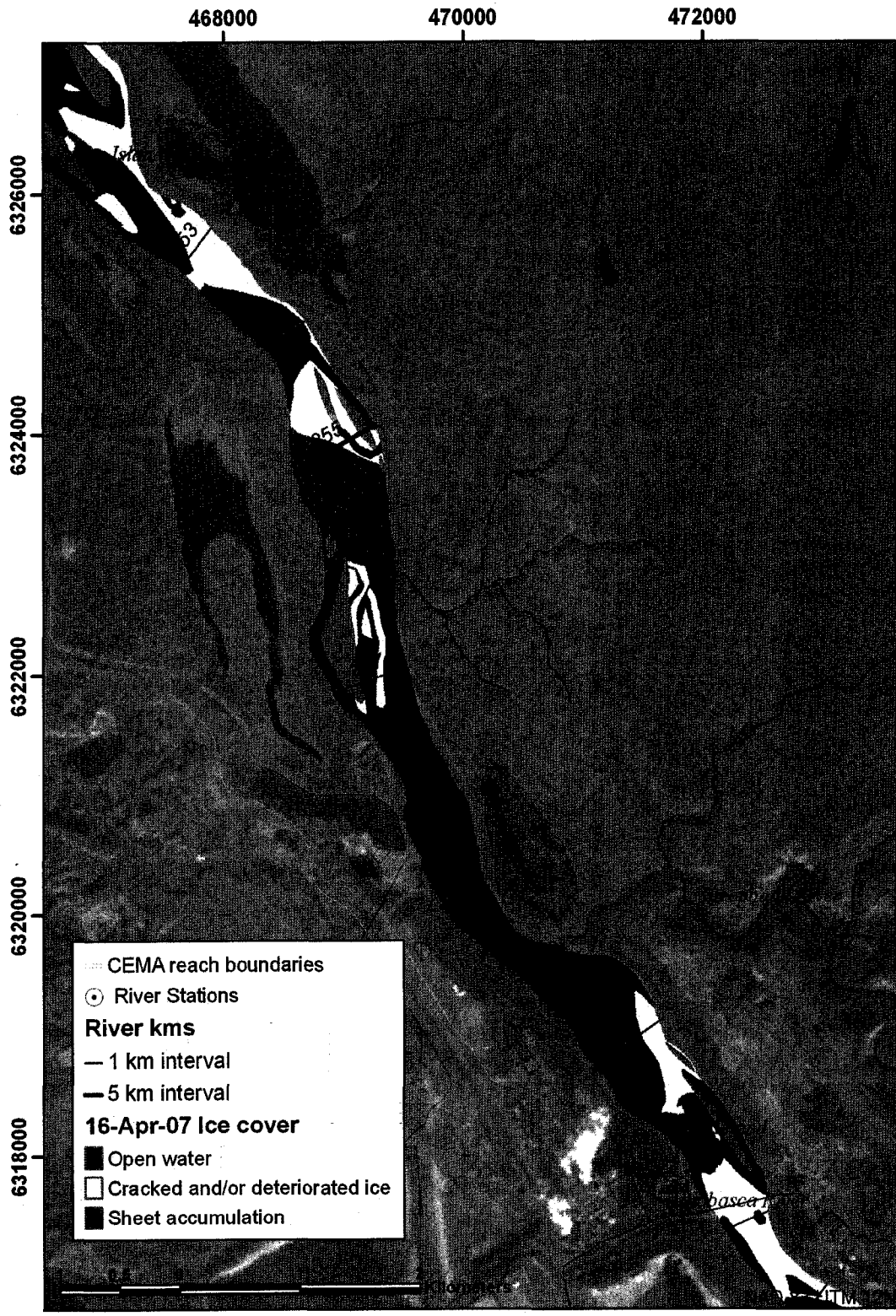


Figure B6.4 Ice cover mapping: April 16, 2007 - km 264 to 252

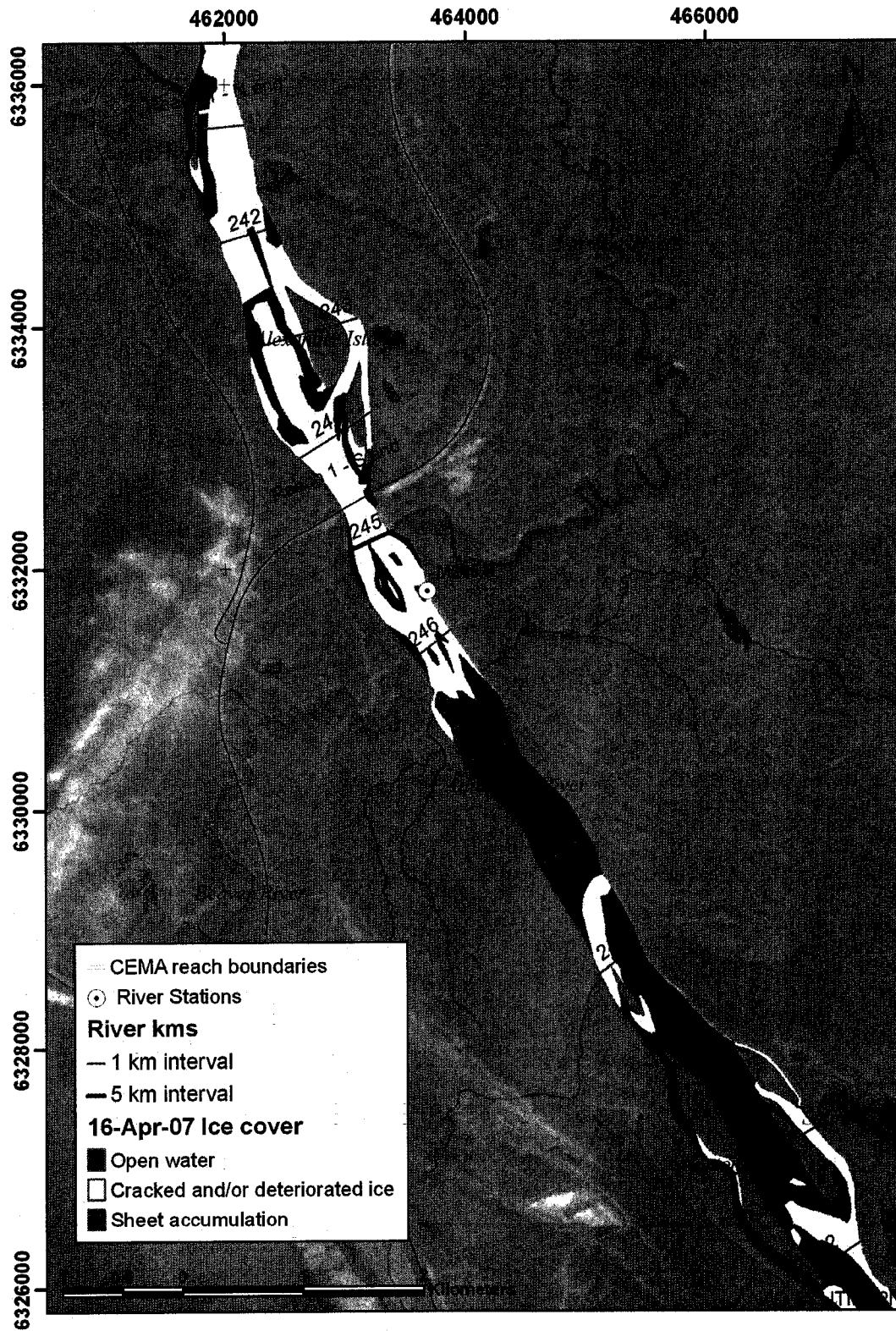


Figure B6.5 Ice cover mapping: April 16, 2007 - km 252 to 241

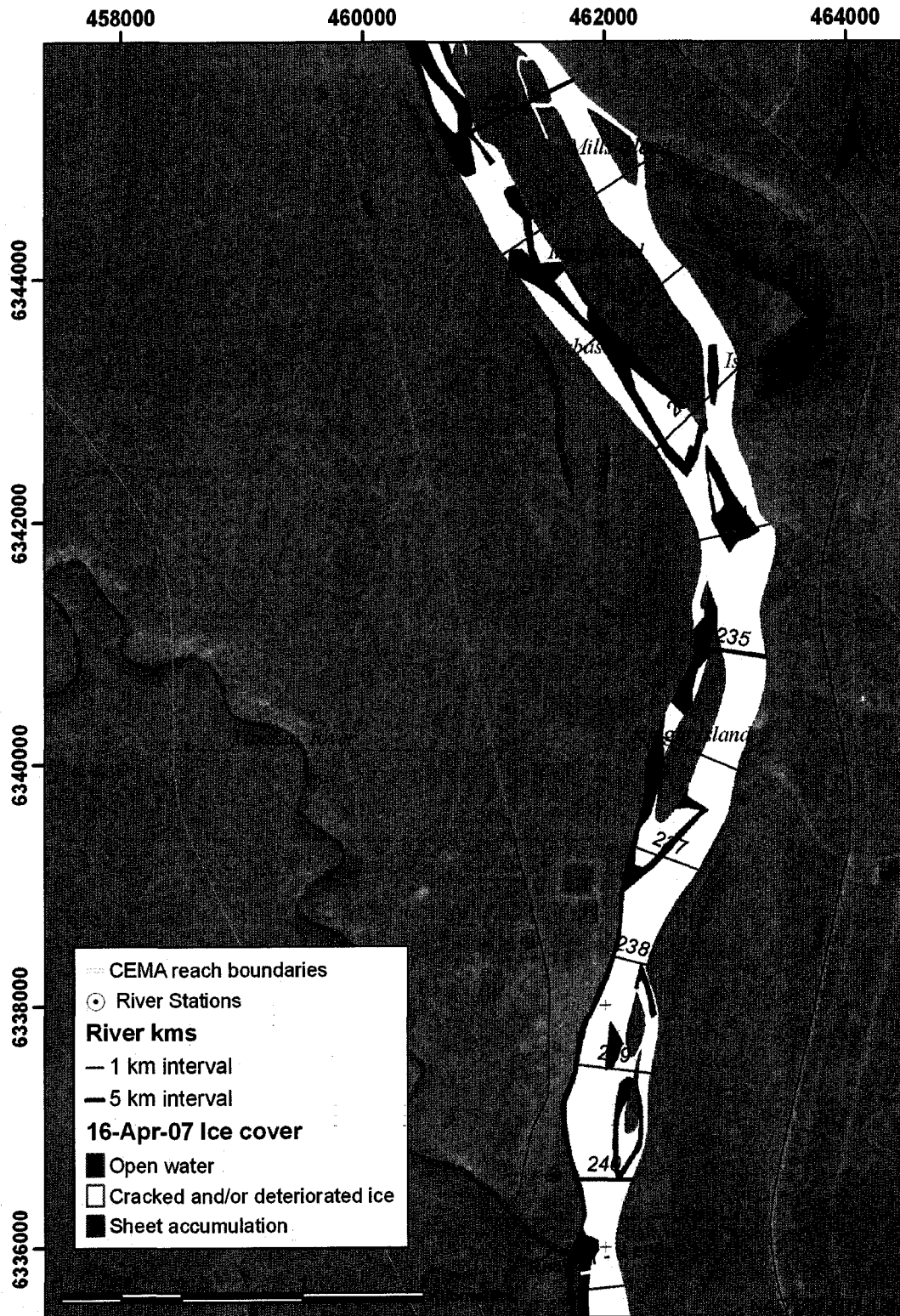


Figure B6.6 Ice cover mapping: April 16, 2007 - km 241 to 230

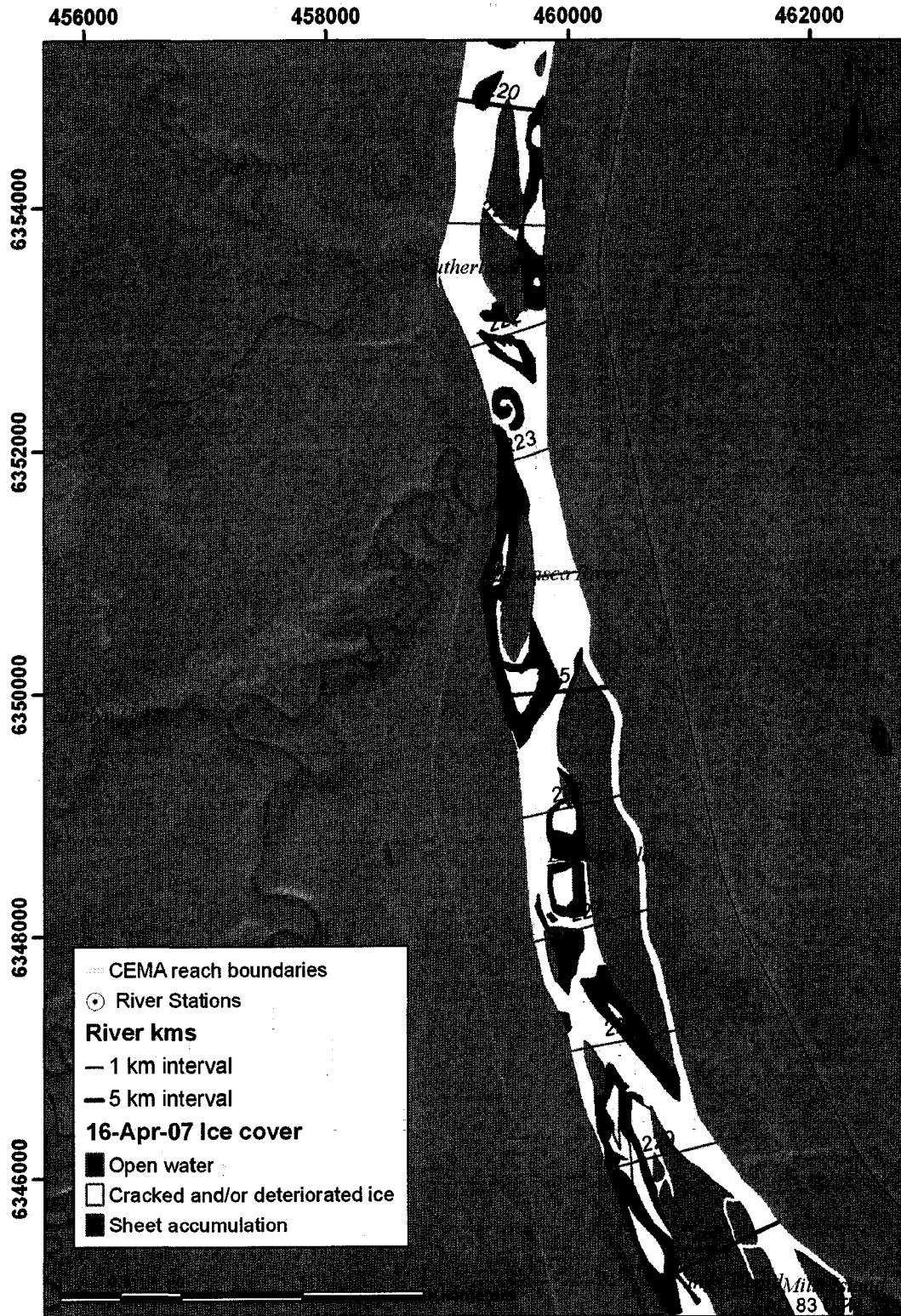


Figure B6.7 Ice cover mapping: April 16, 2007 - km 230 to 220

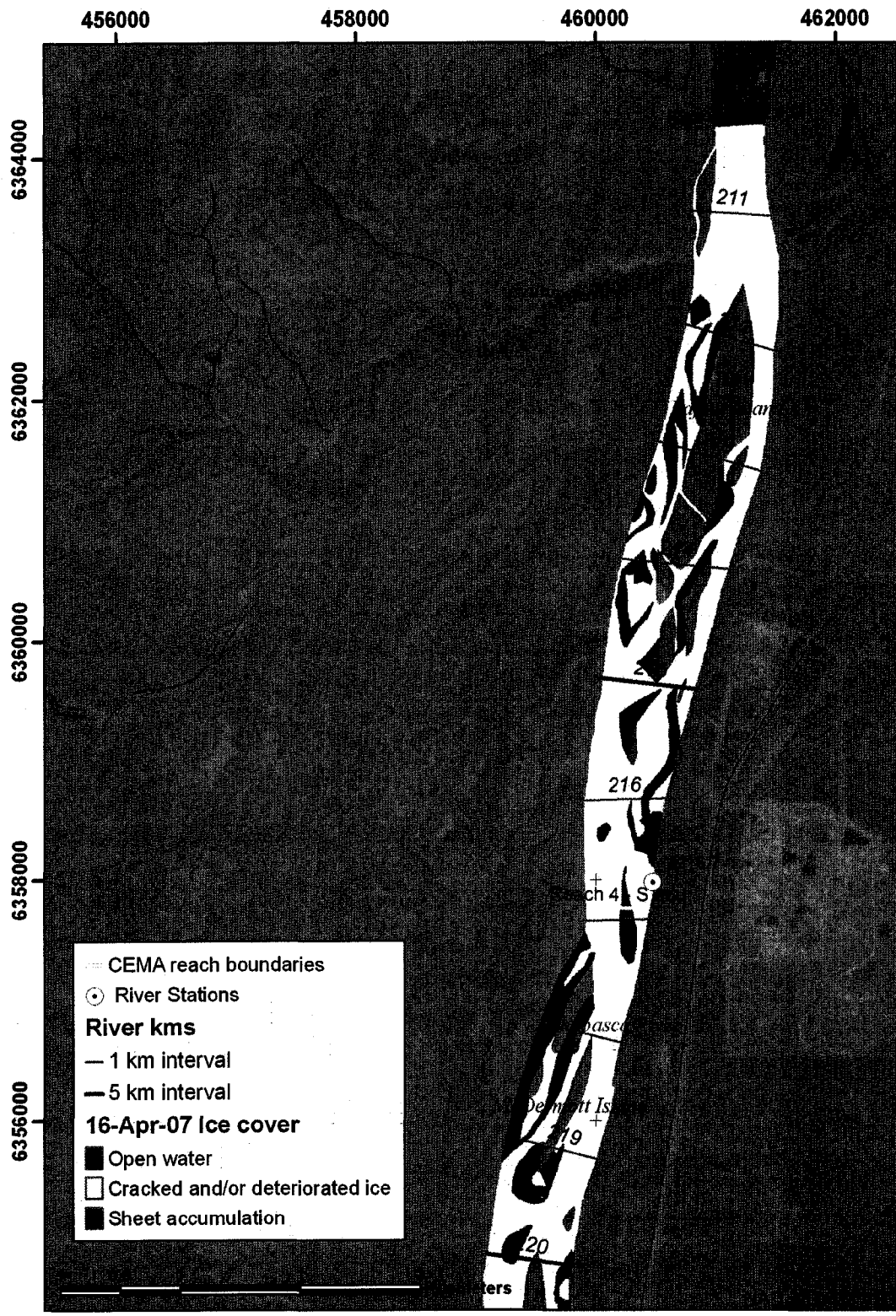


Figure B6.8 Ice cover mapping: April 16, 2007 - km 220 to 210

Appendix B5 Ice cover mapping – April 17, 2007

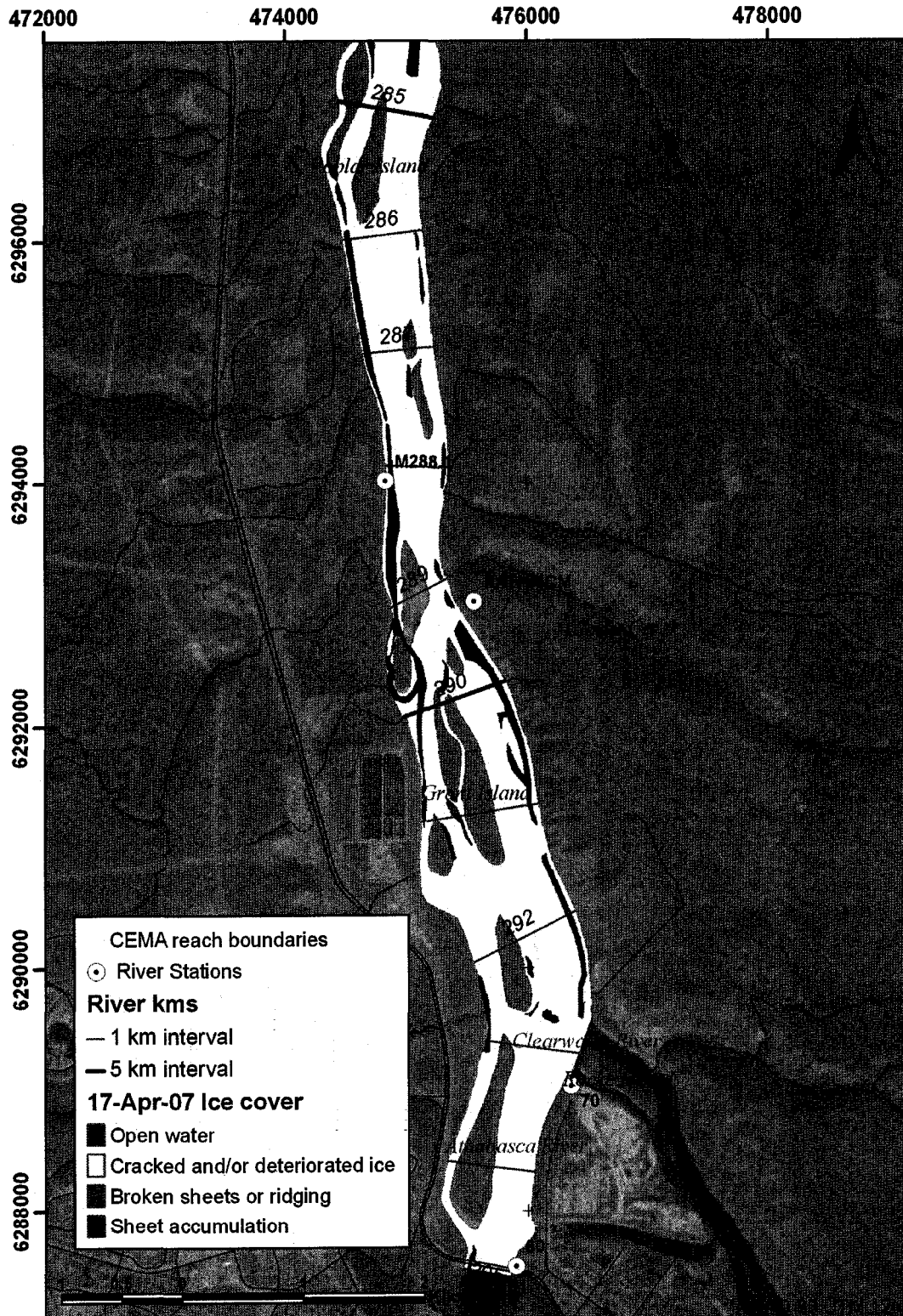


Figure B7.1 Ice cover mapping: April 17, 2007 - km 295 to 285

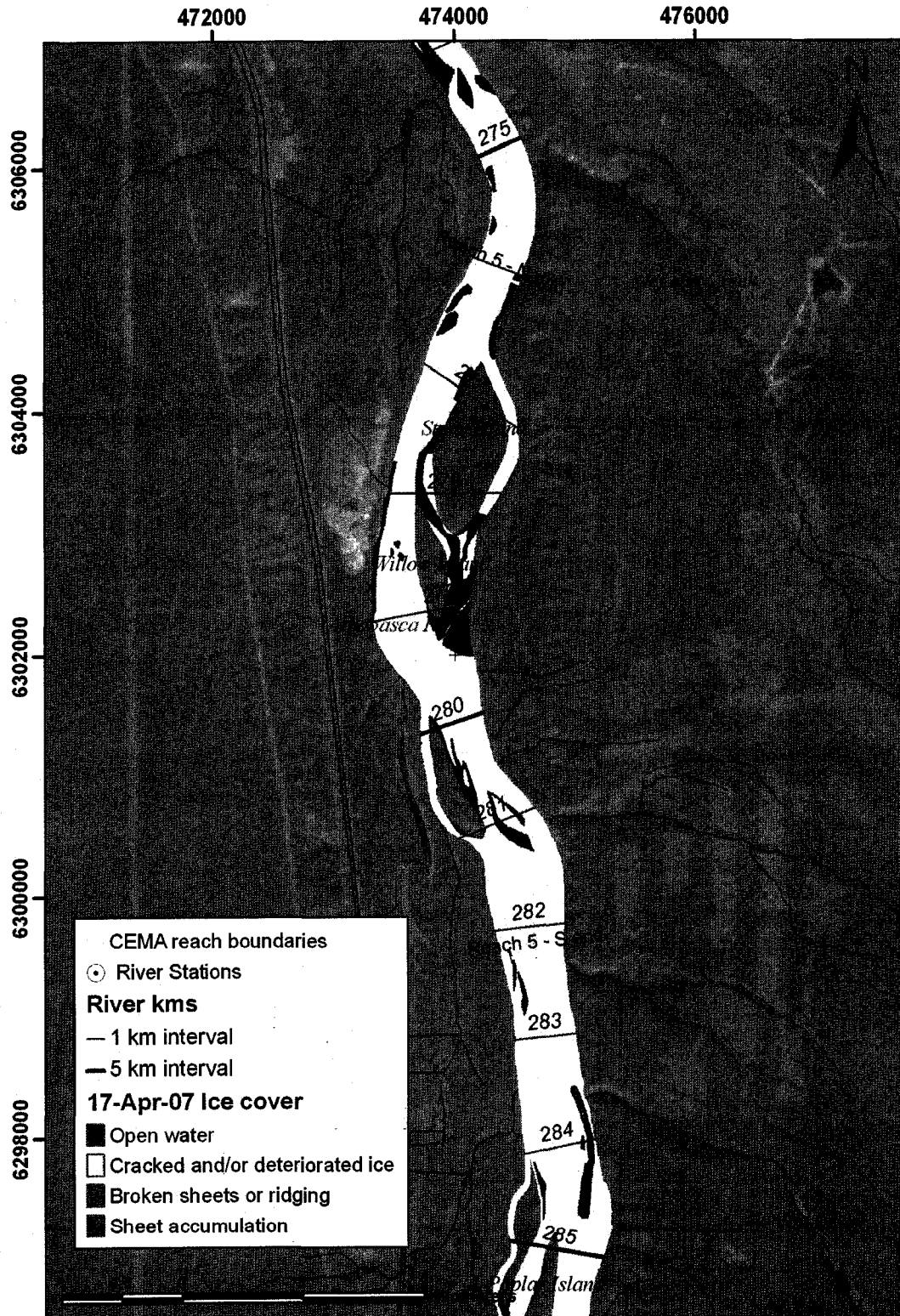


Figure B7.2 Ice cover mapping: April 17, 2007 - km 285 to 274

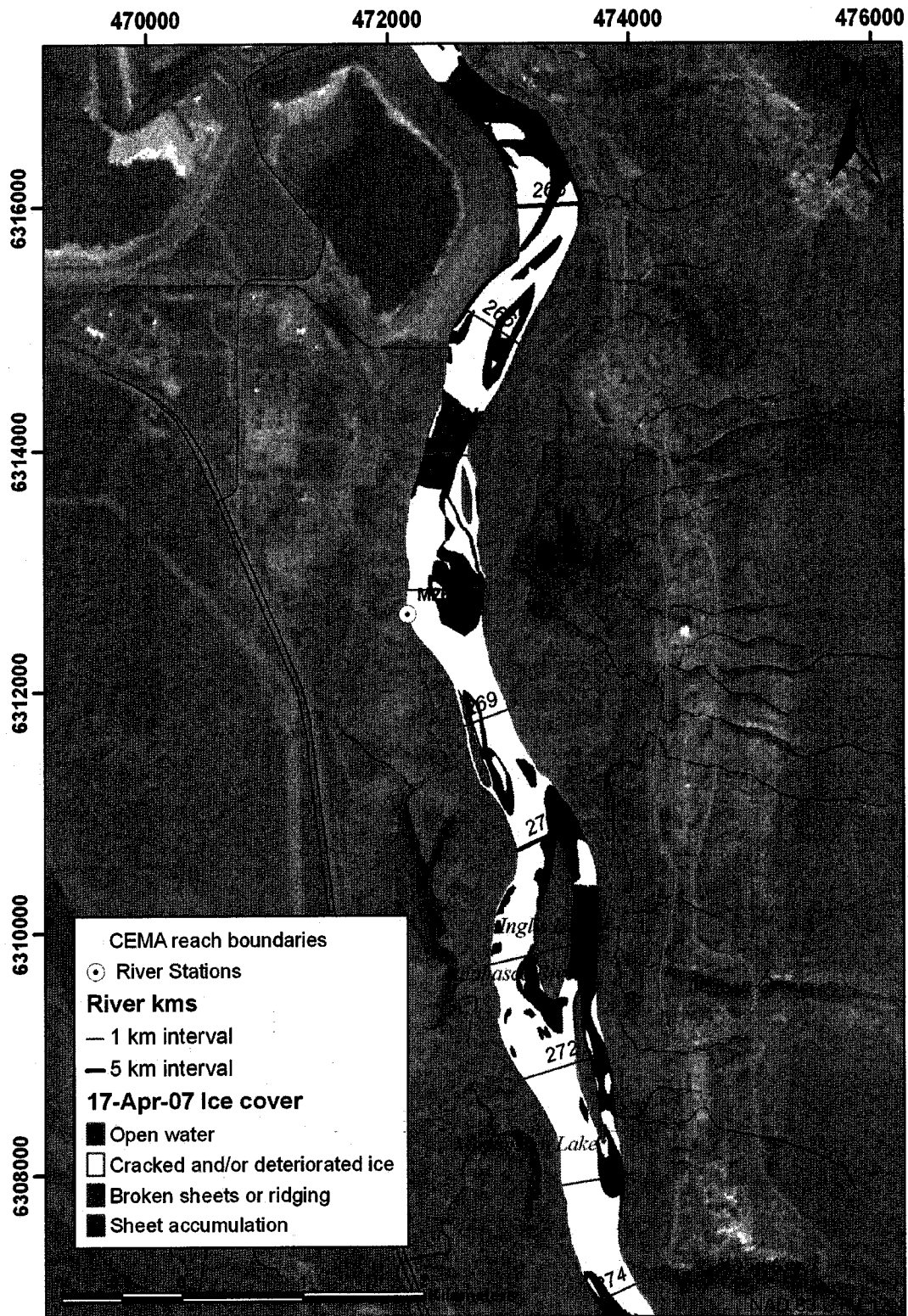


Figure B7.3 Ice cover mapping: April 17, 2007 - km 274 to 264

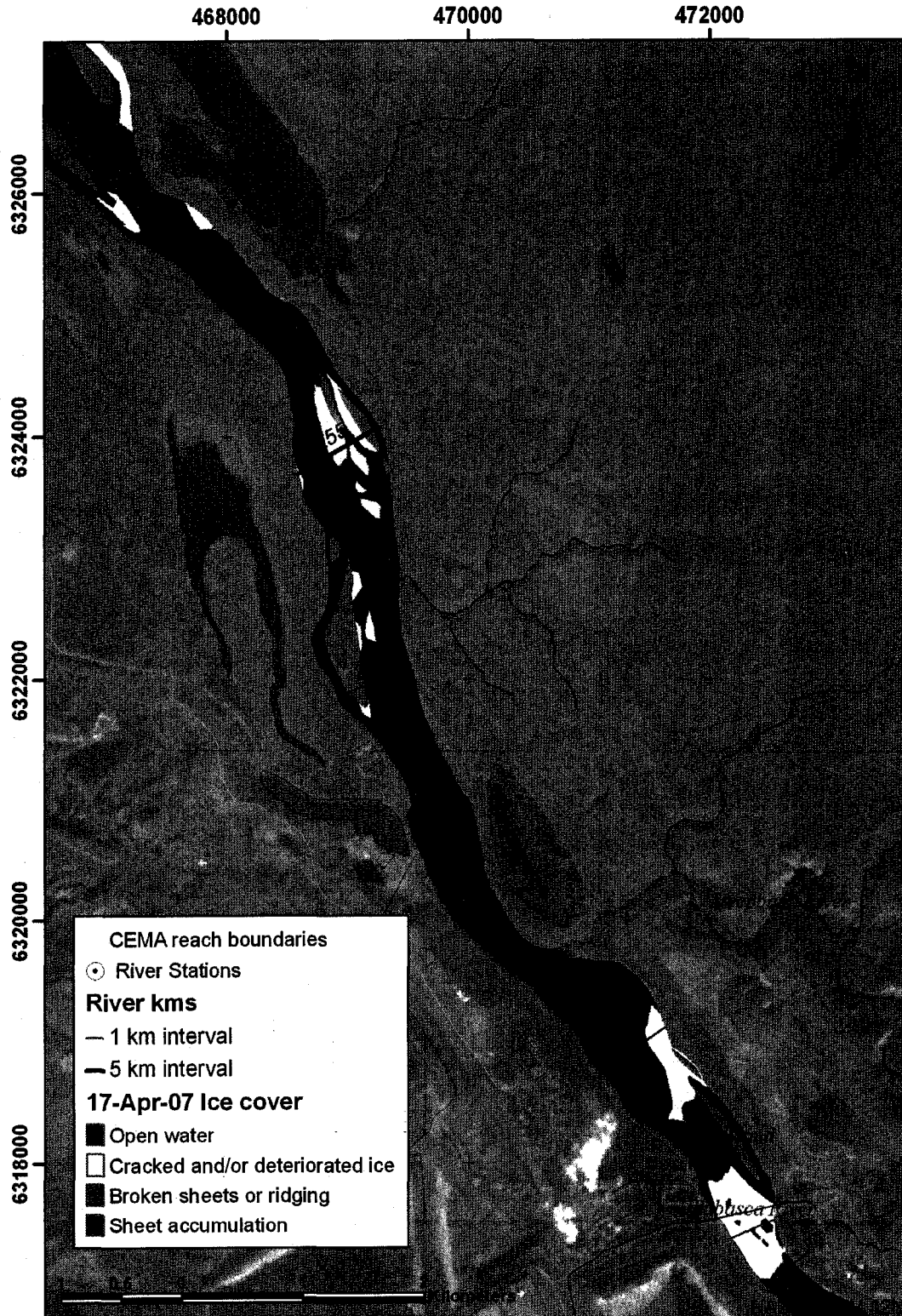


Figure B7.4 Ice cover mapping: April 17, 2007 - km 264 to 252

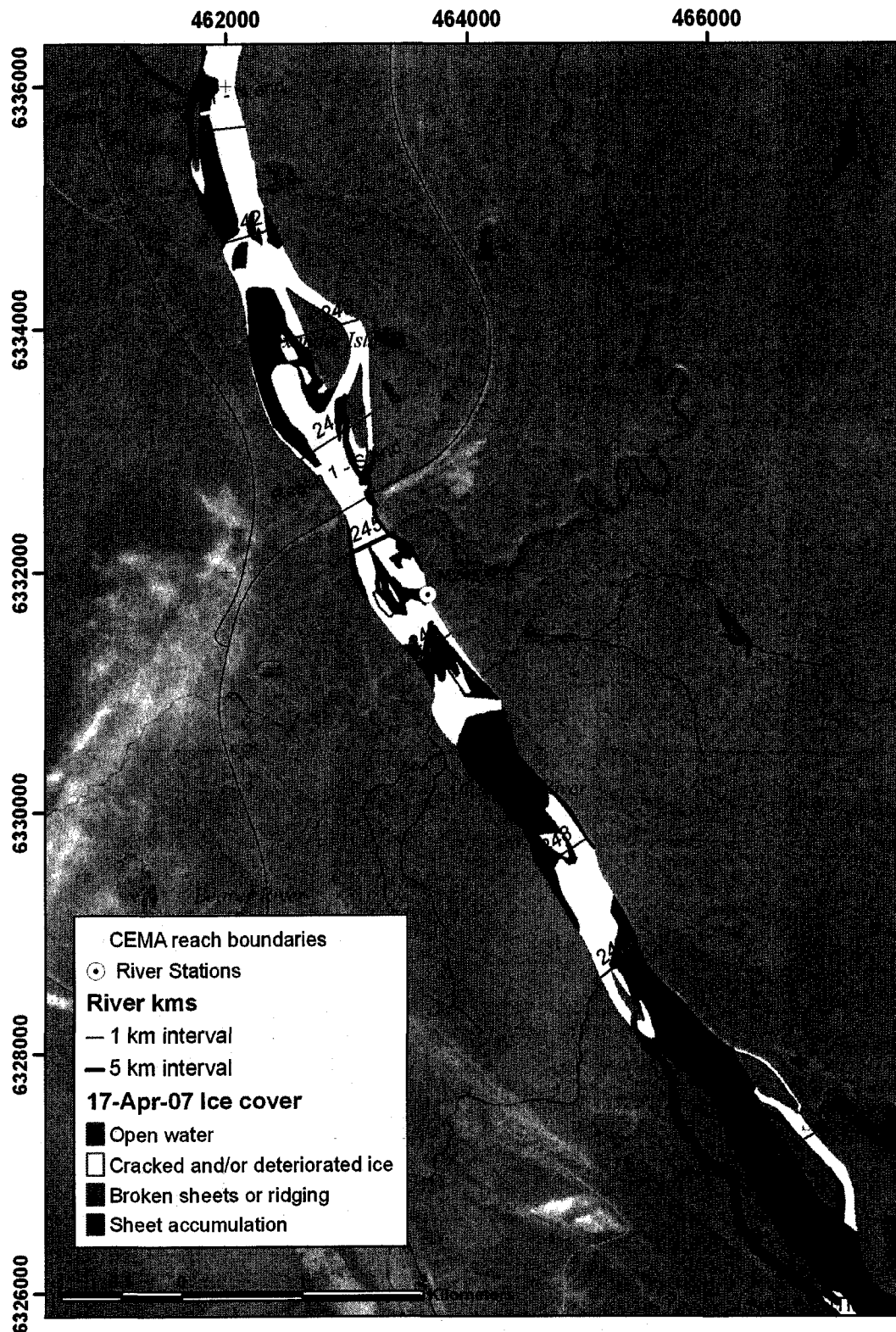


Figure B7.5 Ice cover mapping: April 17, 2007 - km 252 to 241

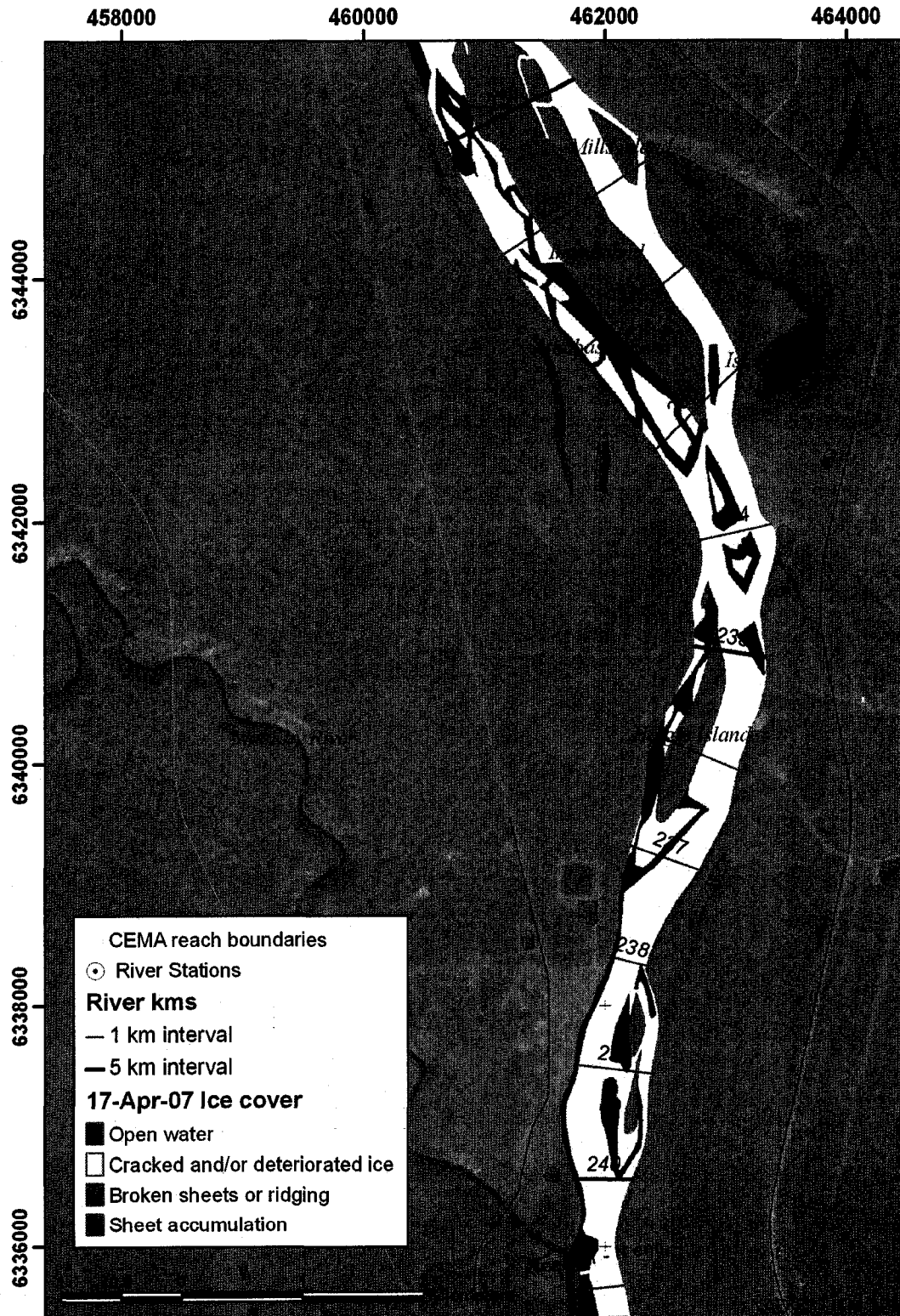


Figure B7.6 Ice cover mapping: April 17, 2007 - km 241 to 230

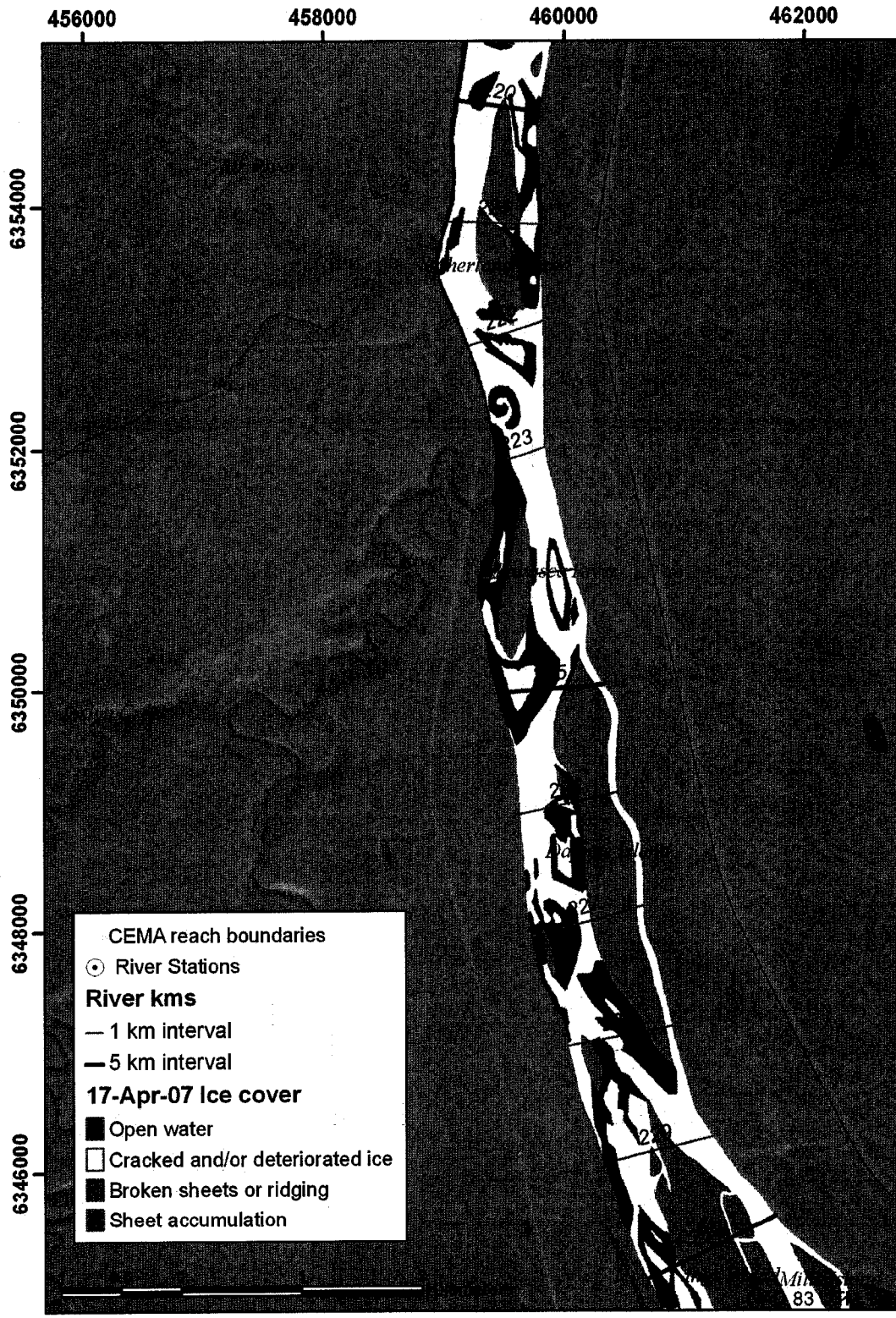


Figure B7.7 Ice cover mapping: April 17, 2007 - km 230 to 220

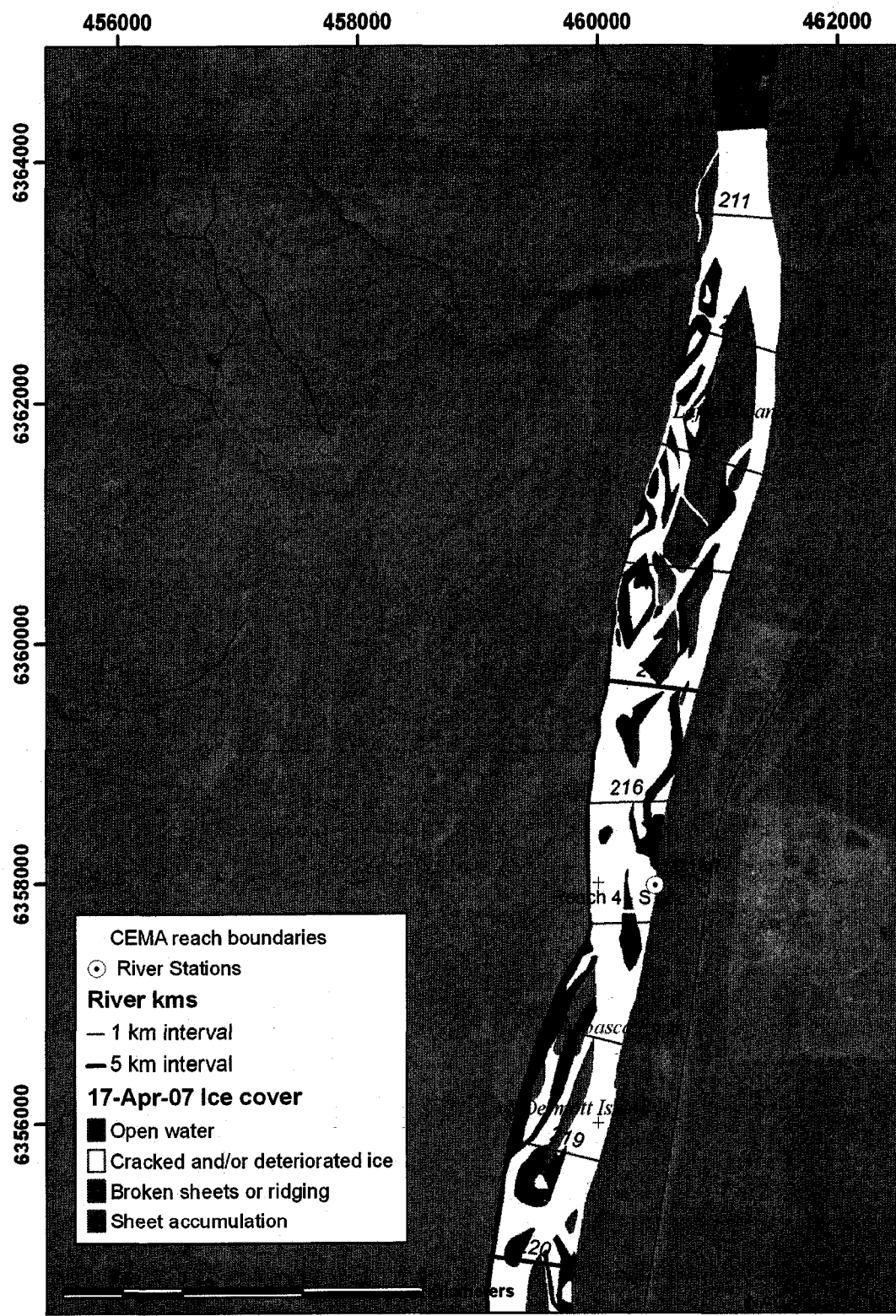


Figure B7.8 Ice cover mapping: April 17, 2007 - km 220 to 210